

University of Vermont

**UVM ScholarWorks**

---

Graduate College Dissertations and Theses

Dissertations and Theses

---

2015

## Organic Chemical Characterization Of Primary And Secondary Biodiesel Exhaust Particulate Matter

John Kasumba  
*University of Vermont*

Follow this and additional works at: <https://scholarworks.uvm.edu/graddis>



Part of the [Environmental Engineering Commons](#), and the [Place and Environment Commons](#)

---

### Recommended Citation

Kasumba, John, "Organic Chemical Characterization Of Primary And Secondary Biodiesel Exhaust Particulate Matter" (2015). *Graduate College Dissertations and Theses*. 358.  
<https://scholarworks.uvm.edu/graddis/358>

This Dissertation is brought to you for free and open access by the Dissertations and Theses at UVM ScholarWorks. It has been accepted for inclusion in Graduate College Dissertations and Theses by an authorized administrator of UVM ScholarWorks. For more information, please contact [scholarworks@uvm.edu](mailto:scholarworks@uvm.edu).

ORGANIC CHEMICAL CHARACTERIZATION OF PRIMARY AND SECONDARY  
BIODIESEL EXHAUST PARTICULATE MATTER

A Dissertation Presented

by

John Kasumba

to

The Faculty of the Graduate College

of

The University of Vermont

In Partial Fulfillment of the Requirements  
for the Degree of Doctor of Philosophy  
Specializing in Civil and Environmental Engineering

May, 2015

Defense Date: October 29, 2014  
Dissertation Examination Committee:

Britt A. Holmén, Ph.D, Advisor  
Giuseppe A. Petrucci, Ph.D, Chairperson  
Donna M. Rizzo, Ph.D  
Robert G. Jenkins, Ph.D  
Cynthia J. Forehand, Ph.D., Dean of the Graduate College

## ABSTRACT

Biodiesel use and production has significantly increased in the United States and in other parts of the world in the past decade. This change is driven by energy security and global climate legislation mandating reductions in the use of petroleum-based diesel. Recent air quality research has shown that emission of some pollutants such as CO, particulate matter (PM), SO<sub>2</sub>, hydrocarbons, and carcinogenic polycyclic aromatic hydrocarbons (PAHs) is greatly reduced with biodiesel. However, studies have also shown that some unregulated emissions, such as gas-phase carbonyls, are increased with biodiesel combustion. Very limited research has been done to investigate the particle-phase carbonyl and quinone emissions from biodiesel combustion. Also, very limited studies have investigated the ozone oxidation of biodiesel exhaust PM. Fatty acid methyl esters (FAMES) are found in high abundance in biodiesel exhaust PM. The presence of these FAMES in biodiesel exhaust PM can potentially alter the kinetics of the reactions between ozone and particle-phase PAHs.

In this study, an Armfield CM-12 automotive light-duty diesel engine operated on a transient drive cycle was used to generate PM from various waste vegetable oil (WVO) and soybean biodiesel blends (containing 0%, (B00), 10% (B10), 20% (B20), 50% (B50), and 100% (B100) biodiesel by volume). The primary PM emissions were sampled using Teflon-coated fiberfilm filters. Laboratory PAHs, FAMES, and B20 exhaust PM were exposed to ~0.4 ppm ozone for time periods ranging from 0-24 hours in order to study the effect of FAMES and biodiesel exhaust PM on the ozonolysis of PAHs. Organic chemical analysis of samples was performed using gas chromatography/mass spectrometry (GC/MS). PAHs, carbonyls, FAMES, and n-alkanes were quantified in the exhaust PM of petrodiesel, WVO and soybean fuel blends. The emission rates of the total PAHs in B10, B20, B50, and B100 exhaust PM decreased by 0.006-0.071 ng/μg (5-51%) compared to B00, while the emission rates for the FAMES increased with increasing biodiesel content in the fuel. The emission rates of the total n-alkanes in B10, B20, B50, and B100 exhaust PM decreased by 0.5-21.3 ng/μg (4-86%) compared to B00 exhaust PM. The total emission rates of the aliphatic aldehydes in biodiesel exhaust PM (B10, B20, B50, and B100) increased by 0.019-2.485 ng/μg (36-4800%) compared to petrodiesel. The emission rates of the total aromatic aldehydes, total aromatic ketones, and total quinones all generally decreased with increasing biodiesel content in the fuel.

With the exception of benzo[a]pyrene, the pseudo-first order ozone reaction rate constants of all the PAHs decreased by 1.2-8 times in the presence of the FAMES. Phenanthrene, fluoranthene, and pyrene were the only PAHs detected in the B20 exhaust PM, and their ozone reaction rate constants were about 4 times lower than those obtained when the PAHs alone were exposed to ozone.

The findings of this study indicate that there are both positive and negative effects to emissions associated with biodiesel use in light-duty diesel engines operating on transient drive cycle.

## CITATIONS

Material in Appendix D of this dissertation was published in the journal of Atmospheric Environment in the form:

Kasumba, J., Holmén, B.A., Hiscox, A., Wang, J., Miller, D.. (2011). Agricultural PM<sub>10</sub> Emissions from Cotton Field Disking in Las Cruces, NM. *Atmospheric Environment*, 45, 1668-1674. **DOI:** *10.1016/j.atmosenv.2011.01.004*.

Material in Appendix E of this dissertation was published in the Journal of Agricultural and Food Chemistry in the form:

Holmén, B.A., Kasumba, J., Hiscox, A., Wang, J., Miller, D.. (2013). Mechanized and Natural Soil-to-Air Transfer of Trifluralin and Prometryn from a Cotton Field in Las Cruces, New Mexico. *Journal of Agricultural and Food Chemistry*, 61, 9776-9783. **DOI:** *10.1021/jf4020697*.

My contribution towards this publication was about 60%. I was responsible for developing the extraction and analysis procedures for all the field samples. I also wrote the initial draft of this publication.



## ACKNOWLEDGMENTS

I would like to start by thanking Professor Britt Holmén, my advisor, for mentoring me during my graduate studies at UVM. Her continuous support and push for excellence helped me succeed through my Ph.D. program. I also thank her for reading through all the manuscripts in this dissertation.

I would also like to thank Professor Giuseppe Petrucci for chairing my dissertation committee. I also thank Professors Donna Rizzo and Robert Jenkins for serving on my dissertation committee. I thank them for all the helpful suggestions they gave me when I was writing this dissertation.

I also acknowledge the present members of the Holmén Research Group (Karen Sentoff, Tyler Feralio, Jim Dunshee, Matt Conger, and Ben Rukavina) and the past members (Dan Nielsen, Tucker Stevens, Mitchell Robinson, Terry Barrett, Phil Cannata, Chris Gavitt, Dan Cooney, Timothy Kelly, and Wesley Miller) for their help in the lab, advice, and contributions in group meetings.

I also wish to thank Bruce O'Rourke for helping troubleshoot the GC/MS systems in our laboratory.

Lastly, I thank my family and friends for supporting me throughout my Ph.D. journey. Special thanks to my friends John Hanley, Mr. Joseph Rogers, Mrs. Laurene Rogers, and Laura Obregon for the great love they showed me while I was in this cold part of the world.

## TABLE OF CONTENTS

CITATIONS .....	ii
ACKNOWLEDGMENTS .....	iii
LIST OF TABLES .....	vi
LIST OF FIGURES .....	vii
TABLE OF ABBREVIATIONS .....	ix
<b>Chapter 1 INTRODUCTION .....</b>	<b>1</b>
1.1 Organization of Dissertation .....	1
1.2 Background .....	4
1.3 Overall Research Objectives .....	7
1.4 Research Questions .....	8
1.5 Literature Review .....	9
1.5.1 Chemical Composition of Biodiesel and Biodiesel Exhaust PM .....	9
1.5.2 Chemical Composition of Diesel and Diesel Exhaust PM .....	17
1.5.3 Effects of Biodiesel on the Organic Compounds in PM from Diesel Engines .....	19
1.5.4 Reaction of Ozone with Biodiesel Exhaust PM .....	22
<b>Chapter 2 METHODS.....</b>	<b>26</b>
2.1 Methods for Organic Chemical Analysis of Diesel and Biodiesel Exhaust PM....	26
2.1.1 Fuels used in Emission Tests.....	26
2.1.2 Emissions Test Procedure and Sampling.....	29
2.1.3 Chemicals .....	32
2.1.4 Extraction and Analysis of Target Organic Chemical Compounds .....	35
2.1.5 Quality Control /Quality Assurance .....	38
2.1.6 Data Analysis.....	41
2.2 Methods for Analysis of Fuel Samples .....	43
2.2.1 Fuel and Lubricating Oil Analysis by GC/MS .....	43
2.2.2 Data Analysis.....	45
2.3 Methods for the Ozone Exposure Experiments.....	46
2.3.1 Ozone Exposure Experiments .....	46
2.3.2 Extraction and GC/MS Analysis .....	51
2.3.3 Data Analysis.....	51

<b>Chapter 3 RESULTS AND DISCUSSION .....</b>	<b>54</b>
3.0 Sampling Information .....	54
3.1 Organic Chemical Characterization of Biodiesel Exhaust Particulate Matter from a Light-Duty Diesel Engine.....	57
3.1.1 n-Alkanes Emissions .....	57
3.1.2 PAH Emissions.....	64
3.1.3 FAMES Emissions .....	75
3.1.4 Carbonyl and Quinone Emissions .....	81
3.2 Comparison of Organic Composition of Fuel and Particulate Matter from a Light-Duty Diesel Engine Fueled with Diesel and Biodiesel .....	92
3.2.1 Organic Composition of Fuels.....	92
3.2.2 PM Emissions in Biodiesel Exhaust.....	104
3.2.3 Summary of Formation Pathways .....	120
3.3 Effect of Fatty Acid Methyl Esters on the Heterogeneous Ozonation Reactions of PAHs in Biodiesel Particulate Matter .....	122
3.3.1 Ozonolysis of PAH Mixture Spiked on ¼-inch FF Punches.....	122
3.3.2 Ozonolysis of PAHs in the Presence of FAMES (Spiked Experiments) .....	127
3.3.3 FAMES Ozonolysis Rate Constants for Spiked Mix.....	130
3.3.4 Ozonolysis of PAHs in B20 Biodiesel Exhaust PM.....	132
3.3.5 Ozonolysis of FAMES in B20 Biodiesel Exhaust PM.....	135
3.3.6 Products of the Ozonolysis of PAHs and FAMES.....	140
<b>Chapter 4 SUMMARY AND RECOMMENDATIONS .....</b>	<b>148</b>
<b>Chapter 5 REFERENCES CITED.....</b>	<b>155</b>
APPENDIX A.....	163
APPENDIX B .....	183
APPENDIX C .....	195
APPENDIX D.....	212
APPENDIX E .....	228

## LIST OF TABLES

<b>Table 1.1:</b> Most common fatty acid groups in biodiesel fuel.....	11
<b>Table 1.2:</b> Fatty acid compositional profiles for soybean and canola oils.....	12
<b>Table 1.3:</b> Fatty acid compositional profiles for animal fats. ....	13
<b>Table 1.4:</b> Organic chemical fuel composition of the diesel fuel used in two previous studies.....	18
<b>Table 2.1:</b> Measured properties of the soybean and waste vegetable oil biodiesel fuels, and Trono ULSD fuel.....	28
<b>Table 2.2:</b> CM-12 Engine, dynamometer, and lube oil specifications.....	30
<b>Table 2.3:</b> PAHs in the 16 PAHs mix, n-alkanes in the n-alkanes standard, and FAMEs in the 10 FAMEs mix .....	33
<b>Table 2.4:</b> Structures of the FAMEs used in the study. ....	34
<b>Table 2.5:</b> Concentrations ( $\mu\text{g/g}$ ) of the different WVO biodiesel fuel blends that were analyzed for the different target analytes .....	45
<b>Table 2.6:</b> Concentrations (ppm) of the different soybean biodiesel fuel blends that were analyzed for the different target analytes .....	45
<b>Table 3.1:</b> Sampling conditions during the WVO and soybean engine test sequences ...	56
<b>Table 3.2:</b> PAH emission rates ( $\text{ng}/\mu\text{g}$ ) obtained in the present study with those obtained by Karavalakis et al. (2009) .....	71
<b>Table 3.3:</b> Equations of best fit for the percent reduction of total PAH (phenanthrene, fluoranthene, and pyrene) emissions from the present study and Karavalakis et al. (2009).....	74
<b>Table 3.4:</b> Average percent composition of the main FAMEs detected in the WVO and soybean biodiesel exhaust PM.....	77
<b>Table 3.5:</b> Aromatic hydrocarbons detected in diesel fuel.....	101
<b>Table 3.6:</b> Percent composition (%) of the speciated compound groups in lubricating oil samples used by Mao et al. (2009) .....	104
<b>Table 3.7:</b> Average percent composition of the main FAMEs detected in the WVO and soybean biodiesel fuel and exhaust PM.....	110
<b>Table 3.8:</b> Mass of FAMEs injected in the engine (mg) and sampled on the filters during the different WVO engine runs .....	116
<b>Table 3.9:</b> Mass of FAMEs injected in the engine (mg) and sampled on the filters during the different soybean engine runs.....	117
<b>Table 3.10:</b> Formation pathways of the target organic compounds detected in diesel and biodiesel exhaust PM. ....	121
<b>Table 3.11:</b> Comparison of literature studies on the heterogeneous reaction rates of ozone with PAHs on different substrates and this study .....	126
<b>Table 3.12:</b> Products identified from the ozonolysis of the FAMEs in spiked FF punches and B20 biodiesel exhaust PM after 24 hours of ozone exposure. ....	142

## LIST OF FIGURES

<b>Figure 1.1:</b> FAME concentrations ( $\mu\text{g}/\text{gal}$ Fuel) of the soybean and beef tallow biodiesel fuel blends used by Magara-Gomez et al. (2012).....	16
<b>Figure 1.2:</b> FAME emission rates ( $\mu\text{g}/\text{kg}$ $\text{CO}_2$ ) in the biodiesel exhaust PM of the soybean and beef tallow biodiesel fuel blends used by Magara-Gomez et al. (2012) .....	17
<b>Figure 2.1:</b> Drive cycle used during engine testing .....	30
<b>Figure 2.2:</b> Schematic of the ozone exposure setup.....	48
<b>Figure 3.1:</b> Average emission rates ( $\text{ng}/\mu\text{g}$ ) of n-alkanes in PM resulting from the combustion of (a) WVO and (b) soybean biodiesel blends .....	59
<b>Figure 3.2:</b> Emission rates ( $\text{ng}/\mu\text{g}$ ) of total n-alkanes (sum of emission rates of the detected n-alkanes) in the exhaust PM of (a) WVO biodiesel blends, and (b) soybean biodiesel blends.....	62
<b>Figure 3.3:</b> Average emission rates ( $\text{ng}/\mu\text{g}$ ) of PAHs in PM resulting from the combustion of (a) WVO and (b) soybean biodiesel blends .....	66
<b>Figure 3.4:</b> Emission rates ( $\text{ng}/\mu\text{g}$ ) of total PAH (sum of emission rates of the detected PAHs) in the exhaust PM of (a) WVO biodiesel blends, and (b) soybean biodiesel blends.....	68
<b>Figure 3.5:</b> Percent reduction in total PAH emissions with increasing WVO and soybean biodiesel volume percent. ....	74
<b>Figure 3.6:</b> Average emission rates ( $\text{ng}/\mu\text{g}$ ) of FAMES in PM resulting from the combustion of (a) WVO and (b) soybean biodiesel blends .....	76
<b>Figure 3.7:</b> Emission rates ( $\text{ng}/\mu\text{g}$ ) of total FAMES (sum of emission rates of the speciated FAMES) in the exhaust PM of (a) WVO biodiesel blends, and (b) soybean biodiesel blends .....	79
<b>Figure 3.8:</b> Average emission rates ( $\text{ng}/\mu\text{g}$ ) of (a) Aliphatic aldehydes (b) Aromatic aldehydes (c) Aromatic ketones, and (d) Quinones in PM resulting from the combustion of WVO biodiesel blends .....	82
<b>Figure 3.9:</b> Average emission rates ( $\text{ng}/\mu\text{g}$ ) of (a) Aliphatic aldehydes (b) Aromatic aldehydes (c) Aromatic ketones, and (d) Quinones in PM resulting from the combustion of soybean biodiesel blends.....	83
<b>Figure 3.10:</b> Emission rates ( $\text{ng}/\mu\text{g}$ ) of total (a) Aliphatic aldehydes, (b) Aromatic aldehydes, (c) Aromatic ketones, and (d) Quinones in the exhaust PM resulting from combustion of WVO biodiesel blends .....	85
<b>Figure 3.11:</b> Emission rates ( $\text{ng}/\mu\text{g}$ ) of total (a) Aliphatic aldehydes, (b) Aromatic aldehydes, (c) Aromatic ketones, and (d) Quinones in the exhaust PM resulting from combustion of soybean biodiesel blends.....	87
<b>Figure 3.12:</b> Distribution of n-alkanes in the petrodiesel fuel used to prepare the WVO and soybean biodiesel blends .....	93
<b>Figure 3.13:</b> Concentrations ( $\mu\text{g}/\text{gal}$ ) of n-alkanes measured in the WVO and soybean biodiesel fuel blends .....	94

<b>Figure 3.14:</b> Concentration of n-alkanes ( $\mu\text{g}/\text{gal}$ ) in diesel (B00) and biodiesel fuel blends from both feedstocks .....	95
<b>Figure 3.15:</b> FAME concentrations ( $\text{g}/\text{gal}$ fuel) of the different blends of WVO and soybean biodiesel fuels .....	96
<b>Figure 3.16:</b> Average percent composition of FAMEs in the WVO and soybean biodiesel fuel blends .....	97
<b>Figure 3.17:</b> Chromatograms of diesel (B00), neat biodiesel (B100) fuels, and lubricating oil .....	103
<b>Figure 3.18:</b> Fuel blend ratios of FAME concentrations to methyl linoleate (C18:2n6c) concentration ( $(\text{g}/\text{gal})/(\text{g}/\text{gal})$ ) in the (a) WVO and (b) soybean biodiesel fuel blends .....	111
<b>Figure 3.19:</b> Exhaust PM ratios of FAME emission rates to that of methyl linoleate (C18:2n6c) ( $(\text{ng}/\mu\text{g})/(\text{ng}/\mu\text{g})$ ) in the (a) WVO and (b) soybean exhaust PM .....	112
<b>Figure 3.20:</b> Volatilization ( $k'_2$ ) and effective pseudo-first order ozonation ( $k'_{Eff}$ ) rate constants obtained from the reactions of ozone and 16 PAHs only, and Mixture of 16 PAHs and 10 FAMEs.....	123
<b>Figure 3.21:</b> Pseudo-first order FAME ozonation rate constants obtained from the reactions of ozone with the mixtures of 16 PAHs and 10 FAMEs, and Biodiesel (B20) exhaust PM .....	131
<b>Figure 3.22:</b> Products of the ozonolysis of the FAMEs in B20 biodiesel exhaust PM .	143

## TABLE OF ABBREVIATIONS

ACN	Acetonitrile
ANOVA	Analysis of Variance
ASTM	American Society for Testing and Materials
CO	Carbon monoxide
CO <sub>2</sub>	Carbon dioxide
Comp	Composition
Conc	Concentration
DCM	Dichloromethane
EI	Electron Impact
EPA	Environmental Protection Agency
FAMEs	Fatty acid methyl esters
FF	Fiberfilm filter
GC/MS	Gas chromatography/mass spectrometry
$k'_{Eff}$	Effective first order ozonation rate constant
LSD	Low sulfur diesel
MDL	Method detection limit
MeOH	Methanol
MSD	Mass selective detector
MW	Molecular weight
N <sub>2</sub>	Nitrogen
O <sub>3</sub>	Ozone
PAHs	Polycyclic aromatic hydrocarbons
PFBHA	Pentafluorobenzylhydroxylamine
PM	Particulate matter
ppm	parts per million
POCs	Polar oxygenated compounds
QFF	Quartz fiber filter
RH	Relative humidity
RSD	Relative standard deviation
SD	Standard deviation
SLPM	Standard liters per minute
Soy	Soybean
SO <sub>2</sub>	Sulfur dioxide
TD	Thermal desorption
ULSD	Ultra-low sulfur diesel
WVO	Waste vegetable oil
2F9F	2-fluoro-9-fluorenone
6F4C	6-fluoro-4-chromanone

## **Chapter 1**

### **INTRODUCTION**

#### **1.1 Organization of Dissertation**

This dissertation has been divided into five chapters, i.e., (1) Introduction, (2) Methods, (3) Results and Discussion, (4) Summary and Recommendations, and (5) References Cited. Chapter 1 presents an introduction to this dissertation with background information on prior studies related to the objectives of the studies in this dissertation.

In Chapter 2, the methods employed to answer the questions in Chapter 1 are presented.

Chapter 3 presents the results of the experimental studies of this dissertation. In Section 3.1 of Chapter 3, the results of the effects of soybean and WVO biodiesel fuels on the exhaust PM emission of PAHs, n-alkanes, FAMES, and carbonyls from a light-duty diesel engine are presented. The emission rates of the target analytes in the exhaust PM of the different blends of soybean (B20 and B100) and WVO (B10, B20, B50, and B100) are compared to those of petrodiesel PM. The results of this study show that the emissions of PAHs and n-alkanes generally decreased with increasing biodiesel in the fuel for both feedstocks, but increases in the emissions of aliphatic carbonyls were observed with increasing biodiesel in the fuel. The emission rates of the aromatic aldehydes, aromatic ketones, and quinones generally decreased with increasing biodiesel in the fuel.

Section 3.2 of Chapter 3 summarizes the results from the analysis of the fuel samples that were used in the emission tests in order to understand the origin of the compounds detected in the exhaust PM. Again, emphasis was put on analysis of PAHs,



n-alkanes, FAMEs, and carbonyls. The findings of this study show that some toxic compounds such as PAHs, and carbonyls, that were not detected in the fuel and lubricating oil were formed during combustion in the engine, while other compounds such as FAMEs and some n-alkanes were emitted as unburned fuel.

The results of the investigation of the effects of FAMEs on the ozone oxidation of PAHs in biodiesel exhaust PM are presented in Section 3.3 of Chapter 3. The effect of laboratory standards of FAMEs on the ozone oxidation rates of laboratory standards of PAHs was also investigated. The FAMEs reduced the ozone reaction rates of the PAHs, and product compounds more oxygenated than the parent FAMEs were identified and quantified.

In Chapter 4, the results of the different studies in this dissertation are synthesized to develop overall conclusions and recommendations for future studies, while Chapter 5 presents the references that were cited throughout this dissertation.

Appendix A contains the list of target analytes, detection limits, engine sampling information, reproducibility data for the extractions, and results obtained from the analysis of variance tests. Appendix B contains the raw data for the target analytes obtained from the extraction of the filters analyzed for this dissertation. Appendix C shows summary results for the experimental parameters of the ozone exposure experiments, and the kinetic plots of the reactions between the PAHs and FAMEs with ozone. Appendices D and E show the manuscripts that were published from the herbicides project.

The results of this study show that there are both positive and negative effects of biodiesel use to human health and the environment. Most of the vegetable oil-based

feedstocks used in biodiesel production (e.g., soybean, canola, palm, sunflower, coconut, etc.) are produced from land use activities such as agriculture. Like diesel and biodiesel engine emissions, other anthropogenic activities like agricultural practices such as disking, harvesting, and tillage operations have been previously reported to affect the air quality (PM concentrations) especially in the vicinity of agricultural fields (Clausnitzer and Singer, 1997; Kjelgaard et al., 2004; Qiu and Pattey, 2008). In an effort to understand the effects of anthropogenic activities on air quality, this dissertation also presents work performed to quantify the PM<sub>10</sub> emissions from six different disking events on an agricultural field in New Mexico. This study, previously published in *Atmospheric Environment*, involved application of two pre-emergence herbicides (trifluralin and prometryn) on the agricultural field, followed by sampling of the gas- and particle-phase emissions using a variety of instruments at different heights and locations (near and far from the disking tractor) on the field during disking both pre- and post-herbicide application. In one manuscript of this study, the PM<sub>10</sub> emissions during the disking events were quantified to determine the PM<sub>10</sub> emission factors on the field during the different disking events. Meteorological conditions such as wind speed were found to affect the PM<sub>10</sub> emission factors on the field. The PM<sub>10</sub> emission factors were found to generally increase during disking events, and vertical PM<sub>10</sub> concentration profiles showed maxima at sampling heights between 1 and 2 m above the ground. This work is presented in Appendix D of this dissertation.

Additionally, the gas/particle partitioning behavior of trifluralin and prometryn during the different agricultural events was also investigated. The gas- and particle-phase herbicides emitted during the disking operations were sampled by an Apex personal

sampler that consisted of a Teflon filter-polyurethane foam (Filter-PUF) assembly. The filter sampled particle-phase herbicides, while the PUF cartridge sampled gas-phase herbicides. The PUFs and filters were extracted by supercritical fluid extraction (SFE), and the extracts analyzed using GC/MS. The concentrations of prometryn in both the gas and particle phases were 2-8 times greater than those of trifluralin for all sampling events. The mass fractions of prometryn in the particle phase were greater than those of trifluralin for all sampling events. The results of this study were published in the *Journal of Agricultural and Food Chemistry* and can be found in Appendix E of this dissertation.

## **1.2 Background**

Biodiesel is a fuel derived from renewable biological sources such as vegetable oil or animal fat (Ma and Hanna 1999). Recent research has shown that levels of some biodiesel exhaust emissions (particulate matter (PM), carbon dioxide, carbon monoxide, polycyclic aromatic hydrocarbons (PAHs), sulphur dioxide) are lower than those for petrodiesel (Needham et al., 1985; Last et al., 1995; McDonald et al., 1995; Graboski et al., 1998; Purcell et al., 1996; Schmidt et al., 1996; McCormick et al., 2001; US EPA (2002); Knothe et al., 2006). Furthermore, recent research on and use of biodiesel as an alternative fuel for diesel engines started because of the reduction of petroleum production by the Organization of the Petroleum Exporting Countries (OPEC) and the resulting price rise (Kahn et al., 2002). Hence, there has been an increase in biodiesel use in diesel engines in the United States and Europe in the past decade. Some studies, however, have indicated that potentially toxic unregulated combustion products like PAHs (e.g., Bakeas et al., 2011; Karavalakis et al., 2011; Magara-Gomez et al., 2012)

and carbonyls (e.g., Correa and Arbilla, 2008; Bikas and Zervas, 2007; Turrio-Baldassarri et al., 2004) are emitted in higher concentrations in biodiesel exhaust than in petrodiesel exhaust. For example, Correa and Arbilla (2008) observed that, with the exception of benzaldehyde, the rest of the gas-phase carbonyls measured (formaldehyde, acetaldehyde, acrolein+acetone, propionaldehyde, and butyraldehyde) had significantly higher concentrations in biodiesel than in conventional diesel exhaust (Correa and Arbilla, 2008). Other studies such as Guarieiro et al. (2008) indicated that the gas-phase emissions of some carbonyl compounds in biodiesel exhaust were greater than the corresponding carbonyl emissions in conventional diesel. The reason for the conflicting results could be due to differences in biodiesel feedstocks, engines, and engine operating conditions used by the different studies.

No studies have so far measured or compared the particle-phase carbonyl including quinone emissions in biodiesel exhaust PM to conventional diesel PM. However, studies like Schauer et al. (1999), Jakober et al. (2006), Jakober et al. (2007), and Jakober et al. (2008) have measured gas- and particle-phase concentrations of carbonyls and quinones in conventional diesel, although higher concentrations were detected in the gas-phase compared to the particle-phase. There is a need to measure and quantify the particle-phase carbonyl emissions from biodiesel as well because such compounds have been previously linked to adverse health effects in humans (Henry and Wallace, 1996; Mauderly 1997). Because previous studies found that the gas-phase emissions of aliphatic carbonyls in biodiesel exhaust were significantly higher than those for conventional diesel exhaust, it is hypothesized that the particle-phase concentrations of the aliphatic carbonyls in biodiesel exhaust will also be greater than those for

conventional diesel. Also, given that the aromatic content of biodiesel is lower than that of conventional diesel, it is hypothesized that the emissions of the aromatic carbonyls and quinones are reduced with biodiesel use.

Furthermore, the interaction between biodiesel exhaust PM emissions and atmospheric oxidants such as ozone has not been well explored to date, despite the possibility that the oxidized products of such interactions could be harmful to human health, hence making biodiesel more toxic than petrodiesel. No studies to date have measured or quantified the oxidation products of biodiesel exhaust PM from different biodiesel feedstocks. For about three decades, a lot of effort has been put into studying the reactions between ozone and other pollutants adsorbed on diesel PM such as PAHs and alkanes (e.g., Pitts et al., 1978; Grosjean et al., 1983; Poschl et al., 2001; Tsapakis and Stephanou, 2003; Kwamena et al., 2004; Kahan et al., 2006; Perraudin et al., 2007). No literature data on studies investigating the reactions between ozone and fatty acid methyl esters (FAMES) in biodiesel exhaust PM are available. Such studies are important because they can lead to a better understanding of the atmospheric fate and environmental impact of biodiesel exhaust. The FAMES exist in biodiesel exhaust PM at concentrations about 3 orders of magnitude higher than the PAHs (Magara-Gomez et al., 2012). Therefore, the high abundance of FAMES in biodiesel exhaust PM could hinder the atmospheric oxidation of PAHs, hence leading to long residence times of the PAHs, consequently leading to long range transport of the PAHs. Additionally, because biodiesel is an oxygenated fuel, it is hypothesized that its oxidation products with ozone will be more oxygenated than the parent FAMES. Also, ozonolysis of FAMES leads to formation of aldehydes (Zahardis et al., 2006). Oxygenated organic compounds like

aldehydes have been previously linked to adverse health effects in humans such as oxidative stress (Mauderly 1997). Furthermore, oxygenation of aerosol can affect its properties like hygroscopicity and ability to form cloud condensation nuclei (Sun and Ariya 2006).

This dissertation summarizes the results of the organic chemical characterization (with emphasis on PAHs, n-alkanes, FAMEs, carbonyls, and quinones) of the exhaust PM from different blends of waste vegetable oil (WVO) and soybean biodiesel feedstocks blended with ultra-low sulfur diesel (ULSD) in the same engine. Results of the organic chemical analysis of the fuels used to generate the exhaust PM are also presented in order to understand whether the organic compounds in the exhaust PM are due to unburned fuel (survival during combustion), lubricating oil or combustion of both the fuel and lubricating oil. Lastly, the effect of the FAMEs in biodiesel exhaust PM on the ozonation of PAHs was investigated.

### **1.3 Overall Research Objectives**

- i. To study the organic chemical composition of the particle-phase emissions from combustion of two biodiesel feedstocks (soybean and waste vegetable oil, WVO) and their blends with ULSD (containing 0% (B00), 10% (B10), 20% (B20), 50% (B50), and 100% (B100) biodiesel by volume) in a light-duty diesel engine.
- ii. To investigate the organic chemical composition of the fuels (ULSD, WVO, and soybean biodiesel) used to generate the particulate matter in the light-duty diesel engine.
- iii. To study the effect of the FAMEs in biodiesel exhaust PM on the ozone reactivity of PAHs produced during biodiesel fuel combustion in a light-duty diesel engine.

- iv. To identify and quantify the products formed during the ozone oxidation of FAMES derived from biodiesel combustion.

#### **1.4 Research Questions**

From the overall research objectives, the following research questions were developed in order to guide this research:

1. Does the organic chemical composition of exhaust PM vary with biodiesel feedstock (soybean versus WVO)? Specifically, do the emission rates (ng/ $\mu$ g) of the PAHs, n-alkanes, FAMES, carbonyls, and quinones vary with biodiesel feedstock?

Are the organic compound emission rates statistically different for blends of biodiesel (B00-B100)?

2. How is the organic chemical composition of the fuel different from that of the exhaust PM? Are the compounds emitted in the exhaust PM from unburned fuel, unburned lubricating oil, or are they emitted as a result of combustion of the fuel, lubricating oil, or combustion of both the fuel and lubricating oil?
3. Does the presence of FAMES in biodiesel exhaust PM affect the ozone oxidation rates of other pollutants in the biodiesel exhaust PM such as PAHs?

## 1.5 Literature Review

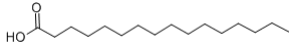
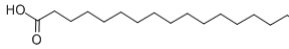
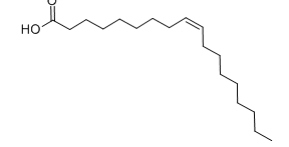
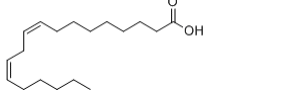
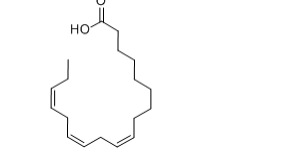
### 1.5.1 Chemical Composition of Biodiesel and Biodiesel Exhaust PM

Biodiesel exhaust PM contains compounds that make up the biodiesel fuel together with the combustion products of petrodiesel/biodiesel. Pure biodiesel (B100) is usually mixed with pure petrodiesel/conventional diesel (B00) to make biodiesel blends of different concentrations. Blends are by volume of fuels mixed, for example B5 contains 5% pure biodiesel and 95% conventional diesel, B20 contains 20% pure biodiesel and 80% conventional diesel, etc. Furthermore, biodiesel consists of mainly fatty acids methyl esters (FAMES) derived from the fatty acids of vegetable oils or animal fats. It is generally assumed that fatty acid compositional profiles remain unchanged during conversion of the feedstocks to fuels via transesterification (Hoekman et al., 2012). Table 1.1 shows the most common fatty acid groups in biodiesel, while Table 1.2 shows the fatty acid compositional profiles of soy and canola biodiesel feedstocks. These data were obtained from Hoekman et al. (2012), who did a thorough literature review on the composition, properties, and specifications of biodiesel fuel. Note that the sums of species in Tables 1.2 and 1.3 exceed 100% for each biodiesel feedstock. The authors explained that this was in part due to rounding issues, and also as a consequence of the way the mean concentration values were determined by the authors. The compositional profiles of biodiesel give a useful insight into the differences in the various biodiesel feedstocks, and they can hence give us an idea on the type of emissions expected from a certain feedstock. As can be seen in Table 1.2, both canola and soybean biodiesel feedstocks are dominated by C<sub>18</sub> compounds. Furthermore, much as both feedstocks are dominated by C<sub>18</sub> compounds, the relative amounts of these compounds (saturated [18:0],



mono-unsaturated [18:1], and di-unsaturated [18:2]) vary considerably in each feedstock. The four most abundant fatty acids in soybean biodiesel are linoleic acid > oleic acid > palmitic acid > linolenic acid, while those for canola biodiesel are oleic acid > linoleic acid > linolenic acid > palmitic acid. Table 1.3 shows the fatty acid compositional profiles of different animal fats-based biodiesel feedstocks. The animal fat feedstocks are dominated by C<sub>16</sub> and C<sub>18</sub> compounds, both saturated (16:0, 18:0) and unsaturated (16:1, 18:1, and 18:2). The relative amounts of the saturated and unsaturated acids for the animal fat biodiesel fuels also vary from one feedstock to another (Table 1.3).

**Table 1.1 Most common fatty acid groups in biodiesel fuel (Hoekmann et al. 2012).**

Compound Name	Formal Name	Abbreviation	Molecular Formula	Molecular Weight	Molecular Structure <sup>a</sup>
Palmitic acid	Hexadecanoic acid	16:0	C <sub>16</sub> H <sub>32</sub> O <sub>2</sub>	256	
Stearic acid	Octadecanoic acid	18:0	C <sub>18</sub> H <sub>36</sub> O <sub>2</sub>	284	
Oleic acid	Cis-9-Octadecadienoic acid	18:1	C <sub>18</sub> H <sub>34</sub> O <sub>2</sub>	282	
Linoleic acid	Cis-9,12-Octadecadienoic acid	18:2	C <sub>18</sub> H <sub>32</sub> O <sub>2</sub>	280	
Linolenic acid	Cis-9,12,15-Octadecatrienoic acid	18:3	C <sub>18</sub> H <sub>30</sub> O <sub>2</sub>	278	

a) chemicalbook.com (accessed Nov 23, 2014)

X:Y implies, number of carbon atoms, and number of double bonds in fatty acid

**Table 1.2 Fatty acid compositional profiles for soybean and canola oils (Hoekman et al., 2012 and references therein).**

<b>Fatty acid</b>		<b>Soybean</b>	<b>Canola</b>
Common Name	Abbrev.		
Capric	10:0		0.1
Lauric	12:0	0.1	
Myristic	14:0	0.1	
Palmitic	16:0	11.6	4.2
Palmitoleic	16:1	0.2	0.3
Heptadecanoic	17:0	0.1	0.1
Stearic	18:0	3.9	2.0
Oleic	18:1	23.7	60.4
Linoleic	18:2	53.8	21.2
Linolenic	18:3	5.9	9.6
Arachidic	20:0	0.3	0.7
Gondoic	20:1	0.3	1.5
Eicosadienic	20:2		0.1
Behenic	22:0	0.3	0.3
Erucic	22:1	0.1	0.5
Lignoceric	24:0	0.1	0.2
Nervonic	24:1	0.3	0.2
Other/unknown		4.1	2.2

**Table 1.3 Fatty acid compositional profiles for animal fats (Hoekman et al., 2012 and references therein).**

Fatty Acid		Animal Fats					
Common Name	Abbrev.	Butter	Hog Lard	Beef Tallow	Fish Oil*	Chicken and Turkey	Sheep
Caprylic	8:0	5.5					
Capric	10:0	3	0.1				
Lauric	12:0	3.6	0.1	0.1 - 0.1	0.4	0.1	
Tridecylic	13:0				0.2		
Myristic	14:0	7 - 11.6	1 - 2	2.1 - 8	10.3	0.8 - 1	3
Myristoleic	14:1			0.9	0.2	0.2	
Pentadanoic	15:0		0.1	0.5	1	0.1	
Pentadecenoic	15:1				0.1		
Palmitic	16:0	24 - 33.4	24 - 30	23.3 - 37	20.8	20 - 25.3	21
Palmitoleic	16:1		2 - 3.3	0.1 - 5	12.7	6 - 7.2	2
Hexadecadienoic	16:2				1.9		
Hexadecatrienoic	16:3				2.3		
Heptadecanoic	17:0		0.4	1 - 1.5	0.8	0.1	
Heptadecenoic	17:1		0.2	0.8	0.3	0.1	
Stearic	18:0	10 - 13	12 - 18	9.5 - 34.2	3.3	6 - 6.5	25
Oleic	18:1	28 - 31	40 - 50	14 - 50	9.8	37.7 - 40	34
Ricinoleic	18:1						5
Linoleic	18:2	1 - 3.1	7 - 13	1.5 - 50	1.6	17 - 24	3
Linolenic	18:3	0.2 - 0.5	0 - 1	0 - 0.7	1.9	0.8 - 2	
Stearidonic	18:4				2.5		
Arachidic	20:0		0.2 - 0.5	0.2 - 1.2	0.2	0.2	
Gondoic	20:1		0.7	0.3 - 0.51	1.3	0.3	
Auricolic	20:2		0.1		0.4		
Eicosatrienoic	20:3				0.4		
Arachidonic	20:4				2.3		
Eicosapentaenoic	20:5				12.5		
Behenic	22:0		0.2	0.1	0.2		
Erucic	22:1		0.1	0.1	0.3		
Adrenic	22:4				0.3		
Clupanodonic	22:5				2.5		
Docosahexaenoic	22:6				7.1		
Lignoceric	24:0				0.1		
Nervonic	24:1				0.3		

\* Fish Oil contains some odd fatty acids not listed

The exhaust PM of the biodiesel fuels mainly consists of the combustion products of the fuels together with the unburned compounds in the biodiesel like fatty acids and FAMES. The combustion products found in conventional diesel PM such as PAHs, hydrocarbons, and carbonyls have all been reported to be found in biodiesel exhaust PM by different researchers, although the relative amounts of PAHs and hydrocarbons have been reported to be less in biodiesel exhaust PM compared to those in conventional diesel PM (Graboski and McCormick 1998; Cardone et al., 2002; Pinto et al., 2005). Wu and Lin (2012) analyzed the trace species in biodiesel exhaust using gas chromatography/mass spectrometry (GC/MS). The authors used soybean biodiesel fuel in a four-cylinder, four-stroke-cycle 2200 c.c precombustion diesel engine (Yueloong Diesel SD22). The biodiesel fuel contained 21.8% saturated FAMES and 78.2% unsaturated FAMES, while the compositions of the fatty acids in the fuel were not reported. The major saturated FAME species in the fuel were methyl palmitate (hexadecanoic acid methyl ester,  $C_{17}H_{34}O_2$ , 11.85%) and methyl stearate (octadecanoic acid methyl ester,  $C_{19}H_{38}O_2$ , 6.61%), while methyl linoleate (methyl octadeca-9,12-dienoate,  $C_{19}H_{34}O_2$ , 74.78%) was the major unsaturated FAME species. The fatty acids and FAMES detected in high concentrations in the biodiesel exhaust were: hexanoic acid (0.0084 ppm), octanoic acid (0.0037 ppm), n-hexadecanoic acid (0.2477 ppm), oleic acid (1.0641 ppm), octadecanoic acid (0.1844 ppm), 1,2-benzenedicarboxylic acid (0.0174 ppm), methyl palmitate (0.5043 ppm), methyl octadeca-9,12-dienoate (1.6111 ppm), methyl oleate (3.1841 ppm), and methyl linolelaidate (1.3454 ppm). Although the authors did not report some of the species (fatty acids and FAMES) observed in the

biodiesel fuel, it can be seen that the major FAMES observed in the biodiesel fuel were also detected in the biodiesel exhaust.

Magara-Gomez et al. (2012) measured the concentrations ( $\mu\text{g}/\text{gal}$ ) of the main FAMES in B50 and B100 fuel blends of soybean and beef tallow biodiesel feedstocks that they used to measure the PM emissions from a John Deere (model 1993) tractor that was not equipped with aftertreatment control technologies. The emission rates ( $\mu\text{g}/\text{kg CO}_2$ ) of the FAMES in the biodiesel exhaust PM were also measured by GC/MS. Methyl linoleate (57.5-60.3%), methyl oleate (18.5-18.6%), methyl palmitate (10.5-12.6%), methyl stearate (4.5-5.0%), and methyl linolenate (6.0-6.1%) were the main FAMES detected in the B50 and B100 blends of soybean biodiesel fuel. The compositions of the FAMES were obtained by dividing the concentration of each individual FAME by the total concentration of all the FAMES detected in the fuel. Methyl oleate (32.5-35.9%), methyl palmitate (26.4-28.7%), methyl stearate (19.4-19.9%), methyl linoleate (13.2-13.5%), methyl myristate (1.7-2.4%), and methyl linolenate (1.2-1.3%), were the main FAMES detected in the B50 and B100 beef tallow biodiesel fuel blends. Note that beef tallow biodiesel (animal fat-based biodiesel) had a higher percentage of saturated FAMES than soybean biodiesel (plant-based biodiesel). Figure 1.1 shows the concentrations of the FAMES detected in the soybean and beef tallow biodiesel fuel blends used by Magara-Gomez et al. (2012).

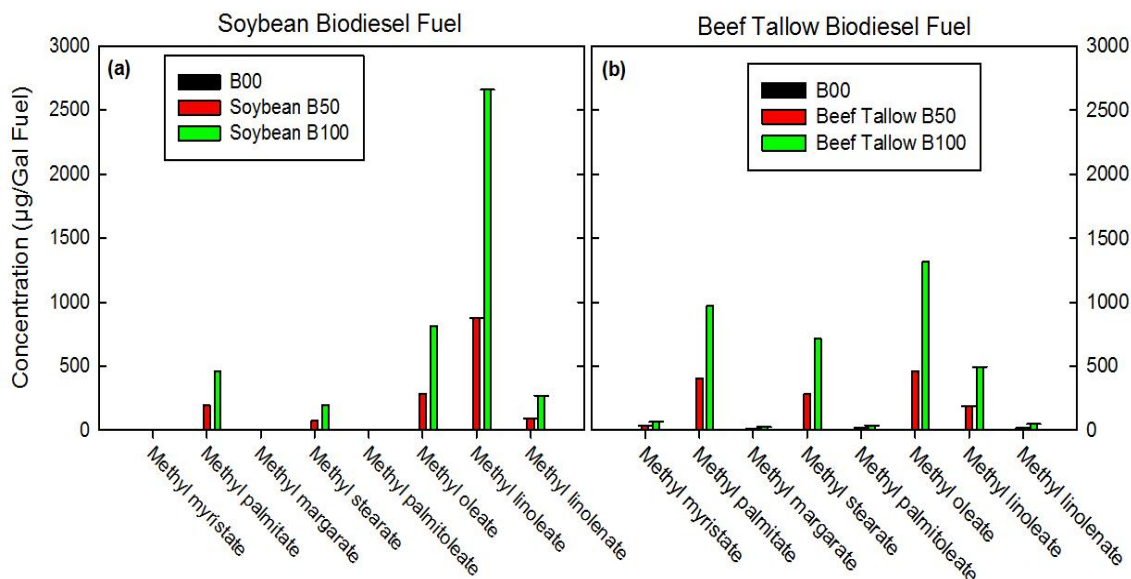


**Figure 1.1 FAME concentrations ( $\mu\text{g}/\text{gal Fuel}$ ) of the soybean and beef tallow biodiesel fuel blends used by Magara-Gomez et al. (2012). Error bars represent one standard deviation.**

The main FAMES in the soybean biodiesel fuel were detected in the exhaust PM for both B50 and B100 fuels i.e. methyl linoleate (53.1-54.5%), methyl oleate (20.7-21.3%), methyl palmitate (12.6-13.7%), methyl stearate (6.1-7.4%), and methyl linolenate (5.2-5.6%). The main FAMES detected in the soybean biodiesel exhaust PM were also detected in the B50 and B100 beef tallow biodiesel exhaust PM but at compositions different than those for the soybean biodiesel exhaust PM. The FAMES were detected in beef tallow biodiesel exhaust PM at the following compositions, methyl linoleate (6.5-13.2%), methyl oleate (27.5-36.9%), methyl palmitate (24.7-40.9%), methyl stearate (23.9-24.3%), and methyl linolenate (0.7-1.3%). Figure 1.2 shows the emission rates of the FAMES in the exhaust PM of the soybean and beef tallow biodiesel fuel blends in the Magara-Gomez et al. (2012) study. The patterns of the FAME compositions in the biodiesel exhaust PM for both feedstocks slightly differed from those

of the corresponding biodiesel fuels. The reason for this observation was possibly because of combustion in the engine, whereby some FAMES in the biodiesel fuel were burned more than others in the engine, hence leading to changes in the FAMES composition in the biodiesel exhaust PM.

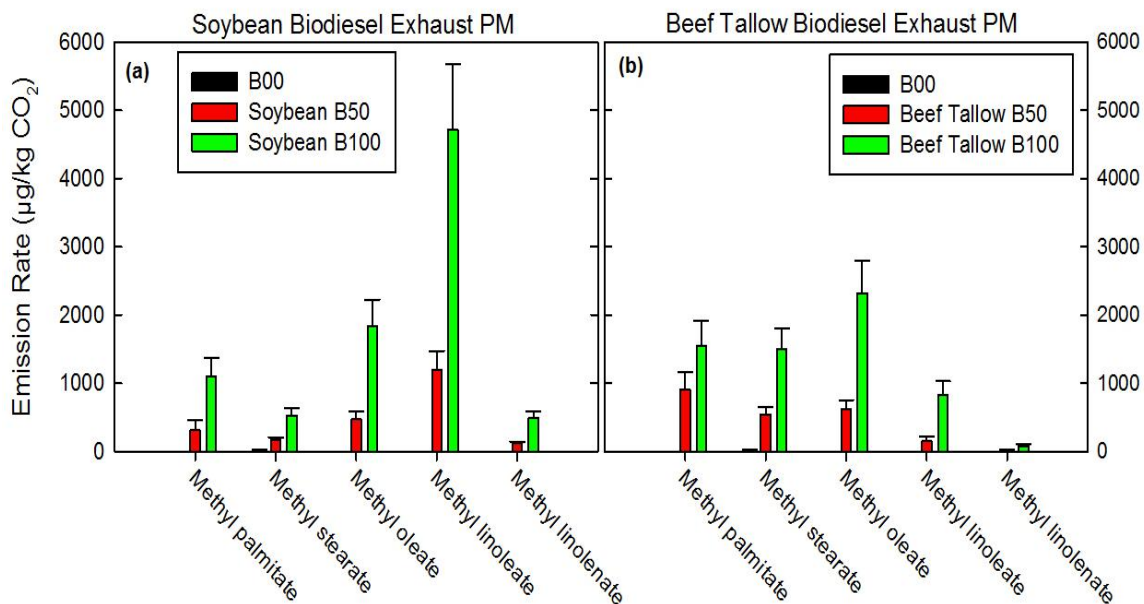


**Figure 1.2 FAME emission rates ( $\mu\text{g}/\text{kg CO}_2$ ) in the biodiesel exhaust PM of the soybean and beef tallow biodiesel fuel blends used by Magara-Gomez et al. (2012). Error bars represent one standard deviation.**

### 1.5.2 Chemical Composition of Diesel and Diesel Exhaust PM

Diesel fuel has been previously reported to consist of saturates (65-85%), aromatics (5-30%), and olefins (0-5%) (WHO 1996). Studies such as Schauer et al. (1999), and Liang et al. (2005) performed detailed organic chemical speciation of low sulfur diesel (LSD). Both these studies found that the LSD used in their respective studies was dominated by saturated alkanes (straight-chain, branched, and cyclic) with 10 to 25 carbon atoms, although the composition of the different classes of alkanes were different in the two studies (Table 1.4). Schauer et al. (1999) found that the diesel fuel



used in their study was composed of about 64% n-alkanes, while Liang et al. (2005) reported that the diesel fuel used in their study was composed of about 28% n-alkanes. In general, both of the fuels used in the two studies were comprised of about 80% saturated alkanes and less than 10% saturated cycloalkanes. Schauer et al. (1999) found the diesel fuel to consist of about 5% PAHs (substituted and unsubstituted), while the composition of PAHs in the diesel fuel used by Liang et al. (2005) was about 4%.

**Table 1.4 Organic chemical fuel composition of the diesel fuel used in two previous studies.**

<b>Compound Class</b>	<b>Liang et al. (2005)</b>		<b>Schauer et al. (1999)</b>	
	<b>Conc (µg/g)</b>	<b>%Comp</b>	<b>Conc (µg/g)</b>	<b>%Comp</b>
n-Alkanes	190763	27.90	108908	63.60
Branched Alkanes	368404	53.87	48860	28.53
Saturated Cycloalkanes	52798	7.72	4080	2.38
Unsubstituted PAHs	1793	0.26	3268	1.91
Substituted PAHs	25302	3.70	6085	3.55
Others	44796	6.55	31.7	0.02
<b>Total</b>	<b>683856</b>	<b>100</b>	<b>171233</b>	<b>100</b>

Diesel exhaust PM consists of unburned fuel constituents and products from the combustion of the fuel. The main constituents of particles originating from diesel combustion are elemental carbon in the form of soot and organic compounds, which include pyrogenic compounds and partially oxidized fuel and lubricating oil components, unburned lubricating oil, and unburned fuel (Rogge et al., 1993; Fraser et al., 2003; Brandenberger et al., 2005; Erickson et al., 2012). Further, because diesel fuel consists largely of aliphatic hydrocarbons containing 10-25 carbon atoms, it is expected that these components and their thermally altered breakdown products also will be present in diesel

exhaust (Schauer et al., 1999). Many recent studies have focused on understanding the organic chemical characteristics of particulate emissions from diesel engines (e.g., Rogge et al., 1993; Schauer et al., 1999; Liang et al., 2005, etc.) because of the health effects and environmental impacts linked to diesel exhaust. From the detailed organic chemical speciation studies of PM from medium-duty and heavy-duty diesel engines by Rogge et al. (1993) and Schauer et al. (1999), diesel PM was found to consist of n-alkanes (C<sub>15</sub> to C<sub>29</sub>), branched alkanes, saturated cycloalkanes, aromatic hydrocarbons including substituted and unsubstituted PAHs, carbonyls, n-alkanoic acids, and other compounds that existed in very small concentrations. Some of the compounds detected in the diesel exhaust PM such as alkanes and PAHs are emitted both as unburned fuel and lubricating oil, and fuel combustion products, while n-alkanoic acids, terpanes, hopanes, steranes, alkanedioic acids, and aromatic acids have been attributed to combustion of the fuel and lubricating oil (e.g., Rogge et al., 1993, Schauer et al., 1999; Liang et al., 2005). Studies by Jakober et al. (2006, 2007, and 2008) quantified particle-phase carbonyls including quinones in diesel exhaust PM and such compounds have been attributed to diesel fuel combustion.

### **1.5.3 Effects of Biodiesel on the Organic Compounds in PM from Diesel Engines**

The effects of biodiesel fuel on the organic compounds such as hydrocarbons including n-alkanes, PAHs, carbonyls, and FAMES in exhaust PM from diesel engines have been characterized by several studies (e.g., Correa and Arbilla 2006; Payri et al., 2009, Karavalakis et al., 2009; Bakaes et al., 2011; Karavalakis et al., 2011; Magara-Gomez et al., 2012).

Magara-Gomez et al. (2012) measured the emission rates ( $\mu\text{g}/\text{kg CO}_2$ ) of the n-alkanes, PAHs, and FAMEs in the exhaust PM from a John Deere tractor fueled with ULSD fuel, soybean (B50 and B100), and beef tallow (B50 and B100) biodiesel fuels. The emission rates of the total n-alkanes decreased by 35%, 82%, 69%, and 87% for soybean B50, soybean B100, beef tallow B50, and beef tallow B100 biodiesel fuel blends, respectively, compared to ULSD. The emission rates of the total PAHs decreased by 74%, 80%, 77%, and 84% for soybean B50, soybean B100, beef tallow B50, and beef tallow B100 biodiesel fuels, respectively, compared to ULSD. On the other hand, the emission rates of the total FAMEs in the exhaust PM increased with increasing biodiesel in the fuel (Figure 1.2). The emission rates of the total FAMEs in the soybean B100 exhaust PM were about 4 times greater than those in the soybean B50 exhaust PM, while the emission rates of the total FAMEs in beef tallow B100 exhaust PM were about 3 times greater than those in the beef tallow B50 exhaust PM (Figure 1.2).

Karavalakis et al. (2009) measured the emission rates of PAHs from a diesel passenger vehicle equipped with an indirect injection diesel engine (1998 model year Toyota Corolla 2.0 TD with 4 cylinders, 86×85 mm, bore×stroke, 23:1 compression ratio, 61 kW maximum power at 4000 rpm, 174 Nm maximum torque at 2000 rpm, and 1300 kg weight) fueled with LSD and soy methyl ester biodiesel blends of B5, B10, and B20 using a real-world drive cycle in Athens (Athens Drive Cycle, ADC) developed by the authors. The emissions from the diesel passenger car under the ADC drive cycle were then compared with the emissions from a chassis dynamometer operated with modified New European Drive Cycle (NEDC), and Athens Drive Cycle (ADC). The emission rates of the total PAHs in the exhaust PM of the diesel passenger vehicle under the ADC

drive cycle decreased by about 20%, 41%, and 14% for B5, B10, and B20, respectively, compared to LSD. The emission rates of the total PAHs in the exhaust PM from the chassis dynamometer under the NEDC decreased by about 17%, 38%, and 11%, for B5, B10, and B20, respectively, compared to LSD.

The effects of biodiesel on the emissions of gas-phase carbonyls from diesel engines have been studied by a number of researchers (e.g., Correa and Arbilla 2008; Guarieiro et al., 2008; Karavalakis et al., 2009; Karavalakis et al., 2011). Most of the previous studies found that the emissions of gas-phase carbonyls increased with increasing biodiesel content in the fuel. Cahill and Okamoto (2012) measured the emission rates of both gas- and particle-phase carbonyls from two heavy-duty diesel trucks (2000 and 2008 model vehicles) fueled with ULSD and B50 and B100 blends of soy biodiesel, animal biodiesel, and renewable diesel fuels. Only ULSD and the B50 and B100 blends of soy biodiesel fuels were tested for the 2008 model vehicle. The tests were performed on a chassis dynamometer using simulated city (Urban Dynamometer Driving Schedule, UDDS) and high speed cruise (Heavy, Heavy-Duty Diesel Truck 50 mph cruise cycle) drive cycles. The authors found that the emission rates of the aromatic aldehydes that mostly partition in the particle phase generally decreased between 16% and 67% for both vehicles and drive cycles when biodiesel and renewable diesel fuels were used instead of ULSD although some fuels showed slightly higher emissions rates than ULSD.

#### **1.5.4 Reaction of Ozone with Biodiesel Exhaust PM**

There is currently no literature data showing the reactions between atmospheric oxidants such as ozone and the compounds adsorbed on to biodiesel PM, and it is not known whether such reactions increase or decrease the toxicity of biodiesel exhaust PM. Further, the effects of biodiesel exhaust PM on the ozone reactivity of the compounds in exhaust PM such as PAHs is not well understood. It is therefore important to have studies with the biodiesel exhaust PM exposed to ozone in order to understand the effects of the environmental oxidants like ozone on the atmospheric fate of biodiesel PM and other toxic compounds in the exhaust PM. Such studies can also help us understand the transformational products of biodiesel exhaust PM and the effects of biodiesel on human health and the environment at large. Several researchers have investigated the reactions between ozone and the pollutants adsorbed on diesel exhaust PM, particularly PAHs. Such studies were mainly focused on studying the reaction rates between ozone and the PAHs, and identification and quantitation of the products formed after the reactions between ozone and the PAHs. Furthermore, the heterogeneous reaction kinetics of the PAHs with ozone have been found to take place via the Langmuir-Hinshelwood mechanism by previous studies (Poschl et al., 2001; Kwamena et al., 2004; Kwamena et al., 2007; Zhou et al., 2012). The Langmuir-Hinshelwood reaction mechanism is a two-step mechanism which involves rapid adsorption of ozone on the substrate surface, followed by a slower surface reaction between the adsorbed ozone and the PAHs (Poschl et al., 2001).

Perraudin et al. (2007) studied the kinetics of the reactions of ozone with 13 PAHs adsorbed on atmospheric model particles (graphite and silica to model

carbonaceous and mineral atmospheric particles, respectively). Pseudo-first order and second order reaction rate constants were measured for the reactions of ozone with the PAHs at room temperature over a 15 minute time period. The authors determined the rate constants for the different PAHs and also further stated that the heterogeneous reactions of ozone with particulate PAHs are more rapid than those occurring in the gas-phase, and may be competitive with atmospheric photo degradation (Perraudin et al. 2007). The substrate was found to affect the pseudo-first order ozone reaction rate constants of the PAHs. The ozone reaction rate constants of the PAHs varied between  $(1.5\pm 0.5)\times 10^{-17}$  cm<sup>3</sup> molecule<sup>-1</sup> second<sup>-1</sup> for chrysene and  $(1.3\pm 0.7)\times 10^{-16}$  cm<sup>3</sup> molecule<sup>-1</sup> second<sup>-1</sup> for dibenzo[a,l]pyrene when the PAHs were adsorbed on silica particles, while the rates varied between  $(1.5\pm 0.3)\times 10^{-17}$  cm<sup>3</sup> molecule<sup>-1</sup> second<sup>-1</sup> for fluoranthene and  $(1.4\pm 0.3)\times 10^{-16}$  cm<sup>3</sup> molecule<sup>-1</sup> second<sup>-1</sup> for benzo[a]pyrene when the PAHs were adsorbed on graphite particles.

Kahan et al. (2006) investigated the effects of different types of organic mixtures/substrates representing urban grime (in octanol or decanol) on the heterogeneous reaction rates of ozone with PAHs (naphthalene, anthracene, fluoranthene, phenanthrene, pyrene, and benzo[a]pyrene) at room temperature. The heterogeneous reaction kinetics of all PAHs were found to be well-described by the Langmuir-Hinshelwood mechanism, suggesting surface reactions for the PAHs. The reaction rates of anthracene in octanol and decanol were similar, and the presence of vacuum grease, stearic acid, or cornstarch did not affect the heterogeneous reaction rates of anthracene with ozone. The presence of unsaturated compounds (oleic acid and squalene) at concentrations 3 orders of magnitude higher than anthracene decreased the heterogeneous

reaction rate of anthracene by about 70% and 90%, for oleic acid and squalene, respectively. The heterogeneous reaction rate of benzo[a]pyrene in the presence of oleic acid and squalene was found to decrease by the same magnitude as that of anthracene. Therefore, the presence of the unsaturated site(s) in oleic acid and squalene were responsible for the decrease in the heterogeneous ozone reaction rates of anthracene and benzo[a]pyrene (Kahan et al. 2006).

Other studies (e.g., Poschl et al., 2001; Kwamena et al., 2004; Donaldson et al., 2005; Kwamena et al., 2007; Rudich et al., 2007, Zhou et al., 2012) have all reported matrix effects on the heterogeneous reaction rates of the PAHs with ozone.

In his thesis, Stevens (2010) investigated the heterogeneous reactions between ozone and 16 EPA priority PAHs and coronene adsorbed on a quartz fiber filter (QFF) and NIST diesel PM. This study involved the exposure of the PAHs to ozone (0.4 ppm) for a 24 hour period, and the difference in the PAHs/O<sub>3</sub> heterogeneous reaction rates resulting from the two substrates were determined. The individual PAHs (anthracene, phenanthrene, and fluorene) adsorbed on a QFF were also separately reacted with ozone (0.4 ppm). For the reactions between ozone and PAHs adsorbed on a QFF, 9,10-anthracenedione, 9H-fluoren-9-one, and (1,1'-biphenyl)-2,2'-dicarboxaldehyde were detected, while for the reactions between ozone and the PAHs adsorbed on diesel PM, only 9,10-anthracenedione was detected.

Tsapakis and Stephanou (2003) also studied the decomposition of PAHs by ozone in the gas and particle phases under high volume sampling by using, in parallel, a conventional device and a device protected with an oxidant denuder. The authors used three different sampling regimes; short and long sampling under high ozone

concentration and long sampling under low ozone concentration at three representative sampling sites. It was found that most of the gas- and particle-phase PAHs in the study were susceptible to ozone degradation under high atmospheric ozone concentrations (>50 ppbv) and long sampling times (>24 hrs).

All the above studies indicated that ozone is an important atmospheric oxidant that is capable of reacting with the pollutants in biodiesel exhaust PM, and that the type of substrate affects the heterogeneous reaction rates of the PAHs with ozone.



## **Chapter 2**

### **METHODS**

This chapter is divided into three sections, and each section presents the methods that were employed to answer the questions presented in Chapter 1. Section 2.1 presents the methods used to analyze the organic chemical composition of the biodiesel exhaust PM, Section 2.2 presents the methods used to analyze organic chemical composition of the fuels (petrodiesel, WVO and soybean biodiesel blends), while Section 2.3 presents the methods used to study the kinetics of the heterogeneous reactions between ozone and PAHs, FAMES, and biodiesel exhaust PM.

#### **2.1 Methods for Organic Chemical Analysis of Diesel and Biodiesel Exhaust PM**

##### **2.1.1 Fuels used in Emission Tests**

Ultra-low sulfur diesel (ULSD) fuel was purchased from Trono Fuels (Trono Oil and Gas Inc., Burlington, VT). Soybean vegetable oil was purchased from Catania Spagna Corp (Ayer, MA), while waste vegetable oil (WVO) was sourced from the University of Connecticut (Storrs, CT) dining hall. Verbal communications with the University of Connecticut's dining hall staff indicated that the cooking oil used in the dining hall was mainly canola oil. The 100% soybean and WVO biodiesel fuels were then processed at the University of Connecticut's Biofuels Laboratory. The processed soybean and WVO biodiesel fuels were transported and stored at 13 °C under a N<sub>2</sub> gas headspace to minimize oxidation during storage at the University of Vermont's Transportation Air Quality Laboratory where all the engine test runs were performed.

Blends of B10, B20, and B50 biodiesel fuel were prepared by mechanically blending 10%, 20%, and 50% biodiesel with 90%, 80%, and 50% ULSD by volume, respectively. The pure fuels (ULSD and neat biodiesel) and the biodiesel blends were subsequently stored at 13 °C under a N<sub>2</sub> gas headspace until engine testing. The properties of the soybean and WVO biodiesel fuels and the ASTM D6751 biodiesel standards are shown in Table 2.1 with the ULSD properties and the ASTM D975 diesel fuel standards. All the fuels used in this study met the ASTM fuel specifications. However, it is important to note that two different batches of petrodiesel were used. The first batch was used to prepare the WVO biodiesel blends, while the second batch, purchased from the same supplier, Trono Fuels (Burlington, VT) was used to prepare the soybean biodiesel blends. The fuel densities were determined using an IROX Diesel Analyzer (Grabner Instruments, Austria), while the rest of the fuel properties were tested at the University of Connecticut's Biofuels Laboratory.

**Table 2.1 Measured properties of the soybean and waste vegetable oil biodiesel fuels, and Trono ULSD fuel. Fuel testing was performed at the University of Connecticut’s Biofuels Laboratory, Storrs, CT.**

Property	Units	Soybean	WVO	Trono Fuel (ULSD) Batch1/Batch2	ASTM D6751		ASTM D975 <sup>a</sup>	
					Biodiesel		Petrodiesel	
					Min	Max	Min	Max
Density	kg/m <sup>3</sup>	0.876	0.876	0.809/0.812				
Flash point	°C	167.4	176.5	45.6/ND	130		52	
Kinematic	mm <sup>2</sup> /s	4.166	4.354		1.9	6.0	1.9	4.1
Cloud point	°C	1.13	-0.15		Report			
Sulfur	ppm	<1	2.5	1.2/ND		15		10
Carbon	wt,%	0.033	0.05	0.003/ND		0.05		0.35
Cetane		49.9		46.7/ND	47			40
Oxidative	h	6.28	11.49		3			
Ash content	wt,%	<0.005	-			0.02		0.01
Water	mg/kg	0.01	0.00	0.000/ND		500		500
Acid value	mg KOH/g	0.134	0.196			0.5		
Copper corrosion	Degree of corrosion			1A/ND				No.3A
Phosphorus	wt,%	<0.001	<0.001			0.001		
Free	wt,%	0.007	0.003			0.02		
Total	wt,%	0.050	0.049			0.24		

<sup>a</sup> Value for no.2 diesel fuel; The two density values correspond to the densities obtained for the two Trono diesel fuel batches. Batch1 was used to prepare biodiesel blends for the WVO sequence, while Batch2 was used to prepare biodiesel blends for the soybean sequence. ND means that “No Data” is available for that test.

### **2.1.2 Emissions Test Procedure and Sampling**

A CM-12 Automotive Diesel Engine test bed (Armfield Ltd, United Kingdom) with a light-duty diesel engine was used to generate PM (see engine specifications in Table 2.2). The CM-12 has a Volkswagen 1.9L SDi naturally aspirated industrial diesel engine without exhaust gas recirculation or aftertreatment devices and a Zelu SL/KLAM Eddy Current Dynamometer. Engine emission test runs were performed using a combination of a transient cycle (12% load) followed by three steady-state phases operating at different engine loads (5, 36 and 50% load) when the engine was fueled with ULSD. The transient drive cycle, developed using data collected by driving a Volkswagen TDI Jetta in downtown Burlington, VT, was thought to more realistically mimic real-world driving of light-duty diesel vehicles in urban areas than the federally mandated Chassis dynamometer and engine dynamometer tests for light-duty and heavy-duty vehicles, respectively. Figure 2.1 shows the drive cycle used in this study.

**Table 2.2 CM-12 Engine, dynamometer, and lube oil specifications.**

Engine	
Bore of cylinder	79.5 mm
Number of cylinders	4
Stroke volume	474 cm <sup>3</sup>
Rated speed	95.5 mm
Rated power	60 kW
Maximum torque	130 Nm at 2000 - 2400 RPM
Compression ratio	19.5:1
Power Absorption Unit/ Eddy Current Dynamometer	
Manufacturer	Zelu/ Klam
Model Number	K-40 PAU
Max Power	60kW
Max Torque	145Nm
Lube Oil	
Manufacturer	Castrol
Model Number	SAE 5W-40
Part Number	06249
Type	Synthetic

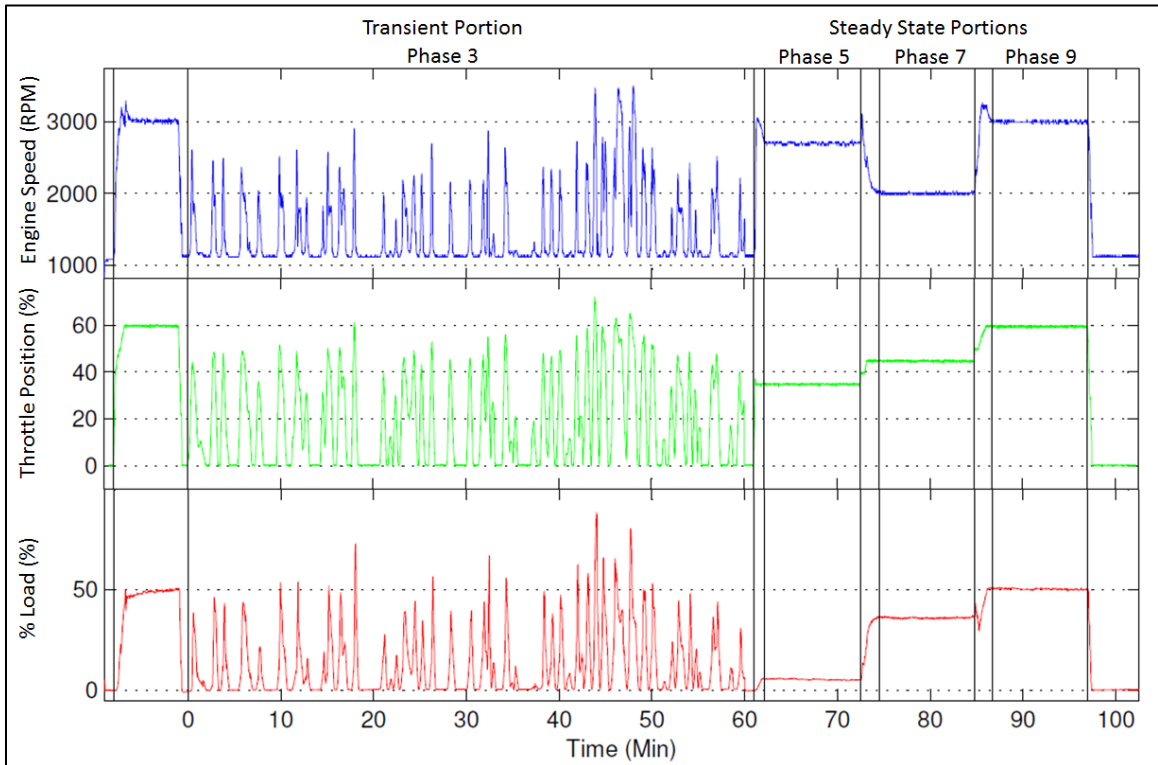


**Figure 2.1 Drive cycle used during engine testing (Feralio and Holmén 2015).**

Engine exhaust was diluted with clean dry, hydrocarbon-free air in a mini-dilution tunnel with a dilution factor of approximately 80 in order to mimic real-world dilution of vehicle exhaust (Holmén et al. 2014). Exhaust particles were sampled on Teflon-coated Fiberfilm filters (FF, T60A20, diameter 47 mm, Pallflex Corp., Putman, CT). One FF sampled the total (gas+particle) emissions for the diluted exhaust, while the second FF sampled the total emissions of the raw (undiluted) exhaust. Exhaust air flowed through each filter at approximately 16 L/min. All filters were pre-weighed (after conditioning for 24 hours in a Coy chamber maintained at 20-25 °C and 30-40% relative humidity) and post-weighed in order to determine the gravimetric mass of the sampled exhaust PM. A Cahn microbalance (Cahn C-33, Thermo Scientific, Waltham, MA) with 1 µg sensitivity was used for weighing the filters. All PM filter samples were stored at -80 °F until they were extracted in order to minimize reactions and volatile losses. In this study, the FF filters that sampled undiluted raw exhaust emissions (gas+PM) were extracted for the organic chemical analysis. The filter temperature during sampling was not directly measured for each test, but ranged from 21 to 45 °C for the runs it was measured. This, therefore, means that the gas-to-particle behavior of the raw exhaust PM sampled in this study was similar to that experienced when raw exhaust is diluted with ambient air.

Engine runs were performed in triplicate for each biodiesel blend. The engine runs for the WVO sequence (0% (B00), 10% (B10), 20% (B20), 50% (B50), and 100% (B100) biodiesel by volume) were performed from June 2013 to September 2013, while one soybean B00 run was performed in December 2013, and the rest of the soybean (B00, B10, B20, B50, and B100) engine runs were performed from April 2014 to May 2014 (see Table A-3 in Appendix A). Four engine blank runs were performed between

June 2013 and May 2014 by operating all sampling instruments the same way as during the emission test runs but with the engine off.

### **2.1.3 Chemicals**

Dichloromethane (DCM, OmniSolv. HR-GC Grade), acetone (OmniSolv. HR-GC Grade), hexanes (OmniSolv. HR-GC Grade), methanol (MeOH, B&J Brand for Purge and Trap GC Analysis), and acetonitrile (ACN, Carbonyl-free B&J Brand) were all purchased from VWR International (West Chester, PA). Pentafluorobenzylhydroxylamine (PFBHA), authentic standards of 26 carbonyls and quinones, 13 even numbered n-alkanes (C<sub>12</sub>-C<sub>36</sub>), and 10 FAMES were all purchased from Sigma-Aldrich (Allentown, PA). A standard of the 16 EPA PAHs was purchased from Ultra Scientific (North Kingstown, RI). Table 2.3 shows the list of PAHs, n-alkanes, and FAMES used in this study, while Table 2.4 shows the structures and properties of the FAMES. Table A-1 in Appendix A shows the full list and concentration in the standards of target analytes (n-alkanes, PAHs, FAMES, and POCs).

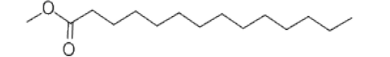
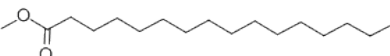
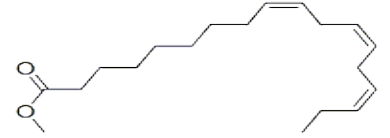
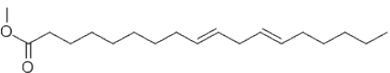
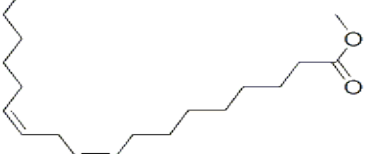
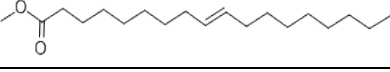
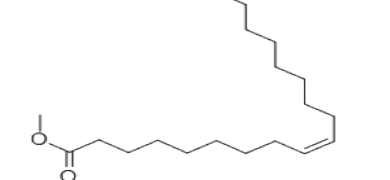
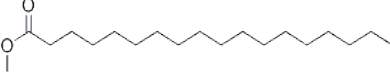
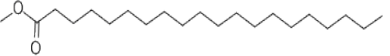
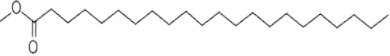
**Table 2.3 PAHs in the 16 PAHs mix, n-alkanes in the n-alkanes standard, and FAMES in the 10 FAMES mix.**

PAHs	Abbrev	FAMES	Abbrev	% in Mix
Naphthalene	Nap	Methyl myristate	C14:0	4
Acenaphthylene	Acy	Methyl palmitate	C16:0	10
Acenaphthene	Ace	Methyl stearate	C18:0	6
Fluorene	Flu	Methyl arachidate	C20:0	2
Phenanthrene	Phen	Methyl behenate	C22:0	2
Anthracene	Anth	Methyl oleate	C18:1n9c	25
Fluoranthene	Fluor	Methyl elaidate	C18:1n9t	10
Pyrene	Pyr	Methyl linoleate	C18:2n6c	34
Benzo[a]anthracene	BaA	Methyl linoleidate	C18:2n6t	2
Chrysene	Chr	Methyl linolenate	C18:3n3c	5
Benzo[b]fluoranthene	BbF			
Benzo[k]fluoranthene	BkF			
Benzo[a]pyrene	BaP			
Indeno[1,2,3-cd]pyrene	IDP			
Benzo[ghi]perylene	BghiP			
Dibenz[a,h]anthracene	DBahA			
<b>n-Alkanes</b>				
Dodecane	DCNE			
Tetradecane	TCNE			
Hexadecane	HCNE			
Octadecane	OCNE			
Eicosane	ECNE			
Docosane	DSNE			
Tetracosane	TSNE			
Hexacosane	HSNE			
Octacosane	OSNE			
Triacotane	TTNE			
Dotriacotane	DTTN			
Tetratriacontane	TTTN			
Hexatriacontane	HTTN			

The PAHs standard was in DCM solvent, and the concentrations of PAHs in the mix were equal (100 µg/mL). The FAMES in the FAMES mix were also in DCM solvent. The n-alkanes were in equal concentrations (50 mg/L) in n-heptane solvent.



**Table 2.4 Structures of the FAMEs used in the study.**

Name	Abbrev	Structure <sup>a</sup>	Chemical Formula	Molecular Weight	Melting Point (°C)	Boiling Point (°C)
Methyl myristate	(C14:0)		C <sub>15</sub> H <sub>30</sub> O <sub>2</sub>	242	18-19 <sup>b</sup>	295 <sup>b</sup>
Methyl palmitate	(C16:0)		C <sub>17</sub> H <sub>34</sub> O <sub>2</sub>	270	30-31 <sup>b</sup>	196 <sup>b</sup>
Methyl linolenate	(C18:3n3c)		C <sub>19</sub> H <sub>32</sub> O <sub>2</sub>	292	-57 <sup>c</sup>	207 /14 mmHg <sup>c</sup>
Methyl linolelaidate	(C18:2n6t)		C <sub>19</sub> H <sub>34</sub> O <sub>2</sub>	294	-35 <sup>d</sup>	207-208/ 11 mmHg <sup>d</sup>
Methyl linoleate	(C18:2n6c)		C <sub>19</sub> H <sub>34</sub> O <sub>2</sub>	294	-35 <sup>a</sup>	346 <sup>c</sup>
Methyl elaidate	(C18:1n9t)		C <sub>19</sub> H <sub>36</sub> O <sub>2</sub>	296	9-10 <sup>a</sup>	220 /24 mmHg <sup>a</sup>
Methyl oleate	(C18:1n9c)		C <sub>19</sub> H <sub>36</sub> O <sub>2</sub>	296	-20 <sup>a</sup>	190-191 <sup>b</sup>
Methyl stearate	(C18:0)		C <sub>19</sub> H <sub>38</sub> O <sub>2</sub>	298	38-39 <sup>b</sup>	215 <sup>b</sup>
Methyl arachidate	(C20:0)		C <sub>21</sub> H <sub>42</sub> O <sub>2</sub>	326	45-48 <sup>a</sup>	369 <sup>c</sup>
Methyl behenate	(C22:0)		C <sub>23</sub> H <sub>46</sub> O <sub>2</sub>	354	54-56 <sup>a</sup>	393 <sup>c</sup>

a) chemicalbook.com (accessed Nov 06, 2014)

b) Perry H. Robert, Chilton H. Cecil (1974). Chemical Engineers HandBook 5th ed. McGraw-Hill Inc. 07-049478-9

c) Tokyo Chemical Industry. <http://www.tcichemicals.com/en/gb/index.html> (accessed Mar 15, 2013)

d) Alfa Aesar. <http://www.alfa.com/> (accessed Nov 06, 2014)

#### 2.1.4 Extraction and Analysis of Target Organic Chemical Compounds

All the triplicate filters for the WVO sequence (B00 through B100) were extracted and analyzed for n-alkanes, PAHs, FAMES, carbonyls, and quinones, while only duplicate B00, B20, and B100 filters for the soybean sequence were similarly extracted and analyzed.

Before extraction, all filters were weighed to ensure that mass change during storage was  $\pm 5\%$  of the mass recorded prior to storage. For extraction, a  $\frac{1}{4}$ -inch punch was cut from each filter using a punch bore and placed in a 180  $\mu\text{L}$  glass thermal desorption vial (glass TD-vial) to which 70  $\mu\text{L}$  of DCM/Hexanes (1:1, v/v) solvent mixture was added to extract the nonpolar compounds by sonicating for 5 minutes. The punch was extracted two more times, and all three extracts were combined in a separate 180  $\mu\text{L}$  glass TD-vial. Polar analytes were then extracted three times with 70  $\mu\text{L}$  aliquots of MeOH and sonicating for 5 minutes each time. The three MeOH extracts were combined in a separate 180  $\mu\text{L}$  glass TD-vial. Both the polar and nonpolar extracts were then gently blown down with  $\text{N}_2$  gas to about 60  $\mu\text{L}$  each. The two extracts were then combined in a new 180  $\mu\text{L}$  glass TD-vial, and the combined extract was blown down to 100  $\mu\text{L}$ . An aliquot (2  $\mu\text{L}$  for Blanks, B00, B10, and B20 filter extracts; 1  $\mu\text{L}$  for B50 filter extracts; for the B100 extracts, 5  $\mu\text{L}$  of the extract was diluted with 15  $\mu\text{L}$  of DCM:Hexanes:MeOH (1:1:2) and 2  $\mu\text{L}$  of the diluted extract was used for GC/MS analysis) was then taken from the 100  $\mu\text{L}$  final combined extract and injected in a gas chromatography/mass spectrometer (5890GC/5972MSD, Agilent Technologies, Wilmington, DE) equipped with a thermal desorption syringeless injector (Lavigne Laboratories, Storrs Mansfield, CT) for analysis of nonpolar compounds such as PAHs

and n-alkanes. Given that the laboratory did not have authentic standards for the odd-numbered n-alkanes, such compounds (odd-numbered n-alkanes) were identified and confirmed using the NIST Library (NIST 2008). For the analysis of polar compounds (carbonyls and quinones), an aliquot (2  $\mu\text{L}$  for Blanks, B00, B10, and B20 filter extract; 1  $\mu\text{L}$  for B50 filter extracts; 5  $\mu\text{L}$  of the extract was diluted with 15  $\mu\text{L}$  of DCM:Hexanes:MeOH (1:1:2) and 2  $\mu\text{L}$  of the diluted extract was derivatized) was then taken from the 100  $\mu\text{L}$  final extract and derivatized with excess (pentafluorobenzylhydroxylamine) PFBHA in a 180  $\mu\text{L}$  TD-vial. This was performed by adding 1  $\mu\text{L}$  of a 2.4 ppm solution of 6-fluoro-4-chromanone (6F4C) quantitation standard to the aliquot followed by 1.5  $\mu\text{L}$  of a 25 mg/mL PFBHA (in MeOH) solution (Jakober et al., 2008). Acetonitrile/dichloromethane (ACN/DCM) solvent mixture (9:1, v/v) was then added to the vial to target a final solution volume of 30  $\mu\text{L}$  and a PFBHA concentration of 5 mM. The sample was then derivatized at 35  $^{\circ}\text{C}$  for 24 hours. At the end of the 24 hour derivatization period, the excess PFBHA was quenched by adding 11  $\mu\text{L}$  of acetone, and the quenching reaction let to proceed for at least 1 hour at room temperature. The derivatized extract was blown down to dryness and then heated at 80  $^{\circ}\text{C}$  for 10 minutes so as to let the excess PFBHA-acetone oxime volatilize. The derivatized sample was then analyzed on the TD-GC/MS. Note that 1  $\mu\text{L}$  of a 2 ppm solution containing 6 deuterated PAH internal standards (2.65 ng of, 1,4-dichlorobenzene-D4, naphthalene-D8, acenaphthene-D10, phenanthrene-D10, chrysene-D12, and perylene-D12) in DCM was added to each sample's nonpolar extract just before TD-GC/MS analysis for quantitation of the nonpolar compounds. The internal standard eluting closest to a given target analyte was used to quantify that particular analyte.

6-Fluoro-4-chromanone, added to the polar fraction extract just before the derivatization reaction, was used as the internal standard to quantify all the derivatized POCs (Jakober et al., 2008).

The TD-GC/MS system operated in splitless mode using 99.999% helium carrier gas flowing at 1.6 mL/min, and a Rxi-XLB 30 m, 0.25 mm ID, and 0.25  $\mu\text{m}$  film thickness (Restek, Bellefonte, PA) column. The injector temperature was 295  $^{\circ}\text{C}$ , while the detector temperature was 290  $^{\circ}\text{C}$ . The oven program used for analysis of all extracts on the TD-GC/MS was as follows: 65  $^{\circ}\text{C}$  initial temperature held for 12 min, 10  $^{\circ}\text{C}/\text{min}$  ramp to 180  $^{\circ}\text{C}$  and held for 3 min, 2.5  $^{\circ}\text{C}/\text{min}$  ramp to 300  $^{\circ}\text{C}$  and held for 15 min. The MSD was operated with electron ionization (EI), and the EI mass spectra were acquired in scan mode ( $m/z$  50 - 650 amu).

The Rxi-XLB column could not resolve the unsaturated FAMEs, and this made the analysis/quantitation of FAMEs simultaneously with either the PAHs/n-alkanes or POCs on the TD-GC/MS impossible. Therefore, FAMEs were separately analyzed on a 6890GC/5973MSD system (Agilent Technologies, Wilmington, DE) equipped with a polar column, SLB-IL 100, 30 m length, 0.25 mm ID, and 0.20  $\mu\text{m}$  film thickness (Sigma Aldrich, Milwaukee, WI) and a 7683 Series liquid autosampler (Agilent). A 1  $\mu\text{L}$  aliquot was drawn from the 100  $\mu\text{L}$  final extract and diluted with 50  $\mu\text{L}$  of hexanes for the Blanks, B00, B10, and B20 filter extracts. The 1  $\mu\text{L}$  aliquot from the B50 extracts was diluted with 100  $\mu\text{L}$  of hexanes, while that from the B100 extracts was diluted with 200  $\mu\text{L}$  of hexanes. An appropriate amount of a 100 ppm standard of 6F4C internal standard was then added to each extract just before GC/MS analysis to target a 6F4C concentration of 2 ppm for quantitation of all FAMEs. The 6890/5973 GC/MS system also operated in

splitless mode using helium carrier gas flowing at 1 mL/min. The injector and detector temperatures were 240 °C and 280 °C, respectively. The oven program used for analysis of all extracts on the 6890/5973 GC/MS system was as follows: 50 °C initial temperature held for 13.5 min, 3 °C/min ramp to 200 °C and held for 30 min. The MSD was also operated in EI mode (m/z 50 - 500 amu).

## 2.1.5 Quality Control /Quality Assurance

### 2.1.5.1 Detection Limits

The method detection limits were estimated according to Method 556 (US EPA 1998) using Equation 2-1 below:

$$\text{Method Detection Limit (MDL)} = St_{(n-1, 1-\alpha=99)} \quad \text{Eq (2 - 1)}$$

where  $S$  = standard deviation of  $n$  runs for a sample whose concentration of the analyte is about 5 times the noise level,  $n$  = number of replicates, and  $t_{(n-1, 1-\alpha=99)}$  is the Student's t-value for the 99% confidence level with  $n-1$  degrees of freedom.

MDLs for the PAHs were determined by analyzing a 0.125 ppm PAH standard (number of runs,  $n = 7$ ) on the TD-GC/MS, while the detection limits for the n-alkanes were determined using a 0.7 ppm standard ( $n=7$ ), and the detection limits for the PFBHA-oximes for the POCs were estimated using 2 µL of a 2 ppm standard ( $n=8$ ). The MDLs for the FAMES were determined by analyzing a 5 ppm standard of the 10 FAMES mix seven times ( $n=7$ ) on the 6890/5973 GC/MS. The MDLs of the n-alkanes, PAHs, PFBHA-oximes for the POCs, and FAMES are shown in (Table A-2 in Appendix A).

In general, good detectability was achieved for most n-alkanes (C<sub>15</sub>-C<sub>26</sub>) and FAMES as all their detected concentrations were above the detection limits. For the PAHs, only phenanthrene, fluoranthene, and pyrene had their concentrations greater than the detection limits. The concentrations of the rest of the PAHs were either equal to or below their respective detection limits. n-Hexanal, n-nonanal, n-decanal, benzaldehyde, m-tolualdehyde, p-tolualdehyde, acetophenone, 9-fluorenone, perinaphthenone, benzophenone, 1,4-benzoquinone, 1,4-naphthoquinone, and anthraquinone were the only POCs that were detected at concentrations greater than the detection limits in the diesel and biodiesel exhaust PM samples.

Detection of majority of the analytes at concentrations greater than their respective detection limits implied that the ¼-inch punches could be used to represent the concentrations of the target analytes on the entire filter. Extraction of ¼-inch punches saved both time and extraction solvents. This is because smaller volumes of extraction solvents were used to extract the ¼-inch punches compared to extraction of the entire filters. This subsequently led to less time needed for sample concentration in form of N<sub>2</sub> gas blowdown compared to the time that would be needed if the extract from the entire filter was to be concentrated.

#### ***2.1.5.2 Engine and Laboratory Blanks***

Engine and laboratory blank filters were extracted and analyzed the same way the filters sampled during engine runs were extracted and analyzed. No n-alkanes, PAHs, or FAMES were detected in the engine blanks, while n-hexanal, n-nonanal, n-decanal, and benzophenone were the only POCs detected in the engine blanks. All samples were

therefore blank corrected for the four target analytes that were detected in the engine blanks.

### ***2.1.5.3 Percent Recoveries and Reproducibility***

Before extraction, each ¼-inch filter punch was spiked with tetracosane-d50 and 2-fluoro-9-fluorenone (2F9F) to assess the extraction efficiencies of the nonpolar and polar compounds in the PM, respectively. The average recovery of tetracosane-d50 was  $80.1 \pm 23.0\%$ , while that of 2F9F was  $109.6 \pm 58.4\%$ . Also, two to four punches were extracted from select filters in order to assess the reproducibility of the extraction and GC/MS analysis procedure. Good reproducibility was obtained for most of the filters where multiple punches were extracted whereby at least 75% of the extracts had %RSD values less than 20% (see Tables A-4 to A-19 in Appendix A). Further, good reproducibility was also achieved for the triplicate and duplicate filters extracted for WVO and soybean blends, respectively, as about 71% of the data had %RSD values less than 20%. Percent RSD values greater than 30% were observed for the high volatility compounds (compounds with less than 14 carbon atoms), and such variability was probably caused by losses during blowdown. No corrections for percent recoveries were performed, and all data, including those with high variability were used for further data analysis.

## 2.1.6 Data Analysis

### 2.1.6.1 Estimation of Individual Analyte Emission Rates

Because the mass of PM collected on each filter varied during each run, the mass of each target analyte in the entire 47 mm filter's PM deposit,  $M_i$ , was first computed (Equation 2-2) and then normalized to the total gravimetric mass of PM sampled:

$$M_i = m_i \times N_p \quad \text{Eq (2 - 2)}$$

where,

$M_i$  = Total Mass of Analyte  $i$  on entire FF Filter (ng),

$m_i$  = Measured mass of Analyte  $i$  in one Filter punch extract (ng), and

$N_p$  = Number of ¼" punches in Filter ( $N_p = 44$ ).

It was assumed that the available diameter for the deposition of PM on a 47 mm diameter filter was 42 mm because the o-ring in the filter holder covered about 2.5 mm of the filter edge. It was further assumed that the PM was uniformly deposited on the filter. Given the above mentioned assumptions, it was estimated that the total number of ¼-inch punches that could be cut from the 42 mm diameter PM deposit on the face of each filter,  $N_p$ , was 44.

Emission rates (Mass of Analyte per mass of PM Sampled, ng/μg) of the analytes were obtained by dividing the mass of analyte (ng) on the filter ( $M_i$  in Equation 2-2) by the gravimetric mass of PM (μg) sampled during that particular run (see Table 3.1 and Table A-3 in Appendix A for PM mass). Average emission rates of each analyte are reported based on the duplicate and triplicate extracted filters for the soybean and WVO biodiesel blend engine runs, respectively. The standard deviation values based on replicate engine test results were used to represent the uncertainties in the analysis and



quantitation of each target analyte. Emission rates of the different biodiesel blends were compared to those of ULSD by a percent difference calculation, (Equation 2-3). The reduction (negative value) or increase (positive value) in emission rates of compounds for the different biodiesel blends compared to B00 are reported for the total gas- and particle-phase emissions collected using the *undiluted FF* filters.

$$\%Difference (\% \Delta) = \frac{Emission\ Rate\ of\ B_{xx}\ PM - Emission\ Rate\ of\ B_{00}\ PM}{Emission\ Rate\ of\ B_{00}\ PM} \times 100 \quad (Eq\ 2 - 3)$$

### 2.1.6.2 Analysis of Variance (ANOVA)

The emission rates of the sum of target analytes for each compound class (n-alkanes, PAHs, FAMEs, aliphatic aldehydes, aromatic aldehydes, aromatic ketones, and quinones) were obtained for each engine run (filter) by summing up the emission rates of all the detected target analytes in each class. Then, the differences in the mean emission rates of the target analytes across all blends of WVO (i.e., WVO B00 vs WVO B10 vs WVO B20 vs WVO B50 vs WVO B100) and soybean (i.e., soybean B00 vs soybean B20 vs soybean B100) biodiesel exhaust PM were determined at a level of significance ( $\alpha$ ) = 0.05 using JMP Pro software (Version 11.2.0, SAS Institute Inc., Cary, NC). Note that the POCs were divided into four subgroups (i.e., aliphatic aldehydes, aromatic aldehydes, aromatic ketones, and quinones). Further, the differences in mean emission rates of the total target analyte groups across similar blends of both WVO and soybean (i.e., WVO B00 vs soybean B00, WVO B20 vs soybean B20, WVO B100 vs soybean B100) biodiesel exhaust PM were also determined at  $\alpha=0.05$ . When the

ANOVA results showed that there were differences in emission rates of the target analytes across the biodiesel blends of any feedstock, a two-way t-test was further applied on each pair of blends to obtain the blends that had statistically significant differences in emission rates. The differences in emission rates were considered to be statistically significant if the p-value was less than the level of significance ( $p\text{-value} < 0.05$ ).

## **2.2 Methods for Analysis of Fuel Samples**

### **2.2.1 Fuel and Lubricating Oil Analysis by GC/MS**

Samples were taken from both WVO and soybean fuel fuel blends, diluted in hexanes, and analyzed for the organic composition by GC/MS. Fuel samples of each of the blends used for the WVO test sequence (B00, B10, B20, B50, and B100) were analyzed for n-alkanes, PAHs, and FAMES. B00, B20, and B100 were the only fuels from the WVO test sequence that were analyzed for carbonyls and quinones. All the blends used for the soybean test sequence (B00, B10, B20, B50, and B100) were analyzed for n-alkanes and PAHs, while B00, B20, and B100 were the only fuels from the soybean test sequence that were analyzed for FAMES. Carbonyls and quinones were not analyzed in any of the fuels used in the soybean test sequence because neither carbonyls nor quinones were detected in the WVO fuel samples (B00, B20, and B100) that were analyzed. Therefore, it was assumed that both carbonyls and quinones would not be present in the soybean biodiesel fuel samples as well. All fuel samples were analyzed in duplicate with the exception of the fuel samples used for the soybean test sequence where 4 replicate fuel samples were used for the FAME analysis. Tables 2.5 and 2.6 show the concentrations of the different WVO and soybean biodiesel fuel

samples, respectively, that were analyzed for the target analytes. In addition to the analysis of the fuel samples, lubricating oil samples were also analyzed by GC/MS for n-alkanes and PAHs. One of the lubricating oil samples was new (unused) oil, while the second sample was used lubricating oil extracted from the engine after the WVO test sequence. Note that the lubricating oil samples were each diluted to 843 ppm with hexanes before GC/MS analysis. Analysis of n-alkanes, PAHs, carbonyls, and quinones was performed on the TD-GC/MS (5890/5972 GC/MSD), while analysis of the FAMES was performed on the 6890/5973 GC/MS. Note that 1  $\mu$ L aliquots of the diluted fuel and lubricating oil samples were injected during GC/MS analysis. Prior to injection in the TD-GC/MS, each 1  $\mu$ L aliquot of fuel sample was spiked with 1  $\mu$ L of a 2 ppm internal standard solution (containing 6 internal standards in DCM, the same internal standards used for quantitation of target analytes in exhaust PM) for quantitation of n-alkanes, and PAHs. Again, the internal standard eluting closest to a particular target analyte was used to quantify that analyte. For the quantitation of FAMES on the liquid autosampler GC/MS, an appropriate volume of a 100 ppm internal standard solution of 6F4C in DCM was added to target a final concentration of 6F4C of 2 ppm in the solution.

**Table 2.5 Concentrations ( $\mu\text{g/g}$ ) of the different WVO biodiesel fuel blends that were analyzed for the different target analytes. N represents the number of samples analyzed.**

Blend	Density (g/mL)	PAHs and n-Alkanes		FAMES		Carbonyls and Quinones	
		Conc ( $\mu\text{g/g}$ )	N	Conc ( $\mu\text{g/g}$ )	N	Conc ( $\mu\text{g/g}$ )	N
B00	0.813	806	2	50	2	806	1
B10	0.817	812	2	100	2		
B20	0.824	819	2	100	2	818	1
B50	0.843	838	2	100	2		
B100	0.876	869	2	50	2	869	1

Fuel density was obtained by weighing a known volume of fuel on a balance. Density of hexanes=0.672g/mL

**Table 2.6 Concentrations (ppm) of the different soybean biodiesel fuel blends that were analyzed for the different target analytes. N represents the number of samples analyzed.**

Blend	Density (g/mL)	PAHs and n-Alkanes		FAMES	
		Conc ( $\mu\text{g/g}$ )	N	Conc ( $\mu\text{g/g}$ )	N
B00	0.812	806	2	50	4
B10	0.816	812	2		
B20	0.822	819	2	50	4
B50	0.842	838	2		
B100	0.876	869	2	50	4

Fuel density was obtained by weighing a known volume of fuel on a balance. Density of hexanes=0.672 g/mL

## 2.2.2 Data Analysis

After GC/MS analysis, the mass of each target analyte in the diluted fuel samples was determined using Equation 2-4;

$$M = \frac{m \times V}{v} \quad \text{Eq (2 - 4)}$$

where  $M$  = mass of target analyte in diluted fuel sample (ng)

$m$  = mass of target analyte in 1  $\mu\text{L}$  sample analyzed on the GC/MS (ng)

$V$  = volume of diluted fuel sample ( $\mu\text{L}$ )

$v$  = volume of diluted fuel sample injected in GC for analysis ( $\mu\text{L}$ )

The concentrations of the target analytes in the original fuel (before dilution) samples were obtained by dividing  $M$  in Equation 2-4 by the volume of fuel that was diluted.

## **2.3 Methods for the Ozone Exposure Experiments**

### **2.3.1 Ozone Exposure Experiments**

#### ***2.3.1.1 Ozone Exposure Setup***

The schematic of the ozone exposure setup is shown in Figure 2.2. Compressed air from the building was pushed through the system. The air was then split into two lines, one through an ENALY 1000BT-12 ozone generator (Shanghai, China) at 1 L/min, and the other through a humidification system at 5 L/min. The air through each line was dried with silica gel, cleaned with activated charcoal, ozone-scrubbed with potassium iodide (KI trap), and finally filtered with a HEPA filter. Air through the humidification system was split into two lines (dry and humidified lines) using a two-way rotameter. The air was humidified using a Perma Pure humidifier (Perma Pure, Tom River, NJ), which was used to maintain the relative humidity (RH) of the air in the system at 50% ( $\pm 5$ ). A temperature and RH data logger (Dickson TR320 Pro series; Dickson, Addison, IL) located at the exit of the system was used to record the temperature and RH of the air in the setup.

Ozone was generated using the ENALY 1000BT-12 ozone generator at a rate of about 1100 mg/hr, which was far in excess of what was required and could be measured by the ozone measurement instrument. Therefore, the excess ozone from the generator was vented out just downstream of the ozone generator. A needle valve downstream of the ozone generator was further used to control the amount of ozone mixed with the humidified air.

The humidified air was mixed with the air from the ozone generator, and the concentration of ozone in the air was measured using a Dasibi 1003-AH ozone monitor (Glendale, CA), and recorded every 30 seconds using LabView. Ozone in the setup was always maintained at a concentration of  $0.4 \pm 0.08$  ppm to ensure excess ozone during the exposure experiments (see Appendix C for calculation of number of ozone molecules in each reactor). The ozone/air mixture was passed through a 6-way rotameter via a 3-way valve into three parallel Teflon 164 mL reactors (Savillex, Eden Prairie, MN). The main purpose of the 3-way valve was to close flow through the 6-way rotameter whenever experiments were temporarily stopped to remove filter punches from the Teflon reactors. Furthermore, only 3 channels of the 6-way rotameter were connected to the reactors, and flow through each reactor was adjusted using the corresponding rotameter channel. Equal flow of air (approx. 0.4 SLPM) through all reactors was maintained during each exposure experiment.

The air exiting each reactor was passed through a potassium iodide trap to remove the excess ozone, then through PUF adsorbents to capture the gas-phase products formed during the ozonation reactions. The air exiting all three reactors was then combined, and the total exit flow through all reactors was periodically measured and recorded. The total

flowrate of the air exiting all three reactors was always maintained at approximately  $1.2 \pm 0.24$  SLPM. Before each exposure experiment, the system was conditioned by pushing air through for at least 2 hours. By doing this, the system was cleaned of any residual contaminants. Furthermore, stable flows, RH, and ozone concentrations were achieved during conditioning before the start of each experiment.

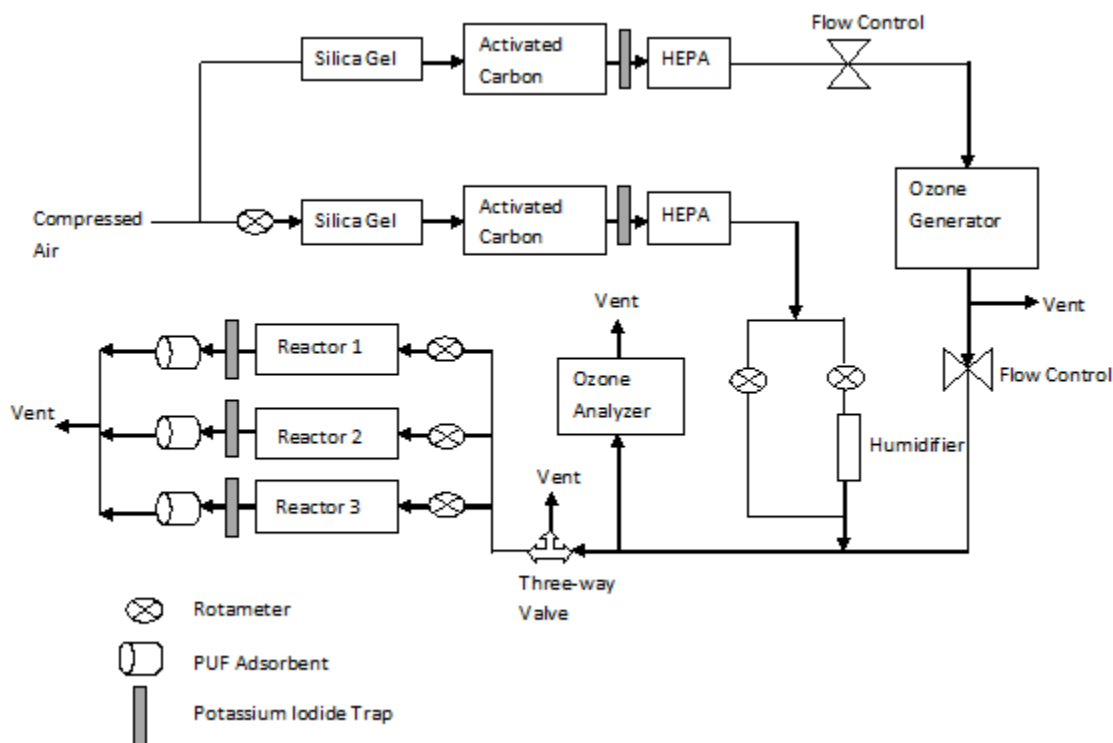


**Figure 2.2 Schematic of the ozone exposure setup.**

### *2.3.1.2 Exposure of PAHs to Ozone*

In the first set of experiments,  $\frac{1}{4}$ -inch punches were cut from a bare 47 mm Teflon-coated FF filter. The punches were then spiked with  $30 \pm 6$  ng of each of the 16 PAHs in the mix (see Table 2.3). The spiked mass of PAHs represented the approximate

mass of each PAH that was previously quantified in B20 exhaust PM (Section 2.1). The spiked punches were placed in the Teflon reactors and exposed to  $\sim 0.4 \pm 0.08$  ppm ozone for periods of 0, 1, 2, 4, 8, and 24 hr (see schematic in Figure 2.2). The 1 and 2 hour exposures were done in Reactor 1, the 4 and 8 hour exposures were done in Reactor 2, while the 24 hour exposure was done in Reactor 3. All reactors were covered with aluminum foil to avoid reactions due to photochemistry. The punches for the  $t=0$  time point were immediately saved for extraction after being spiked with the PAH mix. At the end of each exposure period, the filter punches were removed from their corresponding reactors and stored in a  $-20$  °C freezer until they were ready for extraction and GC/MS analysis. Triplicate punches were exposed to ozone for each time point.

### ***2.3.1.3 Exposure of PAHs and FAMES to Ozone***

In a different set of experiments, 1/4-inch filter punches were first spiked with the 16 PAH mix (approx.  $30 \pm 6$  ng of each PAH in the mix), followed by the 10 FAME mix (approx. 10,000 ng of total FAMES in the mix). The respective quantities of PAHs and FAMES spiked on the 1/4-inch punches were chosen to equal the amounts of PAHs and FAMES detected in the exhaust PM of WVO (however, it was later found that the total amount of FAMES in WVO B20 exhaust PM was about 4 times greater than the amount of FAMES spiked on the punches in these experiments). The spiked punches were exposed to  $0.4 \pm 0.08$  ppm of ozone in a similar manner as those spiked with PAHs only. Again, the 1 and 2 hr exposures were conducted in Reactor 1, the 4 and 8 hr exposures were conducted in Reactor 2, while the 24 hr exposure was conducted in Reactor 3. The punches from this ozone exposure experiment were also stored in the  $-20$  °C freezer until



they were extracted and analyzed by GC/MS. These FAMES+PAHs punches were exposed to ozone in triplicates for each time point.

#### ***2.3.1.4 Exposure of biodiesel (B20) Exhaust PM to Ozone***

Similarly, ¼-inch punches were cut from one of the filters that were used to sample biodiesel (B20) exhaust PM. The punches were also exposed to ozone in a similar way as the filter punches that were spiked with PAHs, and FAMES+PAHs. The exposed punches were stored in a -20 °C freezer until GC/MS analysis. Punches were exposed to ozone in duplicates for each time point.

#### ***2.3.1.5 Controls Experiments***

Note that before each ozone exposure experiment, a control experiment was conducted at the same experimental conditions as the exposure experiments described above but without ozone (ozone generator was off). From the control experiments, the rate of losses due to volatilization for the more volatile PAHs and FAMES were determined. From the control experiments, it was also confirmed that there was no background ozone in the compressed air used as the ozone analyzer registered zero ozone concentrations. Therefore, loss of compounds during the control experiments was entirely due to volatilization.

The average values of ozone concentrations, total exit flowrates, temperature, and RH measured during the control and ozone exposure experiments are shown in Appendix C (Tables C-4, C-5, and C-6).

### **2.3.2 Extraction and GC/MS Analysis**

Extraction, derivatization, and TD-GC/MS analysis of the filter punches from the ozone exposure experiments followed the same procedure used for the extraction and analysis of exhaust PM filter punches in Section 2.1.

Again, the FAMES were separately analyzed on a 6890GC/5973MSD (Agilent) system equipped with a SLB-IL polar column (Restek) and 7683 Series autosampler (Agilent). An aliquot (10  $\mu$ L for the spiked punches, and 1  $\mu$ L for the biodiesel exhaust PM punches) was drawn from the 100  $\mu$ L final extract, blown down to near dryness and then followed by reconstitution with 50  $\mu$ L of hexanes. Solvent exchange was performed because MeOH was found to degrade the polar column. An appropriate amount of a 100 ppm standard of 6F4C was then added to each extract just before GC/MS analysis to target a 6F4C concentration of 2 ppm for quantitation of all FAMES.

### **2.3.3 Data Analysis**

Equation 2-5 shows a simplified chemical equation for the reactions between ozone and each reactant in the system. Because of the excess and constant ozone present during exposure, pseudo-first order kinetics were assumed for the reactions between ozone and the reactants in the system during the ozone exposure experiments. Also, pseudo-first order kinetics were assumed for the control experiments. The pseudo-first order rate constants of the PAHs or FAMES with ozone were obtained by quantifying the concentration of each PAH or FAME remaining on the filter punch at each ozone exposure time. The concentration of unreacted analyte was normalized to its measured initial concentration, and the natural log of the normalized concentration was then plotted

against reaction time. The data were then fit with a linear least-squares regression, and an exponential function was then obtained for each compound (Equation 2-6), where  $[Reactant]_t$  = concentration of PAH or FAME unreacted at any time, t,  $[Reactant]_0$  = initial concentration of PAH or FAME,  $k'$  is the pseudo-first order rate constant determined from the best fit slope obtained from the linear fit of the natural log of the normalized concentration data versus reaction time.



$$\frac{[Reactant]_t}{[Reactant]_0} = Exp(-k't) \quad Eq (2 - 6)$$

Because the experimental setup was a flow system, unavoidable losses of the more volatile FAMES and PAHs due to volatilization were experienced during the ozone exposure experiments. Therefore, to ensure quantification of losses due to heterogeneous reactions with ozone only, an effective ozonation rate constant  $k'_{Eff}$  (Equation 2-7) was calculated for each compound. This was done by subtracting the rate constants obtained during the control experiments from the rate constants obtained during the corresponding ozone exposure experiments. This approach has been previously used by Poschl et al. 2001:

$$k'_{Eff} = k'_1 - k'_2 \quad Eq (2 - 7)$$

where  $k'_{Eff}$  = Compound loss due to reaction with ozone only,

$k'_1$  = Compound loss due to both volatilization and reaction with ozone, and

$k'_2$  = Compound loss due to volatilization (from control experiments).

The standard errors on the slopes obtained from the linear regression of the experimental data to determine the pseudo-first order ozonation rate constants ( $k'_1$  and  $k'_2$ ) were considered as the uncertainties or errors in the pseudo-first order rate constants. The uncertainties in determining  $k'_{Eff}$  were obtained by propagation of error (Equation 2-8).

$$Unc(k'_{Eff}) = \sqrt{Unc(k'_1)^2 + Unc(k'_2)^2} \quad Eq (2 - 8)$$

where  $Unc(k'_{Eff})$  = uncertainty in the effective ozone reaction rate constant

$Unc(k'_1)$  = uncertainty in the ozone reaction+volatilization rate constant

$Unc(k'_2)$  = uncertainty in the volatilization rate constant

## Chapter 3

### RESULTS AND DISCUSSION

This chapter presents the results and discussion of all the experiments that were conducted in this dissertation. Section 3.0 presents the sampling information of the engine runs for the filters that were used in this study. Sections 3.1, 3.2, and 3.3 of this chapter present the results and discussion of the research questions 1, 2, and 3, respectively, posed in Chapter 1.

#### 3.0 Sampling Information

Table 3.1 summarizes the sampling and engine run conditions for the filters that were analyzed in the present study. The engine runs were named based on the fuel blend used and the date a particular run was conducted. Filters were numbered in sequential order following the order of engine runs in which they were used. In general, the mass of PM sampled increased with increasing biodiesel content in the fuel (Table 3.1). Also, the concentration of PM generally increased with increasing biodiesel content in the fuel. The average concentration of PM sampled compared to WVO B00 increased by 10.6%, 25.4%, 87.5%, and 200% for WVO B10, B20, B50, and B100, respectively. For the soybean sequence, the average concentration of PM sampled decreased by 32.3% for soybean B20 biodiesel compared to soybean B00, but then increased by 69.0% for soybean B100 biodiesel.

No particular trends were observed in the volume of fuel used with respect to biodiesel content in the fuel (Table 3.1). For the WVO sequence, the average volume of fuel used compared to WVO B00 decreased by 6.0%, 2.2%, and 1.1% for WVO B10,

B20, and B50, respectively. However, for the WVO B100 biodiesel, the average volume of fuel used increased by 2.4% compared to WVO B00. The average volume of fuel used increased by 6.5% and 11.8% for soybean B20 and B100, respectively, compared to the soybean sequence B00 fuel.

**Table 3.1 Sampling conditions during the WVO and soybean engine test sequences.**

Engine Sampling Date	Run ID	Fuel Type	Filter #	PM Mass Sampled (mg)	PM Conc. ( $\mu\text{g}/\text{m}^3$ ) $\times 10^3$	Volume of Fuel Used (L)	Filter Analysis Date
<b>WVO Sequence</b>							
6/13/2013	1_13JUN2013_Blank	Blank	FF 246	0.02	0.01	-	3/24/2014
8/27/2013	1_27AUG2013_Blank	Blank	FF 271	0.04	0.02	-	3/24/2014
9/28/2013	1_28SEP2013_Blank	Blank	FF 346	0.06	0.03	-	3/24/2014
6/18/2013	1_25JUN2013_B000	B00	FF 256	23.1	10.3	3.65	3/3/2014
6/25/2013	1_05AUG2013_B000	B00	FF 261	27.6	10.5	4.19	3/3/2014
8/6/2013	1_06AUG2013_B000	B00	FF 266	22.6	10.3	3.63	3/3/2014
8/28/2013	1_29AUG2013_B010	B10	FF 276	24.8	11.5	3.62	3/4/2014
8/30/2013	1_30AUG2013_B010	B10	FF 281	23.2	10.6	3.60	3/4/2014
8/31/2013	1_31AUG2013_B010	B10	FF 286	26.6	12.3	3.56	3/4/2014
9/4/2013	1_04SEP2013_B020	B20	FF 291	28.3	12.9	3.74	3/7/2014
9/5/2013	1_05SEP2013_B020	B20	FF 296	29.8	13.3	3.73	3/7/2014
9/6/2013	1_06SEP2013_B020	B20	FF 301	27.9	12.8	3.75	3/7/2014
9/9/2013	1_09SEP2013_B050	B50	FF 306	40.9	18.9	3.80	3/7/2014
9/10/2013	1_10SEP2013_B050	B50	FF 311	46.7	20.8	3.76	3/7/2014
9/11/2013	1_11SEP2013_B050	B50	FF 316	42.6	18.6	3.78	3/7/2014
9/19/2013	1_19SEP2013_B100	B100	FF 331	75.0	32.8	3.98	3/29/2014
9/20/2013	1_20SEP2013_B100	B100	FF 336	74.8	32.9	3.91	3/29/2014
9/20/2013	2_20SEP2013_B100	B100	FF 341	63.8	27.6	3.85	3/29/2014
<b>Soybean Sequence</b>							
4/30/2014	1_30APR2014_Blank	Blank	FF 411	0.04	0.02	-	6/10/2014
12/6/2013	1_06DEC2013_B000	B00	FF 386	54.2	25.0	3.74	6/18/2014
5/2/2014	1_02MAY2014_B000	B00	FF 421	37.6	15.6	3.44	6/18/2014
5/13/2014	1_13MAY2014_B020	B20	FF 466	33.4	14.6	3.79	6/17/2014
5/14/2014	2_14MAY2014_B020	B20	FF 471	31.1	12.9	3.86	6/17/2014
5/23/2014	1_23MAY2014_B100	B100	FF 511	92.3	37.1	4.03	6/23/2014
5/26/2014	1_26MAY2014_B100	B100	FF 516	81.6	31.5	4.00	6/23/2014

### **3.1 Organic Chemical Characterization of Biodiesel Exhaust Particulate Matter from a Light-Duty Diesel Engine**

#### **3.1.1 n-Alkanes Emissions**

Figure 3.1 shows the emission rates of the speciated n-alkanes in WVO and soybean biodiesel exhaust PM. Among the 19 target n-alkane species, the n-alkanes detected with very good certainty in the exhaust PM of all fuel blends were C<sub>15</sub>-C<sub>26</sub> n-alkanes (n-pentadecane, n-hexadecane, n-heptadecane, n-octadecane, n-nonadecane, n-eicosane, n-heneicosane, n-docosane, n-tricosane, n-tetracosane, and n-hexacosane) for both biodiesel feedstocks. n-Tetradecane was detected in the exhaust PM of B00, B10, B20, and B50 of the WVO sequence but the spectra for the WVO B100, soybean B20, and soybean B100 exhaust PM were not clear because of interference from other compounds that co-eluted with n-tetradecane in B100 exhaust PM extracts. Therefore, the n-tetradecane emission rates were not plotted in Figure 3.1. Quite high variability was seen in the B00 n-alkane emission rates of the WVO sequence (0.05-2.46 ng/μg), and the reason for this variability is not well-known, but it could be due to the differences in ambient conditions (temperature and RH) for the different runs. The first run was performed on June 18<sup>th</sup>, 2013, while the second run was performed on June 25<sup>th</sup>, 2013, and the third run was conducted on August 5<sup>th</sup>, 2013. The average ambient temperature was 20.9±0.4 °C, 29.7±0.7 °C, and 23.8±0.7 °C, respectively, for the June 18<sup>th</sup>, June 25<sup>th</sup>, and August 6<sup>th</sup> engine runs, while the average ambient RH was 41.9±3.1%, 59.6±2.6%, and 36.5±3.4%, respectively, for the June 18<sup>th</sup>, June 25<sup>th</sup>, and August 6<sup>th</sup> engine runs. Because the ambient temperature and RH did not appear to vary greatly between the



triplicate runs, it indicates that a different factor could have influenced the variability in the emission rates of the n-alkanes observed in the B00 exhaust PM for the WVO sequence. High variability was also seen in the emission rates of some compounds such as n-octadecane, n-nonadecane, n-eicosane, and n-heneicosane in the B00 and B10 exhaust PM of the WVO sequence. Also, high variability was observed in the n-heptadecane, n-octadecane, and n-nonadecane B00 exhaust PM emission rates of the soybean sequence, while high variability was observed in the emission rates of n-eicosane, n-heneicosane, and n-docosane for the soybean B20 exhaust PM.

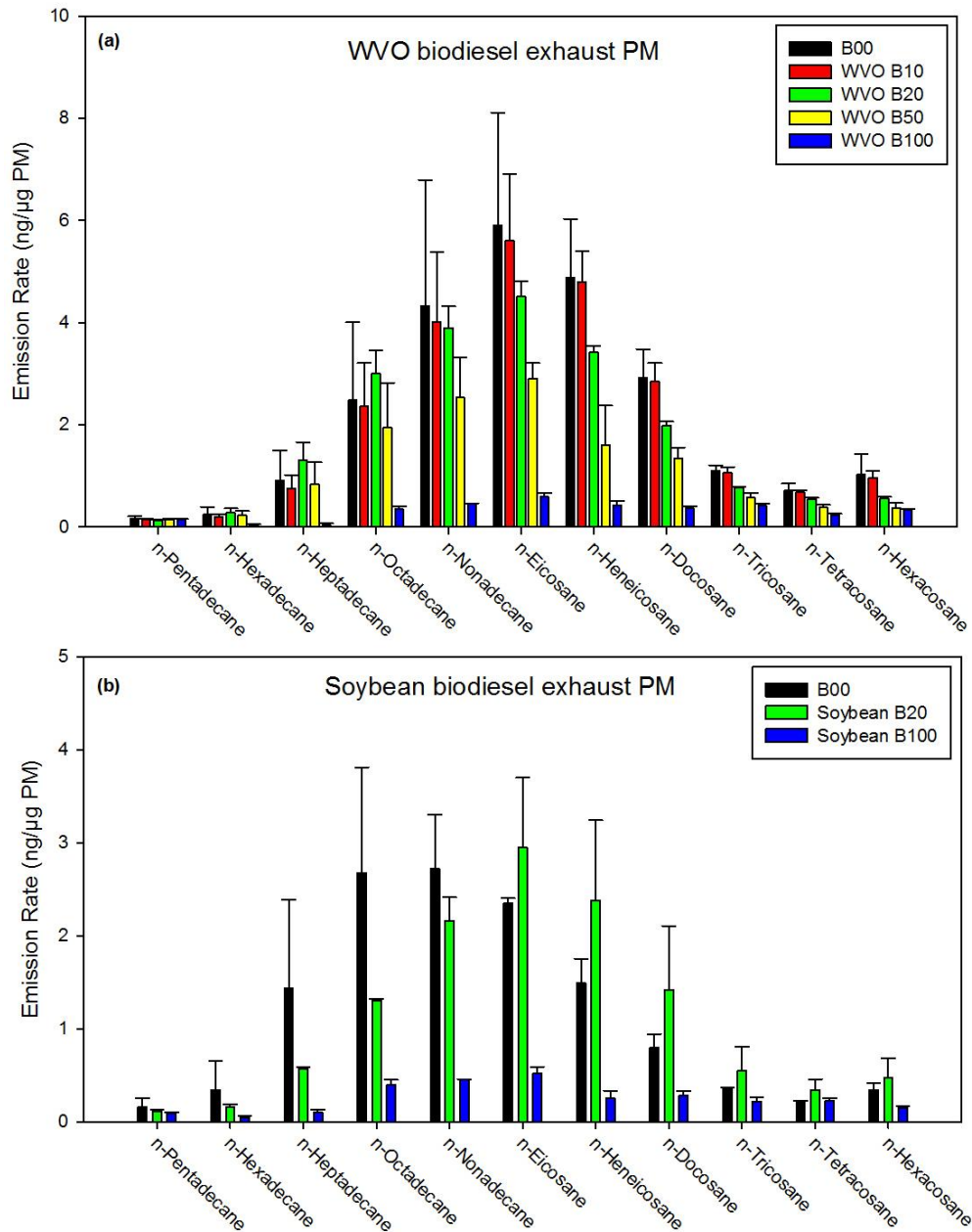


**Figure 3.1** Average emission rates (ng/μg) of n-alkanes in PM resulting from the combustion of (a) WVO and (b) soybean biodiesel blends. Error bars represent one standard deviation across multiple emission tests. For WVO, n = 3; For Soybean, n = 2. Note that the y-axis scales are different for both plots.

Emission rates of most of the individual n-alkanes generally decreased with increasing WVO biodiesel content in the fuel. The only deviations for WVO were seen

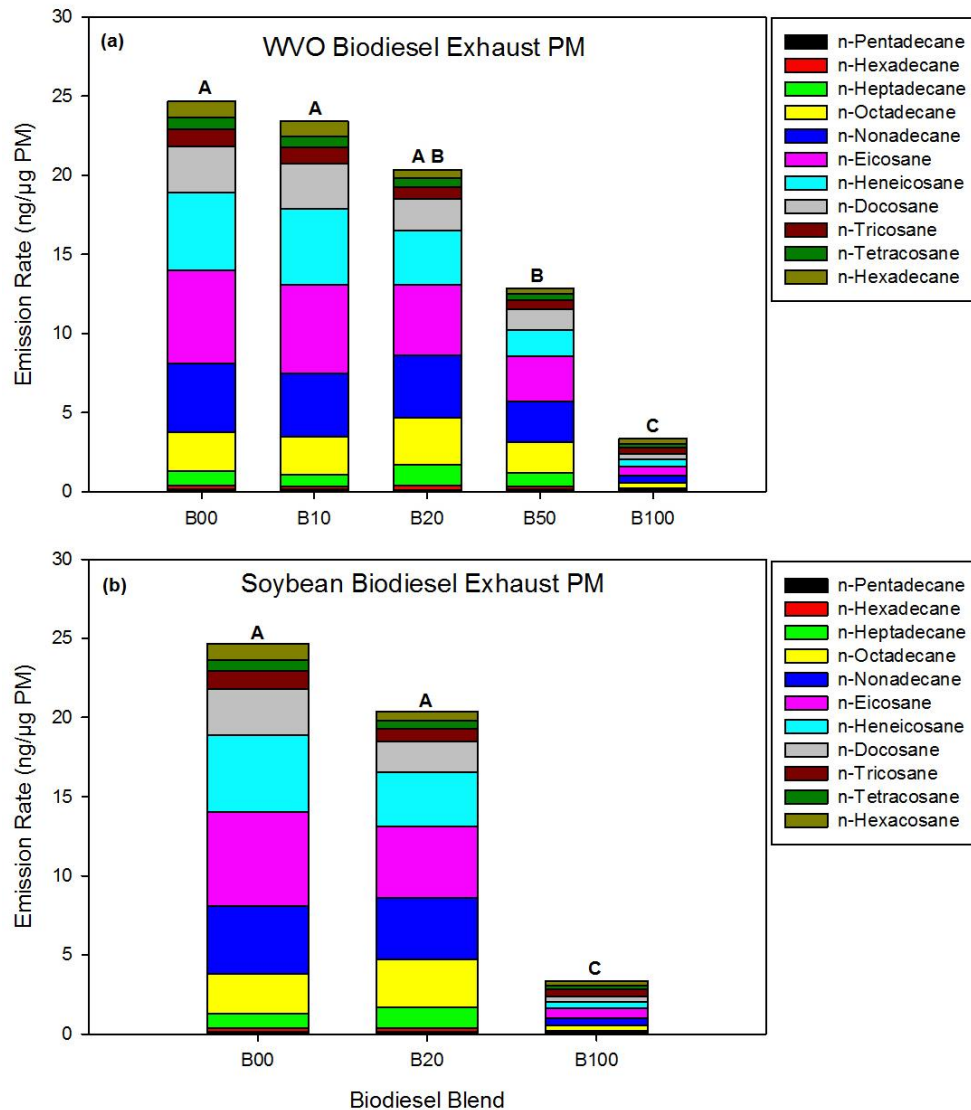
in n-hexadecane, n-heptadecane, and n-octadecane, which showed 15.0%, 43.6%, and 20.9%, respectively, higher emission rates for the WVO B20 blend compared to petrodiesel. Also, n-eicosane, n-heneicosane, n-docosane, n-tricosane, n-tetracosane, and n-hexacosane had 25.5%, 60.0%, 78.5%, 56.5%, 50.3%, and 41.2%, respectively, higher emission rates in the soybean B20 blend compared to B00.

Figure 3.2 shows a plot of the emission rates of the total n-alkanes (sum of emission rates of the detected n-alkanes) in the exhaust PM of the different blends of WVO and soybean biodiesel fuels. Similar letters on top of the bars of different WVO or soybean blends in Figure 3.2 mean that the differences in emission rates of the total n-alkanes were not statistically significant for those WVO or soybean biodiesel blends at  $\alpha=0.05$ . Bars with different letters mean that the differences in emission rates of total n-alkanes for those biodiesel blends were statistically significant at  $\alpha=0.05$ . See Table A-23 in Appendix A for p-values of the statistical tests for all blend pairs of WVO and soybean biodiesel exhaust PM.

For the WVO sequence, the sum of measured n-alkane emission rates reduced by 5.1%, 17.4%, 47.8%, and 86.4% for the B10, B20, B50, and B100 biodiesel blends, respectively, compared to B00. The differences in emission rates of the total n-alkanes in the WVO B00 exhaust PM, WVO B10, and WVO B20 exhaust PM were not statistically significant (Figure 3.2). The differences in emission rates of the total n-alkanes in the WVO B00 exhaust PM were, however, statistically significant from those of WVO B50 and WVO B100 exhaust PM with p-values of 0.0134 and 0.0003, respectively. The differences in emission rates of the total n-alkanes in the WVO B20 and WVO B50

exhaust PM were not statistically significant. See Table A-22 in Appendix A for p-values of the statistical tests for all blend pairs of WVO biodiesel exhaust PM.

The emission rates of the total n-alkanes for soybean B20 and B100 decreased by 3.6% and 78.7%, respectively, compared to B00. The differences in emission rates of the total n-alkanes in the soybean B00 and B20 exhaust PM were not statistically significant (Figure 3.2). The differences in emission rates of the total n-alkanes between soybean B00 and B100 exhaust PM were statistically significant (p-value = 0.0306).



**Figure 3.2** Emission rates (ng/μg) of total n-alkanes (sum of emission rates of the detected n-alkanes) in the exhaust PM of (a) WVO biodiesel blends, and (b) soybean biodiesel blends. For WVO,  $n = 3$ ; For Soybean,  $n = 2$ . Similar letters on top of the bars of different WVO or soybean blends mean that the differences in emission rates of the total n-alkanes were not statistically significant for those WVO or soybean biodiesel blends at  $\alpha=0.05$ . Bars with different letters mean that the differences in emission rates of total n-alkanes for those biodiesel blends were statistically significant at  $\alpha=0.05$ .

The differences in the emission rates of the total n-alkanes with increasing biodiesel content in the fuel clearly suggest that use of either soybean or WVO biodiesel in a light-duty diesel engine instead of ULSD reduces the emission of n-alkanes, thus

reducing the n-alkanes load in the atmosphere. This is not surprising because petrodiesel fuel consists of n-alkanes (Schauer et al., 1999) that make it through the engine as unburned fuel or partially burned hydrocarbons, while neat biodiesel does not contain n-alkanes. Because no n-alkanes are found in the neat biodiesel fuels (WVO B100 and soybean B100), the n-alkanes measured in the exhaust PM of the neat biodiesel fuels could have been derived from the lubricating oil used in the engine. Rogge et al. (1993) suggested that at the elevated temperatures (~250 °C) encountered during engine operation, the n-alkyl hydrocarbons in lubricating oil may undergo mild thermocracking at the tertiary carbon atoms to form n-alkanes in exhaust. To evaluate this possibility, the lubricating oil used during both petrodiesel and biodiesel emission tests was analyzed on the TD-GC/MS, and branched alkanes were detected. This observation, therefore, supports the suggestion that n-alkanes are likely formed during the combustion of the lubricating oil in the engine when high molecular weight branched alkanes are broken to form n-alkanes. It is also possible that the n-alkanes detected in the biodiesel exhaust PM were formed from the pyrolysis of the FAMES (Maher and Bressler 2007).

In general, the total n-alkane emission rates for the WVO sequence were higher than those for the corresponding soybean sequence (B00, B20, and B100). For example, the total n-alkane emission rates for the WVO B00 sequence were 1.9 times higher than the soybean B00 emissions, the WVO B20 emissions were 1.6 times higher than the soybean B20 emissions, while the WVO B100 emissions were 1.2 times higher than the soybean B100 emissions. However, the differences between the emission rates of n-alkanes for the B00 WVO and B00 soybean test sequences were not statistically significant (p-value = 0.1676), while the B20 (p-value = 0.0323) and B100

( $p$ -value = 0.0179) emissions rates for both feedstocks were statistically significant at  $\alpha = 0.05$ . In spite of the fact that the emission rates of the n-alkanes in WVO B100 biodiesel exhaust PM were 1.2 times higher than those in soybean B100, they were very much lower than the soybean B00 and B20 emissions. This suggests that use of the neat biodiesel from either feedstock in a light-duty diesel engine at the engine operating conditions used in this study would reduce emissions of n-alkanes by 80%.

The trends of the emission rates of the n-alkanes are consistent with some prior studies. For example, Magara-Gomez et al. (2012) examined the composition of diesel PM emissions from a 1993 John Deere 7700 model, with a heavy-duty diesel engine that was not equipped with aftertreatment control technologies. They found 35% and 82% reductions in the emission rates of n-alkanes for soybean B50 and B100 blends, respectively. They further found 69% and 87% reductions in the n-alkane emission rates when the engine was fueled with beef tallow B50 and B100, respectively.

### **3.1.2 PAH Emissions**

PAHs originate either from the fuel itself (Schauer et al., 1999; Brandenberger et al., 2005) or result from the pyrolysis of organic compounds from the fuel, lubricating oil, or formed within the combustion chamber (Gangwar et al., 2011). Only three PAHs were detected at concentrations greater than the detection limits in all exhaust PM samples: phenanthrene, fluoranthene, and pyrene for both WVO and soybean biodiesel sequences. The rest of the PAHs were detected at concentrations below their respective detection limits, and are, therefore, not discussed further. Some prior studies (e.g., Magara-Gomez et al., 2012) also reported the PAHs mentioned above as the most dominant PAH species

in the diesel and biodiesel exhaust PM. Karavalakis et al. (2009) observed that, with the exception of benzo[a]pyrene, all the PAHs heavier than pyrene were detected at concentrations below detection limits when emissions from a 1998 model year Toyota Corolla 2.0 TD fueled with different blends of soy methyl esters and operated under the Athens and New European drive cycles were measured.

In general, the emission rates of the detected individual PAHs were lower in the WVO biodiesel exhaust PM (B10 through B100) compared to B00, with the exception of phenanthrene in WVO B20 exhaust PM which had a 0.4% increase compared to B00 (Figure 3.3). For the soybean biodiesel exhaust PM, the emission rates of some of the detected PAHs increased compared to B00 in some cases, while in other cases, they decreased. For example, the emission rates of fluoranthene in soybean B20 and B100 exhaust PM were 48.2% and 59.1% greater than the B00 exhaust PM, while the emission rate of pyrene in B20 exhaust PM was 20.5% higher than that for B00. The emission rates of phenanthrene in both soybean B20 and B100 exhaust PM decreased by 60.1% and 70.2%, respectively, compared to B00, while that of pyrene in soybean B100 decreased by 10.7% compared to B00.



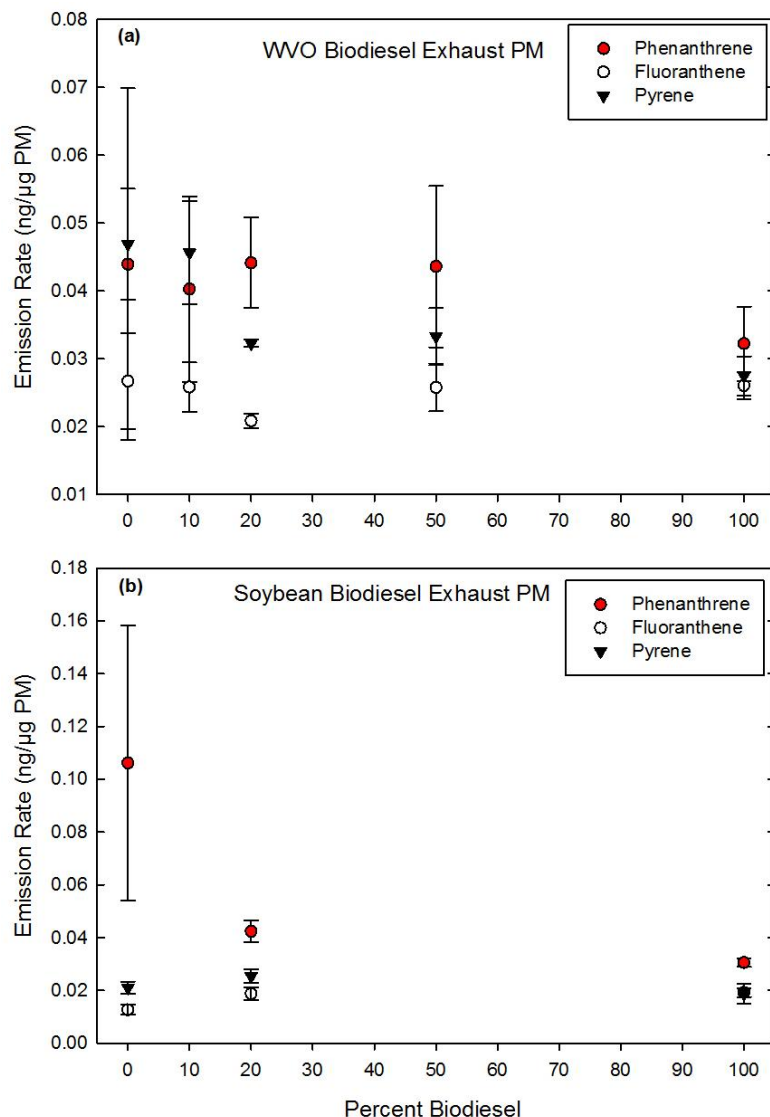


**Figure 3.3** Average emission rates (ng/μg) of PAHs in exhaust PM resulting from the combustion of (a) WVO and (b) soybean biodiesel blends. Error bars represent one standard deviation across multiple emission tests. For WVO,  $n = 3$ ; For Soybean,  $n = 2$ . Note that the y-scales are different for both plots.

The total PAH emission rates (sum of phenanthrene, fluoranthene, and pyrene emission rates) decreased with increasing biodiesel for both feedstocks (Figure 3.4). On average, for the WVO sequence, the reductions (percent difference) in total PAH emissions were 4.9%, 17.2%, 15.1%, and 27.1% for the B10, B20, B50, and B100 exhaust PM, respectively, compared to B00 exhaust PM. However, the differences in

emission rates of the total PAHs for all WVO biodiesel blends were not statistically significant. For the soybean biodiesel sequence, 38.2% and 51.0% reductions in total PAH emissions were observed for the B20 and B100 exhaust PM, respectively, compared to B00. The differences in emission rates of total PAHs for all soybean biodiesel blends were also not statistically significant. The total PAH emission rates for the corresponding WVO and soybean blends were observed to be quite similar, contrary to what was observed with the n-alkane emission rates. The differences in the emission rates of the total PAHs for the WVO B00 versus soybean B00, WVO B20 versus soybean B20, and WVO B100 versus soybean B100 engine runs were not statistically significant at  $\alpha = 0.05$ . Detailed results obtained from the analysis of variance (ANOVA) are shown in the Tables A-20 to A-23 in Appendix A.

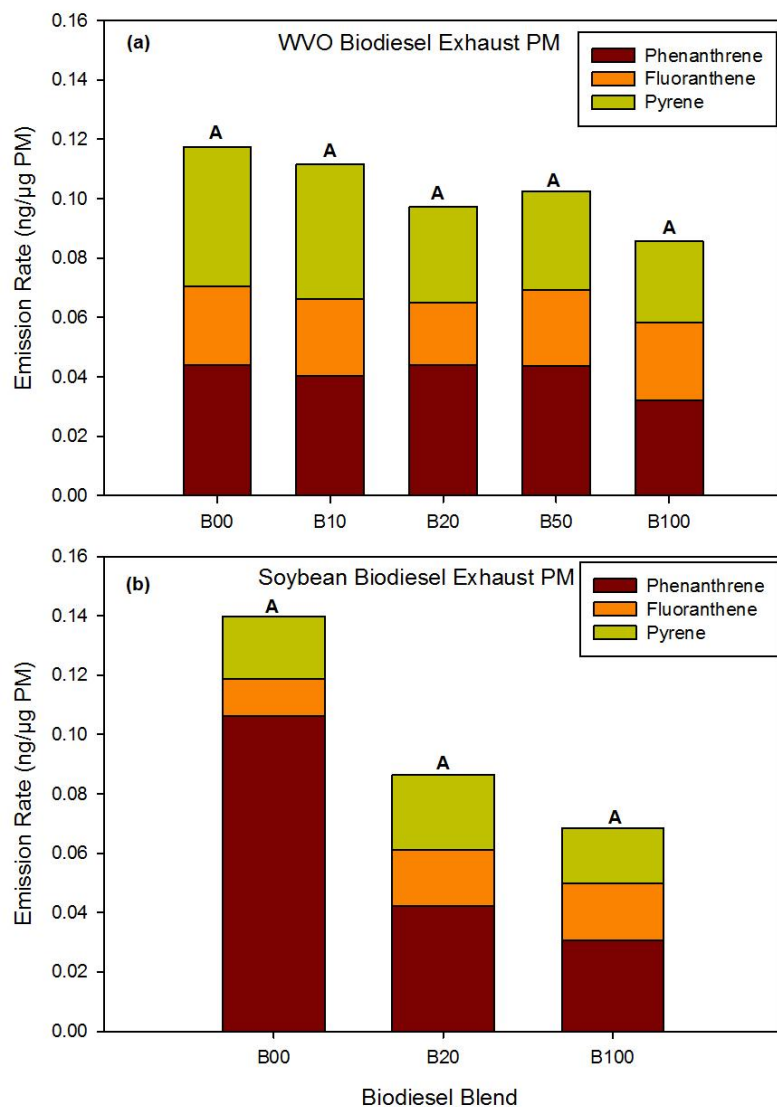


**Figure 3.4** Emission rates (ng/μg) of total PAH (sum of emission rates of the detected PAHs) in the exhaust PM of (a) WVO biodiesel blends and (b) soybean biodiesel blends. For WVO, n = 3; For Soybean, n = 2.

Use of WVO and soybean biodiesel blends in a light-duty diesel engine led to reductions in emissions of some PAHs, although some were seen to increase with some blends, while others did not significantly vary from blend to blend. However, the sum of the emissions of the three detected PAHs appeared to decrease with increasing biodiesel in the fuel which could be beneficial mainly because of the adverse health effects

associated with the PAHs detected in this study. A large majority of previous studies (e.g., Correa and Arbilla, 2006; Chien et al., 2009; Karavalakis et al., 2009; Magara-Gomez et al., 2012) all showed that PAH emission rates decreased with increasing biodiesel content in the fuel. The reduction in PAH emissions with increasing biodiesel can be explained by the complete absence of PAHs in the biodiesel fuel, unlike petrodiesel (Cardone et al., 2002; Correa and Arbilla, 2006; Chien et al., 2009; Karavalakis et al., 2009). More importantly, biodiesel's higher oxygen content of approx. 11% (Demirbas 2007) most likely enables more complete fuel combustion compared to diesel fuel in which the oxygen content is zero, hence leading to a decrease in PAH emissions (Chien et al., 2009). The presence of PAHs in the neat WVO B100 and soybean B100 biodiesel exhaust PM samples (Figures 3.3 and 3.4) suggests that factors other than fuel aromaticity and the presence of PAHs in the fuel influence the PAH emissions. Rogge et al. (1993) suggested that fuel aromaticity, engine load, PAH accumulation in lubricating oil, lubricating oil combustion, and cold start behavior all influence the emission of PAHs in gasoline and diesel engines. Therefore, a combination of two or more of the above mentioned factors outlined by Rogge et al. (1993) may somewhat explain why PAHs were detected in the neat biodiesel exhaust samples studied here.

### ***3.1.2.1 Comparison of PAH Emission Rates with Previous Studies***

In a study by Karavalakis et al. (2009), the PAH emissions from a diesel passenger vehicle equipped with an indirect diesel injection engine (1998 model year Toyota Corolla 2.0 TD with 4 cylinders, 86×85 mm, bore×stroke, 23:1 compression ratio,

61 kW maximum power at 4000 rpm, 174 Nm maximum torque at 2000 rpm, and 1300 kg weight) were measured when the vehicle was fueled with LSD (B00) and soy methyl ester blends (B5, B10, and B20). The emission tests were conducted under real Athens driving conditions (Athens Drive Cycle, ADC) and compared with those of a modified New European Drive Cycle (NEDC) using a chassis dynamometer. The PM was sampled on 47 mm Pallflex glass-fiber filters. The filters were extracted and analyzed for several analytes including PAHs. Table 3.2 shows the emission rates of the PAHs (phenanthrene, fluoranthene, and pyrene) obtained in the Karavalakis et al. (2009) study. The emission rates of all the PAHs detected in the present study for the corresponding biodiesel blends were about an order of magnitude lower than those in the Karavalakis et al. (2009) study (Table 3.2). The reasons for the lower emission rates of the PAHs in this study compared to that of Karavalakis et al. (2009) could be due to differences in: (a) fuels used (ULSD in this study versus LSD), (b) engine types (light-duty diesel engine in this study versus medium-duty diesel engine), and (c) drive cycles.

**Table 3.2 PAH emission rates (ng/μg) obtained in the present study with those obtained by Karavalakis et al. (2009).**

<b>ADC Drive Cycle (Karavalakis et al., 2009)</b>			
<b>Blend</b>	<b>Phen</b>	<b>Fluor</b>	<b>Pyr</b>
B00	0.577	0.385	0.346
B5	0.542	0.417	0.208
B10	0.435	0.348	0.174
B20	0.600	0.500	0.400
<b>NEDC Drive Cycle (Karavalakis et al., 2009)</b>			
B00	0.625	0.500	0.688
B5	0.571	0.500	0.643
B10	0.538	0.462	0.692
B20	0.692	0.615	0.769
<b>WVO Sequence (This Study)</b>			
B00	0.044	0.027	0.047
B10	0.040	0.026	0.046
B20	0.044	0.021	0.032
<b>Soybean Sequence (This Study)</b>			
B00	0.106	0.013	0.021
B20	0.042	0.019	0.025

According to the EPA 2002 review, the percent reductions in emissions with respect to biodiesel content in the fuel of pollutants like PM, CO, and hydrocarbons in biodiesel exhaust compared to petrodiesel exhaust can be approximated with linear models. For the reason mentioned above, the percent reductions in emission of PAHs in biodiesel exhaust PM compared to petrodiesel exhaust PM were fit with linear models in the present study. Additionally, percent reductions in the emissions of PAHs with respect to biodiesel content in the fuel from the Karavalakis et al. (2009) study were computed and linear models for the two drive cycles used in that study were obtained. The linear models obtained in this study were subsequently compared to those obtained from the Karavalakis et al. (2009) study.

The percent reductions in PAH emissions as a function of biodiesel content in the fuel showed a fairly linear relationship with WVO biodiesel ( $R^2 = 0.5917$ ), while a weak

linear relationship was observed for soybean biodiesel where fewer blends were analyzed ( $R^2 = 0.2899$ ) (Figure 3.5 and Table 3.3). The low  $R^2$  value for soybean was likely due to the very high variability obtained in the duplicate B00 emission rates for the soybean sequence. Figure 3.5 suggests that the PAH emissions generally decrease with increasing WVO and soybean biodiesel content in a light-duty diesel engine, and such reductions could be approximated with a linear relationship. Also, note that the percent reduction in the emission of PAHs was maximum at the B100 biodiesel blends for both WVO and soybean sequences. This may imply that B100 could be the optimal blend required for the maximum reduction of engine-out PAHs in the light-duty diesel engine used in this study.

Compared to the Karavalakis et al. (2009) study, the equation of best fit for the percent reduction in emissions of PAHs for the soybean sequence was somewhat similar to that of the New European Drive Cycle (NEDC, Figure 3.5 and Table 3.3). Note that in the Karavalakis et al. (2009) study, the biodiesel blends used were B00, B5, B10, and B20. Furthermore, the percent reductions in the emission of PAHs in the NEDC and Athens Drive Cycle (ADC) in the Karavalakis et al. (2009) study were lower for the B20 biodiesel blend compared to the B5 and B10 blends, and this possibly led to the very low  $R^2$  value observed in the NEDC and ADC results (Table 3.3). The similarity in the equations of best fit (due to the somewhat similar slopes, although with different  $R^2$  values) for the soybean sequence and the NEDC drive cycle from Karavalakis et al. (2009) could partly be due to the similarity in feedstocks (i.e., soybean biodiesel in this study and soy methyl ester in the Karavalakis et al. (2009) study). Note that the data were forced to linear models without intercepts (Table 3.3). It is also possible that the

soybean sequence ( $R^2 = 0.2899$ ) could be better fit with a nonlinear model that shows a minimum percent reduction in PAH emission rates at a soybean biodiesel blend ratio between 20% and 100%. For the Karavalakis et al. (2009) study, minima in the percent reductions in PAH emission rates were observed at B10 for both drive cycles, which explains the very low  $R^2$  values obtained for the ADC and NEDC drive cycles. This, therefore, means that the percent reductions in PAH emission rates in the Karavalakis et al. (2009) study and the soybean sequence in this study could possibly be better fit with a nonlinear model. Note that only 3 biodiesel blends (B5, B10, and B20) were used in the Karavalakis et al. (2009) study, while only 2 biodiesel blends (B20 and B100) were used in the present study. Therefore, in order to establish whether a nonlinear model better predicts the percent reductions in PAH emission rates with respect to soybean biodiesel content in the fuel, more data needs to be collected with more biodiesel blends.



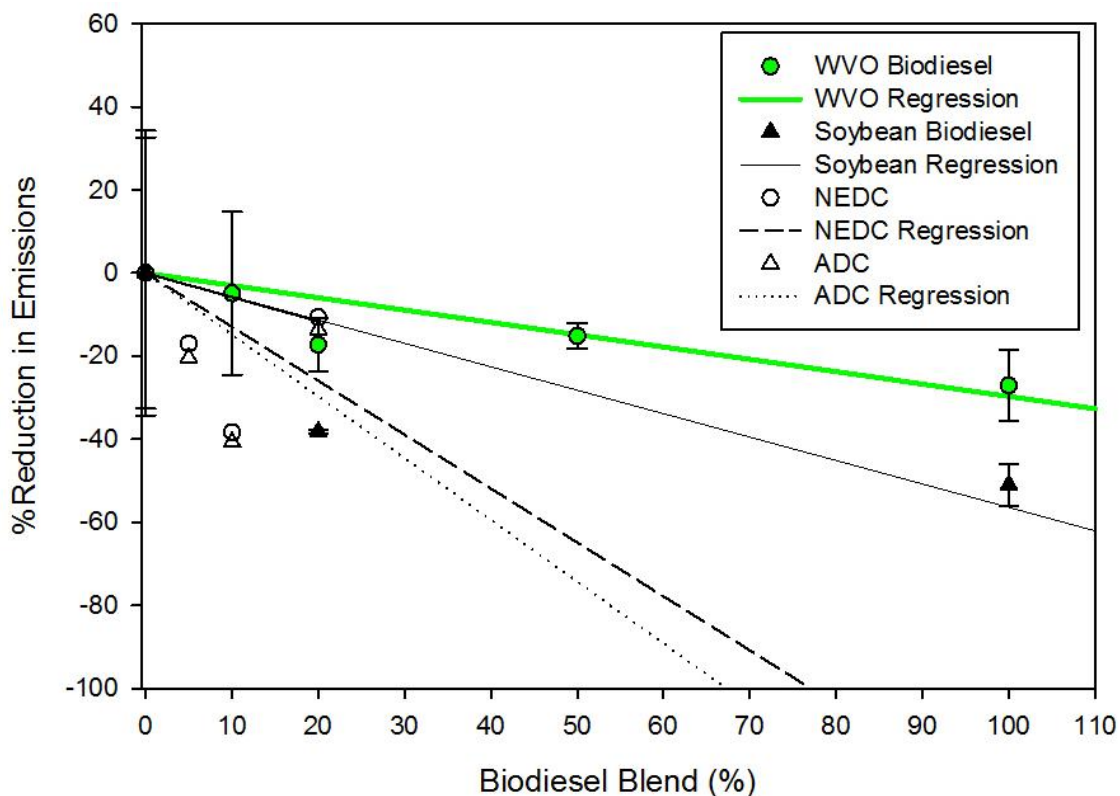


**Figure 3.5** Percent reduction in total PAH emissions with increasing WVO and soybean biodiesel volume percent.

**Table 3.3** Equations of best fit for the percent reduction of total PAH (phenanthrene, fluoranthene, and pyrene) emissions from the present study and Karavalakis et al. (2009). Values in parantheses mean one standard error obtained on the slope.

Feedstock/Study	Equation of best fit	R <sup>2</sup>
WVO (This Study)	$y = -0.2362 \pm (0.0691)x$	0.5197
Soybean (This Study)	$y = -0.4099 \pm (0.3100)x$	0.2899
Soy methyl ester (NEDC)	$y = -0.4742 \pm (1.1442)x$	0.0000
Soy methyl ester (ADC)	$y = -0.5811 \pm (1.2189)x$	0.0000

### 3.1.3 FAMES Emissions

Figure 3.6 shows the emission rates of the FAMES speciated in the WVO and soybean biodiesel exhaust PM. In general, the emission rates of the FAMES increased with increasing biodiesel in the fuel, as expected. No FAMES were detected in petrodiesel exhaust PM samples suggesting that there were no FAMES formed during the combustion of petrodiesel, no FAMES in the lubricating oil that would have ended up in the exhaust PM, and that there was no carryover from previous biodiesel runs. The most dominant FAMES detected (i.e., >10% contribution to total FAMES) in the biodiesel exhaust PM were methyl linoleate, methyl oleate, methyl palmitate, and methyl elaidate for both feedstocks in no particular order of decreasing/increasing concentration across all blends. With the exception of methyl elaidate, the most dominant FAMES in the biodiesel exhaust PM (methyl linoleate, methyl oleate, and methyl palmitate) were also the most dominant FAMES in the biodiesel fuel samples (see Section 3.2 for detailed fuel analysis results). Table 3.4 shows the percent composition data of the main FAMES detected in the WVO and soybean biodiesel exhaust PM.

The amounts of methyl oleate relative to those of methyl linoleate in the B20 and B100 exhaust PM for the WVO biodiesel appeared to be greater than those for the soybean biodiesel (Figure 3.6). These differences could partly be due to the higher concentrations of methyl linoleate in the soybean biodiesel compared to WVO biodiesel. Because of the high concentrations of methyl linoleate in the soybean biodiesel (see Section 3.2 for fuel analysis results), it is possible that a lot of methyl linoleate was emitted as unburned fuel when soybean biodiesel was used, while most of the methyl linoleate was burned when WVO biodiesel was used.

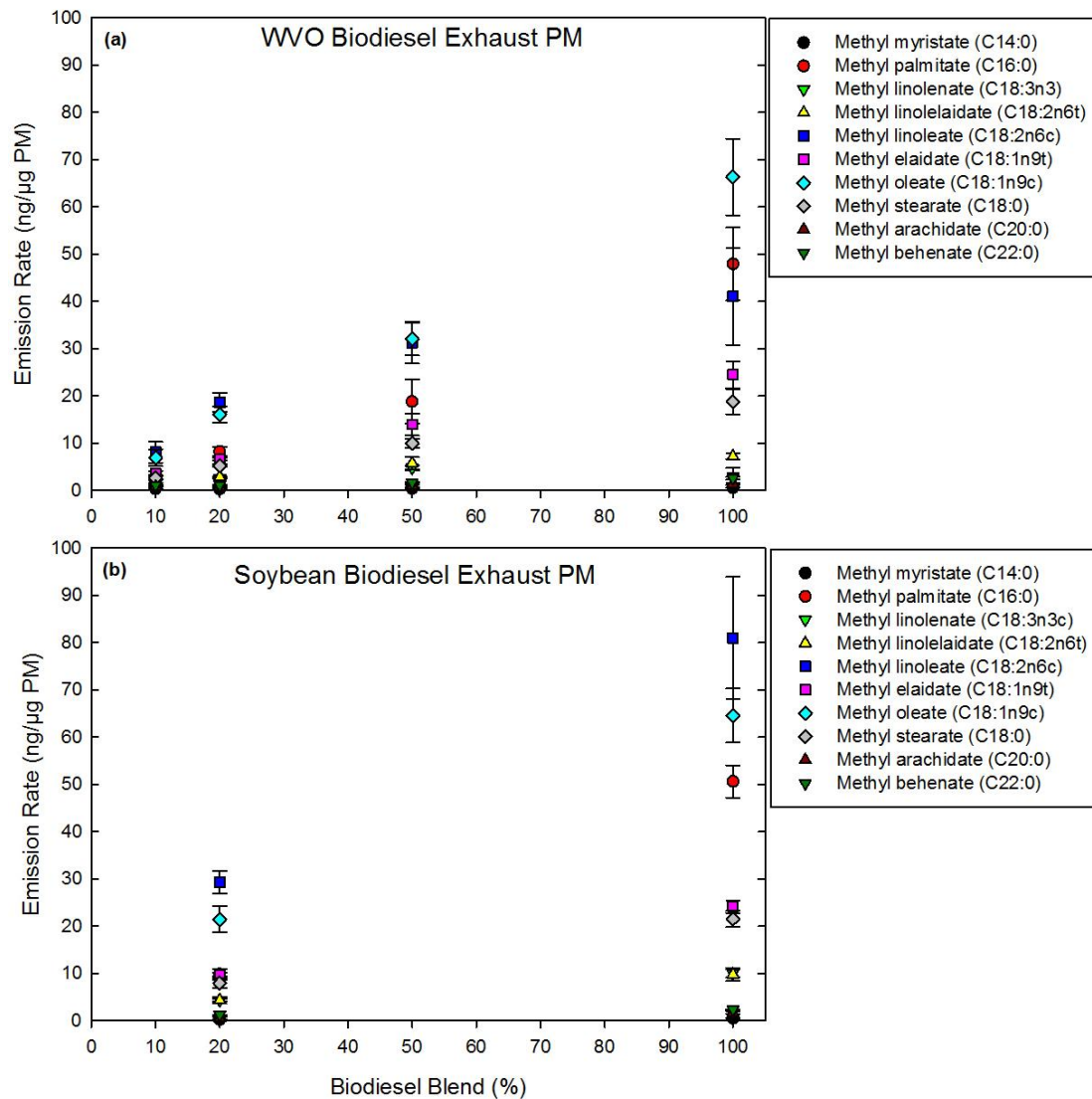


**Figure 3.6 Average emission rates (ng/μg) of FAMES in exhaust PM resulting from the combustion of (a) WVO and (b) soybean biodiesel blends. Error bars represent one standard deviation across multiple emission tests. For WVO, n = 3; For Soybean, n = 2.**

**Table 3.4 Average percent composition of the main FAMES detected in the WVO and soybean biodiesel exhaust PM. SD means one standard deviation based on triplicate (n=3) and duplicate (n=2) engine runs for WVO and soybean sequences, respectively.**

Compound	WVO Biodiesel								Soybean Biodiesel			
	B10	SD	B20	SD	B50	SD	B100	SD	B20	SD	B100	SD
Methyl myristate (C14:0)	1.10	0.19	0.50	0.05	0.40	0.04	0.30	0.03	0.30	0.010	0.20	0.030
Methyl palmitate (C16:0)	8.60	3.10	13.1	0.61	15.7	2.89	22.5	0.40	11.1	2.07	19.0	0.31
Methyl linolenate (C18:3n3c)	4.60	0.11	4.20	0.38	4.00	0.48	1.30	0.63	4.90	0.51	3.80	0.010
Methyl linoleaidate (C18:2n6t)	9.60	3.12	4.60	0.51	4.80	0.86	3.40	0.33	4.90	0.04	3.70	0.82
Methyl linoleate (C18:2n6c)	26.3	2.76	29.8	1.40	26.1	0.78	19.1	2.11	32.9	0.42	30.3	2.31
Methyl elaidate (C18:1n9t)	12.2	2.83	10.7	0.43	11.7	2.00	11.5	0.46	11.0	0.34	9.10	1.26
Methyl oleate (C18:1n9c)	22.6	1.80	25.7	1.30	26.8	0.43	31.2	1.72	24.0	1.45	24.3	0.11
Methyl stearate (C18:0)	8.70	0.42	8.40	0.36	8.30	0.31	8.80	0.37	8.90	0.48	8.10	0.020
Methyl arachidate (C20:0)	2.60	0.46	1.20	0.07	0.80	0.18	0.70	0.09	0.60	0.34	0.60	0.050
Methyl behenate (C22:0)	3.80	1.25	1.80	0.18	1.40	0.15	1.20	0.28	1.40	0.08	0.90	0.060
<b>Total</b>	<b>100</b>		<b>100</b>		<b>100</b>		<b>100</b>		<b>100</b>		<b>100</b>	

Figure 3.7 shows the total FAME emission rates (sum of the speciated FAMEs) for the WVO and soybean biodiesel sequences. The emission rates of the total speciated FAMEs in the WVO B100 exhaust PM were approximately 7, 3, and 2 times greater than those for the WVO B10, B20, and B50 exhaust PM, respectively. The differences in emission rates of the total FAMEs in WVO B10 and WVO B20 exhaust PM were not statistically significant, while the differences in total FAME emission rates for the rest of the WVO biodiesel pairs were statistically significant (Figure 3.7). See Table A-22 in Appendix A for p-values of the differences in emission rates of the different WVO biodiesel pairs.

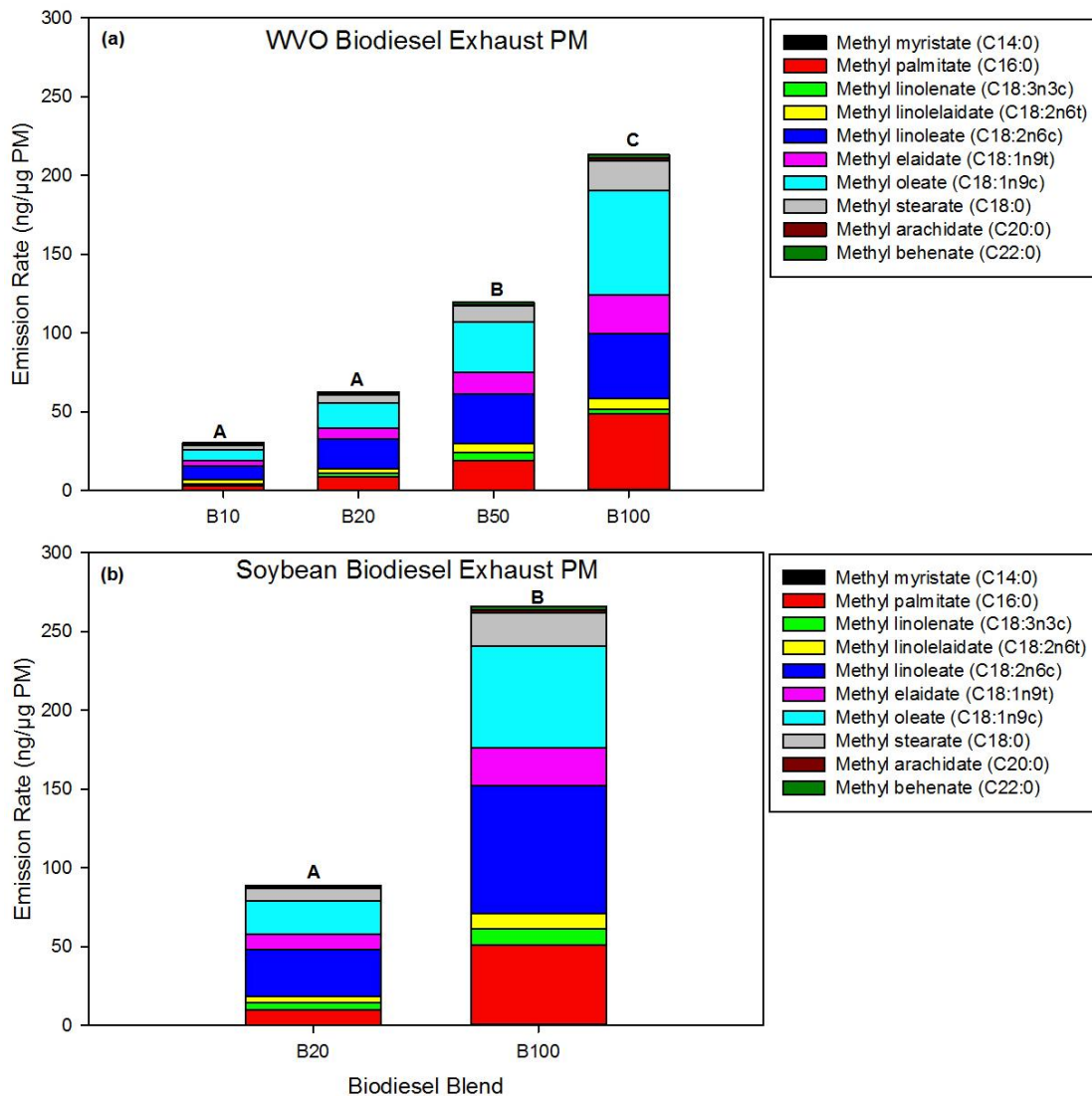


**Figure 3.7** Emission rates (ng/ $\mu$ g) of total FAMES (sum of emission rates of the speciated FAMES) in the exhaust PM of (a) WVO biodiesel blends, and (b) soybean biodiesel blends. For WVO, n = 3; For Soybean, n = 2.

The emission rates of the total speciated FAMES in soybean B100 exhaust PM were 3 times higher than those in soybean B20 exhaust PM, and the differences were statistically significant (p-value=0.0083). These observations are consistent with previous studies, for example, Magara-Gomez et al. (2012) observed increasing emissions of FAMES with increasing biodiesel content in the fuel when a John Deere

agricultural tractor was fueled with soybean and beef tallow biodiesel feedstocks. The authors found that the emission rates of the total FAMES in the soybean B100 exhaust PM were about 4 times greater than those of the soybean B50 PM, while the emission rates of the total FAMES in the beef tallow B100 exhaust PM were about 3 times greater than those of beef tallow B50 PM. The increase in FAME emission rates with increasing biodiesel indicates that the amount of unburned biodiesel fuel in the exhaust increased as the concentration of biodiesel in the fuel increased.

Because of the unique emission of FAMES from biodiesel combustion, FAMES could be used as molecular markers of biodiesel combustion. No studies, however, have used FAMES as biomarkers of biodiesel combustion. The main reasons for not including such species as potential markers of biodiesel combustion could be due to lack of knowledge about detailed organic aerosol chemical speciation, the wide variety of biodiesel sources, and thus, variety in FAMES composition (Hoekman et al., 2012; Magara-Gomez et al., 2012).

The emission rates of the total FAMES in soybean B20 exhaust PM were 1.4 times higher than those in WVO B20 exhaust PM, and the difference was statistically different (p-value = 0.0114). The emission rates of the total FAMES in soybean B100 exhaust PM were 1.2 times higher than those in WVO B100 exhaust PM, but the differences were not statistically significant (p-value = 0.1499). The differences in the emission rates of the total FAMES in WVO B20 and soybean B20 could be partly due to differences in the sampling conditions such as ambient temperature and RH experienced during the emissions tests of the two feedstocks.

### **3.1.4 Carbonyl and Quinone Emissions**

The emission rates of the speciated carbonyls (22 target analytes) and quinones (4 target analytes) in WVO and soybean biodiesel exhaust PM are shown in Figures 3.8 and 3.9, respectively. Carbonyls were divided into four different groups: aliphatic aldehydes (7 target analytes), aliphatic ketones (6 target analytes), aromatic aldehydes (4 target analytes), and aromatic ketones (5 target analytes). The emission rates of the carbonyls in the exhaust PM of the different biodiesel blends compared to petrodiesel exhaust PM either increased or decreased based on the group of compounds. The variations in the emission rates of the various carbonyl groups in the different WVO and soybean biodiesel blends are discussed below.



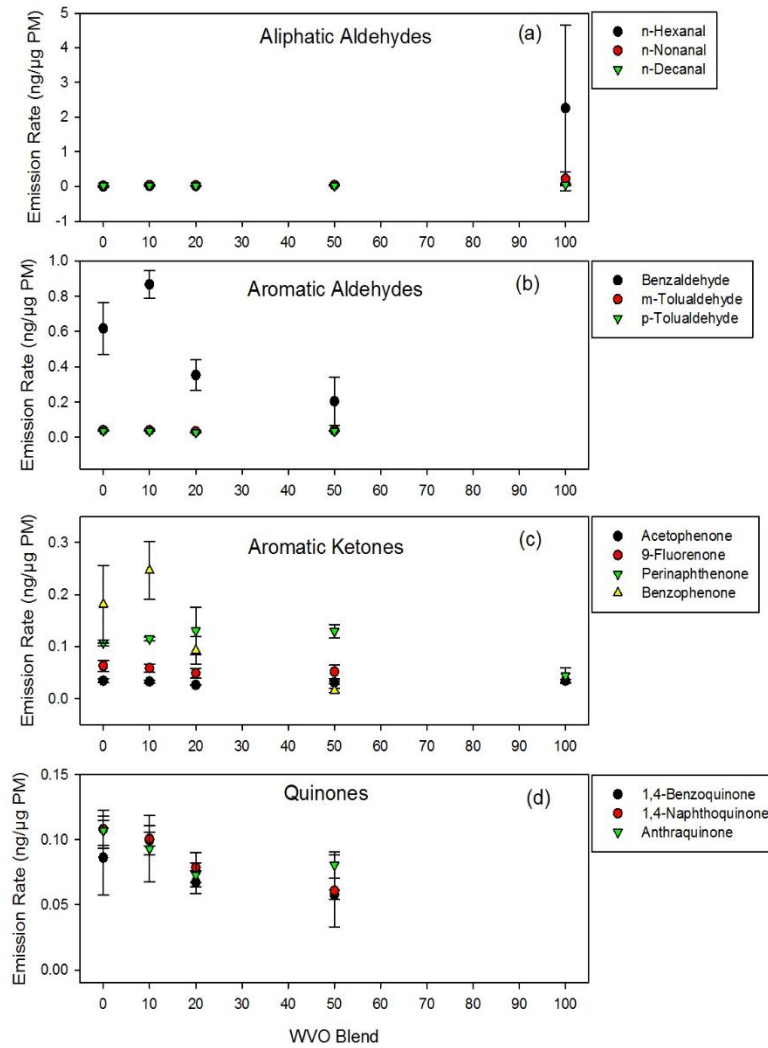


**Figure 3.8 Average emission rates (ng/μg) of (a) Aliphatic aldehydes (b) Aromatic aldehydes (c) Aromatic ketones, and (d) Quinones in exhaust PM resulting from the combustion of WVO biodiesel blends. Error bars represent one standard deviation across triplicate (n=3) emission tests. Note that the y-axis scales are different for all plots.**

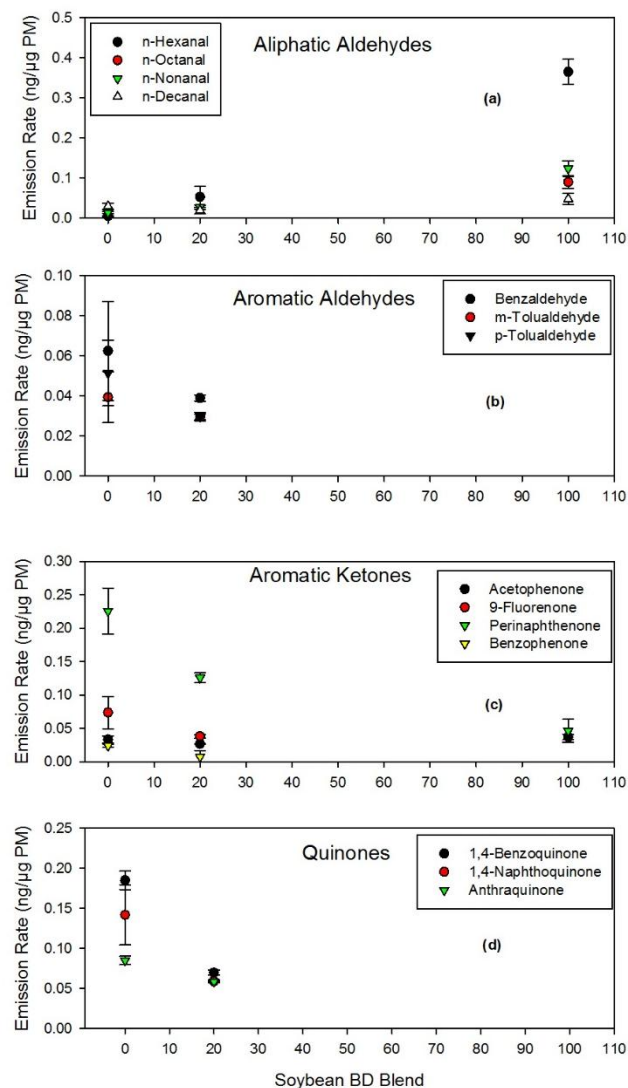


**Figure 3.9** Average emission rates (ng/ $\mu$ g) of (a) Aliphatic aldehydes (b) Aromatic aldehydes (c) Aromatic ketones, and (d) Quinones in PM resulting from the combustion of soybean biodiesel blends. Error bars represent one standard deviation across duplicate (n=2) emission tests. Note that the y-axis scales are different for all plots.

In general, the emission rates of the three aliphatic aldehydes (n-hexanal, n-nonanal, and n-decanal) increased with increasing WVO biodiesel in the fuel (Figure 3.10). High variability was observed in the n-hexanal emission rates for WVO B100, and that could be due to losses of n-hexanal during blowdown because of its relatively high

volatility. The emission rates of the total aliphatic aldehydes (sum of emission rates of the 3 detected species) increased by 56.2%, 35.9%, and 103% for WVO B10, B20, and B50 exhaust PM, respectively, compared to B00. The total aliphatic aldehyde emission rates measured in WVO B100 increased by 4800.0% compared to petrodiesel, due to the extremely high, but variable n-hexanal emissions. The differences in emission rates of the total aliphatic aldehydes of the different blends of WVO biodiesel fuel (WVO B10, WVO B20, and WVO B50) and B00 were not significant, while the differences between the WVO B100 and B00 were significant (Figure 3.10). The emission rates of the aliphatic aldehyde species in soybean biodiesel exhaust PM also increased with increasing biodiesel content in the fuel (Figures 3.9 and 3.11). n-Octanal, which was not detected in any WVO tests, was detected in the soybean B100 exhaust PM, although it was not detected in the B00 and B20 blends of the soybean feedstock. The emission rates of the total aliphatic aldehydes increased by 106.0% and 1200.0% in the soybean B20 and B100 exhaust biodiesel PM, respectively, compared to petrodiesel PM. The differences in the emission rates of the total aliphatic aldehydes in soybean B20 and B00 were not significant, while the difference in emissions of total aliphatic aldehydes in soybean B100 and B00 were significant (Figure 3.11). Furthermore, the differences in the emission rates of the total aliphatic aldehydes for the corresponding WVO and soybean biodiesel blends (B00, B20, and B100) were not statistically significant.

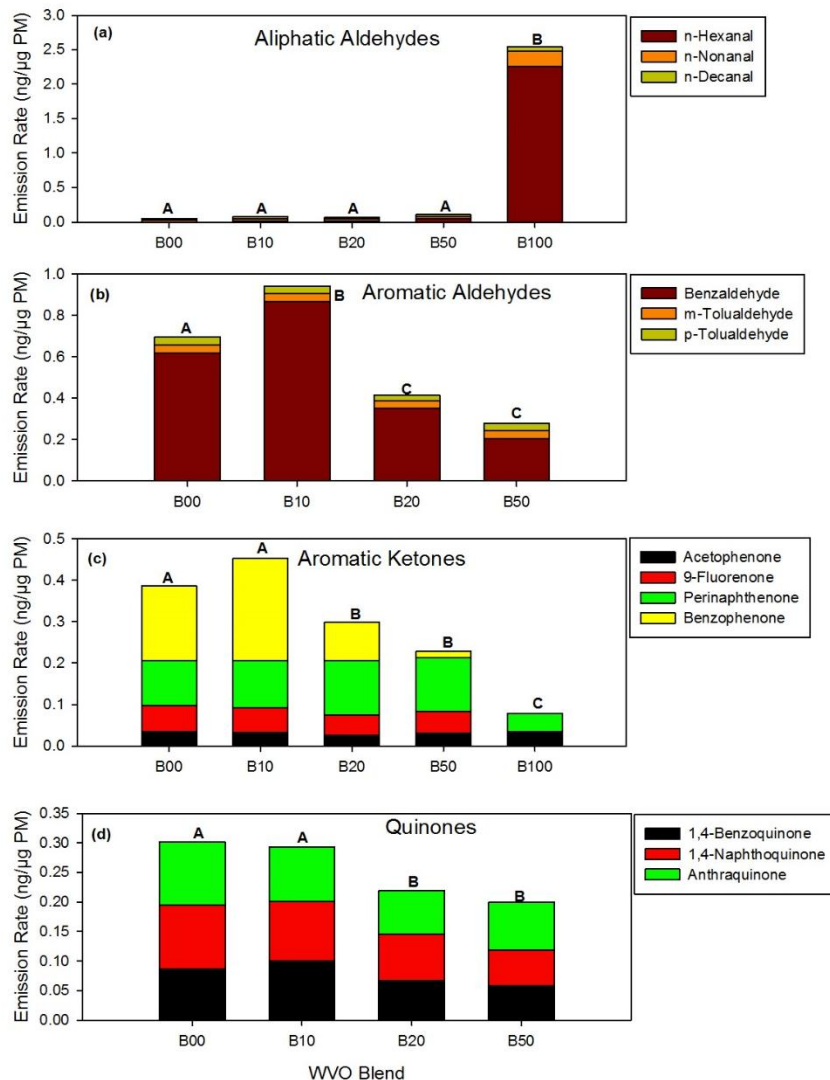


**Figure 3.10** Emission rates (ng/μg) of total (a) Aliphatic aldehydes, (b) Aromatic aldehydes, (c) Aromatic ketones, and (d) Quinones in the exhaust PM resulting from combustion of WVO biodiesel blends.  $n = 3$ . Note that the y-axis scales are different for all plots.

Increasing the biodiesel content in the fuel increased the emission rates of the aliphatic aldehydes for both biodiesel feedstocks. Such compounds would partition in both the gas and particle phases because of their properties. Previous studies (e.g., Turrio-Baldassarri et al., 2004; Pang et al., 2006; Correa and Arbilla, 2008; Karavalakis et al., 2011, and Cahill and Okamoto, 2012) that measured gas-phase aliphatic aldehydes

in diesel and biodiesel exhaust PM found that the emissions increased with increasing biodiesel content in the fuel. The gas-phase aliphatic aldehydes that were studied in those previous studies were formaldehyde, acetaldehyde, propionaldehyde, and butyraldehyde. Cahill and Okamoto (2012) also measured gas plus particle-phase n-nonanal and n-decanal, which they found to increase with increasing biodiesel content when emissions from two heavy-duty diesel trucks fueled with petrodiesel, soybean biodiesel, animal biodiesel, and renewable diesel were measured. The increase in aliphatic aldehyde emissions with increasing biodiesel is attributed to oxidation of the methyl ester molecules in biodiesel (Correa and Arbilla, 2008). It is important to note that some studies have, however, reported decreases in aliphatic aldehydes with increasing biodiesel content in the fuel (e.g., Guarieiro et al., 2008). The disparities in emissions with use of biodiesel may be due to differences in factors such as biodiesel feedstock, engine type, drive cycle, and operating conditions (Correa and Arbilla, 2008).

Aliphatic ketones such as 2-pentanone, 2-hexanone, 2-heptanone, 2-nonanone, and 2-octanone were not detected with very good certainty. The concentrations of these compounds were below the method detection limits and, therefore, their results are not discussed.

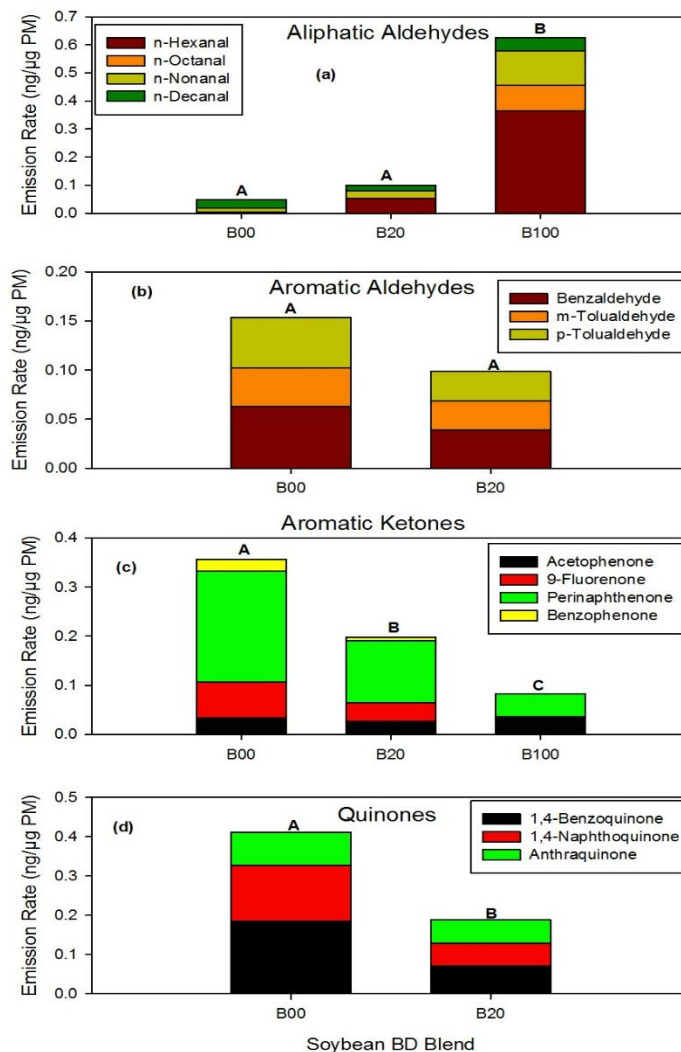


**Figure 3.11** Emission rates (ng/μg) of total (a) Aliphatic aldehydes, (b) Aromatic aldehydes, (c) Aromatic ketones, and (d) Quinones in the exhaust PM resulting from combustion of soybean biodiesel blends.  $n = 2$ . Note that the y-axis scales are different for all plots.

The aromatic aldehydes detected in the exhaust PM of both feedstocks include, benzaldehyde, m-tolualdehyde, and p-tolualdehyde (Figures 3.8 to 3.11). In general, the emission rates of the aromatic aldehydes decreased with increasing fuel biodiesel content. Benzaldehyde was the most dominant aromatic aldehyde detected in the WVO biodiesel exhaust, but it was detected at an order of magnitude lower concentration in the soybean

blends. Surprisingly, benzaldehyde increased in the WVO B10 exhaust PM compared to B00. Because of the high emission rate of benzaldehyde for WVO B10, the emission rates of the total aromatic aldehydes increased by 35.7% in WVO B10 compared to B00. The emission rates of the total aromatic aldehydes decreased by 40.6% and 60.0% in WVO B20 and B50, respectively, compared to B00. The aromatic aldehydes in WVO B100 were below the detection limits. The differences in total aromatic aldehyde emission rates of the different WVO blends and B00 were significant (Figure 3.10)

The emission rates of the total measured aromatic aldehydes in soybean B20 decreased by 36.0% compared to B00, while all aromatic aldehyde concentrations were below the detection limits in the soybean B100 exhaust PM (Figure 3.11). The differences in total aromatic aldehyde emission rates of soybean B20 and B00 were not significant, while the differences in total aromatic aldehyde emission rates of soybean B100 and B00 were significant. The emissions of gas- and particle-phase aromatic aldehydes have been previously reported to decrease with increasing biodiesel (Pang et al., 2006; Correa and Arbilla, 2008; Karavalakis et al., 2011, and Cahill and Okamoto 2012). It is likely that aromatic aldehydes are emitted as a result of the incomplete combustion of the aromatic compounds in the fuel. Because there are no aromatic compounds in biodiesel, the emissions of the aromatic aldehydes decrease with increasing biodiesel content in the fuel (Correa and Arbilla, 2008; Karavalakis et al., 2011).

Because of the moderately high vapor pressures of the three detected aromatic aldehydes of 1.01, 0.349, and 0.263 mm Hg at 25 °C for benzaldehyde, m-tolualdehyde, and p-tolualdehyde, respectively, all of them (detected aromatic aldehydes) partition

mostly in the gas phase. It is, therefore, likely that some of the emissions of the detected aromatic aldehydes were gas-phase emissions that adsorbed on the exhaust PM.

Four aromatic ketones (acetophenone, 9-fluorenone, perinaphthenone, and benzophenone) were detected in both WVO and soybean biodiesel exhaust PM (Figures 3.8 to 3.11). Benzophenone was the most abundant aromatic ketone detected in the WVO biodiesel exhaust PM, while perinaphthenone was the most abundant aromatic ketone detected in the soybean biodiesel exhaust PM. As observed for the aromatic aldehydes, the emission rates of the aromatic ketones generally decreased with increasing biodiesel content in the fuel. However, the emission rates of perinaphthenone increased by 7.3%, 21.7%, and 20.7% in WVO B10, B20, and B50, respectively, compared to B00. The benzophenone emission rates increased by 35.8% in WVO B10 compared to B00. The emission rates of the total aromatic ketones compared to B00 increased by 17.2% in WVO B10 and decreased by 22.7%, 40.9%, and 79.6% in WVO B20, WVO B50, and WVO B100, respectively. The increase for WVO B10 was mainly due to the high emission rates of benzophenone and perinaphthenone. On the other hand, the emission rates of perinaphthenone decreased with increasing biodiesel in the soybean sequence, where 44.3% and 79.5% decreases were observed for soybean B20 and B100 exhaust PM, respectively, compared to B00. The total aromatic ketone emission rates decreased by 44.6% in soybean B20 exhaust PM compared to B00. The 9-fluorenone and benzophenone concentrations in WVO and soybean B100 were below the detection limits. For the WVO sequence, the differences in total aromatic ketone emission rates between all fuel blends and B00 were significant with the exception of B10 (Figure 3.10). Also, the differences in total aromatic ketone emission rates between soybean B20,



soybean B100 and B00 were significant (Figure 3.11). With the exception of the B20 biodiesel blends, the differences in total aromatic ketone emission rates of the other corresponding WVO and soybean biodiesel blends (B00 and B100) were not significant.

The observations made for the aromatic ketones concur with those made for the aromatic aldehydes, whereby the emission rates generally decreased with increasing biodiesel in the fuel. These results support prior suggestions that the absence of aromatic compounds in biodiesel fuel leads to the reduction in emission of aromatic compounds (Cahill and Okamoto 2012).

Three quinones detected with high confidence in the exhaust PM of both WVO and soybean biodiesel were 1,4-benzoquinone, 1,4-naphthoquinone, and anthraquinone. The emission rates of the quinones generally decreased with increasing biodiesel, with the exception of 1,4-benzoquinone which increased by 15.5% in WVO B10 exhaust PM compared to B00. The concentrations of all quinones were below the detection limits in both WVO and soybean B100 exhaust PM. The emission rates of the total quinones decreased by 2.7%, 27.4%, and 34% in WVO B10, B20, and B50, respectively, compared to B00. The differences in total quinone emission rates between WVO B10 and B00 were not significant, while the differences between WVO B20, B50, and B100 and B00 were significant (Figure 3.10). For soybean feedstock biodiesel, there was a higher total quinone emission rate decrease for B20 of 54.5% compared to B00 than observed for WVO. Further, no quinones were detected in soybean B100 exhaust PM. The differences in total quinone emission rates between the soybean biodiesel fuel blend and B00 were significant (Figure 3.11). With the exception of neat biodiesel fuels where

quinones were not detected, the total quinone emission rates for the corresponding WVO and soybean fuels blends (B00 and B20) were significant.

No prior studies have quantified the emissions of quinones in biodiesel exhaust PM although quinones, including those identified in the present study, have been previously measured and quantified in exhaust from light-duty gasoline vehicles and heavy-duty diesel engines fueled with petrodiesel in both the gas and particle phases (e.g., Cho et al., 2004; Valavanidis et al., 2006; Jakober et al., 2007). Results here show that the emissions of the three quinones generally decreased with increasing biodiesel content for both biodiesel feedstocks at >20% blend ratio. These results support the observation that aromatic compound emissions in diesel exhaust PM originate from the incomplete combustion of the aromatic compounds in petrodiesel fuel. The absence of aromatic compounds in biodiesel fuel therefore leads to the 3-50% reduction in the emission of quinones in biodiesel exhaust PM for the B10 to B50 blends, and complete removal of quinones in the exhaust when operating on 100% neat biodiesel.

## **3.2 Comparison of Organic Composition of Fuel and Particulate Matter from a Light-Duty Diesel Engine Fueled with Diesel and Biodiesel**

The main objective of this section was to compare the organic chemical composition of the fuels (B00, WVO blends, and soybean blends) to that of the PM generated from combustion of the respective fuels in the CM-12 light-duty diesel engine.

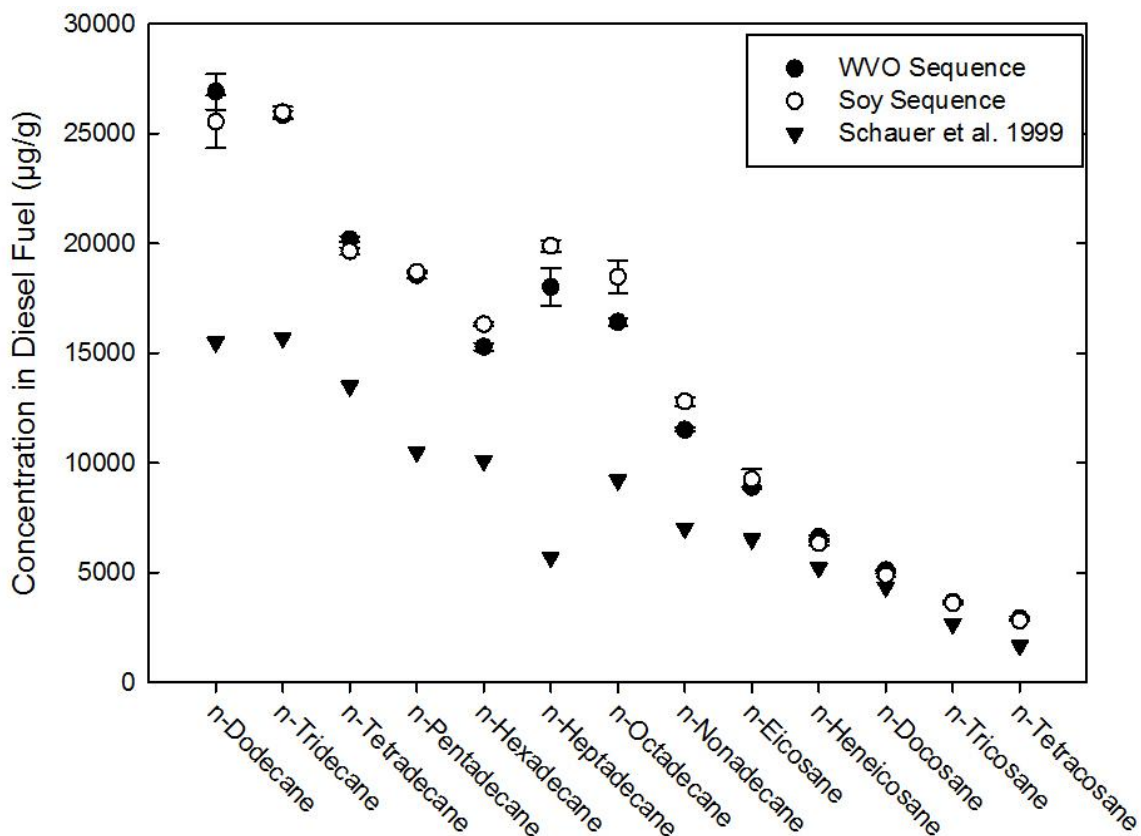
### **3.2.1 Organic Composition of Fuels**

#### ***3.2.1.1 n-Alkanes in Fuel***

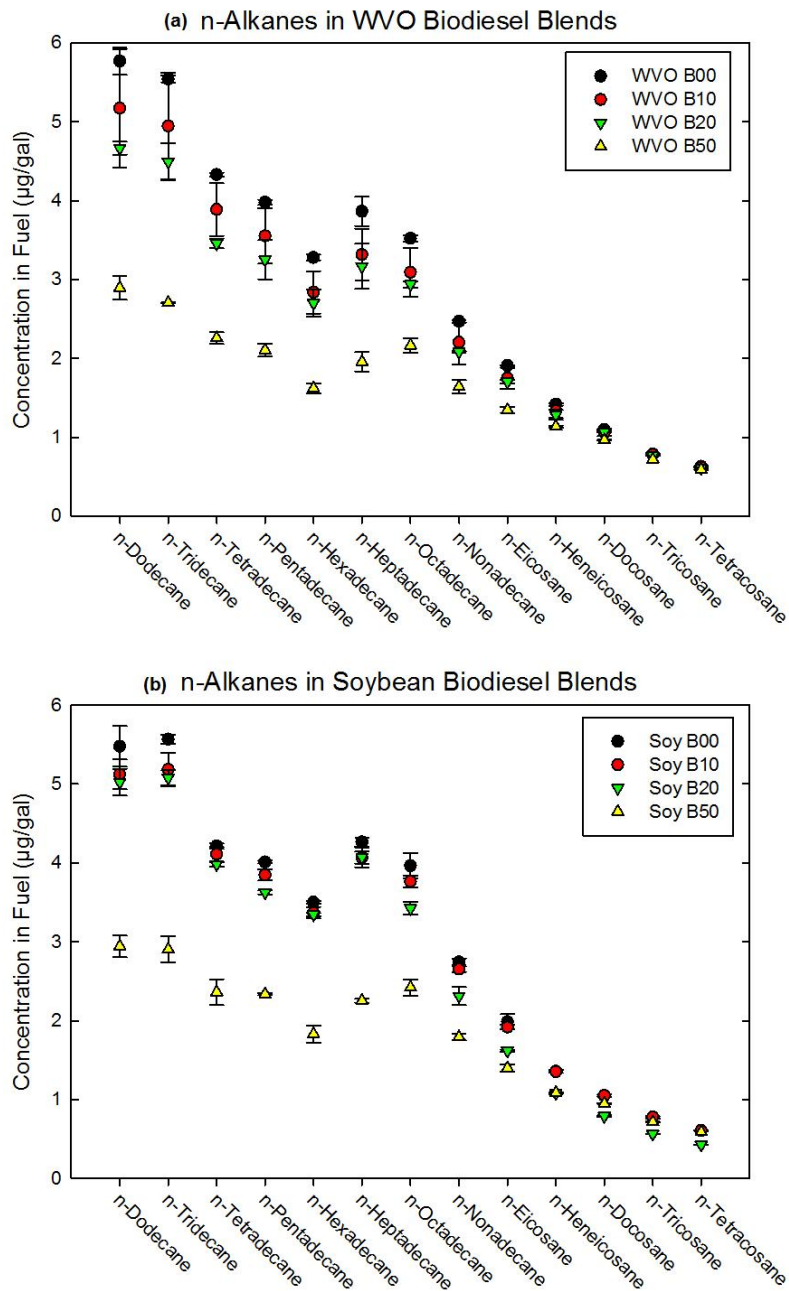
The n-alkanes speciated in the petrodiesel fuel used to prepare the WVO biodiesel and soybean biodiesel fuel blends are shown in Figure 3.12. The n-alkanes detected ranged from C<sub>12</sub> to C<sub>24</sub>, and their concentrations in any fuel blend generally decreased with increasing number of carbon atoms. These results are in agreement with previous studies such as Rogge et al. (1993), Schauer et al. (1999), and Erickson et al. (2012) that reported that aliphatic hydrocarbons in diesel fuel range from C<sub>10</sub> to C<sub>25</sub>. Compared to the California diesel fuel used by Schauer et al. (1999), all the individual n-alkanes existed at higher concentrations (1.1 to 3.5 times higher) in the diesel fuel used in the present study (Figure 3.12). n-Dodecane was the most abundant n-alkane detected in the diesel fuel. Note that fuel concentration units in this study are expressed in µg/gal, but the units in Figure 3.12 are expressed in µg/g for the sake of comparison with the results from the Schauer et al. (1999) study.

Figure 3.13 shows the distributions of the n-alkanes in the WVO biodiesel and soybean biodiesel fuel blends. The concentrations of the n-alkanes were greatest in the

B00 fuel for both the WVO and soybean test sequences, as expected. No n-alkanes were detected in the neat WVO and soybean fuels. In general, the concentrations of the individual n-alkane species in the WVO and soybean biodiesel fuel blends decreased with increasing biodiesel content in the fuel. Furthermore, the concentrations of the total n-alkanes (sum of all n-alkanes) linearly decreased with increasing biodiesel in the fuel for both feedstocks (Figure 3.14). The regression equations for the total n-alkanes in the WVO and soybean biodiesel blends were quite similar. This, therefore, implies that in terms of n-alkanes content in the fuel, the petrodiesel batch used to prepare the WVO biodiesel blends was similar to that used to prepare the soybean biodiesel blends.



**Figure 3.12** Distribution of n-alkanes in the petrodiesel fuel used to prepare the WVO and soybean biodiesel blends. Error bars refer to one standard deviation. n = 2.



**Figure 3.13** Concentrations ( $\mu\text{g/gal}$ ) of n-alkanes measured in the WVO and soybean biodiesel fuel blends. Error bars refer to one standard deviation.  $n = 2$ . No n-alkanes were detected in the neat biodiesel fuels.

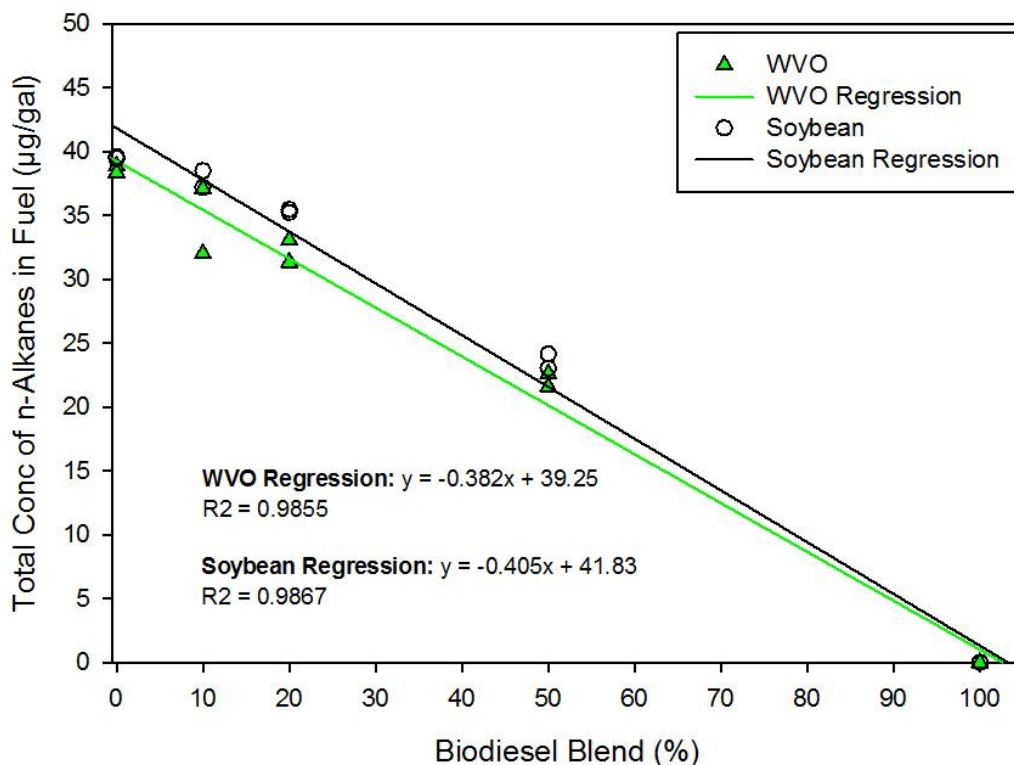
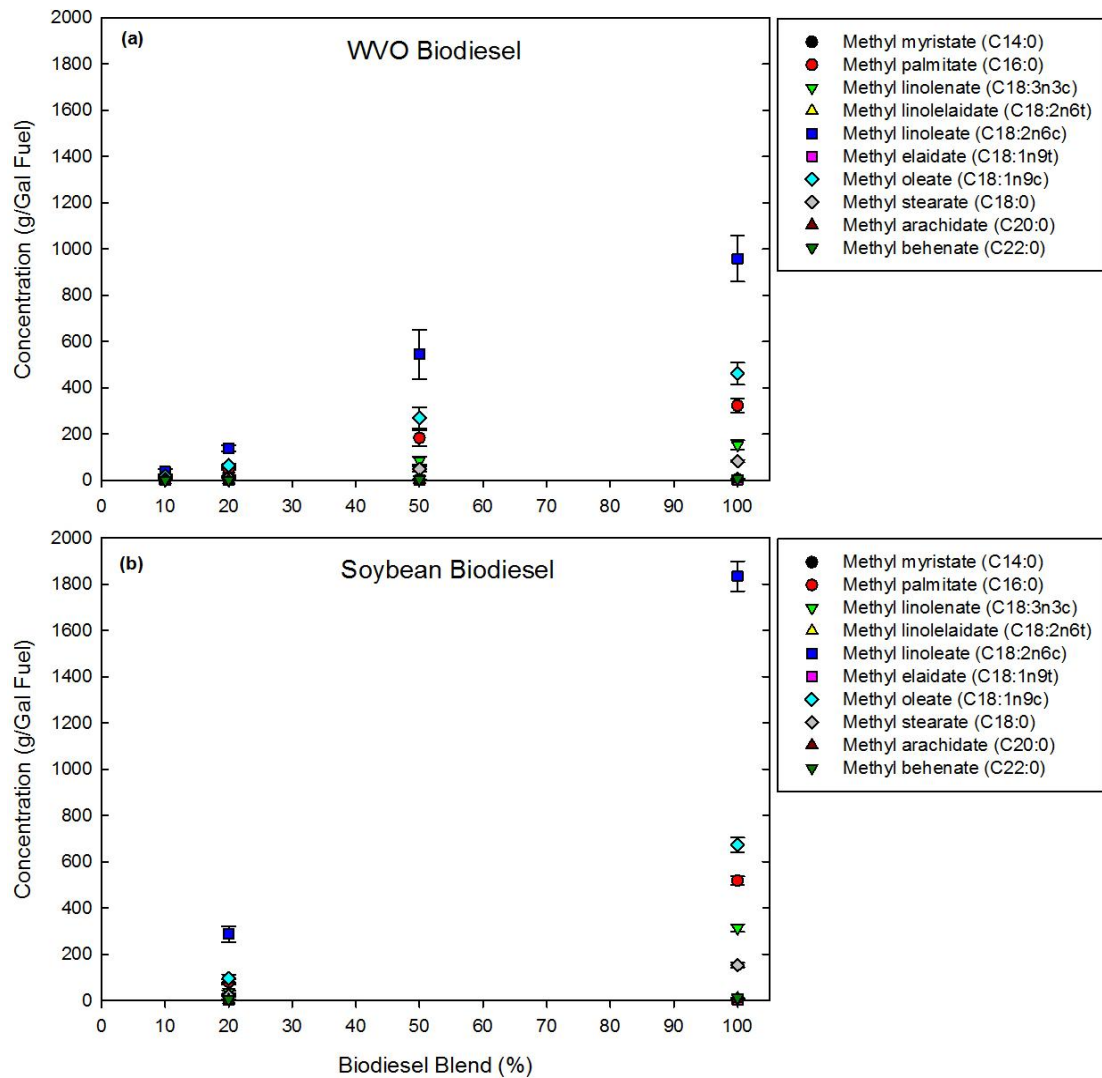


**Figure 3.14 Concentration of n-alkanes ( $\mu\text{g}/\text{gal}$ ) in diesel (B00) and biodiesel fuel blends from both feedstocks.**

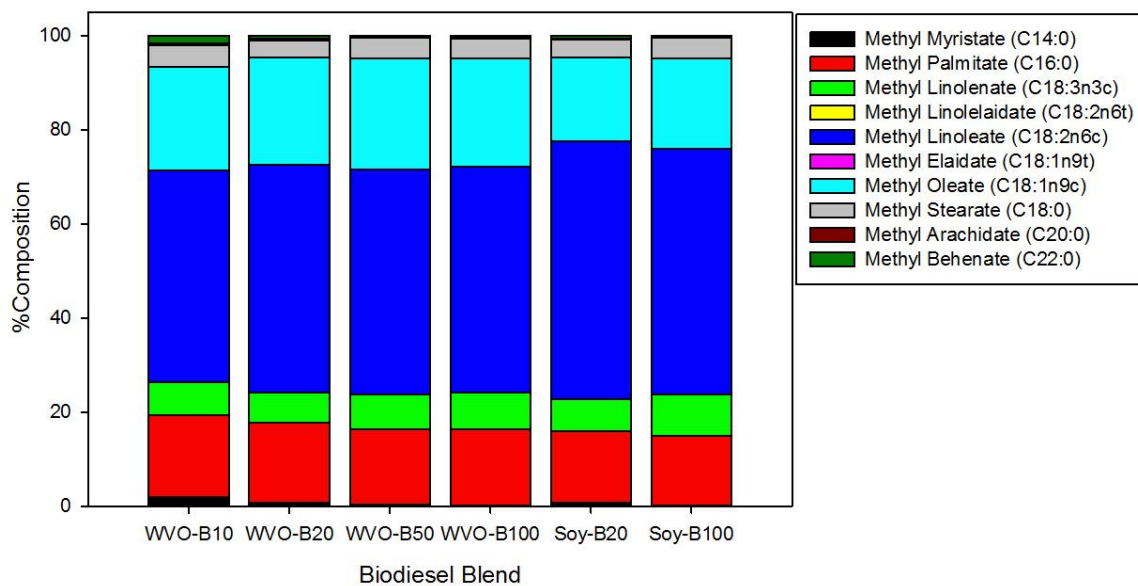
### 3.2.1.2 FAMES in Fuel

Figure 3.15 shows the concentrations of the FAME species in the WVO and soybean biodiesel fuel blends. Figure 3.16 shows the percent composition of the FAMES in the WVO and soybean biodiesel fuel blends. The speciated FAMES in this study were methyl esters of the most naturally occurring fatty acids in plant oils. The most dominant FAMES in the neat WVO biodiesel (B100) fuel were methyl linoleate ( $48.0 \pm 0.1\% = 959 \pm 99.5 \text{ g}/\text{gal}$ ), methyl oleate ( $23.1 \pm 0.1\% = 461.2 \pm 47.9 \text{ g}/\text{gal}$ ), and methyl palmitate ( $16.2 \pm 0.2\% = 323.2 \pm 30.0 \text{ g}/\text{gal}$ ). Based on the FAMES compositional profiles in the literature (e.g., Hoekman et al., 2012 and references therein), the WVO biodiesel used in this study was most likely derived from soybean cooking oil. This is because the FAMES

compositional profiles for WVO were more similar to those of soybean than any other feedstock reported in the literature. The FAMES compositional profiles for the B10, B20, and B50 WVO fuel blends were all similar to those of the neat WVO biodiesel as seen in Figure 3.16.



**Figure 3.15 FAME concentrations (g/gal fuel) of the different blends of WVO and soybean biodiesel fuels. Error bars refer to one standard deviation. For WVO, n = 2; For Soybean, n = 4. No FAMES were detected in the petrodiesel fuel, while methyl linolelaidate and methyl elaidate were not detected in any of the biodiesel fuel blends.**



**Figure 3.16 Average percent composition of FAMES in the WVO and soybean biodiesel fuel blends.**

Further, methyl linolelaidate and methyl elaidate were not detected in any of the biodiesel blends even when large concentrations (100 ppm) of the fuels were analyzed. For the neat soybean biodiesel (B100), the most dominant FAMES were methyl linoleate ( $52.2 \pm 0.3\% = 1833.3 \pm 65.1$  g/gal), methyl oleate ( $19.1 \pm 0.2\% = 671.6 \pm 32.2$  g/gal), and methyl palmitate ( $14.7 \pm 0.2\% = 517.3 \pm 19.0$  g/gal). The FAME profiles observed in soybean B20 were similar to those observed in the neat soybean B100 biodiesel fuel. The soybean B20 biodiesel had methyl linoleate ( $54.6 \pm 0.9\% = 286.1 \pm 33.6$  g/gal), methyl oleate ( $18.0 \pm 1.1\% = 94.2 \pm 17.3$  g/gal), and methyl palmitate ( $15.2 \pm 0.3\% = 79.7 \pm 10.3$  g/gal). The compositional profiles of the FAMES in the neat soybean biodiesel obtained in this study are similar to those reported in the literature by Hoekman et al. (2012). The authors reported that the most abundant FAMES in soybean biodiesel are methyl linoleate ( $53.8 \pm 3.5\%$ ), methyl oleate ( $23.7 \pm 2.4\%$ ), and methyl palmitate ( $11.6 \pm 2.0\%$ ) when they



compiled data from a variety of literature studies that measured FAMES in soybean biodiesel.

It is important to note that much as the neat B100 WVO and soybean biodiesel fuels had quite similar FAME compositional profiles, the amounts (mass) of the individual FAMES in soybean biodiesel were greater than those in WVO biodiesel (Figure 3.16). This observation could partly suggest that the soybean waste cooking oil used in the preparation of the WVO biodiesel fuel probably lost some of the fatty acids during the process of cooking/frying as it became waste/used cooking oil. Therefore, the fatty acids lost during cooking/frying for the case of the waste cooking oil were not available for transesterification of the waste cooking oil. It is also highly possible that the waste cooking oil used in making the WVO biodiesel had a small amount of canola waste cooking oil mixed with a very large amount of soybean waste cooking oil. This is because the percent composition of methyl oleate was slightly higher in the WVO biodiesel compared to that in soybean biodiesel ( $23.1\pm 0.1\%$  in WVO versus  $19.1\pm 0.2\%$  in soybean biodiesel). Also, the percent composition of methyl linoleate in the WVO biodiesel was slightly lower than that in the soybean biodiesel. The average percent compositions of methyl oleate and methyl linoleate in canola biodiesel have been previously reported to be  $\sim 60.4\pm 2.9\%$  and  $\sim 21.2\pm 1.8\%$ , respectively (Hoekman et al., 2012). Therefore, it is likely that a small amount of canola waste cooking oil was added to the soybean waste cooking oil to make the WVO biodiesel used in the present study.

The ratios of the total FAMES in the neat WVO biodiesel (B100) fuel to those in the WVO biodiesel fuel blends were  $22.9\pm 5.9$ ,  $6.6\pm 0.6$ , and  $1.7\pm 0.3$  for B10, B20, and B50, respectively. With the exception of WVO B10 that had a very large deviation from

the expected value of 10, the rest of the WVO biodiesel fuel blends had the ratios of the total FAMES in agreement with the expected values (5 for B20, and 2 for B50). For the soybean biodiesel fuel, the ratio of the total FAMES in the neat soybean fuel (B100) to that of soybean B20 was  $6.5 \pm 0.8$  as opposed to the expected value of 5. The lack of agreement between the experimental and expected ratios especially for the B10 biodiesel blends could be due to analytical problems associated with analyzing the B10 biodiesel samples because of the low concentrations of the target analytes in such fuel samples. It is also possible that there were errors made in mixing the B10 biodiesel blends in the laboratory, and that the B10 blends were not actually 10% biodiesel.

### ***3.2.1.3 PAHs/Aromatic Hydrocarbons in Fuel***

None of the 16 EPA PAHs were detected in the two petrodiesel fuel batches or any of the WVO and soybean biodiesel fuel blends and neat B100 biodiesel fuel. Some old and recent studies have reported detection of PAHs in diesel fuel. For example, Williams et al. (1989), Schauer et al. (1999), Mi et al. (2000), Brandenberger et al. (2005), and Lim et al. (2005) all reported detection of unsubstituted PAHs in the diesel fuel used in their respective studies. Schauer et al. 1999 reported naphthalene, fluorene, phenanthrene, anthracene, and pyrene concentrations in a commercial California diesel fuel ranging between 5 and 600  $\mu\text{g/g}$ . A study in Australia by Lim et al. (2005) reported that the total PAH concentration (naphthalene, acenaphthylene, acenaphthene, fluorene, phenanthrene, anthracene, fluoranthene, and pyrene) in ULSD (sulfur content = 50 ppm) was about 3 times lower than that of low sulfur diesel (LSD, sulfur content = 500 ppm). Lim et al. (2005) further found that the total aromatic content of the LSD was about 1.7

times higher than that of the ULSD. Nelson et al. (2008) also found that the diesel fuels that had higher amounts of sulfur had higher concentrations of PAHs when diesel fuels with 24-1700 ppm of sulfur were analyzed for PAHs. It is therefore possible that the high sulfur content of the diesel fuels used in previous studies was responsible for the high concentrations of PAHs detected in those fuels. For the present study, the sulfur content of the diesel fuel was 1.2 ppm (Table 2.1).

The aromatic hydrocarbons detected in the petrodiesel fuel used in this study are shown in Table 3.5. The only PAHs detected were substituted naphthalenes (naphthalene, 1,2,3,4-tetrahydro, naphthalene, 2-chloro, and naphthalene, 1,6,7-trimethyl) and substituted benzenes (Table 3.5). Unsubstituted PAHs were not detected in the diesel fuel used in this study probably because of the recent efforts to reformulate the diesel fuel, which would lead to a reduction in the emissions due to diesel combustion such as the unsubstituted PAHs. The reformulation of the current diesel fuel is possibly performed by reducing the aromatic composition of the fuel, and by also reducing the amount of aromatic additives in the diesel (Westerholm and Li 1994; Marr et al., 1999). Furthermore, because previous studies showed a relationship between the sulfur content and PAH concentrations in the diesel fuel, it is likely that the regulations requiring use of ULSD in diesel engines also led to the reduction of PAHs in diesel fuel. The EPA's Clean Air Highway Diesel rule of 2001 (US EPA 2006), that took effect in 2006 requires use of diesel fuel with a sulfur content not greater than 15 ppm in the United States. Therefore, these regulations on diesel fuel could have led to the low PAH concentrations in the diesel fuels in use since the 2006 diesel fuel regulation went into effect.

**Table 3.5 Aromatic hydrocarbons detected in diesel fuel.**

<b>Benzenes</b>	<b>Naphthalenes</b>	<b>Other Aromatics</b>
Benzene, 1-methyl-4-(1-methylethyl)	Naphthalene, 2-chloro	Isopropyl phenyl ketone
Benzene, 1,2,3,5-tetramethyl	Naphthalene, 1,6,7-trimethyl	1H-Indene, 2,3-dihydro-4,7-dimethyl
Benzene, 1-ethyl-2,5-dimethyl	Naphthalene, 1,2,3,4-tetrahydro	2H-1-Benzopyran-2-one, 3-methyl
Benzene, pentamethyl	2(1H)naphtholenone, 3,4-dihydro	1(3H)-Isobenzofuranone, 3-propylidene
Benzene, 1-ethyl-3-(1-methylethyl)	1H-Imidazole, 4,5-dihydro-2-(1,2,3,4-tetrahydro-1-naphthalenyl)	N-Nitrosodiphenylamine
Benzene, 1-(1,1-dimethylethyl)-3-methyl		1(3H)-Isobenzofuranone, 3-butylidene
Benzene, 1,3-bis(1-methylethyl)		

#### ***3.2.1.4 Carbonyls and Quinones in Fuel***

For the three fuel blends that were derivatized (i.e., WVO B00, WB20, and WVO B100), none of the target carbonyls and quinones were detected. This, therefore, indicates that the petrodiesel fuels, and WVO biodiesel fuels did not contain any of the target carbonyls and quinones. Because no carbonyls were seen in the WVO biodiesel blends, it was assumed that the soybean biodiesel blends did not contain carbonyls and quinones, and thus, the soybean biodiesel blends were not analyzed for the carbonyls and quinones. Any of the carbonyls and quinones detected in the exhaust PM would thus be a result of fuel and lubricating oil combustion in the engine.

#### ***3.2.1.5 Analysis of the Lubricating Oil***

No target PAHs were detected in the two lubricating oil samples that were analyzed by TD-GC/MS. None of the target n-alkanes (C<sub>12</sub> to C<sub>36</sub>) were detected as well. However, hydrocarbons with molecular weights equal to the molecular weights of the

target n-alkanes were detected but not quantified. Most of the hydrocarbons detected in the lubricating oil were unresolvable, and eluted under the unresolved complex mixture (UCM) in the chromatogram (Figure 3.17). The lubricating oil UCM most likely consisted of branched alkanes and cycloalkanes with 24 to 36 carbon atoms (Mao et al., 2009) that could not be separated by our chromatographic technique. Hydrocarbon compounds with up to 40 carbon atoms were also detected although at relatively low abundances. Lubricating oils have been previously reported to have final boiling points ranging between 400 and 500 °C, and they also consist of hydrocarbon mixtures with C<sub>14</sub> to C<sub>45</sub> (Rogge et al., 1993). Furthermore, it can be seen in Figure 3.17 that the petrodiesel fuel consisted mainly of the low and medium boiling point n-alkanes (C<sub>11</sub>-C<sub>24</sub>), while the WVO and soybean biodiesel feedstocks consisted of FAMES.

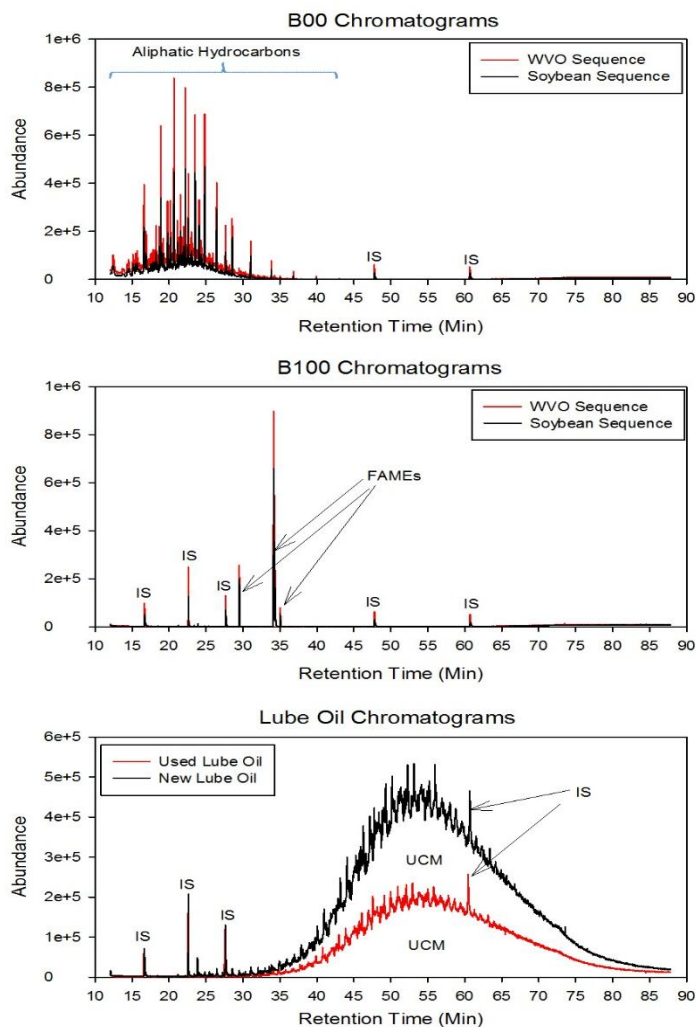


**Figure 3.17 Chromatograms of diesel (B00), neat biodiesel (B100) fuels, and lubricating oil. IS means Internal Standard, which were acenaphthene-d10, phenanthrene-d10, anthracene-d10, chrysene-d12, and perylene-d12 in order of elution; UCM means Unresolved Complex Mixture.**

Some studies that have previously performed the organic chemical speciation of lubricating oil reported that lubricating oil mostly consists of branched alkanes, cycloalkanes, and aromatic compounds (e.g., Mao et al., 2009). For example, Mao et al. (2009) investigated the chemical nature of three different brands of brand new (unused) lubricating oil (Castrol SAE30, Esso SAE15W40, and Elf LDX5W40) using high-

performance liquid chromatography followed by two-dimensional gas chromatography. Using this technique, the authors were able to more comprehensively characterize the chemical composition of the lubricating oil than the technique employed in the present study. It was found that all the three oil brands were dominated by branched alkanes and cycloalkanes (Table 3.6). The monoaromatics and PAHs each accounted for less than 10% of the organic carbon mass of all three lubricating oil brands. In the present study, it was not possible to distinguish between the cycloalkanes and monoaromatics because of the difficulty in resolving the UCM. Further, failure to detect the PAHs suggests that there were no PAHs in the lubricating oil used in the present study.

**Table 3.6 Percent composition (%) of the speciated compound groups in lubricating oil samples used by Mao et al. (2009).**

Compounds	Castrol SAE30	Esso SAE15W40	Elf LDX5W40
Branched alkanes	32.8±2.3	35.9±2.4	74.3±2.6
Cycloalkanes	49.5±5.8	46.0±5.1	20.2±6.6
Monoaromatics	8.2±2.9	8.4±2.5	3.0±1.7
PAHs	9.5±3.2	9.7±2.7	2.5±2.4

### 3.2.2 PM Emissions in Biodiesel Exhaust

#### 3.2.2.1 *n*-Alkanes in Biodiesel Exhaust PM

The average emission rate data for the speciated *n*-alkanes in WVO and soybean biodiesel exhaust PM have already been presented in Figures 3.1 and 3.2, and the variations in the emission rates of the *n*-alkanes with respect to biodiesel content in the fuel were discussed in Section 3.1. The most dominant *n*-alkanes in the biodiesel exhaust PM for both feedstocks were the medium molecular weight C<sub>15</sub> to C<sub>26</sub> *n*-alkanes (*n*-pentadecane, *n*-hexadecane, *n*-heptadecane, *n*-octadecane, *n*-nonadecane, *n*-eicosane,

n-heneicosane, n-docosane, n-tricosane, n-tetracosane, and n-hexacosane), and their emission rates generally decreased with increasing biodiesel content in the fuel. In contrast, the most abundant n-alkanes in the diesel fuel and biodiesel fuel blends were both low and medium molecular weight C<sub>12</sub> to C<sub>19</sub> n-alkanes (n-dodecane, n-tridecane, n-tetradecane, n-pentadecane, n-hexadecane, n-heptadecane, n-octadecane, and n-nonadecane) as seen in Figures 3.12 and 3.13. The concentrations of the n-alkane species in the WVO and soybean biodiesel fuel blends also decreased with increasing biodiesel content in the fuel, as expected. The amounts of the C<sub>12</sub> to C<sub>16</sub> n-alkane species compared to those with more than 16 carbon atoms (> C<sub>16</sub>) were lower in the exhaust PM than in the different fuel blends (B00 to B50). The reason for this observation is that the n-alkanes (C<sub>12</sub> to C<sub>16</sub>) are more volatile than larger n-alkanes (> C<sub>16</sub>), and were possibly lost during filter sampling of the exhaust PM due to their volatility. Schauer et al. (1999) found that n-dodecane, n-tridecane, and n-tetradecane all partitioned in only the gas-phase, while n-pentadecane and n-hexadecane mostly partitioned into the gas-phase when gas- and particle-phase tailpipe emissions from medium-duty diesel trucks were measured. As seen in Figures 3.12 and 3.13, n-alkanes with more than 24 carbon atoms (> C<sub>24</sub>) were not detected in the fuel, but they were detected in the exhaust PM. This observation means that the n-alkanes with more than 24 carbon atoms (> C<sub>24</sub>) were probably formed as a result of (a) combustion of the fuel, (b) combustion of the lubricating oil, or (c) combustion of the lubricating oil and fuel. Detection of the n-alkanes in the exhaust PM of WVO B100 and soybean B100 as seen in Figures 3.1 and 3.2 was quite surprising given that no n-alkanes were detected in the neat biodiesel fuels (WVO B100 and soybean B100). Previous studies (e.g., Magara-Gomez et al., 2012)



also reported detection of n-alkanes in the exhaust PM of the neat B100 biodiesel fuels when a 1993 John Deere 7700 model tractor that was not equipped with aftertreatment control technologies was fueled with soybean and animal fat biodiesel feedstocks. Therefore, the n-alkanes detected in the WVO B100 and soybean B100 exhaust PM were either a result of the combustion of the biodiesel fuel, or combustion of the lubricating oil. It is also possible that the n-alkanes in the exhaust PM of the neat fuels were formed from the combustion of the FAMES. Maher and Bressler (2007) and references therein proposed that n-alkanes are formed during the pyrolysis of saturated and unsaturated triglycerides of vegetable oils. During the thermocracking of saturated triglycerides,  $\text{RCOO}^{\cdot}$  and  $\text{RCH}_2\text{O}^{\cdot}$  free radicals are formed (Maher and Bressler, 2007). The odd n-alkanes are formed by decarboxylation of  $\text{RCOO}^{\cdot}$  followed by disproportionation and ethylene elimination (Maher and Bressler, 2007). The even n-alkanes are produced by loss of a ketene from  $\text{RCH}_2\text{O}^{\cdot}$  followed by disproportionation and ethylene elimination (Maher and Bressler, 2007). Because triglycerides of vegetable oils are fatty acid analogues of the FAMES in biodiesel fuel, it is possible that the n-alkanes are formed via the same mechanisms during biodiesel combustion in a diesel engine. Compounds such as n-pentadecane, n-hexadecane, n-heptadecane, n-octadecane, n-nonadecane, n-eicosane, n-heneicosane, n-docosane, n-tricosane, and n-tetracosane would be the n-alkanes formed from the pyrolysis of the FAMES in the biodiesel fuels used in this study according to the mechanisms proposed by Maher and Bressler 2007. Another possible mechanism through which the n-alkanes in the exhaust PM of the neat B100 biodiesel fuels could be formed is the combustion of the lubricating oil. High molecular weight branched alkanes ( $\text{C}_{20}\text{-C}_{40}$ ) were detected in the lubricating oil (fresh and used lube oil) used in the present

study. It is possible that the high molecular weight branched alkanes in the lubricating oil were broken into n-alkanes during combustion in the engine. At elevated temperatures (~250 °C) encountered during engine operation, the n-alkyl hydrocarbons in lubricating oil may undergo thermocracking at the tertiary carbon atoms to form n-alkanes in the exhaust (Rogge et al., 1993). This explains how high molecular weight n-alkanes may appear in the exhaust PM even when the fuels or lubricating oil did not contain n-alkanes (Rogge et al., 1993).

### ***3.2.2.2 FAMES in Biodiesel Exhaust PM***

The emission rate data for the FAMES speciated in the WVO and soybean biodiesel exhaust PM have already been presented in Figures 3.6 and 3.7, and the changes in emission rates with respect to biodiesel content in the fuel have also been discussed in Section 3.1. Detection of methyl linolelaidate and methyl elaidate in the exhaust PM, but not in any of the WVO and soybean biodiesel fuel blends, including the neat B100 biodiesel fuels, was quite surprising. Although methyl linolelaidate and methyl elaidate were detected in the biodiesel exhaust PM, their emission rates in the exhaust PM of the WVO and soybean biodiesel blends were lower than those for the most abundant FAMES (methyl linoleate, methyl oleate, and methyl palmitate) detected in the biodiesel fuels. These two FAMES (methyl linolelaidate and methyl elaidate) were potentially formed from the combustion of the FAMES originally found in the fuels. It is likely that during combustion, the FAMES native to the fuel rearrange to form new/different FAMES. The mechanism by which new FAMES are formed during engine combustion should be a subject of future research. However, such FAMES could be

formed through interactions of the multiple free radicals formed at the high engine temperatures during combustion. Further understanding of such mechanisms could help better elucidate how fuel combusts in the engine. It could also help us understand and predict the possible compounds that could be formed in the engine when certain types of fuels or methyl esters are used.

The FAME compositional profiles in the exhaust PM were quite different from those observed in the WVO and soybean biodiesel fuel blends (Table 3.7). For example, the most dominant FAMES in the WVO B100 exhaust PM had the following compositions: methyl linoleate ( $19.2 \pm 2.1\% = 41 \pm 10.3 \text{ ng}/\mu\text{g}$ ), methyl oleate ( $31.1 \pm 1.7\% = 66 \pm 8.1 \text{ ng}/\mu\text{g}$ ), methyl palmitate ( $22.5 \pm 0.4\% = 48 \pm 7.7 \text{ ng}/\mu\text{g}$ ), and methyl elaidate ( $11.5 \pm 0.5\% = 24 \pm 2.8 \text{ ng}/\mu\text{g}$ ). Note that only the 10 most common FAMES derived from plant and animal oils were quantified in the biodiesel exhaust PM, and a compound was considered to be among the most dominant FAMES if its contribution to the total FAMES was greater than 10%. The FAMES compositions in the WVO B100 exhaust PM were somewhat different than the profiles observed in the WVO B100 biodiesel fuel (i.e. methyl linoleate ( $48.0 \pm 0.1\%$ ), methyl oleate ( $23.1 \pm 0.1\%$ ), methyl palmitate ( $16.2 \pm 0.2\%$ ), and methyl elaidate ( $0\%$ )). The most dominant FAMES in the soybean B100 exhaust PM also had the following compositions: methyl linoleate ( $30.4 \pm 2.3\% = 81 \pm 12.9 \text{ ng}/\mu\text{g}$ ), methyl oleate ( $24.3 \pm 0.1\% = 65 \pm 5.7 \text{ ng}/\mu\text{g}$ ), methyl palmitate ( $19.0 \pm 0.3\% = 51 \pm 3.4 \text{ ng}/\mu\text{g}$ ), and methyl elaidate ( $9.0 \pm 1.3\% = 24 \pm 1.3 \text{ ng}/\mu\text{g}$ ). This too is somewhat different than the profiles observed in the soybean B100 biodiesel fuel: i.e., methyl linoleate ( $52.2 \pm 0.3\%$ ), methyl oleate ( $19.1 \pm 0.2\%$ ), methyl palmitate ( $14.7 \pm 0.2\%$ ), and methyl elaidate ( $0\%$ ). Differences between the compositions of the FAMES in the soybean B20

as well as WVO B10, B20, and B50 biodiesel fuel blends and the corresponding biodiesel exhaust PM samples were also observed as seen in Figures 3.18 and 3.19. Note that Figures 3.18 and 3.19 show the ratios of the different FAMES to that of methyl linoleate (the most abundant FAME in the biodiesel fuels and their blends) in the WVO and soybean biodiesel fuel blends and biodiesel exhaust PM as a function of biodiesel content in the fuel, respectively. Raw concentration data of the FAMES in the WVO and soybean biodiesel exhaust PM are provided in Appendix B.

**Table 3.7 Average percent composition of the main FAMES detected in the WVO and soybean biodiesel fuel and exhaust PM. For WVO, n = 3; For Soybean, n = 2. SD means 1 standard deviation for the multiple fuel or PM analyses. ND means that the FAME was not detected. Some values are less or greater than 100% because of rounding.**

Compound	WVO Biodiesel Fuel								Soybean Biodiesel Fuel			
	B10	SD	B20	SD	B50	SD	B100	SD	B20	SD	B100	SD
Methyl myristate	1.90	0.50	0.70	0.10	0.30	0.10	0.20	0.10	0.70	0.10	0.10	0.10
Methyl palmitate	17.4	0.50	17.1	0.10	16.0	0.10	16.2	0.20	15.2	0.30	14.7	0.20
Methyl linolenate	7.00	1.60	6.50	0.30	7.50	0.20	7.60	0.20	6.90	0.80	8.90	0.30
Methyl linolelaidate	ND		ND		ND		ND		ND		ND	
Methyl linoleate	45.0	2.50	48.3	0.50	47.7	0.40	48.0	0.10	54.7	0.90	52.2	0.30
Methyl elaidate	ND		ND		ND		ND		ND		ND	
Methyl oleate	21.9	0.20	22.8	0.40	23.7	0.50	23.1	0.10	17.9	1.10	19.1	0.20
Methyl stearate	4.70	0.40	3.70	0.10	4.30	0.10	4.20	0.20	3.80	0.30	4.30	0.20
Methyl arachidate	0.40	0.10	0.30	0.10	0.20	0.10	0.20	0.10	0.20	0.10	0.20	0.10
Methyl behenate	1.70	0.20	0.70	0.10	0.40	0.10	0.40	0.10	0.60	0.10	0.30	0.10
Total	100.0		101.1		100.1		99.9		100.0		99.8	
Compound	WVO Biodiesel PM								Soybean Biodiesel PM			
	B10	SD	B20	SD	B50	SD	B100	SD	B20	SD	B100	SD
Methyl myristate	1.10	0.20	0.50	0.10	0.40	0.10	0.30	0.10	0.30	0.10	0.20	0.10
Methyl palmitate	9.00	3.10	13.1	0.60	15.7	2.90	22.5	0.40	11.1	2.10	19.0	0.30
Methyl linolenate	4.60	0.10	4.10	0.40	4.00	0.50	1.40	0.60	4.90	0.50	3.80	0.10
Methyl linolelaidate	9.20	3.10	4.60	0.50	4.80	0.90	3.40	0.30	4.90	0.10	3.70	0.80
Methyl linoleate	26.6	2.80	29.8	1.40	26.2	0.80	19.2	2.10	32.9	0.40	30.4	2.30
Methyl elaidate	11.9	2.80	10.7	0.40	11.7	2.00	11.5	0.50	11.0	0.30	9.00	1.30
Methyl oleate	22.8	1.80	25.7	1.30	26.8	0.40	31.1	1.70	24.1	1.50	24.3	0.10
Methyl stearate	8.60	0.50	8.40	0.40	8.30	0.30	8.80	0.40	9.00	0.50	8.10	0.10
Methyl arachidate	2.50	0.50	1.20	0.10	0.80	0.20	0.70	0.10	0.60	0.30	0.60	0.10
Methyl behenate	3.60	1.30	1.80	0.20	1.40	0.20	1.20	0.30	1.40	0.10	0.90	0.10
	99.9		99.9		100		100		100.0		100.0	

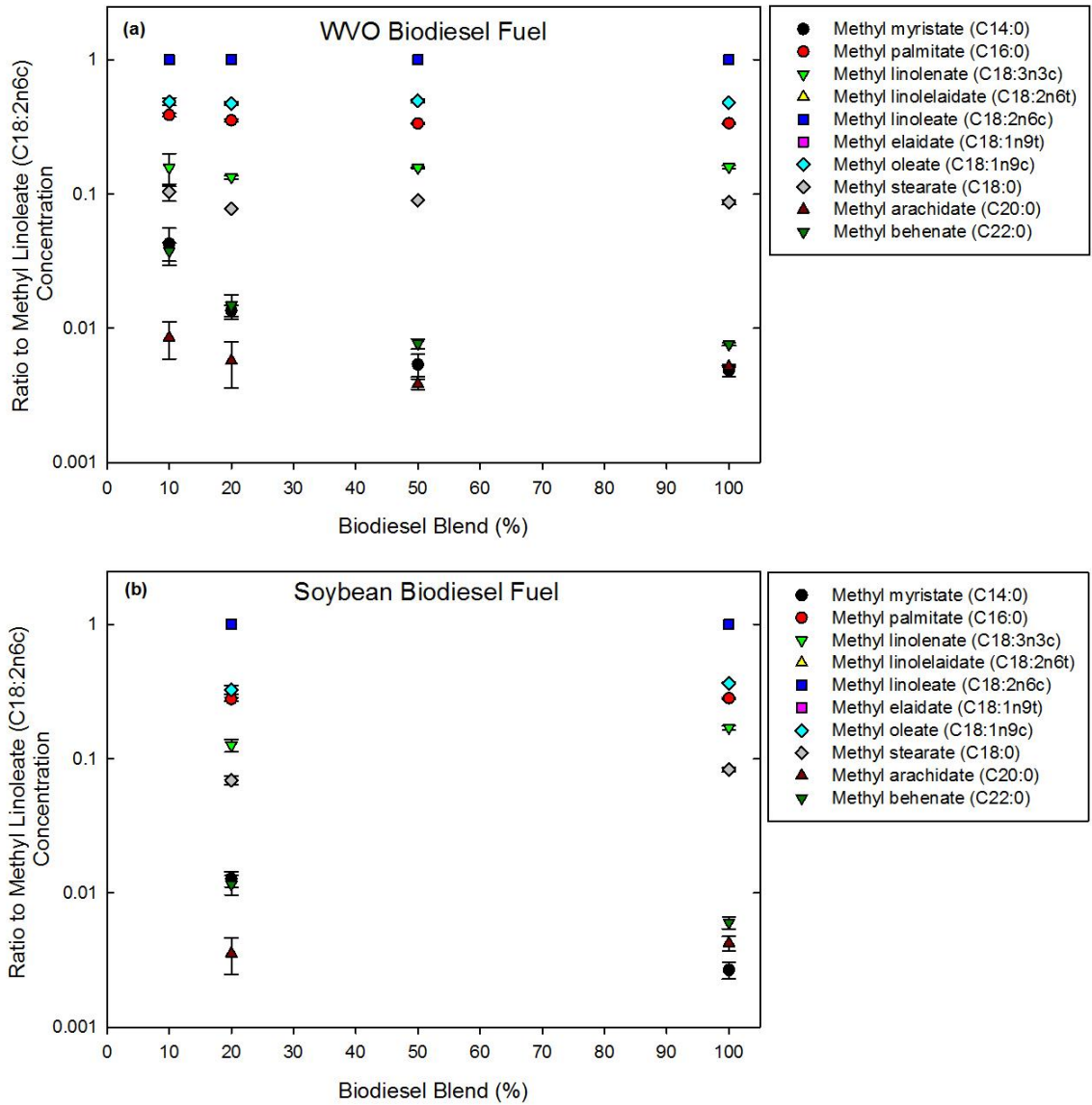


**Figure 3.18 Fuel blend ratios of FAME concentrations to methyl linoleate (C18:2n6c) concentration ((g/gal)/(g/gal)) in the (a) WVO and (b) soybean biodiesel fuel blends. Error bars represent one standard deviation. Note that the y-axes are log scales.**

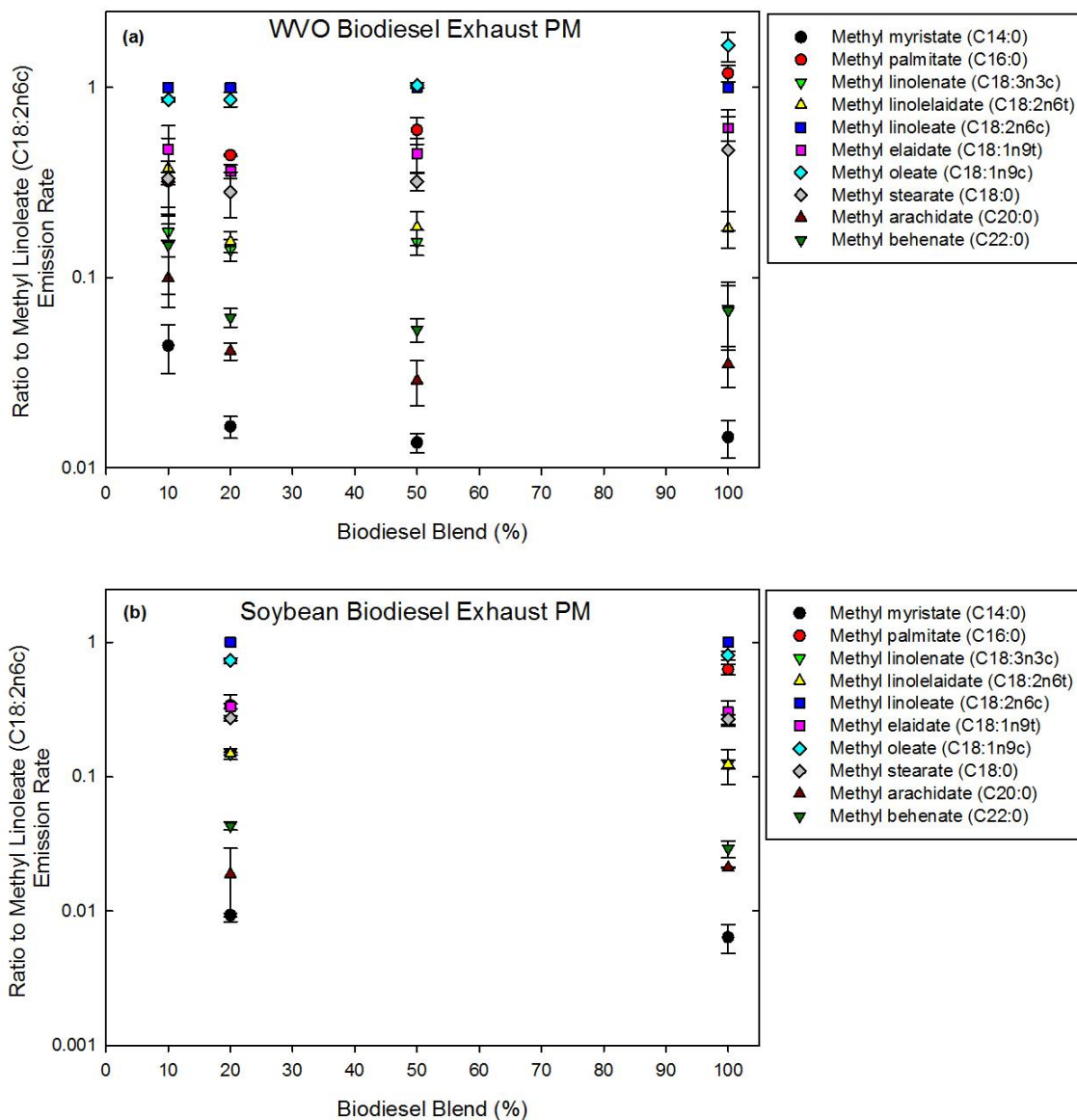


**Figure 3.19 Exhaust PM ratios of FAME emission rates to that of methyl linoleate (C18:2n6c) ((ng/μg)/(ng/μg)) in the (a) WVO and (b) soybean exhaust PM. Error bars represent one standard deviation. Note that the y-axes are log scales, and the scales are different for the two plots.**

The ratios of the concentrations of the individual FAMES to that of methyl linoleate in the different biodiesel fuel blends of both feedstocks were relatively constant and below 1 (Figure 3.18). This means that the concentrations of the other FAMES relative to that of methyl linoleate in the different fuel blends of both WVO and soybean

biodiesel were independent of biodiesel content in the fuel, as expected. On the contrary, the ratios of the emission rates of the individual FAMES to that of methyl linoleate in the exhaust PM varied from blend to blend, depending on the number of double bonds in the FAME. In general, the emission rates of the saturated FAMES (methyl palmitate and methyl stearate) relative to that of methyl linoleate increased with increasing biodiesel in the fuel, although the increases were less in the soybean biodiesel exhaust PM compared to WVO exhaust PM. The emission rates of the monounsaturated FAMES (methyl oleate and methyl elaidate) relative to that of methyl linoleate in the exhaust PM also increased with increasing biodiesel in the fuel. Note that methyl elaidate was not detected in the biodiesel fuel. The emission rates of methyl linolenate (3 double bonds) and methyl linolelaidate (2 double bonds) relative to that of methyl linoleate decreased with increasing biodiesel in the fuel. Furthermore, the percent of methyl linoleate in the exhaust PM generally decreased with increasing biodiesel in the fuel, and its (methyl linoleate) relative percent abundance in the exhaust PM was less than that in the corresponding biodiesel fuel blends (Table 3.7). These observations imply that the unsaturated FAMES with two or more C=C double bonds in the fuel were burned more effectively in the engine than the monounsaturated and saturated FAMES. This is not surprising because the monounsaturated FAMES have only one C=C double bond that can be oxidized during combustion, while methyl linoleate has two C=C double bonds available for oxidation during combustion. Additionally, methyl linoleate appeared to be burned more effectively than the monounsaturated and saturated FAMES not only because of its two C=C double bonds, but also because it was the most abundant FAME in the biodiesel fuels. Methyl linolenate, which has three C=C double bonds, appeared to



burn more effectively in the engine than methyl linoleate because it has more double bonds than methyl linoleate. In spite of the fact that both the saturated and unsaturated FAMES in biodiesel are oxygenated, it appears that the degree of unsaturation of the FAMES is a more important factor for biodiesel combustion in a diesel engine than the presence of oxygen atoms in the FAMES. The double bonds are more prone to decomposition (Karavalakis et al., 2011) because of the presence of the pi electrons in the C=C double bond, and therefore, this further explains why the more unsaturated a FAME is, the more it is transformed during combustion in the engine. These results suggest that the number of double bonds contained in a FAME determines the effectiveness of the combustion of that particular FAME in a diesel engine. The majority of the FAMES with two or more C=C double bonds are burned more than those with one or no C=C double bonds during combustion, and those with one or no double bonds are mainly emitted as unburned fuel. These results further suggest that the unsaturation of a biodiesel fuel might be advantageous for biodiesel combustion because the more-unsaturated FAMES burn better than the less-unsaturated or saturated FAMES.

### ***3.2.2.3 Mass Balance on the FAMES***

In order to ascertain whether the FAMES in the biodiesel fuel were really oxidized during combustion in the engine, mass balance calculations were applied to the different engine runs. The total mass of each individual FAME injected in the engine during a particular run was determined from the concentration of that FAME in the fuel (mg/gal) and the amount of fuel (gal) consumed during that run. The volume of fuel used during each run was determined by dividing the weight of the fuel used by the density of the fuel. Note that the weight of fuel in the tank was measured using a GBK 70A weighing

scale (Adam Equipment Inc., Danbury, CT) on which the fuel tank sat during emissions testing. The total mass of each individual FAME emitted during the run was determined from the GC/MS analysis results of the filters. Note that it was assumed that the FAMES were not lost due to volatilization during engine sampling. For the FAMES that were detected in both the biodiesel fuel samples and biodiesel exhaust PM for both feedstocks, the mass in the biodiesel fuel was always greater than the mass in the biodiesel exhaust PM (Tables 3.8 and 3.9). This, therefore, means that such FAMES were lost during combustion in the engine, and that FAMES detected in the biodiesel exhaust PM were possibly emitted as unburned fuel. On the other hand, it is also possible that such FAMES were emitted as combustion products, but because they were measured in the biodiesel exhaust PM at lower amounts than in the fuel, it was not possible to confirm whether those FAMES were products of combustion. The possibility of formation of new FAMES during combustion is supported by detection of methyl linolelaidate and methyl elaidate in the biodiesel exhaust PM, in spite of the fact that they were not detected in the biodiesel fuel samples.

From the FAMES mass balance calculations, it can be seen that a small fraction (less than 0.1%) of the FAMES injected in the engine were emitted as unburned fuel, assuming that there were no losses during sampling. This observation implies that the emissions due to unburned fuel are negligible compared to the amount of fuel injected in the engine.

**Table 3.8 Mass of FAMES injected in the engine (mg) and sampled on the filters during the different WVO engine runs. ND means that the analyte was not detected.**

	<b>WVO B10 Run 1</b>	<b>WVO B10 Run 2</b>	<b>WVO B20 Run 1</b>	<b>WVO B20 Run 2</b>	<b>WVO B50 Run 1</b>	<b>WVO B50 Run 2</b>	<b>WVO B100 Run 1</b>	<b>WVO B100 Run 2</b>
<b>Mass of FAMES in Fuel</b>								
<b>Compounds</b>	Mass (mg)	Mass (mg)	Mass (mg)	Mass (mg)	Mass (mg)	Mass (mg)	Mass (mg)	Mass (mg)
Methyl myristate	1.47E+03	1.46E+03	1.85E+03	1.86E+03	2.86E+03	2.87E+03	4.88E+03	4.72E+03
Methyl palmitate	1.12E+04	1.66E+04	4.55E+04	5.14E+04	2.06E+05	1.59E+05	3.62E+05	3.07E+05
Methyl linolenate	5.31E+03	5.54E+03	1.66E+04	2.01E+04	9.79E+04	7.31E+04	1.76E+05	1.41E+05
Methyl linolelaidate	ND	ND	ND	ND	ND	ND	ND	ND
Methyl linoleate	2.83E+04	4.37E+04	1.27E+05	1.47E+05	6.16E+05	4.70E+05	1.08E+06	9.03E+05
Methyl elaidate	ND	ND	ND	ND	ND	ND	ND	ND
Methyl oleate	1.44E+04	2.04E+04	6.12E+04	6.81E+04	2.99E+05	2.38E+05	5.20E+05	4.34E+05
Methyl stearate	3.24E+03	4.08E+03	9.85E+03	1.14E+04	5.56E+04	4.22E+04	9.13E+04	8.09E+04
Methyl arachidate	2.95E+02	2.92E+02	9.23E+02	6.19E+02	2.22E+03	1.92E+03	5.58E+03	4.72E+03
Methyl behenate	1.18E+03	1.46E+03	2.15E+03	1.86E+03	4.45E+03	3.83E+03	8.37E+03	6.75E+03
<b>Total</b>	<b>6.55E+04</b>	<b>9.36E+04</b>	<b>2.65E+05</b>	<b>3.02E+05</b>	<b>1.28E+06</b>	<b>9.90E+05</b>	<b>2.25E+06</b>	<b>1.88E+06</b>
<b>Mass of FAMES in PM</b>								
Methyl myristate	1.00 E-02	1.00E-02	1.00E-02	1.00E-02	2.00E-02	2.00E-02	4.00E-02	4.00E-02
Methyl palmitate	3.00E-02	8.0E-02	2.80E-01	2.10E-01	9.1E-01	5.90E-01	4.20E+00	2.60E+00
Methyl linolenate	3.00E-02	4.0E-02	7.00E-02	7.00E-02	1.90E-01	2.2E-01	3.60E-01	8.00E-01
Methyl linolelaidate	7.00E-02	6.0E-02	8.00E-02	8.00E-02	2.00E-01	2.70E-01	6.00E-01	4.50E-01
Methyl linoleate	1.30E-01	2.30E-01	6.20E-01	4.80E-01	1.36E+00	1.21E+0	3.84E+00	1.96E+00
Methyl elaidate	8.00E-02	1.10E-01	2.00E-01	1.80E-01	5.30E-01	6.70E-01	2.06E+00	1.39E+00
Methyl oleate	1.2E-01	2.00E-01	5.10E-01	3.90E-01	1.40E+00	1.28E+00	5.67E+00	3.91E+00
Methyl stearate	5.0E-02	7.00E-02	1.60E-01	1.40E-01	4.20E-01	4.20E-01	1.64E+00	1.09E+00
Methyl arachidate	2.0E-02	2.00E-02	2.00E-02	2.00E-02	3.00E-02	4.00E-02	1.2E-01	9.00E-02
Methyl behenate	3.0E-02	3.00E-02	3.00E-02	3.00E-02	7.00E-02	7.00E-02	1.90E-01	1.80E-01
<b>Total</b>	<b>5.60E-01</b>	<b>8.40E-01</b>	<b>2.00E+00</b>	<b>1.61E+00</b>	<b>5.14E+00</b>	<b>4.78E+00</b>	<b>1.87E+01</b>	<b>1.18E+01</b>

**Table 3.9 Mass of FAMES injected in the engine (mg) and sampled on the filters during the different soybean engine runs.**

	<b>Soy B20 Run 1</b>	<b>Soy B20 Run 2</b>	<b>Soy B100 Run 1</b>	<b>Soy B100 Run 2</b>
<b>Mass of FAMES in Fuel</b>				
<b>Compounds</b>	Mass (mg)	Mass (mg)	Mass (mg)	Mass (mg)
Methyl myristate	3.51E+03	3.45E+03	5.14E+03	4.74E+03
Methyl palmitate	7.19E+04	8.24E+04	5.41E+05	5.06E+05
Methyl linolenate	3.33E+04	3.72E+04	3.26E+05	3.06E+05
Methyl linolelaidate	ND	ND	ND	ND
Methyl linoleate	2.66E+05	2.96E+05	1.92E+06	1.79E+06
Methyl elaidate	ND	ND	ND	ND
Methyl oleate	8.24E+04	1.00E+05	7.09E+05	6.51E+05
Methyl stearate	1.82E+04	2.17E+04	1.64E+05	1.44E+05
Methyl arachidate	7.01E+02	1.03E+03	8.81E+03	6.93E+03
Methyl behenate	3.51E+03	3.45E+03	1.10E+04	1.13E+04
<b>Total</b>	<b>4.79E+05</b>	<b>5.46E+05</b>	<b>3.68E+06</b>	<b>3.42E+06</b>
<b>Mass of FAMES in PM</b>				
<b>Compounds</b>	Mass (mg)	Mass (mg)	Mass (mg)	Mass (mg)
Methyl myristate	1.00E-02	1.00E-02	4.00E-02	4.00E-02
Methyl palmitate	3.60E-01	2.80E-01	4.89E+00	3.93E+00
Methyl linolenate	1.30E-01	1.50E-01	9.80E-01	7.70E-01
Methyl linolelaidate	1.40E-01	1.40E-01	8.10E-01	8.80E-01
Methyl linoleate	9.20E-01	9.60E-01	8.32E+00	5.86E+00
Methyl elaidate	3.20E-01	3.10E-01	2.14E+00	2.04E+00
Methyl oleate	6.50E-01	7.30E-01	6.33E+00	4.94E+00
Methyl stearate	2.40E-1	2.70E-01	2.10E+00	1.65E+00
Methyl arachidate	2.00E-2	1.00E-02	1.80E-01	1.20E-01
Methyl behenate	4.00E-02	4.00E-02	2.20E-01	1.90E-01
<b>Total</b>	<b>2.82E+00</b>	<b>2.90E+00</b>	<b>2.60E+01</b>	<b>2.04E+01</b>

ND means that the analyte was not detected

### **3.2.2.4 PAHs in Biodiesel Exhaust PM**

The PAH emission rates data for the exhaust PM of both WVO and soybean biodiesel blends have already been discussed in Section 3.1. None of the PAHs detected in the exhaust PM were detected in the fuel samples and lubricating oil (fresh or used), although aromatic hydrocarbons were detected in petrodiesel and the biodiesel blends of both WVO and soybean biodiesel fuels (B10, B20, and B50). However, no aromatic hydrocarbons were seen in the neat B100 WVO and soybean biodiesel fuels, suggesting

that the PAHs detected in the exhaust PM could not be due to the unburned fuel or lubricating oil. Therefore, the PAHs were possibly a result of the combustion of the fuel, combustion of the lubricating oil, or combustion of the lubricating oil and the fuel in the engine. Detection of the PAHs in the exhaust PM of the neat B100 fuels of WVO and soybean biodiesel was, however, surprising given that the neat biodiesel fuels did not have aromatic hydrocarbons in them. It is likely that the unsubstituted PAHs in the petrodiesel and biodiesel exhaust PM were formed during combustion. Richter and Howard (2000) and Cole et al. (1984) outlined possible pathways (radical interactions) through which PAHs could be formed during combustion of aliphatic and aromatic fuels. This, therefore, implies that the PAHs detected in the present study were formed as a result of the combustion of the fuels and lubricating oil.

Schauer et al. (1999) measured the concentrations of the methyl-substituted and unsubstituted PAHs in the diesel fuel and diesel exhaust PM. The authors found that the ratios of the methyl-substituted PAHs to those of the unsubstituted PAHs were greater in the diesel fuel than the exhaust PM. The authors did not give an explanation for the observations, but it is possible that the unsubstituted PAHs were either formed during combustion, or that the methyl-substituted PAHs were transformed during combustion. Several previous studies have attributed the PAHs in the exhaust PM to unburned fuel or lubricating oil (e.g., Williams et al., 1989; Mi et al., 2000; Brandenberger et al., 2005) when LSD was used in both light-duty and heavy-duty diesel engines, but the results of the present study suggest that no PAHs are emitted as a result of unburned fuel probably because of the very low contents of sulfur (1.2 ppm) and aromatic hydrocarbons in the petrodiesel.

Given that the neat B100 WVO and soybean biodiesel fuels consisted of only FAMES, it is likely that the PAHs detected in the exhaust PM of the neat B100 biodiesel fuels were due to the combustion of the hydrocarbons in the lubricating oil or by thermocracking of the FAMES. Previous studies such as Lin et al. (2006), Chien et al. (2009), and Magara-Gomez et al. (2012) all reported detection of PAHs in the exhaust PM of the neat B100 biodiesel fuels used in their respective studies. However, the authors did not explain the likely causes of PAHs detected in the biodiesel exhaust PM, but it is possible that the PAHs were formed from the combustion of the lubricating oil, or combustion of the lubricating oil and the FAMES through interactions of the free radicals formed at the high temperatures encountered in the engine during combustion.

### ***3.2.2.5 Carbonyls and Quinones in Biodiesel Exhaust PM***

The emission rate data of the speciated carbonyls and quinones in WVO and soybean biodiesel exhaust PM, and the variations in the emission rates with respect to biodiesel content in the fuel have been discussed in Section 3.1. For the B00, WVO B20, and WVO B100 fuel samples analyzed, no target carbonyls and quinones were detected. These observations suggest that all the carbonyls and quinones detected in the exhaust PM of all the fuel blends used in the present study were potentially products of the partial oxidation of the fuel and lubricating oil constituents during combustion in the diesel engine. Several studies (e.g., Schauer et al., 1999; Turrio-Baldassarri et al., 2004; Pang et al., 2006; Correa and Arbilla, 2008; Jakober et al., 2008; Karavalakis et al., 2011, and Cahill and Okamoto, 2012) have measured the carbonyl emissions in either diesel or biodiesel exhaust PM, but no studies have measured the concentrations of carbonyls in

diesel and biodiesel fuels. Studies by Cho et al., 2004; Valavanidis et al., 2006 and Jakober et al., 2007 have quantified the emissions of quinones from light-duty gasoline vehicles and heavy-duty diesel engines fueled with petrodiesel. However, no studies have to date investigated the concentrations of quinones in either petrodiesel or biodiesel fuels, as well as the emissions of quinones in biodiesel exhaust PM.

### **3.2.3 Summary of Formation Pathways**

Table 3.10 summarizes the possible pathways through which the target analytes could be formed in the diesel and biodiesel exhaust PM. Of all the target analytes, it is only n-alkanes and FAMES that could be found in the exhaust PM as a result of unburned fuel, while none of the target analytes were as a result of unburned lubricating oil. All the target analytes could be formed from the combustion of the fuel, while PAHs and n-alkanes could be formed from the combustion of the lubricating oil. Carbonyls, quinones, and FAMES were not thought to be formed from the combustion of lubricating oil, but because of the complex nature of the combustion process in the engine that involves interaction of different free radicals to form various products, this pathway (combustion of lubricating oil) for the formation of carbonyls, quinones, and FAMES could be likely. Interaction of the different combustion products of the fuel and lubricating oil could be another pathway through which all the target analytes could be formed. During engine sampling, the target analytes could adsorb on the tailpipe walls, and they could be desorbed from the tailpipe walls during subsequent engine runs. Therefore, the sampling artifact (desorption from tailpipe walls) might be another

pathway through which the target analytes could be found in the diesel and biodiesel exhaust PM.

**Table 3.10 Formation pathways of the target organic compounds detected in diesel and biodiesel exhaust PM.**

Formation Pathway	PAHs	n-Alkanes	Carbonyls including Quinones	FAMEs
Unburned Fuel	o	√	o	√
Unburned Lubricating Oil	o	o	o	o
Combustion of Fuel	√	√	√	√
Combustion of Lubricating Oil	√	√	No Data	No Data
Interaction of Combustion Products	√	√	√	√
Desorption from Tailpipe Walls	√	√	√	√

o means that the pathway is not likely. √ means that it is a possible pathway.



### **3.3 Effect of Fatty Acid Methyl Esters on the Heterogeneous Ozonation**

#### **Reactions of PAHs in Biodiesel Particulate Matter**

The volatile PAHs such as naphthalene, acenaphthylene, acenaphthene, and fluorene were not detected in any of the spiked samples including the controls. They were also not detected in the biodiesel exhaust PM punches. These volatile PAHs were possibly lost during sample extract blowdown, and therefore, they are not discussed further. Detectability of the rest of the PAHs and FAMES in the filter punches that were spiked (with PAH and FAME standards) and exposed to ozone was quite good. Also, phenanthrene, fluoranthene, and pyrene were the only PAHs detected in the B20 biodiesel exhaust PM with very high confidence (see Section 3.1).

#### **3.3.1 Ozonolysis of PAH Mixture Spiked on ¼-inch FF Punches**

The volatilization and effective pseudo-first order ozonation rate constants for all the detected PAHs spiked on the ¼-inch FF punches with and without the FAMES are shown in Figure 3.20 (see Equation 2-7 for the definitions of the different rate constants). Phenanthrene ( $0.090 \pm 0.020 \text{ hr}^{-1}$ ), anthracene ( $0.065 \pm 0.012 \text{ hr}^{-1}$ ), fluoranthene ( $0.100 \pm 0.010 \text{ hr}^{-1}$ ), and pyrene ( $0.067 \pm 0.009 \text{ hr}^{-1}$ ) had the highest losses due to volatilization in the presence of PAHs only. This was not surprising because of the relatively high vapor pressures of these lower molecular weight PAHs. The volatilization rates of phenanthrene ( $0.140 \pm 0.021 \text{ hr}^{-1}$ ) and anthracene ( $0.141 \pm 0.019 \text{ hr}^{-1}$ ) increased by 55.4% and 118.7%, respectively, when the PAHs were spiked with the FAMES, which was surprising, while the volatilization rates of fluoranthene ( $0.027 \pm 0.017 \text{ hr}^{-1}$ ) and pyrene ( $0.025 \pm 0.017 \text{ hr}^{-1}$ ) decreased by 72.9% and 61.8%, respectively. The

volatilization losses of phenanthrene ( $0.005 \pm 0.027 \text{ hr}^{-1}$ ), fluoranthene ( $0.002 \pm 0.027 \text{ hr}^{-1}$ ), and pyrene ( $0.0 \pm 0.026 \text{ hr}^{-1}$ ) in the B20 biodiesel exhaust PM samples were even lower than for the spiked filter punches, suggesting that the PAHs strongly adsorb onto the PM components, hence reducing their volatilization rates. As expected, the high molecular weight PAHs (chrysene through dibenz[a,h]anthracene) had very low losses in the control experiments, and these losses could be attributed to volatilization during sample handling.

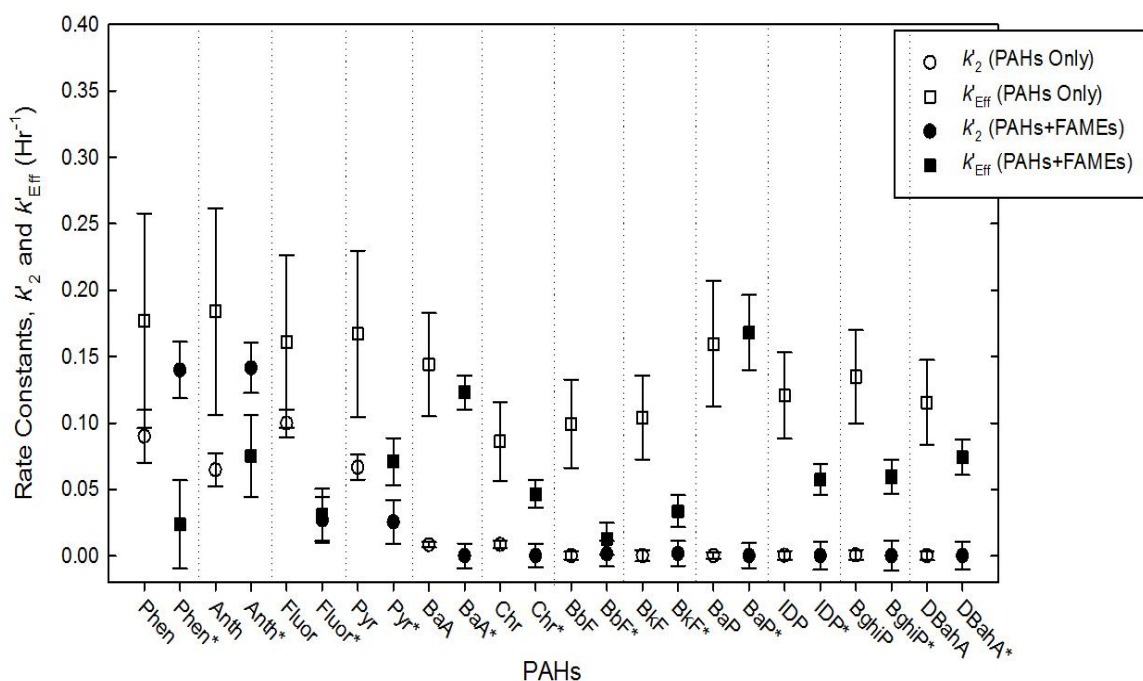


**Figure 3.20** Volatilization ( $k'_2$ ) and effective pseudo-first order ozonation ( $k'_{Eff}$ ) rate constants obtained from the reactions of ozone and 16 PAHs only, and Mixture of 16 PAHs and 10 FAMEs. \* indicates volatilization and pseudo-first order ozonation rate constants of PAHs spiked on 1/4-inch punches with FAMEs. Open symbols indicate control and ozone exposure experiments with 16 PAH mixture only, while closed symbols indicate control and ozone exposure experiments conducted with 16 PAH mixture and 10 FAME mixture. Error bars indicate standard error.

From Figure 3.20, it is quite evident that all the PAHs reacted with ozone, albeit at different rates. During the reactions of the PAHs with ozone in the absence of the

FAMEs, anthracene ( $k'_{Eff}=0.184\pm 0.078 \text{ hr}^{-1}$ ) was the most reactive PAH, while chrysene ( $k'_{Eff}=0.095\pm 0.029 \text{ hr}^{-1}$ ) was the least reactive. The other PAHs that had relatively high pseudo-first order ozonation rate constants were phenanthrene ( $k'_{Eff}=0.177\pm 0.081 \text{ hr}^{-1}$ ), pyrene ( $k'_{Eff}=0.167\pm 0.063 \text{ hr}^{-1}$ ), fluoranthene ( $k'_{Eff}=0.161\pm 0.065 \text{ hr}^{-1}$ ), and benzo[a]pyrene ( $k'_{Eff}=0.160\pm 0.047 \text{ hr}^{-1}$ ), while the other PAHs that had low rates of reaction were benzo[b]fluorathene ( $k'_{Eff}=0.099\pm 0.033 \text{ hr}^{-1}$ ) and benzo[k]fluoranthene ( $k'_{Eff}=0.104\pm 0.032 \text{ hr}^{-1}$ ).

The ozone reactivity of the PAHs spiked on 1/4-inch FF punches did not seem to follow any trend with respect to molecular weight. The effective ozone reaction rate constants of all PAHs were in the same order of magnitude, and anthracene (MW=178) was the most reactive PAH, with chrysene (MW=228) being the least reactive PAH. Previous studies, for example, Perraudin et al. (2007) also found anthracene as the most reactive PAH when a group of 10 PAHs adsorbed on silica and graphite particles were exposed to ozone (Table 3.11). The authors further found that chrysene was the least reactive PAH for the PAHs adsorbed on graphite particles, while fluoranthene was the least reactive PAH on silica particles. The ozonation rate constants of both anthracene and benzo[a]pyrene in the present study were of the same order of magnitude, consistent with the Perraudin et al. (2007) findings. It is, however, important to note that the ozonation rate constants in the study of Perraudin et al. (2007) were two orders of magnitude greater than those obtained in the current study. The difference in the ozonation rate constants obtained in the Perraudin et al. (2007) study and the present study could be due to differences in substrates, ozone exposure durations, and ozone concentrations used in the two different studies. In the Perraudin et al. (2007) study, the

longest exposure time was 15 minutes, while the longest exposure time for the present study was 24 hours. Furthermore, PAH degradation reached a plateau for the graphite particles used in the Perraudin et al. (2007) study even when the ozone concentrations and ozone exposure times were increased, which suggested that the particulate PAHs were not available for oxidation for this type of particles. This kind of phenomenon was not observed in the present study, and could partly explain the difference in ozone reaction rates between the two studies.

**Table 3.11 Comparison of literature studies on the heterogeneous reaction rates of ozone with PAHs on different substrates and this study. ND means that the analyte was not detected.**

Study	This Study	This Study	This Study	Kamens et al. 1985	Alebic-Juretic et al. 2000	Kahan et al. 2006	Perraudin et al. 2007 <sup>d</sup>	Perraudin et al. 2007 <sup>d</sup>
Substrate	FF Filter (PAHs)	FF Filter (PAHs + FAMES)	(B20 Exhaust PM)	Wood smoke	Silica gel	Urban grime	Silica particles	Graphite particles
PAH	$k'_{Eff}(\text{hr}^{-1})$	$k'_{Eff}(\text{hr}^{-1})$	$k'_{Eff}(\text{hr}^{-1})$	$K_{Obs}(\text{hr}^{-1})$	$k_{Obs}(\text{hr}^{-1})$	$k_{Obs}(\text{hr}^{-1})$	$K_{Obs}(\text{hr}^{-1})$	$K_{Obs}(\text{hr}^{-1})$
Max Exposure Time	24 hr	24 hr	24 hr	>24 hr	N/A	0.5 hr	15 min	15 min
[O <sub>3</sub> ] (ppm)	0.4	0.4	0.4	0.57	0.1	14 - 916	1.6 - 13.1	1.6 - 13.1
Phen	0.177 ± 0.081	0.024 ± 0.033	0.043 ± 0.034			9.50E-04 <sup>c</sup>	9.94	10.37
Anth	0.184 ± 0.078	0.075 ± 0.031	ND			5.94E-03 <sup>b,c</sup>	60.48	42.34
Fluor	0.161 ± 0.065	0.031 ± 0.020	0.047 ± 0.034		0.046	≤ 3.31E-04 <sup>b</sup>	6.48	8.21
Pyr	0.167 ± 0.063	0.071 ± 0.018	0.047 ± 0.033	0.438	0.446	1.66E-03 <sup>c</sup>	25.49	10.80
BaA	0.144 ± 0.039	0.123 ± 0.013	ND	0.636	1.048		37.58	12.10
Chr	0.086 ± 0.030	0.047 ± 0.010	ND	3.540 <sup>a</sup>			13.39	6.48
BbF	0.099 ± 0.033	0.013 ± 0.012	ND					
BkF	0.104 ± 0.032	0.033 ± 0.012	ND	0.624			15.55	8.21
BaP	0.160 ± 0.047	0.168 ± 0.028	ND	0.504	1.048	1.02E-02 <sup>b</sup>	60.48	22.90
IDP	0.121 ± 0.032	0.058 ± 0.012	ND				16.42	8.21
BghiP	0.135 ± 0.035	0.059 ± 0.013	ND				9.07	8.21
DahA	0.116 ± 0.032	0.074 ± 0.013	ND					

<sup>a</sup>Chrysene/triphenylene; <sup>b</sup>Dissolved in octanol; <sup>c</sup>Dissolved in decanol; <sup>d</sup>Calculated from second order rate constants using a reference ozone concentration of  $1.2 \times 10^{14}$  molecule.cm<sup>-3</sup>.

### 3.3.2 Ozonolysis of PAHs in the Presence of FAMES (Spiked Experiments)

Exposure of the PAHs spiked on ¼-inch FF punches to ozone in the presence of FAMES decreased the rates of reaction of the PAHs with ozone between 1.2 to 8 times for all PAHs with the exception of benzo[a]pyrene. Benzo[b]fluoranthene ( $k'_{Eff} = 0.013 \pm 0.012 \text{ hr}^{-1}$ ), phenanthrene ( $k'_{Eff} = 0.024 \pm 0.033 \text{ hr}^{-1}$ ), and fluoranthene ( $k'_{Eff} = 0.031 \pm 0.020 \text{ hr}^{-1}$ ) had the largest decrease in reactivity with ozone when the PAHs were exposed to ozone together with the FAMES, as their rates of reaction with ozone decreased by about 8, 7.5, and 5 times, respectively. The ozone reaction rates of benzo[a]anthracene ( $k'_{Eff} = 0.123 \pm 0.013 \text{ hr}^{-1}$ ), and dibenz[a,h]anthracene ( $k'_{Eff} = 0.074 \pm 0.013 \text{ hr}^{-1}$ ) slightly decreased by 1.2 and 1.6 times, respectively, when the PAHs were exposed to ozone in the presence of FAMES. The benzo[a]pyrene reactivity with ozone did not appear to be affected when the PAHs were exposed to ozone together with the FAMES. This result for benzo[a]pyrene is contrary to the findings of a study by Kahan et al. (2006), who found that the presence of oleic acid, an unsaturated fatty acid, decreased the ozone reactivity of benzo[a]pyrene dissolved in either octanol or decanol by about 70%.

In general, the presence of the FAMES, most especially the unsaturated FAMES which are susceptible to attack by ozone, likely led to the observed reduction in reaction rates of the PAHs. The evidence for this observation is that the unsaturated FAMES had higher reaction rates with gas-phase ozone than the PAHs, as discussed below in Subsection 3.3.3. The C=C double bonds in the unsaturated FAMES provide competition to the PAHs for oxidation by ozone as explained in more detail in Subsection 3.3.3. The unsaturated FAMES are more readily attacked by ozone, hence leading to a decrease in

the reaction rates of the PAHs. It was also observed that the concentrations of the unsaturated FAMES decreased with reaction time, whereas the concentrations of the saturated FAMES almost stayed constant. Furthermore, the concentrations of the FAMES were about three orders of magnitude greater than those of the PAHs, and this suggested that the large concentration of FAMES relative to that of the PAHs meant that the PAHs had a lower chance of getting oxidized compared to the FAMES. Therefore, this could also have led to the observed decrease in the reactivity of the PAHs.

In the Kahan et al. (2006) study, the effects of different substrates on the heterogeneous reaction rates of anthracene with ozone were also investigated. The degradation rates of anthracene were not affected by either dissolving it in octanol or decanol. They further found that the presence of vacuum grease or silicone-based grease substrate, stearic acid, or cornstarch did not affect the rate of reaction of anthracene with ozone. However, the presence of unsaturated compounds, oleic acid and squalene (at concentrations three orders of magnitude higher than the PAHs), significantly reduced the heterogeneous reaction rate of anthracene with ozone by about 70% and 90%, respectively. The authors further reported that the decrease in the reaction rate of benzo[a]pyrene in the presence of either oleic acid or squalene was similar in magnitude to that observed for anthracene. The authors argued that the decrease in the reaction rates of both anthracene and benzo[a]pyrene were due to the presence of the unsaturated site(s) in oleic acid and squalene, which reduced the effective surface concentration of ozone available for PAH oxidation.

The suggestions outlined by Kahan et al. (2006) for the decrease in the reactivity of anthracene and benzo[a]pyrene exposed to ozone in the presence of oleic acid could

also be made to the present study. In the current study, five unsaturated FAME species (methyl oleate (C18:1n9c), methyl elaidate (C18:1n9t), methyl linoleate (C18:2n6c), methyl linolelaidate (C18:2n6t), and methyl linolenate (C18:3n3c)) were providing competition to the oxidation of the PAHs by ozone at a total concentration of one order of magnitude higher than the total PAH concentration, thus reducing the available surface concentration of ozone. This ultimately could have led to the depletion of the ozone available for the oxidation of the PAHs.

Kahan et al. (2006) further investigated the reactivity of naphthalene, phenanthrene, anthracene, fluoranthene, pyrene, and benzo[a]pyrene in octanol or decanol solvents to  $10^{14}$ - $10^{16}$  molec.  $\text{cm}^{-3}$  of ozone for 30 minutes (Table 3.11). They found that the relative reaction rates of the PAHs they studied followed the following order: benzo[a]pyrene > anthracene > naphthalene > pyrene > phenanthrene > fluoranthene. In the present study, a similar reactivity pattern was observed when the PAHs were exposed to ozone in the presence of FAMES i.e., benzo[a]pyrene > anthracene > pyrene > fluoranthene > phenanthrene. The only difference in the reactivity order presented by Kahan et al. (2006) and that in the present study is that fluoranthene was slightly more reactive than phenanthrene in this study. It is also important to note that the relative rate constants obtained by Kahan et al. (2006) were about one to three orders of magnitude lower than those obtained in the present study. The different substrates, flowrates, exposure times, RH, and temperature used in the two different studies could account for the observed differences in rate constants.



### 3.3.3 FAMES Ozonolysis Rate Constants for Spiked Mix

Figure 3.21 shows the volatilization and effective pseudo-first order ozonation rate constants of the same FAMES for the reactions with 0.4 ppm ozone and the no-ozone control. The rates of reaction of the unsaturated FAMES during the control experiment (with no ozone in the system) were very low (Figure 3.21). As expected, the more volatile FAMES had the largest losses due to volatilization, with methyl myristate having the highest volatilization rate constant ( $0.065 \pm 0.004 \text{ hr}^{-1}$ ). The rest of the FAMES had very minimal volatilization losses. When the FAMES were exposed to ozone, some unsaturated FAMES reacted with ozone faster than the PAHs (Figures 3.20 and 3.21). Methyl linolenate, with three C=C double bonds, had the highest effective ozone reaction rate ( $k'_{\text{Eff}} = 0.329 \pm 0.023 \text{ hr}^{-1}$ ), followed by methyl linoleate ( $k'_{\text{Eff}} = 0.288 \pm 0.024 \text{ hr}^{-1}$ ) with two C=C double bonds. Of the unsaturated FAMES, methyl linolelaidate, a trans-FAME with two C=C double bonds had the lowest effective ozone reaction rate constant ( $k'_{\text{Eff}} = 0.087 \pm 0.015 \text{ hr}^{-1}$ ). The effective rates of ozone reaction of the saturated FAMES were very low, with methyl myristate having the highest rate of reaction ( $k'_{\text{Eff}} = 0.056 \pm 0.008 \text{ hr}^{-1}$ ), while methyl arachidate and methyl behenate had the lowest ozonation rate constants of ( $k'_{\text{Eff}} = 0.004 \pm 0.003 \text{ hr}^{-1}$ ), and ( $k'_{\text{Eff}} = 0.005 \pm 0.004 \text{ hr}^{-1}$ ), respectively.

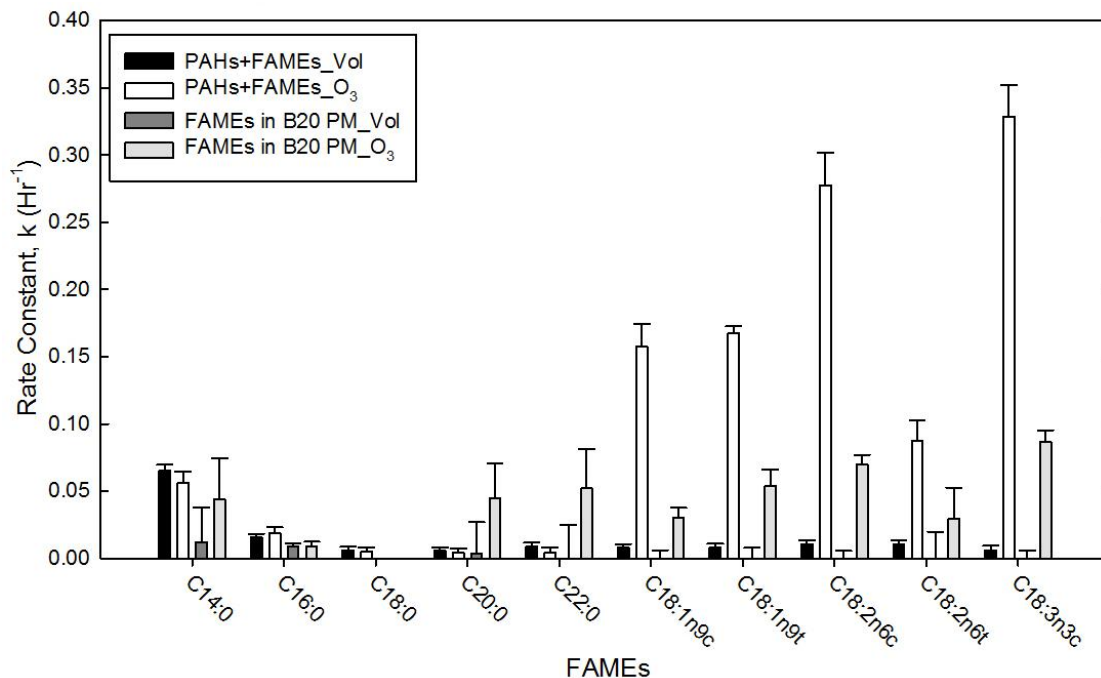


**Figure 3.21 Pseudo-first order FAME ozonation rate constants obtained from the reactions of ozone with the mixtures of 16 PAHs and 10 FAMES, and Biodiesel (B20) exhaust PM.**

The reaction rate constants of the unsaturated FAMES with ozone varied between 0.087 and 0.329 hr<sup>-1</sup>, while those of the saturated FAMES varied between 0.005 and 0.056 hr<sup>-1</sup>. The reaction rate constants of the PAHs in the presence of the FAMES ranged from 0.013 to 0.168 hr<sup>-1</sup>. These observations suggest that some of the unsaturated FAMES are more reactive with ozone than the PAHs, likely because the C=C double bonds in the unsaturated FAMES provide the sites for attack by ozone. The saturated FAMES do not have C=C double bonds, therefore, their reactions with ozone were relatively slower than those of the unsaturated FAMES and most PAHs. These results mean that the unsaturated FAMES were probably the main compounds responsible for the reduced reactivity of the PAHs when the PAHs were exposed to ozone in the presence of the FAMES. Note that the FAMES existed in the standard mixture at different

concentrations (Table 2.3), and this suggests that the contributions of the individual FAMES to the observed reduction in ozone reaction rates of the PAHs was a factor of the individual FAME concentrations in the mixture. The FAMES standard mixture contained 34%, 25%, and 10% of methyl linoleate, methyl oleate, and methyl elaidate, respectively (this mixture was developed for biodiesel GC analysis, and is chemically similar to soybean B100 biodiesel), and this suggests that these unsaturated FAMES (methyl linoleate, methyl oleate, and methyl elaidate) probably contributed the most to the reduction in PAHs reactivity when the PAHs were exposed to ozone in the presence of the FAMES. Future studies should aim at quantifying the contributions of the individual FAMES to the reduction in PAH reactivity with ozone when the PAHs are exposed to ozone in the presence of the FAMES.

### **3.3.4 Ozonolysis of PAHs in B20 Biodiesel Exhaust PM**

For the PAHs detected in the biodiesel (B20) filter punches, the rates of ozone reaction for phenanthrene ( $k'_{Eff} = 0.043 \pm 0.034 \text{ hr}^{-1}$ ) and fluoranthene ( $k'_{Eff} = 0.047 \pm 0.034 \text{ hr}^{-1}$ ) were slightly greater than those obtained when spiked PAHs were exposed to ozone in the presence of FAMES, but greatly lower than those when the PAHs alone were exposed (Table 3.11). In contrast, the reactivity of pyrene ( $k'_{Eff} = 0.047 \pm 0.033 \text{ hr}^{-1}$ ) in the biodiesel exhaust PM was lower than that observed when spiked PAHs were exposed to ozone together with the FAMES. The rates of reaction of phenanthrene, fluoranthene, and pyrene in the case where only the PAHs were exposed to ozone were respectively, 4.1, 3.4, and 3.5 times greater than those in the biodiesel exhaust PM. It was quite surprising that the ozone reaction rates of phenanthrene and fluoranthene in B20 biodiesel exhaust PM would be higher than those obtained when the spiked PAHs were exposed to

ozone in the presence of FAMES. The rate of reaction of pyrene with ozone in the biodiesel exhaust PM decreased compared to when the PAHs were exposed to ozone in the presence of FAMES, probably because the constituents of the matrix in the biodiesel exhaust PM were competing for the ozone with pyrene. Furthermore, diffusion of ozone to the sites where pyrene is could have been hindered more in the solid biodiesel exhaust PM matrix compared to the case where PAHs were spiked on bare filter punches. The rates of reaction of phenanthrene and fluoranthene with ozone in the biodiesel exhaust PM were greater than those obtained when the spiked PAHs were exposed in the presence of FAMES and the reason for this observation is not well known.

Previous studies have investigated the effects of several substrates on the ozone reactivity of PAHs. For example, Perraudin et al. (2007) found that the ozone reactivity of the PAHs differed between silica and graphite particles deposited on FF filters. They used an average ozone concentration of  $1.2 \times 10^{14}$  molec.  $\text{cm}^{-3}$ . However, contrary to the results in the present study, the second order rate constants obtained by Perraudin et al. (2007) were about three orders of magnitude higher than those observed in this study. Note that in the present study, the second order rate constants in the Perraudin et al. (2007) study were converted to first order rate constants by multiplying the second order rate constants by the median ozone concentration used ( $1.2 \times 10^{14}$  molec.  $\text{cm}^{-3}$ ) in order to compare the results from the two studies. Furthermore, based on the three PAHs that were detected in the WVO B20 exhaust PM in this study, the ozonation rate constants in the Perraudin et al. (2007) study varied as follows: pyrene > phenanthrene > fluoranthene, which is different than the order observed in this study (pyrene = fluoranthene > phenanthrene).

Kamens et al. (1985) also investigated the pseudo-first order kinetics of the reactions between ozone and the PAHs in wood smoke (Table 3.11). They used an ozone concentration of about 0.57 ppm, and the pseudo-first order rate constant of pyrene was  $0.438 \text{ hr}^{-1}$ , one order of magnitude greater than the pyrene degradation rate observed ( $0.047 \pm 0.033 \text{ hr}^{-1}$ ) for biodiesel exhaust PM in the present study. The difference in the ozonation rate constants of pyrene observed in the present study and that of Kamens et al. (1985) may be explained by the difference in substrates and experimental conditions used. Furthermore, the existence of the FAMES in the biodiesel exhaust PM could also have led to such a low rate of reaction of pyrene observed in our study. Note that Kamens et al. (1985) detected more PAHs (benzo[a]anthracene, chrysene, benzo[k]fluoranthene, and benzo[a]pyrene) in the wood smoke than the PAHs detected in the biodiesel exhaust PM in this study.

Alebic-Juretic et al. (2000) obtained the pseudo-first order rate constants of some PAHs adsorbed on silica particles and exposed to 100 ppb of ozone. The fluoranthene rate constant obtained by Alebic-Juretic et al. (2000) was similar to that obtained in the present study for biodiesel exhaust PM substrate, but the pyrene rate constant was one order of magnitude greater than that obtained in this study.

The effect of vapor pressure on the ozone reaction rates of the PAHs was investigated, but no relationships were obtained suggesting that the reactions between ozone and the PAHs did not occur in the gas-phase. Other factors such as PAH properties like structure and ionization potential could also have affected the ozone reaction rates of the PAHs, but they were not investigated in the present study. The effect

of such properties (structure and ionization potential) on the reactivity of PAHs should be a subject of future investigation.

### 3.3.5 Ozonolysis of FAMES in B20 Biodiesel Exhaust PM

Pseudo-first order kinetics were also assumed for the volatilization and ozonation of the FAMES in WVO biodiesel exhaust PM. Note that the ¼-inch punches were not weighed prior to the control or ozone exposure experiments, but it was later discovered that the mass of PM deposited on the individual punches varied from punch to punch from a single filter by about 30%. In order to account for the differences in mass of biodiesel exhaust PM on each punch, the concentration of each FAME in a punch was normalized to that of methyl stearate (MW=298), a saturated FAME that is nonvolatile and was relatively unreactive to ozone (see Figure 3.21). The rate constants for the volatilization of the FAMES in the biodiesel exhaust PM were lower than those for the FAMES spiked on ¼-inch FF punches with PAHs. This indicates that the FAMES in the biodiesel exhaust PM were strongly adsorbed on to the particulate matter, leading to a reduction in their volatilization rates. As expected, it was methyl myristate that had the highest volatilization rate constant ( $0.012 \pm 0.026 \text{ hr}^{-1}$ ), but it was about 5 times lower than that seen in the case of FAMES spiked on FF punches ( $0.065 \pm 0.004 \text{ hr}^{-1}$ ) with PAHs.

Methyl linolenate was again seen to have the highest effective ozone reaction rate constant ( $0.086 \pm 0.009 \text{ hr}^{-1}$ ) in B20 exhaust PM although it was lower than that observed when the FAMES were spiked on ¼-inch FF punches with PAHs. Methyl linoleate ( $0.070 \pm 0.007 \text{ hr}^{-1}$ ), had the second highest effective ozone reaction rate constant, followed by methyl elaidate ( $0.054 \pm 0.012 \text{ hr}^{-1}$ ) and methyl behenate ( $0.052 \pm 0.029 \text{ hr}^{-1}$ ). Surprisingly, methyl behenate and methyl arachidate, which are high molecular weight

saturated FAMES, had effective rate constants greater than that of methyl oleate ( $0.030 \pm 0.008 \text{ hr}^{-1}$ ), which is an unsaturated FAME with one C=C double bond. The lower effective ozone reaction rate of methyl oleate compared to those of methyl arachidate and methyl behenate in the B20 exhaust PM was contrary to what was observed when FAMES spiked on ¼-inch FF punches with PAHs were exposed to ozone, where methyl oleate had a higher effective rate constant than methyl arachidate and methyl behenate. The reaction rate for methyl palmitate in B20 exhaust PM in the ozone exposure experiment ( $0 \pm 0.004 \text{ hr}^{-1}$ ) was surprisingly lower than that for the corresponding control experiment ( $0.009 \pm 0.002 \text{ hr}^{-1}$ ). The reason for this observation is not known, but it could partly be due to experimental errors. In general, the effective ozone reaction rate constants of the saturated FAMES in the biodiesel exhaust PM were somewhat similar to those observed when the FAMES were spiked on ¼-inch FF punches with PAHs. However, the ozone reaction rates for the unsaturated FAMES in the B20 exhaust PM were about 3 to 5 times lower than those observed when the FAMES were spiked on ¼-inch FF punches with PAHs. The reason for this observation could be that the FAMES are strongly protected by the biodiesel exhaust PM matrix, which hinders the interactions of ozone with the FAMES for the heterogeneous reactions to occur.

No studies have investigated the reaction kinetics of the FAMES in either biodiesel fuel or biodiesel exhaust PM with ozone, making it difficult to compare the FAMES reaction rates from this study to prior studies. However, numerous recent studies have investigated the reaction kinetics between ozone and fatty acid aerosols, most especially oleic acid (e.g., Moise and Rudich 2002; Thornberry and Abbatt 2004; Hearn et al., 2005; Hung et al., 2005; Ziemann 2005; Rosen et al., 2008). FAMES are the ester

analogues to the fatty acids, and because the ozone attack happens on the unsaturated carbon sites of the fatty acids and the FAMES, it is postulated that the relative reaction kinetics of fatty acids and their analogous FAMES with ozone should be equivalent at a given set of experimental conditions. This, therefore, means that it is fair to state that if you know the rate constant of a certain fatty acid at a certain experimental condition, the rate constant of the corresponding FAME will be approximately equal to the rate constant of the fatty acid. For example, Hearn et al. (2005) found that the reactive uptake coefficients (a dimensionless parameter) of oleic acid and methyl oleate particles exposed to ozone in a flow tube were  $(1.38 \pm 0.06) \times 10^{-3}$  and  $(1.23 \pm 0.10) \times 10^{-3}$ , respectively, a result that showed that the reactive uptake coefficients of oleic acid and methyl oleate were not different. Note that the reactive uptake coefficient of a compound is proportional to its rate of reaction (Thornberry and Abbatt, 2004; Rosen et al., 2008). A pseudo-first order rate constant of  $7.2 \text{ hr}^{-1}$  was reported by Hung et al. (2005) when oleic acid droplets were exposed to 300 ppm of ozone. Rosen et al. (2008) coated silica and polystyrene latex (PSL) particles with oleic acid and exposed them to ozone concentrations ranging from 4 to 28 ppm and estimated maximum pseudo-first order ozonation rate constants of  $7920 \text{ hr}^{-1}$  and  $2304 \text{ hr}^{-1}$ , respectively. Furthermore, Ziemann (2005) exposed oleic acid particles to 2.8 ppm of ozone at room temperature and RH  $\sim 0.1\%$  in a PTFE chamber and reported a pseudo-first order rate constant of  $\sim 54 \text{ hr}^{-1}$ . When the pseudo-first order rate constants of oleic acid in the previous studies were normalized to the ozone concentrations used in the respective studies (reaction rate constant divide by ozone concentration), the normalized rate constants were about 1 to 4 orders of magnitude greater than the normalized methyl oleate rate constants obtained in



this study (FF punches spiked with FAMES and PAHs, and biodiesel B20 exhaust PM). This discrepancy could mean that (i) the assumption that the pseudo-first order rate constant of the reaction between a fatty acid and ozone is approximately equal to that of the FAME analogue of the fatty acid is not valid, (ii) the competition for ozone from the other unsaturated FAMES in the mix used in this study led to the decrease in reactivity of methyl oleate when the FAMES were spiked on ¼-inch FF punches, and (iii) B20 exhaust PM matrix contributed to the reduction in reactivity of methyl oleate.

Thornberry and Abbatt (2004) studied the kinetics of the heterogeneous reactions between ozone and liquid films of oleic acid, linoleic acid, and linolenic acid in a pyrex flow tube at room temperature (298 K) and 0% RH for about 35 minutes. The authors reported gas-surface reaction probabilities for ozone loss of  $(8.0 \pm 1.0) \times 10^{-4}$ ,  $(1.3 \pm 0.1) \times 10^{-3}$ , and  $(1.8 \pm 0.2) \times 10^{-3}$  for oleic acid, linoleic acid and linolenic acid, respectively. The reaction probability for the reactive uptake of ozone by organic liquids is defined as the fraction of collisions with the liquid interface leading to removal of ozone from the gas phase (de Gouw and Lovejoy 1998). The gas-surface reaction probability of a compound is proportional to its pseudo-first order rate constant (de Gouw and Lovejoy, 1998; Thornberry and Abbatt 2004). Therefore, we can clearly see from the work of Thornberry and Abbatt (2004) that the pseudo-first order rate constants increased with increasing degree of unsaturation of the fatty acids and the ozone reaction rate of linolenic acid was 1.4 and 2.3 times higher than those of linoleic acid and oleic acid, respectively. Interestingly, the ozone reaction rate of methyl linolenate was 1.2 and 2 times greater than those of methyl linoleate and methyl oleate, respectively, when the FAMES were spiked on ¼-inch FF punches with PAHs in the present study, which is in

close agreement with the results from the study of Thornberry and Abatt (2004) for the fatty acid analogues. Also, the reaction rate of methyl linolenate was 1.2 and 2.9 times higher than those of methyl linoleate and methyl oleate in the B20 exhaust PM. Similarly, de Gouw and Lovejoy (1998) reported that the reaction probabilities of unsaturated organics were greater than those for the saturated organics when a wide range of organic liquids were exposed to ozone. The trends of the rates of reaction of the FAMES with ozone based on the degree of unsaturation in the present study are in agreement with the trends observed in the reactivity of fatty acids with ozone in previous studies.

Ziemann (2005) examined the reactivity of ozone with oleic acid particles in its (oleic acid) pure state and in mixtures. The particle mixtures included: oleic acid in 10:90 mixtures (by mass) with dioctyl sebacate (DOS), hexadecanoic acid ( $C_{16}$ ), and heptadecanoic acid ( $C_{17}$ ). DOS is a high molecular weight (MW=426) liquid ester, while the  $C_{16}$  and  $C_{17}$  monocarboxylic acids are solids at room temperature. It was found that the reactivity of oleic acid in DOS ( $0.020 \pm 0.01 \text{ s}^{-1}$ ) was unaltered, while the reaction rates in  $C_{16}$  ( $0.005 \pm 0.02 \text{ s}^{-1}$ ) and  $C_{17}$  ( $0.012 \pm 0.02 \text{ s}^{-1}$ ) were 1.3 to 3 times slower than that of pure oleic acid ( $0.015 \pm 0.01 \text{ s}^{-1}$ ). Ziemann (2005) concluded that the reactivity of oleic acid was unhindered in a liquid matrix but significantly reduced in a liquid/solid matrix. In the present study, the 3 to 5 times decrease in the reactivity of the FAMES with ozone in B20 biodiesel exhaust PM compared to the pure FAMES spiked on ¼-inch FF filter punches with PAHs is therefore consistent with the literature. The reduction in reactivity of the FAMES could be due to the uptake of ozone by the other compounds in the biodiesel PM matrix on which the FAMES are adsorbed.

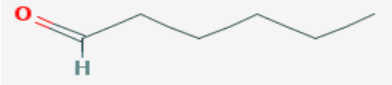
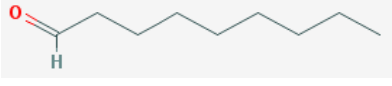
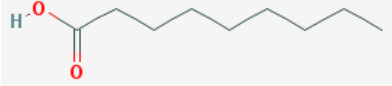
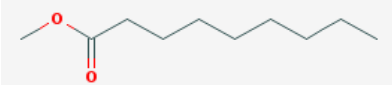
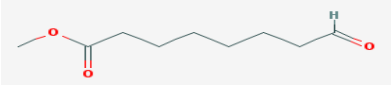
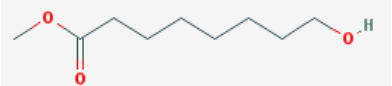
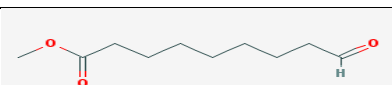
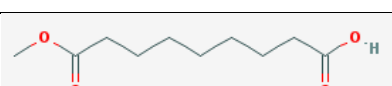

### 3.3.6 Products of the Ozonolysis of PAHs and FAMEs

No ozonolysis products of the PAHs were seen in either the spiked ¼-inch FF punches or in the B20 biodiesel exhaust PM. Because the concentrations of PAHs in the spiked ¼-inch FF punches and in the B20 biodiesel exhaust PM were very low, it is likely that the concentrations of the particle-phase ozonolysis products of the PAHs were below the instrument detection limits. It is also possible that some of the ozonolysis products of the PAHs were gaseous, and thus, did not stay on the filter punches. Therefore, the ozonolysis products of the PAHs will not be discussed.

The main products detected from the ozonolysis of the FAMEs were n-hexanal, n-nonanal, nonanoic acid methyl ester, nonanoic acid, methyl,8-oxooctanoate, octanoic acid,8-hydroxy-methyl ester, nonanoic acid,9-oxo-methyl ester, azelaic acid,dimethyl ester, and azelaic acid,monomethyl ester as shown in Table 3.12. With the exception of n-hexanal and n-nonanal, product identification was based on the NIST 2008 Library search using the AMDIS tool. For n-hexanal and n-nonanal, their authentic standards were used to confirm their spectral identities using the spectra and measured GC retention times. For the other products, identities were confirmed using the match factors obtained in the NIST library search (if the probability of correct identification was greater than 60%). Furthermore, a product's identity was confirmed if that particular compound was consistently detected in the samples that were exposed to ozone. Additionally, the absence of those compounds (products) in the control samples for the case where the FAMEs+PAHs were spiked on ¼-inch FF punches confirmed their presence as ozonation products in the samples that were exposed to ozone. Note that all the FAME ozonolysis products were detected in both the B20 biodiesel exhaust PM samples exposed to ozone

as well as in the B20 biodiesel exhaust PM control samples (Figure 3.22). However, the concentrations of the FAME ozonolysis products were at lower concentrations in the B20 exhaust PM control samples than in the B20 exhaust PM samples exposed to ozone as seen in Figure 3.22. These observations imply that the ozonolysis products of the FAMES were initially present in the B20 biodiesel exhaust PM, and that further oxidation of the FAMES in the biodiesel exhaust PM by ozone added in these experiments led to their increased concentrations.

**Table 3.12 Products identified from the ozonolysis of the FAMES in spiked FF punches and B20 biodiesel exhaust PM after 24 hours of ozone exposure.**

Name	Structure <sup>a</sup>	Molecular Weight	Spiked ¼" FF Punches (ng)	B20 Exhaust PM (ng)
n-Hexanal		100	31.6±26.2	913.8±334.8
n-Nonanal		142	342.8±54.8	1305.0±470.9
Nonanoic acid		158	176.0±9.2	785.8±259.2
Nonanoic acid methyl ester		172	181.0±65.8	598.8±206.8
Methyl,8-oxooctanoate		172	68.5±7.1	143.8±35.0
Octanoic acid,8-hydroxy-methyl ester		174	188.3±27.2	142.8±17.3
Nonanoic acid,9-oxo-methyl ester		186	1259.5±170.4	6277.5±2744.3
Azelaic acid, monomethyl ester		202	510.3±11.7	1963.5±577.7
Azelaic acid, dimethyl ester		216	16.8±3.2	122.3±18.7

a) Pubchem <https://pubchem.ncbi.nlm.nih.gov/search/search.cgi> (Last accessed on 11/19/14)

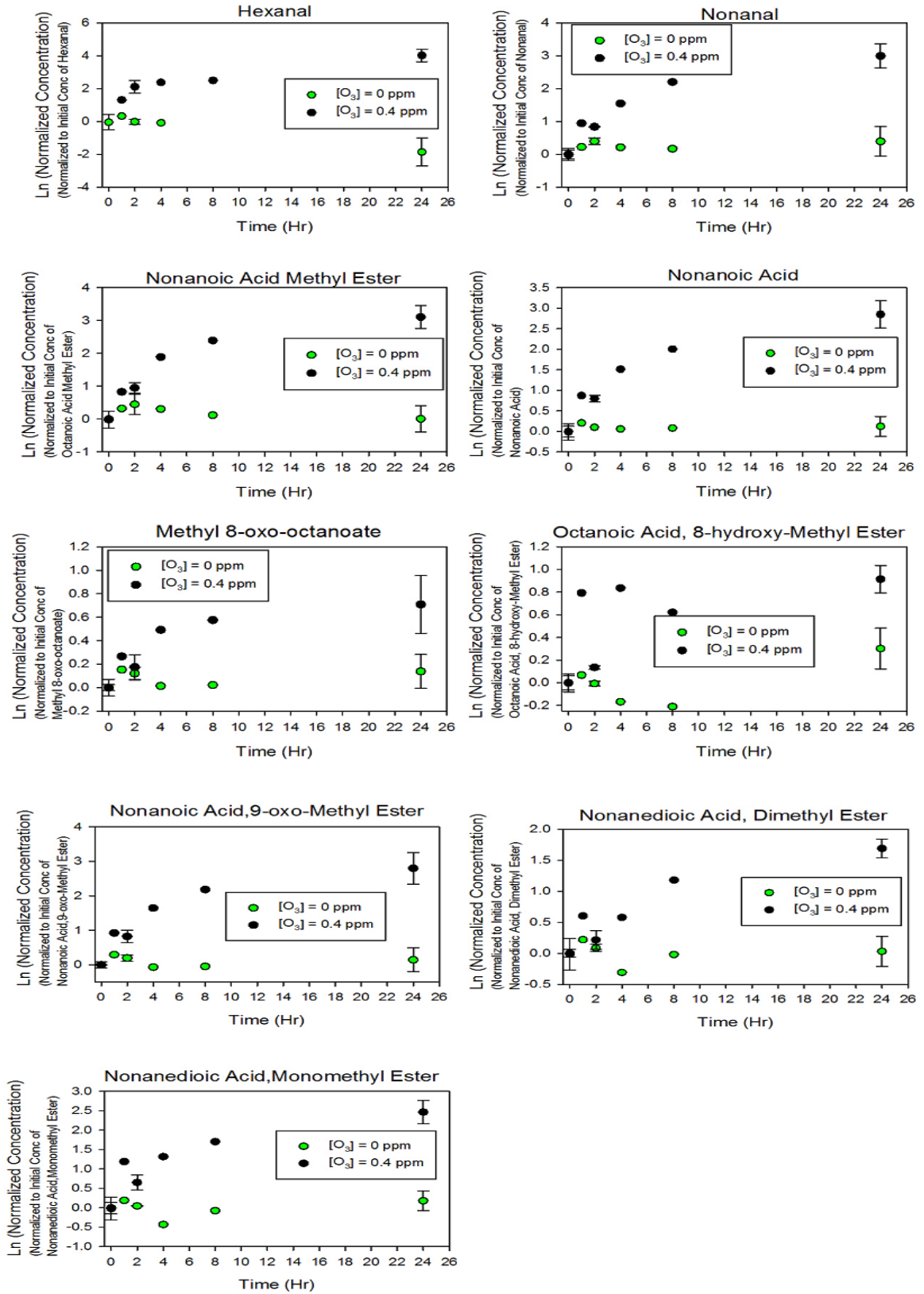


Figure 3.22 Products of the ozonolysis of the FAMES in B20 biodiesel exhaust PM.

The ozonolysis of an unsaturated organic molecule, such as oleic acid, results in products associated with the decomposition of a 1,2,3-trioxolane intermediate, and these products are typically aldehydes or carboxylic acids under oxidative conditions (Zahardis et al., 2006). As observed by Zahardis et al. (2006), the main products of the ozonolysis of the FAMES in the spiked FF punches and B20 biodiesel exhaust PM were aldehydes and carboxylic acids (Table 3.12). Nonanoic acid,9-oxo-methyl ester was the most abundant product seen in the spiked FF punches and in the B20 biodiesel exhaust PM, accounting for at least 40% of all the products observed at any time ( $t \geq 1$  hr) after the beginning of the ozone exposure. This was not surprising because nonanoic acid,9-oxo-methyl ester can be formed by the cleavage of the double bond between the 9<sup>th</sup> and 10<sup>th</sup> carbon atoms from the carbonyl group for all the unsaturated FAMES used in this study. Nonanoic acid,9-oxo-methyl ester was likely a product of the ozonolysis of methyl linolenate, methyl linolelaidate, methyl linoleate, methyl elaidate, and methyl oleate. The second most abundant product identified was azelaic acid,monomethyl ester, and it is also likely that it was formed by ozonolysis of all the unsaturated FAMES. n-Nonanal was the next most abundant product identified, and it was probably due to the ozonolysis of methyl oleate and methyl elaidate. It is only the cleavages of methyl oleate and methyl elaidate isomers that can lead to the formation of n-nonanal when the double bond between the 9<sup>th</sup> and 10<sup>th</sup> carbon atoms from the carbonyl group is broken during ozonation (Zahardis et al., 2006). Nonanoic acid and nonanoic acid methyl ester were also likely formed by the ozonolysis of all the unsaturated FAMES due to the cleavage of the double bond between the 9<sup>th</sup> and 10<sup>th</sup> carbon atoms from the carbonyl group. n-Hexanal was probably formed from the ozonolysis of methyl linolelaidate and methyl

linoleate isomers and it was likely formed as a result of the cleavage of the double bond between the 12<sup>th</sup> and 13<sup>th</sup> carbons from the carbonyl group. Methyl 8-oxooctanoate and octanoic acid,8-hydroxy methyl ester were always identified by the NIST Library in the spiked ¼-inch punches as well as in the B20 biodiesel exhaust PM ozonolysis products. The match factors by the NIST Library were always high (> 80%) for these two compounds, but their mechanism of formation is unclear because no likely cleavage leading to such compounds could be identified. It is possible that these compounds were formed from the interaction of the several Criegee intermediates formed during the ozonolysis of the FAMES. More work needs to be done in the future to understand the mechanisms of formation of these compounds because they are more oxygenated than the parent FAMES, which suggests that they could potentially pose more adverse environmental and health effects than the FAMES. Lastly, a compound tentatively identified as azelaic acid,dimethyl ester was also seen both in the ¼-inch FF punches spiked with FAMES+PAHs exposed to ozone and in the B20 biodiesel exhaust PM ozonolysis samples. The identification of this compound was less certain given that its match factors were always low (< 50%) although it was consistently seen in all the samples exposed to ozone. Additionally, its mechanism of formation is also unclear given that there is no likely cleavage that could lead to such a compound. It is, however, possible that this compound was formed from the reactions of the Criegee intermediates. None of the detected compounds were suspected to be as a result of the ozonolysis of the saturated FAMES because they have no C=C double bonds. Moreover, as already seen from the kinetics results of the FAMES, the saturated FAMES were not lost by



ozonolysis. The only realistic mechanism for the loss of the saturated FAMES in this study is volatilization.

It is important to note that the products identified in the present study most likely existed in the particle-phase of the B20 biodiesel exhaust PM because of their high molecular weights. The very light compounds could not be detected due to the methodology employed in this study, but it is likely that a lot of high volatility compounds with molecular weights less than 100 were formed. Most of the low molecular weight compounds would most likely be formed from the cleavage of the double bonds in methyl linolenate, and methyl linoleate to a lesser extent, as suggested by Zahardis et al. (2006).

The ozonolysis of a mixture of methyl oleate, methyl linoleate, and methyl linolenate particles has been previously investigated using a photoelectron resonance capture ionization mass spectrometer, PERCI-AMS (Zahardis et al., 2006). The authors exposed a mixture of the three unsaturated FAMES to ozone at a partial pressure of  $1 \times 10^{-4}$  for 46 seconds. They identified the ozonolysis products and suggested the possible mechanisms for the formation of those products. A list of 30 first-generation chemical products of the ozonolysis of the three FAMES (methyl oleate, methyl linoleate, and methyl linolenate) was subsequently predicted, of which 25 were detected by the PERCI. With the exception of nonanoic acid methyl ester, methyl,8-oxooctanoate, octanoic acid,8-hydroxy-methyl ester, and azelaic acid,dimethyl ester, the other compounds detected in this study were detected/predicted to be formed during ozonolysis in the Zahardis et al. (2006) study. However, it is important to note that the majority of the first-generation products predicted by Zahardis et al. (2006) were either of low

molecular weight ( $MW < 100$ ), or they were unsaturated. No unsaturated products were detected in this study. The reason for this observation could be due to the longer exposure/reaction times employed in this study, which potentially allowed the complete oxidation of the unsaturated compounds predicted by Zahardis et al. (2006). Furthermore, as mentioned earlier, compounds with molecular weights less than 100 were not detected. Such low molecular weight compounds are very volatile and would not stay in the particle-phase or on the filter punches, making their detection in this study impossible. Some of such low molecular weight compounds include: propanal, malonaldehyde, propanoic acid, 3-oxopropanoic acid, hex-3-enal, malonic acid, and many others as listed by Zahardis et al. (2006).

Figure 3.22 shows the concentrations of the ozonolysis products ( $C_t/C_0$ ) of the FAMES over time. The concentration of a compound at any time,  $C_t$ , was normalized to the initial concentration of that compound,  $C_0$ , and the natural log of the normalized concentration was plotted against exposure time. The initial concentration was defined as the compound concentration at the time point when that compound was first detected. From the plots (Figure 3.22), the concentrations of the products were observed to increase with time, implying that the ozonolysis of the FAMES was responsible for the observed increasing concentrations of those reaction products. Note that the ozone reaction continued to produce products over 24 hours of reaction. The rate of increase of the products was initially fast, but then slowed down with time.

## Chapter 4

### SUMMARY AND RECOMMENDATIONS

In this study, the effect of the use of different blends of two biodiesel feedstocks (WVO and soybean) on the emissions of unregulated pollutants was investigated. Fuels containing 0% (B00), 10% (B10), 20% (B20), 50% (B50), and 100% (B100) biodiesel were prepared by blending ULSD with the neat WVO and soybean biodiesel fuels. Although the study was limited to analysis of raw exhaust PM, the organic chemical speciation of the PM emitted from the different biodiesel blends gives great insight on the relative emission characteristics of soybean and waste cooking oil biodiesel combustion. Data like this could be further used in source apportionment studies to identify the potential biodiesel combustion sources because of the unique existence of FAMES in biodiesel exhaust PM. More detailed exhaust PM composition studies like this, however, would need to be performed with different biodiesel feedstocks in order to more accurately use such data in source apportionment models to identify emissions from particular biodiesel feedstocks.

The findings of this study suggest that use of WVO and soybean biodiesel blends in a light-duty diesel engine operating in an urban drive cycle leads to significant reductions in the emissions of some compounds that are harmful to human health and the environment such as PAHs, n-alkanes, and some carbonyls and quinones. Based on the practical and most widely used biodiesel blends in diesel engines (B10 and B20), biodiesel use leads to reductions in the emission of n-alkanes, PAHs, quinones, and some carbonyls compared to petrodiesel. Furthermore, although there were reductions in the emissions with increasing biodiesel content in the fuel, complete elimination of PAH and

n-alkane emissions, however, was not observed even with the 100% biodiesel fuels. Thus, compounds like PAHs and n-alkanes are not only emitted as a result of unburned fuel, but also due to some possible combustion mechanisms in the engine, such as free radical interactions and combustion of lubricating oil with the petrodiesel/biodiesel fuel.

The use of WVO and soybean biodiesel blends also leads to an increase in the emissions of some toxic compounds such as the aliphatic carbonyls with less than 10 carbon atoms, which have been previously reported to be responsible for oxidative stress (Mauderly 1997). Therefore, use of biodiesel in diesel engines has both positive and negative effects on the emissions of unregulated compounds that affect human health and the environment. In order to promote biodiesel for use in diesel engines, there has to be a tradeoff with regard to the emission of some of the unregulated pollutants. If attention is paid to reducing emissions of PAHs, n-alkanes, aromatic aldehydes, aromatic ketones, and quinones, then biodiesel is a suitable substitute for conventional diesel. However, if reducing emissions of aliphatic and low molecular weight carbonyls ( $< C_{10}$ ) is the primary concern, then biodiesel would not be a suitable substitute for petrodiesel as it leads to increased emission of such compounds. Note that the light-duty diesel engine used in this study did not have a diesel particulate filter, diesel oxidation catalyst, or any aftertreatment device. Installation of an aftertreatment device on the engine could potentially have affected the emissions of some compounds studied. Overall, based on previous studies that found that biodiesel use in heavy-duty diesel engines led to reductions in the emission of most criteria pollutants (e.g., McCormick et al., 2001; EPA, 2002; Krahl et al., 2005; Knothe et al., 2006), coupled with the results from this study, biodiesel may be a more appropriate fuel to use in diesel engines instead of petrodiesel

because it leads to decreases in the emission of most unregulated pollutants as well. Further, based on the results of this study, the reductions in the emissions of PAHs and n-alkanes in the exhaust PM of both soybean and WVO biodiesel feedstocks compared to petrodiesel were not statistically different, and the increases in the emissions of the POCs and FAMEs from both feedstocks compared to petrodiesel were also not statistically different. This implies that use of either soybean or WVO biodiesel in a light-duty diesel engine would have similar advantages and disadvantages to the unregulated emissions investigated in this study. Furthermore, the neat fuels of either WVO or soybean biodiesel would be the most beneficial fuel to use in a light-duty diesel engine, although running of diesel engines with neat biodiesel fuels is quite impractical for cold weather and engine capability issues (Knothe 2005).

Given that the emission rates of most target analytes of both WVO and soybean biodiesel fuel blends were not statistically different, it suggests that there is no advantage of using one feedstock over the other in terms of the unregulated emissions studied in this dissertation. However, given that WVO biodiesel fuel is made from used cooking oil, it is more advantageous to use as biodiesel fuel than soybean biodiesel because it is waste that is converted into fuel after the virgin oil is used for cooking. Therefore, cooking oil can be used as both food and fuel when WVO is used, unlike soybean biodiesel where food is used for fuel.

With the exception of the neat fuels of WVO and soybean biodiesel, n-alkanes ( $C_{11}$ - $C_{24}$ ) were detected in all the WVO and soybean blends together with petrodiesel, while branched alkanes were detected in the lubricating oil. Detection of the n-alkanes ( $C_{14}$ - $C_{26}$ ) in the exhaust PM of petrodiesel and the different blends of biodiesel suggests

that n-alkanes are emitted as a result of unburned fuel, and from the combustion of the branched alkanes in the lubricating oil. The n-alkanes detected in the exhaust PM of the neat B100 biodiesel fuels were potentially formed from the combustion of the high MW branched alkanes and cycloalkanes in the lubricating oil. Although the emissions of n-alkanes in diesel engines are significantly reduced with biodiesel use, it is difficult to completely eliminate the emission of n-alkanes even with neat biodiesel if no changes are made to the current lubricating oil formulations. Compared to older studies (e.g., Williams et al., 1989; Schauer et al., 1999; Mi et al., 2000; Brandenberger et al., 2005) that detected significantly high concentrations of PAHs in diesel fuel, it appears that the current diesel fuels contain very low concentrations of PAHs as observed in the present study. This implies that the EPA's Clean Air Highway Diesel rule of 2001 (US EPA 2006) possibly led to cleaner diesel fuel with a maximum sulfur content of 15 ppm that consequently led to the cleaner diesel fuels used currently. The PAHs detected in the exhaust PM of petrodiesel and the different blends of biodiesel were probably formed during the combustion of the constituents of the fuel and lubricating oil and the free radical interactions in the engine. The unsubstituted PAHs detected in the exhaust PM of the neat biodiesel fuels were possibly formed from the free radical interactions in the engine during the combustion of the lubricating oil and the biodiesel fuel. This also highlights the importance of the need to reformulate lubricating oil in order to eliminate emission of carcinogenic PAHs if diesel engines are fueled with biodiesel fuel. The emission of FAMES as unburned fuel increased with increasing biodiesel in the fuel, but it was found that the degree of combustion of the FAMES increased with increasing number of C=C double bonds. Carbonyls and quinones were not detected in any of the

fuel samples, but they were detected in the exhaust PM, which suggests that the carbonyl and quinone formation was from the partial oxidation of the fuel and lubricating oil constituents.

Because of the similarity in the organic chemical compositions of both WVO and soybean biodiesel fuels used in this study, the two biodiesel feedstocks had very minimal differences in the emission rates of the compounds studied. In the future, it will be important to use biodiesel feedstocks that have different chemical compositions. For example, studies should be conducted with animal-based and vegetable oil-based biodiesel feedstocks because the animal-based feedstocks have higher proportions of saturated FAMES than vegetable oil-based feedstocks. The differences in saturation of the FAMES in the animal-based and vegetable oil-based feedstocks could play a role in the emissions because the unsaturated FAMES are easier to oxidize due to the presence of C=C doubles, unlike the saturated FAMES that have no C=C double bonds.

In this study, it was difficult to distinguish between the emissions due to the combustion of the lubricating oil from those due to the combustion of the fuel. In the future, experiments should be designed to be able to separate the emissions due to the combustion of the lubricating oil only from those due to combustion of the fuel only. From such experiments, it will be possible to determine whether the emissions in the exhaust PM are truly due to fuel combustion, and hence better comparison of emissions due to fuel combustion could be assessed.

The kinetics of the reactions of ozone with PAHs and PAHs+FAMES, and in B20 biodiesel exhaust PM were also investigated. The results indicate that the pseudo-first order ozonation rate constants of the PAHs decreased between 1.2 to 8 times when they

were exposed to ozone in the presence of the FAMES, and (3-4 times) when B20 biodiesel exhaust PM was exposed to ozone. The unsaturated FAMES had higher pseudo-first order ozone reaction rate constants than saturated FAMES and PAHs, as expected. The pseudo-first order ozone reaction rates of the unsaturated FAMES were lower in the B20 biodiesel exhaust PM than in the spiked FF filters, indicating that the reactivity of the compounds during heterogeneous oxidation depends on the type of matrix used. These results suggest that the real-world atmospheric lifetimes of the PAHs in biodiesel exhaust PM increase because of the reduced reactivity of the PAHs due to the matrix in the biodiesel exhaust PM. The PAHs in the biodiesel exhaust PM would therefore be capable of staying in the atmosphere for long times and would consequently be transported to farther distances from their sources.

Chemical transformation of primary pollutants can lead to reaction products that impact the environment and human health. Ozonolysis of the FAMES leads to formation of more oxygenated compounds. For example, most of the ozonolysis products of the FAMES were either equally as oxygenated as their parent FAMES (e.g., nonanoic acid and nonanoic acid methyl ester), or more oxygenated (e.g., methyl,8-oxooctanoate, octanoic acid,8-hydroxy-methyl ester, nonanoic acid,9-oxo-methyl ester, azelaic acid,monomethyl ester, and azelaic acid,dimethyl ester) than the parent FAMES. Increases in the molecular oxygen content of particles can increase the hygroscopicity of the particles, thereby impacting the ability of the particles to act as cloud condensation nuclei (Sun and Ariya 2006; Zahardis et al., 2006). The formation of carbonyls such as n-hexanal and n-nonanal from the ozonolysis of the unsaturated FAMES suggests that biodiesel exhaust PM could be more detrimental to both the environment and human



health than the original FAMEs because they can cause oxidative stress in humans (Mauderly 1997). The results of this study suggest that biodiesel emissions from a light-duty diesel engine could lead to long atmospheric lifetimes of some pollutants such as PAHs, and could also lead to formation of more oxygenated high molecular weight/particle-bound products.

For a better understanding of the effects of biodiesel exhaust PM on the heterogeneous reactions of ozone with PAHs in biodiesel exhaust PM, in the future, exhaust PM from petrodiesel and other biodiesel fuel blends such as B10, B50, and B100 should be conducted. By conducting such studies, the effect of biodiesel content in the fuel on the ozone oxidation rates of the PAHs in biodiesel exhaust PM could be better assessed.

## Chapter 5

### REFERENCES CITED

- Alebic-Juretic, A., Cvitas, T., Klasinc, L., 2000. Kinetics of heterogeneous ozone reactions. *Chemosphere*, 41, 667-670.
- Bakeas, E., Karavalakis, G., Stournas, S., 2011. Biodiesel emissions profile in modern diesel vehicles. Part 1: effect of biodiesel origin on the criteria emissions. *Sci. Total Environ.*, 409, 1670-1676.
- Bikas, G., Zervas, E., 2007. Non-regulated pollutants emitted from Euro 3 diesel vehicles as a function of their mileage. *Energy and Fuels* 21, 2731-2736.
- Brandenberger, S., Mohr, M., Grob, K., Neukom, H.P., 2005. Contribution of unburned lubricating oil and diesel fuel to particulate emission from passenger cars. *Atmos. Environ.*, 39, 6985-6994.
- Cahill, M.T., Okamoto, R.A., 2012. Emissions of acrolein and other aldehydes from biodiesel-fueled heavy-duty vehicles. *Environ. Sci. Technol.*, 46, 8382-8388.
- Cardone, M., Prati, M.V., Seggiani, M., Senatore, A., Vitolo, S., 2002. Brassica carinata as an alternative oil crop for the production of biodiesel in Italy: engine performance and regulated and unregulated exhaust emissions. *Environ. Sci. Technol.*, 36, 4656-4662.
- Chien, S-M., Huang, Y-J., Chuang, S-C., Yang, H-H., 2009. Effects of biodiesel blending on particulate and polycyclic aromatic hydrocarbon emissions in nano/ultrafine/fine/coarse ranges from diesel engine. *Aerosol and Air Quality Research*, 9, 18-31.
- Cho, A.K., Di Stefano, E., You, Y., Rodriguez, C.E., Schmitz, D.A., Kumagai, Y., Miguel, A.H., Eiguren-Fernandez, A., Kobayashi, T., Avol, E., Froines, J.R., 2004. Determination of four quinones in diesel exhaust particles, SRM 1649a, and atmospheric PM2.5. *Aerosol Sci. Technol.*, 38, 68-81.
- Clausnitzer, H., Singer, M.J., 1997. Intensive land preparation emits respirable dust. *California Agriculture*, 51, 27-30.
- Cole J.A., Bittner, J.D., Longwell, J.P., Howard, J.B., 1984. Formation Mechanisms of Aromatic Compounds in Aliphatic Flames. *Combustion and Flame*, 56, 51-70.
- Correa, S.M., Arbilla, G., 2006. Aromatic hydrocarbons emissions in diesel and biodiesel exhaust. *Atmos. Environ.*, 40, 6821-6826.

- Correa, S.M., Arbilla, G., 2008. Carbonyl emissions in diesel and biodiesel exhaust. *Atmos. Environ.*, 42, 769-775.
- de Gouw, A.J., Lovejoy, R.E., 1998. Reactive uptake of ozone by liquid organic compound. *Geophysical Research Letters*, 25, 931-934.
- Demirbas, A., 2007. Importance of biodiesel as transportation fuel. *Energy Policy*, 35, 4661-4670.
- Donaldson, D.J., Mmereki, B.T., Chaudhuri, S.R., Handley, S., Oh, M., 2005. Uptake and reaction of atmospheric organic vapours on organic films. *Faraday Discuss.*, 130, 227-239.
- Erickson, M.H., Wallace, H.W., Jobson, B.T., 2012. Quantification of diesel exhaust gas phase organics by a thermal desorption proton transfer reaction mass spectrometer. *Atmos. Chem. Phys. Discuss.*, 12, 5389-5423.
- Feralio, S.T., Holmén A.B., 2015. Varying effect of biodiesel blend on total ultrafine particle emissions from a light-duty diesel engine. *Environ. Sci. Technol.*, (In Press).
- Fraser, M.P., Buzcu, B., Yue, Z.W., McGaughey, G.R., Desai, N.R., Allen, D.T., Seila, R.L., Lonneman, W.A., Harley, R.A., 2003. Separation of fine particulate matter emitted from gasoline and diesel vehicles using chemical mass balancing techniques. *Environ. Sci. Technol.*, 37, 3904-3909.
- Gangwar, J., Gupta, T., Gupta, S., Agarwal, K.A., 2011. Emissions from diesel versus biodiesel fuel used in a CRDI SUV engine: PM mass and chemical composition. *Inhalation Toxicology*, 23, 449-458.
- Graboski, M.S., McCormick, R.L., 1998. Combustion of fat and vegetable oil derived fuels in diesel engines. *Progr. Energy Combustion Sci.*, 24, 125-164.
- Grosjean, D., Fung, K., Harrison, J., 1983. Interactions of polycyclic aromatic hydrocarbons with atmospheric pollutants. *Environ. Sci. Technol.*, 17, 673-679.
- Guarieiro, L., Pereira, P., Torres, E., Olimpio da Rocha, G., de Andrade, J., 2008. Carbonyl compounds emitted by a diesel engine fuelled with diesel and biodiesel–diesel blends: Sampling optimization and emissions profile. *Atmos. Environ.*, 42, 8211–8218.
- Hearn, D.J., Lovett, J.A., Smith, D.G., 2005. Ozonolysis of oleic acid particles: evidence for a surface reaction and secondary reactions involving Criegee intermediates. *Phys. Chem. Chem. Phys.*, 7, 501-511.

- Henry, T.R., Wallace, K.B., 1996. Differential mechanisms of cell killing by redox cycling and arylating quinones, *Arch. Toxicol.*, 70, 482-489.
- Hoekmann, S.K., Broch A., Robbins, C., Cenicerros, E., Natarajan, M., 2012. Review of biodiesel composition, properties, and specifications. *Renewable and sustainable energy reviews*, 16, 143-169.
- Holmén, B.A., Feralio, T., Dunshee, J., Sentoff, K., 2014. Tailpipe emissions and engine performance of a light-duty diesel engine operating on petro- and bio-diesel fuel blends. TRC Report 14-008; The University of Vermont, Transportation Research Center.
- Hung, H-M., Katrib, Y., Martin, T.S., 2005. Products and mechanisms of the reaction of oleic acid with ozone and nitrate radical. *J. Phys. Chem. A*, 109, 4517-4530.
- Jakober, A.C., Charles, M.J., Kleeman, J.M., Green, G.P., 2006. LC-MS analysis of carbonyl compounds and their occurrence in diesel emissions. *Anal. Chem.*, 78, 5086-5093.
- Jakober, A.C., Riddle, G.S., Robert, A.M., Destailats, H., Charles, M.J., Green, G.P., Kleeman, J.M., 2007. Quinone emissions from gasoline and diesel motor vehicles. *Environ. Sci. Technol.*, 41, 4548-4554.
- Jakober, A.C., Robert, A.M., Riddle, G.S., Hugo, D., Charles, M.J., Green, G.P., Kleeman, J.M., 2008. Carbonyl emissions from gasoline and diesel motor vehicles. *Environ. Sci. Technol.*, 42, 4697-4703.
- Kahan, F.T., Kwamena, N-OA., Donaldson, J.D., 2006. Heterogeneous ozonation kinetics of polycyclic aromatic hydrocarbons on organic films. *Atmos. Environ.*, 40, 3448-3459.
- Kahn, J., Rang, H., Kriis, J., 2002. Advances in biodiesel fuel research. *Proc. of Estonian Acad. Sci. Chem.*, 51, 75-117.
- Kamens, M.R., Perry, M.J., Saucy, A.D., Bell, A.D., Newton, L.D., Brand, B., 1985. Factors which influence polycyclic aromatic hydrocarbon decomposition on wood smoke particles. *Environ. International*, 11, 131-136.
- Karavalakis, G., Stournas, S., Bakeas, E., 2009. Effects of diesel/biodiesel blends on regulated and unregulated pollutants from a passenger vehicle operated over the European and the Athens driving cycles. *Atmos. Environ.*, 43, 1745-1752.
- Karavalakis, G., Boutsika, V., Stournas, S., Bakeas, E., 2011. Biodiesel emissions profile in modern diesel vehicles. Part 2: Effect of biodiesel origin on carbonyl, PAH, nitro-PAH and oxy-PAH emissions. *Sci. Total Environ.*, 409, 738-747.

- Kjelgaard, J., Sharratt, B., Sundram, I., Lamb, B., Claiborn, C., Saxton, K., Chandler, D., 2004. PM<sub>10</sub> emission from agricultural soils on the Columbia Plateau: comparison of dynamic and time-integrated field-scale measurements and entrainment mechanisms. *Agricultural and Forestry Meteorology*, 125, 259-277.
- Knothe, G., 2005. Dependence of biodiesel fuel properties on the structure of fatty acid alkyl esters. *Fuel Processing Technol.*, 86, 1059-1070.
- Knothe, G., Sharp, C.A., Ryan, T.W., 2006. Exhaust emissions of biodiesel, petrodiesel, neat methyl esters, and alkanes in a new technology engine. *Energy Fuels*, 20, 403-408.
- Krahl, J., Munack, A., Schroder, O., Stein, H., Bunger, J. Influence of biodiesel and different petrodiesel fuels on exhaust emissions and health effects. In *The Biodiesel Handbook*; Knothe, G., Van Gerpen, J., Krahl, J., Eds.; AOCS Press: Champaign, IL, 2005, 175-182.
- Kwamena, A.N., Thornton, A.J., Abbatt, P.D.J, 2004. Kinetics of surface-bound Benzo[a]pyrene and ozone on solid organic and salt aerosols. *J. Phys. Chem. A*, 108, 11626-11634.
- Kwamena, N.-O.A., Staikova, M. G., Donaldson, D.J., George, I. J., Abbatt, J.P.D., 2007. Role of the aerosol substrate in the heterogeneous ozonation reactions of surface-bound PAHs. *J. Phys. Chem. A*, 111, 11050-11058.
- Last, R.J., Kruger, M., Durnholz, M., 1995. Emissions and performance characteristics of a 4-Stroke, direct injected diesel engine fueled with blends of biodiesel and low sulfur diesel fuel. Technical Paper 950054; SAE: Warrendale, PA.
- Liang, F., Lu, M., Keener, T.C., Liu, Z., Khang, S.J., 2005. The organic composition of diesel particulate matter, diesel fuel and engine oil of a non-road diesel generator. *J Environ. Monit.*, 7, 983-988.
- Lim, H.-J., Carlton, A.G., Turpin, B.J., 2005. Isoprene forms secondary organic aerosol through cloud processing: model simulations. *Environ. Sci. Technol.* 39, 4441-4446.
- Lin, Y-C., Lee, W-J., Hou, H-C., 2006. PAH emissions and energy efficiency of palm-biodiesel blends fueled on diesel generator. *Atmos. Environ.*, 40, 3930-40.
- Ma, F., Hanna, M.A., 1999. Biodiesel production: a review. *Bioresource Technology*. 70, 1-15.
- Magara-Gomez, K.T., Olson, M.R., Okuda, T., Walz, K.A., Schauer, J.J., 2012. Sensitivity of diesel Particulate material emissions and composition to blends of petroleum diesel and biodiesel fuel. *Aerosol Sci. Technol.*, 46, 1109-1118.

- Maher, K.D., Bressler, D.C., 2007. Pyrolysis of triglyceride materials for the production of renewable fuels and chemicals. *Bioresource Technology*, 98, 2351-2368.
- Mao, D., Van De Weghe, H., Lookman, R., Vanermen, G., De Brucker, N., Diels, L., 2009. Resolving the unresolved complex mixture in motor oils using high-performance liquid chromatography followed by comprehensive two-dimensional gas chromatography. *Fuel*, 88, 312-318.
- Marr, C.L., Kirchstetter, W.T., Harley, A.R., 1994. Characterization of polycyclic aromatic hydrocarbons in motor vehicle fuels and exhaust emissions. *Environ. Sci. Technol.*, 33, 3091-3099.
- Mauderly, J.L., 1997. Health issues concerning inhalation of petroleum diesel and biodiesel exhaust. In: *Plant Oils as Fuels: Present State of Science and Future Developments* (Martini N, Schell J, eds). Berlin:Springer, 92–103.
- McCormick, L.R., Graboski, S.M., Alleman, L.T., Herring, M.A., 2001. Impact of biodiesel source material and chemical structure on emissions of criteria pollutants from a heavy-duty engine. *Environ. Sci. Technol.*, 35, 1742-1747.
- McDonald, J.F., Purcell, D.L., McClure, B.T., Kittelson, D.B., 1995. Emissions characteristics of soy methyl ester fuels in an IDI compression ignition engine. Technical Paper 950400; SAE: Warrendale, PA.
- Mi, H-H., Lee, W-J., Chen, C-B., Yang, H-H., Wu, S-J., 2000. Effect of fuel aromatic content on PAH emission from a heavy-duty diesel engine. *Chemosphere*, 41, 1783–1790.
- Moise, T., Rudich, Y., 2002. Reactive Uptake of Ozone by Aerosol-Associated Unsaturated Fatty Acids: Kinetics, Mechanism, and Products. *J. Phys. Chem. A*, 106, 6469-6476.
- Needham, J. R., Doyle, D. M., 1985. The Combustion and ignition quality of alternative fuels in light-duty diesels; Technical Paper 852101; SAE: Warrendale, PA.
- Nelson, F.P., Tibbett, R.A., Day, J.S., 2008. Effects of vehicle type and fuel quality on real world toxic emissions from diesel vehicles. *Atmos. Environ.*, 42, 5291-5303.
- Pang, X., Shi, X., Mu, Y., He, H., Shuai, S., Chen, H., Li, R., 2006. Characteristics of carbonyl compounds from a diesel-engine using biodiesel-ethanol-diesel as fuel. *Atmos. Environ.*, 40, 7057-7065.
- Payri, F., Bermúdez, V.R., Tormos, B., Linares, W.G., 2009. Hydrocarbon emissions speciation in diesel and biodiesel exhausts. *Atmos. Environ.*, 43, 1273-1279.

- Perraudin, E., Budzinski, H., Villenave, E., 2007. Kinetic Study of the Reactions of Ozone with Polycyclic Aromatic Hydrocarbons Adsorbed on Atmospheric Model Particles. *J. Atmos. Chem.*, 56:57-82.
- Pinto, A.C., Guarieiro, L.N., Renzende, J.C., Ribeiro, N.M., Torres, E.A., Lopez, E.A., et al 2005. Biodiesel: An overview. *J Braz. Chem. Soc.* 16(6B):1313-1330.
- Pitts, Jr. J.N., Van Cauwenberghe, K.A., Grosjean, D., Schmid, J.P., Fitz, D.R., Belser, Jr. W.L., Knudson, G.B., Hynds P.M., 1978. Atmospheric reactions of polycyclic aromatic hydrocarbons: facile formation of mutagenic nitro derivatives. *Science*, 202(4367), 515-519.
- Poschl, U., Letzel, T., Schauer, C., Niessner, R., 2001. Interaction of ozone and water vapor with spark discharge soot aerosol particles coated with benzo(a)pyrene: O<sub>3</sub> and H<sub>2</sub>O adsorption, benzo(a)pyrene degradation, and atmospheric implications. *J. Phys. Chem. A*, 105, 4029-4041.
- Purcell, D.J., McClure, B.T., McDonald, J., Basu, H. N., 1996. Transient testing of soy methyl ester fuels in an indirect injection, compression ignition engine; *J. Am. Oil Chem. Soc.*, 73, 381-388.
- Qiu, G., Pattey, E., 2008. Estimating PM<sub>10</sub> emissions from spring wheat harvest using an atmospheric tracer technique. *Atmos. Environ.*, 42, 8315-8321.
- Richter, H., Howard, J.B., 2000. Formation of polycyclic aromatic hydrocarbons and their growth to soot - a review of chemical reaction pathways. *Progress in Energy and Combustion Science*, 26, 565-608.
- Rogge, F.W., Hildemann, M.L., Mazurek, A.M., Caw, R.G., Simoneit, T.R.B., 1993. Sources of Fine Organic Aerosol. 2. Noncatalyst and Catalyst-Equipped Automobiles and Heavy-Duty Diesel Trucks. *Environ. Sci. Technol.*, 27, 636-651.
- Rosen, P.E., Garland, R.E., Baer, T., 2008. Ozonolysis of Oleic Acid Adsorbed to Polar and Nonpolar Aerosol Particles. *J. Phys. Chem. A*, 112, 10315-10324.
- Rudich, Y., Donahue, N.M., Mentel, F.T., 2007. Aging of Organic Aerosol: Bridging the Gap between Laboratory and Field Studies. *Annu. Rev. Phys. Chem.* 58, 321-52.
- Schauer, J.J., Kleeman, M.J., Cass, G.R., Simoneit, B.R.T., 1999. Measurement of emissions from air pollution sources. 2. C<sub>1</sub> through C<sub>30</sub> organic compounds from medium duty diesel trucks. *Environ. Sci. Technol.*, 33, 1578-1587.
- Schmidt, K., Van Gerpen, J., 1996. The effect of biodiesel fuel composition on diesel combustion and emissions. Technical Paper 961086; SAE: Warrendale, PA.

- Stevens, N.T., 2010. Observations on the atmospheric aging of PAHs adsorbed to diesel particulate matter and quartz fiber filters at an atmospherically relevant ozone concentration (M.S. Thesis, University of Vermont).
- Sun, J., Ariya, A.P., 2006. Atmospheric organic and bio-aerosols as cloud condensation nuclei (CCN): A review. *Atmos. Environ.*, 40, 795-820.
- Thornberry, T., Abbatt, J.P.D., 2004. Heterogeneous reaction of ozone with liquid unsaturated fatty acids: detailed kinetics and gas-phase product studies. *Phys. Chem. Chem. Phys.*, 6, 84-93.
- Tsapakis, M., Stephanou, E.G., 2003. Collection of gas and particle semi-volatile organic compounds: use of an oxidant denuder to minimize polycyclic aromatic hydrocarbons degradation during high-volume air sampling. *Atmos. Environ.*, 37, 4935-4944.
- Turrio-Baldassarri, L., Battistelli, C.L., Conti, L., Crebelli, R., de Berardis, B., Iamiceli, A.L., Gambino, M., Iannaccone, S., 2004. Emission comparison of urban bus engine fueled with diesel oil and biodiesel blend. *Sci. Total Environ.*, 327, 147-162.
- U.S. Environmental Protection Agency, Method 556, 1998. Determination of carbonyl compounds in drinking water by pentafluorobenzylhydroxylamine derivatization and capillary gas chromatography with electron capture detection. National Exposure Research Laboratory, Office of Research and Development, US Environmental Protection Agency, Cincinnati, OH.
- U.S. Environmental Protection Agency, 2002. A comprehensive analysis of biodiesel impacts on exhaust emissions. Draft Technical Report 420-P-02-001; National Service Center for Environmental Publications: Cincinnati, OH, October 2002; <http://www.epa.gov/otaq/models/analysis/biodsl/p02001.pdf>.
- U.S. Environmental Protection Agency, 2006. Introduction of cleaner-burning diesel fuel enables advanced pollution control for cars, trucks and buses. Program Update 420-F-06-064; Office of Transportation and Air Quality: October 2006; <http://www.epa.gov/oms/highway-diesel/regs/420f06064.pdf>.
- Valavanidis, A., Fiotakis, K., Vlahogianni, T., Papadimitriou, V., Pantikaki, V., 2006. Determination of selective quinones and quinoid radicals in airborne particulate matter and vehicular exhaust particles. *Environ. Chem.*, 3, 118-123.
- Westerholm, R., Li, H., 1994. A multivariate statistical analysis of fuel-related polycyclic aromatic hydrocarbon emissions from heavy-duty diesel vehicles. *Environ. Sci. Technol.*, 28, 965-972.



- Williams, P.T., Abbass, M.K., Andrews, G.E., Bartle, K.D., 1989. Diesel particulate-emissions-the role of unburned fuel. *Combustion and Flame* 75, 1–24.
- World Health Organization, 1996. Diesel fuel and exhaust emissions. International Program on Chemical Safety. Environmental Health Criteria 171, Geneva, Switzerland.
- Wu, G.Y-P., Lin, Y-F., 2012. Trace species formation pathway analysis of biodiesel engine exhaust. *Applied Energy*, 91, 29-35.
- Zahardis, J., LaFranchi, W.B., Petrucci, A.G., 2006. The heterogeneous reaction of particle-phase methyl esters and ozone elucidated by photoelectron resonance capture ionization: Direct products of ozonolysis and secondary reactions leading to the formation of ketones. *International Journal of Mass Spectrometry*, 253, 38-47.
- Zhou, S., Lee, A.K.Y., McWhinney, R.D., Abbatt, J.P.D., 2012. Burial effects of organic coatings on the heterogeneous reactivity of particle-borne benzo[a]pyrene (BaP) toward ozone. *J. Phys. Chem. A*, 116, 7050-7056.
- Ziemann, J.P., 2005. Aerosol products, mechanisms, and kinetics of heterogeneous reactions of ozone with oleic acid in pure and mixed particles. *Faraday Discuss.*, 130, 469-490.

## APPENDIX A

**Table A-1. Target compounds quantified.**

Compounds	Compound ID	CAS Number	Conc	Supplier	Cat #
<b>PAHs Mix (100 µg/mL each in DCM)</b>					
				Ultra Scientific	PM-611
Naphthalene	NAP	91-20-3	100		
Acenaphthylene	ACY	208-96-8	100		
Acenaphthene	ACE	83-32-9	100		
Fluorene	FLU	86-73-7	100		
Phenanthrene	PHEN	85-01-8	100		
Anthracene	ANTH	120-12-7	100		
Fluoranthene	FLUOR	206-44-0	100		
Pyrene	PYR	129-00-0	100		
Benzo[a]anthracene	BaA	56-55-3	100		
Chrysene	CHR	218-01-9	100		
Benzo[b]fluoranthene	BbF	205-99-2	100		
Benzo[k]fluoranthene	BkF	207-08-9	100		
Benzo[a]pyrene	BaP	50-32-8	100		
Indeno[1,2,3-cd]pyrene	IDP	193-39-5	100		
Benzo[ghi]perylene	BghiP	191-24-2	100		
Dibenz[a,h]anthracene	DBahA	53-70-3	100		
<b>POCs</b>					
2-Pentanone	2PNN	107-87-9	Pure	Sigma Aldrich	68950-100ML
3-Pentanone	3PNN	96-22-0	Pure	Sigma Aldrich	127604-100ML
2-Hexanone	2HXN	591-78-6	Pure	Sigma Aldrich	02473-5ML
2-Heptanone	2HPN	110-43-0	Pure	Sigma Aldrich	02476-1ML
2-Octanone	2OCT	111-13-7	Pure	Sigma Aldrich	02479-1ML
2-Nonanone	2NNE	821-55-6	Pure	Sigma Aldrich	108731-5G
n-Hexanal	HXNL	66-25-1	Pure	Sigma Aldrich	115606-2ML
n-Heptanal	HPTL	111-71-7	Pure	Sigma Aldrich	W254002
n-Octanal	OCTL	124-13-0	Pure	Sigma Aldrich	O5608-25ML

n-Nonanal	NNNL	124-19-6	Pure	Sigma Aldrich	442719
n-Decanal	DECL	112-31-2	Pure	Sigma Aldrich	D7384-25G
Undecanal	UDCL	112-44-7	Pure	Sigma Aldrich	U2202-25G
Dodecanal	DDCL	112-54-9	Pure	Sigma Aldrich	W261505
Benzaldehyde	BZDE	100-52-7	Pure	Sigma Aldrich	B1334-2G
m-Tolualdehyde	mTOL	620-23-5	Pure	Sigma Aldrich	T35505-5G
o-Tolualdehyde	oTOL	529-20-4	Pure	Sigma Aldrich	117552-25G
p-Tolualdehyde	pTOL	104-87-0	Pure	Sigma Aldrich	T35602-100G
Acetophenone	ACNE	98-86-2	Pure	Sigma Aldrich	42163-1ML-F
1-Indanone	1IND	83-33-0	Pure	Sigma Aldrich	I2304-10G
9-Fluorenone	9FLN	486-25-9	Pure	Sigma Aldrich	F1506-5G-A
Perinaphthenone	PNNN	548-39-0	Pure	Sigma Aldrich	P10801-1G
Benzophenone	BZP	119-61-9	Pure	Sigma Aldrich	239852-50G
1,4-Benzoquinone	BQN	106-51-4	Pure	Sigma Aldrich	PHR1028-1G
1,4-Naphthoquinone	NQN	130-15-4	Pure	Sigma Aldrich	70372-50G
Acenaphthoquinone	ACNQ	82-86-0	Pure	Sigma Aldrich	A201-25G-A
Anthraquinone	ATQ	84-65-1	Pure	Sigma Aldrich	31466-250MG
<b>n-Alkanes Mix (50 mg/L each in n-heptane)</b>					
				Sigma Aldrich	68281-2ML-F
Dodecane	DDCN	112-40-3	50		
Tetradecane	TDCN	629-59-4	50		
Hexadecane	HDCN	544-76-3	50		
Octadecane	ODCN	593-45-3	50		
Eicosane	ECSN	112-95-8	50		
Docosane	DCSN	629-97-0	50		
Tetracosane	TCSN	646-31-1	50		

Hexacosane	HCSN	630-01-3	50		
Octacosane	OCSN	630-02-4	50		
Triacosane	TCTN	638-68-6	50		
Dotriacontane	DCTN	544-85-4	50		
Tetraacosane	TECTN	14167-59-0	50		
Hexatriacontane	HCTN	630-06-8	50		
<b>FAMEs Mix, 100 mg Neat</b>					
			(% of each FAME in Mix)	Sigma Aldrich	18917-1AMP
Myristic Acid Methyl Ester	MAME	124-10-7	4		
Palmitic Acid Methyl Ester	PAME	112-39-0	10		
Stearic Acid Methyl Ester	SAME	112-61-8	6		
Oleic Acid Methyl Ester	OAME	112-62-9	25		
Elaidic Acid Methyl Ester	EAME	1937-62-8	10		
Linoleic Acid Methyl Ester	LIEC	112-63-0	34		
Linolelaidic Acid Methyl Ester	LDIC	2566-97-4	2		
Linolenic Acid Methyl Ester	LNIC	301-00-8	5		
Arachidic Acid Methyl Ester	AAME	1120-28-1	2		
Behenic Acid Methyl Ester	BAME	929-77-1	2		
<b>Internal, Quantitation and Recovery Standards</b>					
Phenanthrene-d10	Phen-d10	1517-22-2	1000 µg/mL in DCM	Ultra Scientific	IST-230
Perylene-d12	Pery-d12	1520-96-3	2000 µg/mL in DCM	Ultra Scientific	ATS-150-1
Anthracene-d10	Anth-d10	1719-06-8	1000 µg/mL in DCM	Ultra Scientific	IST-110
Tetracosane-d50	TECSN-d50	16416-32-3	Pure	Sigma Aldrich	451770-100MG
6-Fluoro-4-chromanone	6F4C	66892-34-0	Pure	Sigma Aldrich	364991-1G
2-Fluoro-9-fluorenone	2F9F	343-01-1	Pure	Sigma Aldrich	F9000-1G
<b>Other Chemicals</b>					
Pentafluorobenzylhydroxylamine	PFBHA	57981-02-9	Pure	Sigma Aldrich	76735-1G

### Determination of Detection Limits

Method detection limit (MDL) is defined as the amount of analyte that can be identified, measured, and reported with 99% confidence that the amount of analyte in a sample is greater than zero (Method 556, US EPA 1998).

The method detection limits were estimated according to Method 556 (US EPA 1998) using the equation below

$$\text{Method Detection Limit (MDL)} = St_{(n-1, 1-\alpha = 99)} \quad \text{Eq (A - 1)}$$

where  $S$  = standard deviation of  $n$  runs for a sample whose concentration of the analyte is about 5 times the noise level,  $n$  = number of replicate, and  $t_{(n-1, 1-\alpha = 99)}$  is the Student's t-value for the 99% confidence level with  $n-1$  degrees of freedom.

MDL for the PAHs were determined by analyzing a 0.125 ppm PAHs standard (number of runs,  $n = 7$ ,  $t_{n-1} = 3.143$ ) on the TD-GCMS, while the detection limits for the alkanes were determined using a 0.7 ppm standard ( $n=7$ ,  $t_{n-1} = 3.143$ ), and the detection limits for the PFBHA-oximes for the POCs were estimated using 2  $\mu\text{L}$  of a 2 ppm standard ( $n=6$ ,  $t_{n-1} = 2.998$ ). The MDLs for the FAMES were determined by analyzing a 5 ppm standard of the 10 FAMES mix seven times ( $n=7$ ,  $t_{n-1} = 3.143$ ) on the 6890/5973 GCMS. The table below shows the MDLs of the alkanes, PAHs, PFBHA-oximes for the POCs, and FAMES.

**Table A-2. Method detection limits of the alkanes, PAHs, FAMES, and PFBHA-oximes for the POCs. n = number of replicate runs.**

<b>Alkanes (n=7)</b>	<b>MDL (ng)</b>	<b>POC-oximes (n=8)</b>	<b>MDL (ng)</b>
Dodecane	0.62	2-Pentanone	0.97
Tetradecane	0.45	3-Pentanone	2.10
Hexadecane	0.31	n-Hexanal	1.40
Octadecane	0.19	n-Heptanal	1.08
Eicosane	0.24	n-Octanal	1.10
Docosane	0.20	2-Nonanone	1.10
Tetracosane	0.21	n-Nonanal	1.05
Hexacosane	0.21	n-Decanal	0.32
Octacosane	0.23	Undecanal	0.15
Triacontane	0.28	2-Hexanone	2.06
Dotriacontane	0.30	2-Heptanone	1.19
Tetracontane	0.21	2-Octanone	1.13
Hexatriacontane	0.34	Dodecanal	0.13
<b>PAHs (n=7)</b>	<b>MDL (ng)</b>	Benzaldehyde	1.06
Naphthalene	0.11	m-Tolualdehyde	0.31
Acenaphthylene	0.12	o-Tolualdehyde	1.44
Acenaphthene	0.17	p-Tolualdehyde	0.23
Fluorene	0.09	Acetophenone	0.45
Phenanthrene	0.13	1-Indanone	0.08
Anthracene	0.10	9-Fluorenone	0.18
Fluoranthene	0.13	Perinaphthenone	0.29
Pyrene	0.14	Benzophenone	0.65
Benzo[a]anthracene	0.16	1,4-Benzoquinone	0.36
Chrysene	0.12	1,4-Naphthoquinone	0.33
Benzo[b]fluoranthene	0.15	Acenaphthoquinone	0.46
Benzo[k]fluoranthene	0.23	Anthraquinone	0.33
Benzo[a]pyrene	0.21	<b>FAMES (n=4)</b>	<b>MDL (ng)</b>
Indeno[1,2,3-cd]pyrene	0.25	Myristic Acid Methyl Ester	0.01
Benzo[ghi]perylene	0.23	Palmitic Acid Methyl Ester	0.02
Dibenz[a,h]anthracene	0.19	Oleic Acid Methyl Ester	0.03
		Elaidic Acid Methyl Ester	0.02
		Stearic Acid Methyl Ester	0.02
		Linolenic Acid Methyl Ester	0.01
		Linoleic Acid Methyl Ester	0.02
		Linolelaidic Acid Methyl Ester	0.02
		Arachidic Acid Methyl Ester	0.02
		Behenic Acid Methyl Ester	0.04

The detection limits for the alkanes and PAHs looked quite reasonable, while the detection limits for some of the POCs did not look so reasonable. For example, the PFBHA-oximes for 2-pentanone, 3-pentanone, and 2-hexanone had quite high detection limits (>5 ng for all the above mentioned compounds) which seems very unrealistic. Other compounds such as n-hexanal, n-heptanone, 2-octanone, and o-tolualdehyde had MDLs greater than 3 ng. Because these

compounds could barely be detected by the TD-GCMS for the concentration used to determine the detection limits, their peak areas were quite variable, which later led to very high standard deviations. The high standard deviations obtained led to high values of detection limits for the above mentioned compounds (see Equation A-1). The rest of the compounds had reasonable detection limits as seen in Table 1. However, the detection limits for the PFBHA-oximes of the POCs were generally seen to be greater than those for the alkanes and PAHs. Most of the FAMEs had plausible detection limits with the exception of linoleic acid methyl ester which had detection limits over 10 ng. The peak areas for palmitic acid, oleic acid, and linoleic acid methyl esters were quite variable, which led to high standard deviation values, and hence high detection limits as seen in Equation A-1.

## **References**

US EPA, Method 556, 1998. Determination of carbonyl compounds in drinking water by pentafluorobenzylhydroxylamine derivatization and capillary gas chromatography with electron capture detection. National Exposure Research Laboratory, Office of Research and Development, US Environmental Protection Agency, Cincinnati, OH.

**Table A-3. Sampling Information.**

<b>Filter #</b>	<b>Sampling Date</b>	<b>Fuel Type</b>	<b>Sampling Time (min)</b>	<b>Vol of Air Sampled (m<sup>3</sup>)</b>	<b>Mass of PM Sampled (mg)</b>	<b>PM Conc. (µg/m<sup>3</sup>) ×10<sup>3</sup></b>
<b>WVO Sequence</b>						
FF 246	6/13/2013	Engine Blank	89.65	1.81	0.02	0.007
FF 256	6/18/2013	B00	98.33	1.92	23.07	10.3
FF 261	6/25/2013	B00	115.92	2.26	27.57	10.5
FF 266	8/06/2013	B00	99.0	1.90	22.61	10.3
FF 271	8/27/2013	Engine Blank	91.07	1.78	0.04	0.018
FF 276	8/28/2013	B10	99.25	1.92	24.82	11.5
FF 281	8/30/2013	B10	97.17	1.91	23.21	10.6
FF 286	8/31/2013	B10	98.08	1.93	26.58	12.3
FF 291	9/04/2013	B20	97.83	1.93	28.30	12.9
FF 296	9/05/2013	B20	97.08	1.96	29.83	13.3
FF 301	9/06/2013	B20	97.08	1.94	27.94	12.8
FF 306	9/09/2013	B50	97.08	1.91	40.91	18.9
FF 311	9/10/2013	B50	97.08	1.97	46.70	20.8
FF 316	9/11/2013	B50	96.08	1.92	42.59	18.6
FF 331	9/19/2013	B100	102.42	2.04	74.97	32.8
FF 336	9/20/2013	B100	97.08	1.93	74.80	32.9
FF 341	9/20/2013	B100	97.42	1.92	63.78	27.6
FF 346	9/28/2013	Engine Blank	211.08	4.52	0.06	0.028
<b>Soy Sequence</b>						
FF386	12/06/2013	B00	98.58	1.94	54.16	24.98
FF411	4/30/2014	Engine Blank	81.07	1.66	0.036	0.02
FF421	5/02/2014	B00	100.28	2.00	37.59	15.64
FF466	5/13/2014	B20	99.25	1.95	33.37	14.58
FF471	5/14/2014	B20	99.58	1.99	31.07	12.89
FF511	5/23/2014	B100	98.73	1.89	92.28	37.09
FF516	5/26/2014	B100	98.90	1.92	81.56	31.48



**Reproducibility check (Relative Standard Deviation, %RSD) data for the multiple punches extracted from a single filter**

**Table A-4. %RSD data of the PAHs for the WVO filters where duplicate punches were extracted.**

Fuel Type	B00	B10	B20	B20	B20	B50	B100
Filter #	FF261	FF281	FF291	FF296	FF301	FF311	FF336
Number of Punches Extracted	2	2	2	2	2	2	2
Compound	%RSD						
Phenanthrene	6.1	21.8	4.3	4.0	9.1	15.7	5.7
Fluoranthene	31.2	11.3	2.8	2.5	5.1	13.9	3.4
Pyrene	30.9	13.8	0.0	1.6	15.3	12.5	0.0

**Table A-5. %RSD data of the PAHs for the soy filters where duplicate punches were extracted.**

Fuel Type	B00	B20	B20	B100
Filter #	FF421	FF466	FF471	FF516
Number of Punches Extracted	2	2	2	2
Compound	%RSD			
Phenanthrene	1.2	10.2	0.0	2.4
Fluoranthene	5.9	5.4	4.9	7.4
Pyrene	18.1	7.9	5.5	0.0

**Table A-6. %RSD data of the n-alkanes for the WVO filters where duplicate punches were extracted.**

Fuel Type	<b>B00</b>	<b>B10</b>	<b>B20</b>	<b>B20</b>	<b>B20</b>	<b>B50</b>	<b>B100</b>
Filter #	<b>FF261</b>	<b>FF281</b>	<b>FF291</b>	<b>FF296</b>	<b>FF301</b>	<b>FF311</b>	<b>FF336</b>
Number of Punches Extracted	2	2	2	2	2	2	2
<b>Compound</b>	<b>%RSD</b>						
Dodecane	1.3	29.3	6.1	12.0	3.4	13.8	0.0
Tridecane	30.6	22.0	25.1	38.2	9.6	5.9	0.6
Tetradecane	6.1	0.0	4.5	11.7	9.5	13.1	1.2
Pentadecane	19.5	9.2	4.1	10.8	4.4	9.7	8.5
Hexadecane	43.4	2.1	1.5	7.4	2.6	10.6	5.9
Heptadecane	30.6	13.9	10.7	2.5	4.0	16.4	10.5
Octadecane	6.5	24.7	5.0	1.1	5.0	16.8	4.1
Nonadecane	14.8	20.8	7.8	0.4	2.7	18.8	2.6
Eicosane	24.3	14.7	6.3	1.8	3.2	20.3	0.8
Heneicosane	35.3	0.0	8.4	0.6	3.4	23.6	1.7
Docosane	45.3	19.4	6.7	6.3	1.2	19.3	10.4
Tricosane	37.2	21.2	12.9	1.2	15.2	13.1	4.3
Tetracosane	37.1	17.4	16.8	2.2	0.3	21.8	5.3
Hexacosane	11.9	17.3	51.0	34.1	6.0	45.8	2.8
Octacosane	28.2	90.7	65.2	14.5	2.0	22.0	2.9
triacontane	16.0	7.8	8.8	27.0	0.4	10.7	0.8
Dotriacontane	3.4	1.0	1.0	2.6	0.0	0.3	0.3
Tetratriacontane	5.5	7.4	9.1	11.4	0.2	0.2	1.4
Hexatriacontane	0.1	0.1	0.1	0.0	0.0	0.1	0.0

**Table A-7. %RSD data of the n-alkanes for the soy filters where duplicate punches were extracted.**

Fuel Type	B00	B20	B20	B100
Filter #	FF421	FF466	FF471	FF516
Number of Punches Extracted	2	2	2	2
Compound	%RSD			
Dodecane	1.8	3.4	1.6	3.4
Tridecane	2.5	11.4	0.0	9.6
Tetradecane	1.4	0.3	1.1	9.5
Pentadecane	3.6	15.9	0.4	4.4
Hexadecane	8.4	41.7	17.8	2.6
Heptadecane	10.9	40.8	5.4	4.0
Octadecane	1.3	46.5	1.2	5.0
Nonadecane	5.0	47.3	0.0	2.7
Eicosane	7.2	48.6	1.4	3.2
Heneicosane	9.0	47.6	1.6	3.4
Docosane	9.4	39.9	3.3	1.2
Tricosane	4.9	33.1	1.4	15.2
Tetracosane	3.9	35.0	3.1	0.3
Hexacosane	14.9	48.7	1.8	6.0
Octacosane	9.0	28.8	38.2	2.0
triacontane	0.4	1.2	3.9	0.4
Dotriacontane	1.5	1.0	1.0	0.0
Tetratriacontane	0.2	0.0	0.7	0.2
Hexatriacontane	0.3	0.0	0.1	0.0

**Table A-8. %RSD data of the carbonyls and quinones for the WVO filters where multiple punches were extracted.**

Fuel Type	B00	B10	B20	B20	B20	B50	B50	B50	B100
Filter #	FF261	FF281	FF291	FF296	FF301	FF306	FF311	FF316	FF336
Number of Punches Extracted	2	2	3	2	3	2	4	2	2
Compound	%RSD								
n-Hexanal	165.8	137.4	72.7	56.8	53.7	42.5	53.3	8.8	7.8
n-Nonanal	70.7	58.6	12.3	67.3	47.2	30.7	20.6	13.3	10.6
n-Decanal	28.5	44.9	15.4	52.4	62.7	30.5	32.0	34.9	37.8
Benzaldehyde	37.8	45.0	25.8	49.7	49.5	6.9	39.4	56.2	57.2
m-Tolualdehyde	7.1	1.7	5.9	4.8	1.4	1.9	4.4	1.9	2.0
p-Tolualdehyde	11.1	1.9	4.3	1.9	4.2	0.0	1.4	0.0	0.0
Acetophenone	10.9	11.2	10.4	2.0	5.7	2.2	4.8	0.0	8.8
9-Fluorenone	15.1	7.3	60.1	14.1	12.4	15.6	38.9	18.7	13.2
Perinaphthenone	35.2	41.5	31.6	22.6	54.5	19.1	21.5	22.2	20.2
Benzophenone	23.8	45.8	144.3	118.9	143.4	5.6	18.4	6.2	26.1
1,4-Benzoquinone	6.9	17.0	12.8	23.8	37.4	0.0	15.9	1.3	4.7
1,4-Naphthoquinone	12.3	1.2	40.1	9.0	17.2	16.9	26.4	23.3	4.9
Anthraquinone	29.0	22.0	36.3	34.9	19.0	8.2	18.8	24.1	3.6

**Table A-9. %RSD data of the carbonyls and quinones for the soy filters where multiple punches were extracted.**

Fuel Type	<b>B00</b>	<b>B00</b>	<b>B20</b>	<b>B20</b>	<b>B100</b>
Filter #	<b>FF386</b>	<b>FF421</b>	<b>FF466</b>	<b>FF471</b>	<b>FF516</b>
Number of Punches Extracted	2	3	2	4	2
<b>Compound</b>	<b>%RSD</b>				
n-Hexanal	158.8	38.7	52.3	38.5	34.1
n-Octanal	62.1	37.5	24.2	20.7	7.5
n-Nonanal	89.3	43.1	42.1	33.1	21.6
n-Decanal	24.4	56.2	22.3	42.4	9.3
Benzaldehyde	21.0	12.9	15.7	3.8	6.9
m-Tolualdehyde	14.1	3.3	1.6	5.8	3.1
p-Tolualdehyde	16.3	7.0	6.6	3.4	1.3
Acetophenone	6.1	14.3	3.5	2.5	0.0
9-Fluorenone	57.9	11.9	44.2	17.2	9.0
Perinaphthenone	27.3	12.1	10.8	9.1	1.3
Benzophenone	143.6	31.5	127.3	240.0	33.9
1,4-Benzoquinone	5.3	13.5	3.9	11.4	7.3
1,4-Naphthoquinone	43.7	5.5	36.5	9.8	8.9
Anthraquinone	30.3	15.6	10.0	15.0	0.0

**Table A-10. %RSD data of the FAMES for the WVO filters where duplicate punches were extracted.**

Fuel Type	<b>B10</b>	<b>B20</b>	<b>B20</b>	<b>B20</b>	<b>B50</b>	<b>B100</b>
Filter #	<b>FF281</b>	<b>FF291</b>	<b>FF296</b>	<b>FF301</b>	<b>FF311</b>	<b>FF336</b>
Number of Punches Extracted	2	2	2	2	2	2
<b>Compound</b>	<b>%RSD</b>					
Methyl myristate (C14:0)	0.0	0.0	0.0	0.0	15.7	28.3
Methyl palmitate (C16:0)	40.8	26.1	5.6	0.7	27.6	20.6
Methyl linolenate (C18:3n3)	28.7	13.9	12.5	2.2	1.6	50.9
Methyl linolelaidate (C18:2n6t)	0.0	13.6	0.0	0.0	14.0	13.5
Methyl linoleate (C18:2n6c)	61.5	22.9	16.7	16.7	24.6	19.1
Methyl elaidate (C18:1n9t)	4.4	15.0	2.3	1.7	24.5	12.7
Methyl oleate (C18:1n9c)	5.2	26.0	1.5	2.4	28.9	17.8
Methyl stearate (C18:0)	0.0	23.9	0.0	10.2	23.3	21.8
Methyl arachidate (C20:0)	34.4	20.2	33.7	15.7	32.6	0.0
Methyl behenate (C22:0)	4.1	14.6	4.6	0.0	8.8	14.1

**Table A-11. %RSD data of the FAMES for the soy filters where duplicate punches were extracted.**

Fuel Type	B20	B100
Filter #	FF466	FF516
Number of Punches Extracted	2	2
Compound	%RSD	
Methyl myristate (C14:0)	0.0	0.0
Methyl palmitate (C16:0)	15.9	28.0
Methyl linolenate (C18:3n3)	17.2	38.0
Methyl linolelaidate (C18:2n6t)	28.8	28.3
Methyl linoleate (C18:2n6c)	12.3	35.4
Methyl elaidate (C18:1n9t)	15.3	27.3
Methyl oleate (C18:1n9c)	10.3	32.1
Methyl stearate (C18:0)	9.6	29.9
Methyl arachidate (C20:0)	26.3	30.3
Methyl behenate (C22:0)	0.0	9.9

**Reproducibility check (Relative Standard Deviation) data for the triplicate and duplicate filters extracted for each fuel blend**

**Table A-12. %RSD data of the PAHs for the triplicate WVO filters extracted.**

Blend	B00	B10	B20	B50	B100
Number of Filters Extracted	3	3	3	3	3
Compound	%RSD				
Phenanthrene	59.0	33.9	15.1	27.4	17.0
Fluoranthene	26.6	14.0	5.3	13.7	7.7
Pyrene	17.4	16.7	1.6	12.7	10.5

**Table A-13. %RSD data of the PAHs for the duplicate soy filters extracted.**

Filter #	B00	B20	B100
Number of Filters Extracted	2	2	2
Compound	%RSD		
Phenanthrene	49.1	9.7	5.2
Fluoranthene	14.9	12.7	8.7
Pyrene	11.1	9.8	20.1

**Table A-14. %RSD data of the n-alkanes for the triplicate WVO filters extracted.**

Blend	B00	B10	B20	B50	B100
Number of Filters Extracted	3	3	3	3	3
Compound	%RSD				
Dodecane	6.5	22.0	2.0	13.7	10.3
Tridecane	7.8	7.8	10.9	9.1	15.1
Tetradecane	16.2	8.9	8.8	26.5	11.0
Pentadecane	32.3	18.1	11.1	7.2	13.1
Hexadecane	63.2	19.5	30.5	39.0	8.1
Heptadecane	64.1	34.9	26.4	52.6	13.9
Octadecane	61.6	35.8	15.6	44.6	3.0
Nonadecane	56.8	34.0	10.9	30.8	15.0
Eicosane	37.4	23.5	6.9	10.3	12.9
Heneicosane	23.4	12.5	3.8	47.8	10.5
Docosane	19.0	12.4	4.0	15.9	4.5
Tricosane	9.5	10.9	2.7	15.7	13.1
Tetracosane	19.7	7.1	5.5	13.7	15.3
Hexacosane	38.6	13.4	6.5	26.3	11.5
Octacosane	41.7	46.4	20.5	52.3	13.3
Triacontane	9.8	17.8	9.0	7.5	8.5
Dotriacontane	9.7	7.4	5.0	7.9	9.5
Tetratriacontane	11.0	9.7	4.1	7.0	9.8
Hexatriacontane	10.6	6.7	3.2	6.7	11.5

**Table A-15. %RSD data of the n-alkanes for the duplicate soy filters extracted.**

Filter #	B00	B20	B100
Number of Filters Extracted	2	2	2
Compound	%RSD		
Dodecane	38.8	12.4	8.7
Tridecane	19.2	7.4	8.0
Tetradecane	42.2	13.0	9.6
Pentadecane	60.3	14.4	8.7
Hexadecane	89.5	19.8	47.4
Heptadecane	66.4	4.2	32.4
Octadecane	42.6	1.3	15.0
Nonadecane	21.4	11.6	0.2
Eicosane	2.4	25.6	14.2
Heneicosane	17.8	36.0	31.1
Docosane	19.2	48.6	16.6
Tricosane	5.6	47.1	19.1
Tetracosane	1.2	35.8	12.4
Hexacosane	22.6	42.0	9.4
Octacosane	20.9	21.0	9.7
Triacontane	22.4	4.9	9.3
Dotriacontane	22.0	6.1	7.2
Tetratriacontane	22.7	5.4	8.8
Hexatriacontane	22.9	5.1	8.7



**Table A-16. %RSD data of the carbonyls and quinones for the triplicate WVO filters extracted.**

Blend	B00	B10	B20	B50	B100
Number of Filters Extracted	3	3	3	3	3
Compound	%RSD				
n-Hexanal	3061.0	108.6	59.7	47.9	105.4
n-Nonanal	48.9	58.3	4.4	30.1	91.7
n-Decanal	35.1	27.5	4.0	37.1	32.7
Benzaldehyde	23.8	9.2	24.5	66.9	94.7
m-Tolualdehyde	9.6	1.9	1.5	4.4	20.8
p-Tolualdehyde	7.8	2.9	1.9	7.2	21.0
Acetophenone	9.3	8.2	4.1	7.2	8.6
9-Fluorenone	16.9	12.2	18.1	24.9	122.9
Perinaphthenone	5.3	3.0	35.0	10.1	32.1
Benzophenone	40.9	22.7	28.0	24.2	
1,4-Benzoquinone	33.1	11.2	13.0	6.2	21.5
1,4-Naphthoquinone	13.5	5.3	14.5	45.5	49.1
Anthraquinone	10.5	27.5	12.6	12.5	107.6

**Table A-17. %RSD data of the carbonyls and quinones for the duplicate soy filters extracted.**

Filter #	B00	B20	B100
Number of Filters Extracted	2	2	2
Compound	%RSD		
n-Hexanal	26.4	49.6	8.7
n-Octanal	11.8	8.8	17.4
n-Nonanal	16.1	19.3	15.4
n-Decanal	27.9	44.3	28.9
Benzaldehyde	39.5	4.0	15.5
m-Tolualdehyde	32.4	4.6	15.1
p-Tolualdehyde	31.8	7.1	9.4
Acetophenone	16.2	1.0	10.6
9-Fluorenone	32.8	7.0	51.6
Perinaphthenone	15.2	5.7	37.2
Benzophenone	10.7	128.5	196.1
1,4-Benzoquinone	6.2	4.8	17.7
1,4-Naphthoquinone	26.5	1.7	24.5
Anthraquinone	6.4	3.1	31.2

**Table A-18. %RSD data of the FAMES for the triplicate WVO filters extracted.**

Blend	B10	B20	B50	B100
Number of Filters Extracted	3	3	3	3
Compound	%RSD			
Methyl myristate (C14:0)	4.0	3.4	2.0	3.6
Methyl palmitate (C16:0)	49.8	11.1	24.7	16.0
Methyl linolenate (C18:3n3)	19.2	5.1	11.1	59.6
Methyl linolelaidate (C18:2n6t)	14.6	3.5	22.8	8.8
Methyl linoleate (C18:2n6c)	27.6	10.4	14.1	25.0
Methyl elaidate (C18:1n9t)	13.2	4.7	16.5	11.5
Methyl oleate (C18:1n9c)	25.1	10.9	10.9	12.2
Methyl stearate (C18:0)	13.7	6.0	9.8	14.2
Methyl arachidate (C20:0)	3.6	7.1	28.2	16.7
Methyl behenate (C22:0)	13.4	2.4	8.1	10.5

**Table A-19. %RSD data of the FAMES for the duplicate soy filters extracted.**

Filter #	B20	B100
Number of Filters Extracted	2	2
Compound	%RSD	
Methyl myristate (C14:0)	5.0	8.7
Methyl palmitate (C16:0)	11.8	6.8
Methyl linolenate (C18:3n3)	17.2	8.7
Methyl linolelaidate (C18:2n6t)	6.2	13.8
Methyl linoleate (C18:2n6c)	8.2	15.9
Methyl elaidate (C18:1n9t)	3.8	5.5
Methyl oleate (C18:1n9c)	12.9	8.8
Methyl stearate (C18:0)	12.3	8.2
Methyl arachidate (C20:0)	48.6	16.4
Methyl behenate (C22:0)	1.2	1.9

**Table A-20. ANOVA results for the differences between the emission rates (ng/μg) of the corresponding blends of the WVO and soybean test sequences. N/A means that the species were not detected.**

	<b>WVO B00 and Soybean B00</b>	<b>WVO B20 and Soybean B20</b>	<b>WVO B100 and Soybean</b>
<b>Species</b>	<b>p-value</b>	<b>p-value</b>	<b>p-value</b>
Total PAHs	0.5995	0.1488	0.1397
Total n-Alkanes	0.1676	0.0323	0.0179
Total FAMES	N/A	0.0114	0.1499
Total Aliphatic Aldehydes	0.6900	0.2985	N/A
Total Aromatic Aldehydes	0.0189	0.0166	N/A
Total Aromatic Ketones	0.6365	0.0034	0.8261
Total Quinones	0.0344	0.0067	N/A

Level of significance,  $\alpha = 0.05$

**Table A-21. ANOVA results for the differences between the emission rates (ng/μg) of the different blends of the WVO (B00, B10, B20, B50, and B100) and soybean (B00, B20, and B100) test sequences.**

	<b>WVO Blends</b>	<b>Soybean Blends</b>
<b>Species</b>	<b>p-value</b>	<b>p-value</b>
Total PAHs	0.4194	0.1656
Total n-Alkanes	0.0017	0.0493
Total FAMES	<.0001	0.0083
Total Aliphatic	0.3238	0.2169
Total Aromatic	0.0005	0.2896
Total Aromatic Ketones	<.0001	0.0005
Total Quinones	0.0034	0.0187

Level of significance,  $\alpha = 0.05$

**Table A-22. p-Values obtained from the pairwise comparison of the emissions rates (ng/μg) from the different WVO blends (B00, B10, B20, B50, and B100) during the Analysis of Variance.**

Total PAHs					Total n-Alkanes				
	B10	B20	B50	B100		B10	B20	B50	B100
<b>B00</b>	0.7321	0.2604	0.4412	0.0899	<b>B00</b>	0.7641	0.2787	0.0134	0.0003
<b>B10</b>		0.42	0.6624	0.1581	<b>B10</b>		0.4222	0.0228	0.0005
<b>B20</b>			0.7039	0.5092	<b>B20</b>			0.094	0.0018
<b>B50</b>				0.3073	<b>B50</b>				0.0405
Total FAMES					Total Aliphatic Aldehydes				
	B10	B20	B50	B100		B10	B20	B50	B100
<b>B00</b>					<b>B00</b>	0.9786	0.9885	0.9557	0.0123
<b>B10</b>		0.065	0.0004	<.0001	<b>B10</b>		0.9901	0.977	0.0129
<b>B20</b>			0.0055	<.0001	<b>B20</b>			0.9671	0.0126
<b>B50</b>				0.0003	<b>B50</b>				0.0136
Total Aromatic Aldehydes					Total Aromatic Ketones				
	B10	B20	B50	B100		B10	B20	B50	B100
<b>B00</b>	0.0325	0.0188	0.0025		<b>B00</b>	0.1015	0.037	0.0015	<.0001
<b>B10</b>		0.0006	0.0001		<b>B10</b>		0.0018	0.0001	<.0001
<b>B20</b>			0.1988		<b>B20</b>			0.0823	0.0001
<b>B50</b>					<b>B50</b>				0.0022
Total Quinones									
	B10	B20	B50	B100					
<b>B00</b>	0.7175	0.0059	0.0017						
<b>B10</b>		0.0102	0.0029						
<b>B20</b>			0.4022						
<b>B50</b>									

Level of significance,  $\alpha = 0.05$

**Table A-23 p-Values obtained from the pairwise comparison of the emissions rates (ng/μg) from the different soybean blends (B00, B20, and B100) during the Analysis of Variance.**

Total PAHs			Total n-Alkanes			Total FAMES			Total Aliphatic Aldehydes		
	B20	B100		B20	B100		B20	B100		B20	B100
<b>B00</b>	0.1527	0.0854	<b>B00</b>	0.912	0.0306	<b>B00</b>			<b>B00</b>	0.3325	0.0016
<b>B20</b>		0.5771	<b>B20</b>		0.0332	<b>B20</b>		0.0083	<b>B20</b>		0.0022
Total Aromatic Aldehydes			Total Aromatic Ketones			Total Quinones					
	B20	B100		B20	B100		B20	B100			
<b>B00</b>	0.2896		<b>B00</b>	0.001	0.0002	<b>B00</b>	0.0187				
<b>B20</b>			<b>B20</b>		0.0026	<b>B20</b>					

Level of significance,  $\alpha = 0.05$



**Table B-2 Mass (ng) of target PAHs in the soybean engine test sequence filters. P means mass detected in the ¼ inch punch extracted from each filter, while F means computed mass of analyte on entire filter calculated using Eq (2-2).**

Filter #	BD Blend		Nap	Acy	Ace	Flu	Phen	Anth	Fluor	Pyr	BaA	Chr	BbF	BkF	BaP	IDP	BghiP	DBahA
FF 386	B00	P	7.0E+00	<b>2.0E+00</b>	<b>4.0E+00</b>	5.0E+00	1.8E+02	<b>3.0E+00</b>	1.4E+01	2.4E+01	<b>2.0E+00</b>	ND	ND	ND	<b>5.0E+00</b>	<b>9.0E+00</b>	ND	<b>7.0E+00</b>
		F	3.1E+02	<b>8.8E+01</b>	<b>1.8E+02</b>	2.2E+02	7.7E+03	<b>1.3E+02</b>	6.1E+02	1.1E+03	<b>8.8E+01</b>	ND	ND	ND	<b>2.2E+02</b>	<b>3.9E+02</b>	ND	<b>3.1E+02</b>
FF 421 Punch 1	B00	P	7.0E+00	<b>1.0E+00</b>	<b>1.0E+00</b>	<b>2.5E+00</b>	5.9E+01	<b>1.0E+00</b>	1.2E+01	1.7E+01	<b>1.5E+00</b>	ND	<b>2.0E+00</b>	<b>1.5E+00</b>	<b>3.0E+00</b>	4.5E+00	ND	3.5E+00
		F	3.1E+02	<b>4.4E+01</b>	<b>4.4E+01</b>	<b>1.1E+02</b>	2.6E+03	<b>4.4E+01</b>	5.0E+02	7.4E+02	<b>6.6E+01</b>	ND	<b>8.8E+01</b>	<b>6.6E+01</b>	<b>1.3E+02</b>	2.0E+02	ND	1.5E+02
FF 421 Punch 2	B00	P	4.0E+00	2.5E+00	<b>1.5E+00</b>	<b>3.0E+00</b>	6.0E+01	<b>1.0E+00</b>	1.3E+01	2.2E+01	<b>1.0E+00</b>	ND	<b>2.0E+00</b>	<b>1.5E+00</b>	<b>2.5E+00</b>	5.0E+00	<b>2.0E+00</b>	ND
		F	1.8E+02	1.1E+02	<b>6.6E+01</b>	<b>1.3E+02</b>	2.6E+03	<b>4.4E+01</b>	5.5E+02	9.6E+02	<b>4.4E+01</b>	ND	<b>8.8E+01</b>	<b>6.6E+01</b>	<b>1.1E+02</b>	2.2E+02	<b>8.8E+01</b>	ND
FF 466 Punch 1	B20	P	3.0E+00	1.5E+00	<b>1.0E+00</b>	<b>2.0E+00</b>	3.7E+01	<b>5.0E+01</b>	1.4E+01	1.9E+01	<b>1.0E+00</b>	1.0E+00	3.0E+00	<b>1.5E+00</b>	<b>2.5E+00</b>	<b>4.5E+00</b>	<b>3.0E+00</b>	<b>3.5E+00</b>
		F	1.3E+02	6.6E+01	<b>4.4E+01</b>	<b>8.8E+01</b>	1.6E+03	<b>2.2E+01</b>	5.9E+02	8.3E+02	<b>4.4E+01</b>	4.4E+01	1.3E+02	<b>6.6E+01</b>	<b>1.1E+02</b>	<b>2.0E+02</b>	<b>1.3E+02</b>	<b>1.5E+02</b>
FF 466 Punch 2	B20	P	5.0E+01	<b>1.0E+00</b>	<b>1.5E+00</b>	<b>1.5E+00</b>	3.2E+01	<b>1.5E+00</b>	1.3E+01	1.7E+01	<b>1.0E+00</b>	ND	<b>2.5E+00</b>	ND	ND	4.5E+00	<b>2.0E+00</b>	ND
		F	2.2E+01	<b>4.4E+01</b>	<b>6.6E+01</b>	<b>6.6E+01</b>	1.4E+03	<b>6.6E+01</b>	5.5E+02	7.4E+02	<b>4.4E+01</b>	ND	<b>1.1E+02</b>	ND	ND	2.0E+02	<b>8.8E+01</b>	ND
FF 471 Punch 1	B20	P	2.5E+00	<b>1.0E+00</b>	<b>1.0E+00</b>	<b>1.5E+00</b>	2.8E+01	ND	1.5E+01	2.0E+01	<b>1.5E+00</b>	ND	<b>2.0E+00</b>	<b>1.5E+00</b>	<b>3.0E+00</b>	<b>4.5E+00</b>	3.5E+00	ND
		F	1.1E+02	<b>4.4E+01</b>	<b>4.4E+01</b>	<b>6.6E+01</b>	1.2E+03	ND	6.6E+02	8.8E+02	<b>6.6E+01</b>	ND	<b>8.8E+01</b>	<b>6.6E+01</b>	<b>1.3E+02</b>	<b>2.0E+02</b>	1.5E+02	ND
FF 471 Punch 2	B20	P	2.0E+00	1.0E+00	1.0E+00	<b>1.5E+00</b>	2.8E+01	ND	1.4E+01	1.9E+01	<b>1.5E+00</b>	ND	<b>2.5E+00</b>	<b>1.5E+00</b>	<b>3.0E+00</b>	<b>4.5E+00</b>	<b>2.0E+00</b>	ND
		F	8.8E+01	4.4E+01	4.4E+01	<b>6.6E+01</b>	1.2E+03	ND	6.1E+02	8.1E+02	<b>6.6E+01</b>	ND	<b>1.1E+02</b>	<b>6.6E+01</b>	<b>1.3E+02</b>	<b>2.0E+02</b>	<b>8.8E+01</b>	ND
FF 511	B100	P	2.0E+00	1.0E+01	<b>4.0E+00</b>	<b>8.0E+00</b>	6.2E+01	ND	3.8E+01	3.4E+01	<b>8.0E+00</b>	ND	<b>8.0E+00</b>	ND	ND	ND	1.2E+01	ND
		F	8.8E+01	4.4E+02	<b>1.8E+02</b>	<b>3.5E+02</b>	2.7E+03	ND	1.7E+03	1.5E+03	<b>3.5E+02</b>	ND	<b>3.5E+02</b>	ND	ND	ND	5.3E+02	ND
FF 516 Punch 1	B100	P	2.0E+00	6.0E+00	<b>4.0E+00</b>	<b>8.0E+00</b>	5.8E+01	ND	4.0E+01	4.0E+01	<b>4.0E+00</b>	ND	ND	ND	ND	ND	1.2E+01	ND
		F	8.8E+01	2.6E+02	<b>1.8E+02</b>	<b>3.5E+02</b>	2.5E+03	ND	1.8E+03	1.8E+03	<b>1.8E+02</b>	ND	ND	ND	ND	ND	5.3E+02	ND
FF 516 Punch 2	B100	P	ND	<b>6.0E+00</b>	<b>6.0E+00</b>	<b>8.0E+00</b>	6.0E+01	<b>2.0E+00</b>	3.6E+01	4.0E+01	<b>4.0E+00</b>	ND	1.0E+01	ND	ND	ND	1.0E+01	ND
		F	ND	<b>2.6E+02</b>	<b>2.6E+02</b>	<b>3.5E+02</b>	2.6E+03	<b>8.8E+01</b>	1.6E+03	1.8E+03	<b>1.8E+02</b>	ND	4.4E+02	ND	ND	ND	4.4E+02	ND

ND means the target analyte was "Not Detected" during GC/MS analysis. *Italicized* values mean that the mass spectrum of the target analyte did not match that of the routinely used authentic standards, but the Q-value of the target analyte was greater than 50%. **Bold Italicized** values mean that the Q-value for the target analyte was less than 50%.

Table B-3 Mass (ng) of target n-alkanes in the WVO engine test sequence filters. P means mass detected in the ¼ inch punch extracted from each filter, while F means computed mass of analyte on entire filter calculated using Eq (2-2). This Table shows compounds dodecane (DDCN) through heneicosane (HNCN).

Filter #	BD Blend		DDCN	TRDC	TDCN	PDCN	HDCN	HPCN	ODCN	NDCN	ECSN	HNCN
FF 256	B00	P	2.5E+01	3.0E+01	5.8E+01	5.6E+01	4.5E+01	1.5E+02	4.0E+02	8.3E+02	1.9E+03	2.1E+03
		F	1.1E+03	1.3E+03	2.5E+03	2.5E+03	1.9E+03	6.6E+03	1.7E+04	3.6E+04	8.3E+04	9.0E+04
FF 261 Punch 1	B00	P	2.7E+01	4.5E+01	5.6E+01	8.5E+01	1.1E+02	5.0E+02	1.8E+03	2.9E+03	3.2E+03	2.2E+03
		F	1.2E+03	2.0E+03	2.4E+03	3.7E+03	4.7E+03	2.2E+04	7.9E+04	1.3E+05	1.4E+05	9.5E+04
FF 261 Punch 2	B00	P	<b>2.6E+01</b>	<b>2.9E+01</b>	6.1E+01	1.1E+02	2.0E+02	7.7E+02	2.0E+03	3.6E+03	4.5E+03	3.6E+03
		F	<b>1.1E+03</b>	<b>1.3E+03</b>	2.6E+03	4.9E+03	9.0E+03	3.4E+04	8.7E+04	1.6E+05	2.0E+05	1.6E+05
FF 266	B00	P	<b>2.3E+01</b>	<b>2.6E+01</b>	6.6E+01	1.1E+02	2.0E+02	7.5E+02	1.9E+03	3.2E+03	4.1E+03	3.2E+03
		F	<b>1.0E+03</b>	<b>1.1E+03</b>	2.9E+03	4.7E+03	8.8E+03	3.3E+04	8.3E+04	1.4E+05	1.8E+05	1.4E+05
FF 276	B10	P	<b>2.0E+01</b>	3.1E+01	7.8E+01	9.6E+01	1.3E+02	5.1E+02	1.8E+03	3.1E+03	4.0E+03	3.1E+03
		F	<b>8.8E+02</b>	1.4E+03	3.4E+03	4.2E+03	5.9E+03	2.2E+04	7.7E+04	1.4E+05	1.8E+05	1.4E+05
FF 281 Punch 1	B10	P	2.2E+01	<b>2.9E+01</b>	<b>6.3E+01</b>	6.5E+01	8.6E+01	2.6E+02	8.9E+02	1.7E+03	2.7E+03	2.4E+03
		F	9.6E+02	<b>1.2E+03</b>	<b>2.8E+03</b>	2.8E+03	3.7E+03	1.1E+04	3.9E+04	7.3E+04	1.2E+05	1.0E+05
FF 281 Punch 2	B10	P	3.4E+01	<b>3.9E+01</b>	<b>6.3E+01</b>	7.4E+01	8.3E+01	2.2E+02	6.3E+02	1.2E+03	2.2E+03	2.4E+03
		F	1.5E+03	<b>1.7E+03</b>	<b>2.8E+03</b>	3.2E+03	3.6E+03	9.4E+03	2.7E+04	5.4E+04	9.6E+04	1.0E+05
FF 286	B10	P	2.3E+01	<b>3.5E+01</b>	<b>8.6E+01</b>	7.3E+01	1.3E+02	5.5E+02	1.6E+03	2.3E+03	3.1E+03	2.7E+03
		F	1.0E+03	<b>1.5E+03</b>	<b>3.7E+03</b>	3.2E+03	5.6E+03	2.4E+04	6.8E+04	1.0E+05	1.4E+05	1.2E+05
FF 291 Punch 1	B20	P	<b>2.2E+01</b>	2.9E+01	8.5E+01	6.8E+01	1.2E+02	7.0E+02	1.8E+03	2.5E+03	2.9E+03	2.3E+03
		F	<b>9.6E+02</b>	1.3E+03	3.7E+03	3.0E+03	5.3E+03	3.1E+04	7.9E+04	1.1E+05	1.3E+05	1.0E+05
FF 291 Punch 2	B20	P	<b>2.4E+01</b>	4.2E+01	9.0E+01	7.2E+01	1.2E+02	6.0E+02	1.7E+03	2.2E+03	2.7E+03	2.1E+03
		F	<b>1.1E+03</b>	1.8E+03	3.9E+03	3.1E+03	5.2E+03	2.6E+04	7.4E+04	9.7E+04	1.2E+05	9.0E+04
FF 296 Punch 1	B20	P	<b>2.3E+01</b>	<b>4.3E+01</b>	1.0E+02	8.3E+01	2.5E+02	1.1E+03	2.4E+03	3.0E+03	3.4E+03	2.5E+03
		F	<b>9.8E+02</b>	<b>1.9E+03</b>	4.4E+03	3.6E+03	1.1E+04	4.8E+04	1.0E+05	1.3E+05	1.5E+05	1.1E+05
FF 296 Punch 2	B20	P	<b>2.6E+01</b>	4.1E+01	1.2E+02	9.0E+01	2.3E+02	1.2E+03	2.4E+03	2.9E+03	3.3E+03	2.4E+03
		F	<b>1.1E+03</b>	1.8E+03	5.1E+03	3.9E+03	9.9E+03	5.2E+04	1.1E+05	1.3E+05	1.4E+05	1.0E+05
FF 301 Punch 1	B20	P	<b>2.2E+01</b>	2.3E+01	9.2E+01	7.9E+01	1.8E+02	8.0E+02	1.7E+03	2.3E+03	2.8E+03	2.1E+03
		F	<b>9.4E+02</b>	1.0E+03	4.0E+03	3.5E+03	7.8E+03	3.5E+04	7.6E+04	1.0E+05	1.2E+05	9.3E+04
FF 301 Punch 2	B20	P	<b>2.6E+01</b>	4.0E+01	1.1E+02	9.2E+01	2.0E+02	7.8E+02	1.8E+03	2.3E+03	2.7E+03	2.1E+03
		F	<b>1.1E+03</b>	1.8E+03	4.7E+03	4.0E+03	8.6E+03	3.4E+04	7.7E+04	1.0E+05	1.2E+05	9.2E+04
FF 306	B50	P	<b>4.7E+01</b>	<b>6.9E+01</b>	<b>2.9E+02</b>	1.4E+02	2.8E+02	1.2E+03	2.6E+03	3.1E+03	3.0E+03	7.1E+02
		F	<b>2.1E+03</b>	<b>3.0E+03</b>	<b>1.3E+04</b>	6.2E+03	1.2E+04	5.1E+04	1.2E+05	1.4E+05	1.3E+05	3.1E+04
FF 311 Punch 1	B50	P	<b>5.1E+01</b>	8.1E+01	4.6E+02	1.4E+02	2.4E+02	8.2E+02	1.8E+03	2.3E+03	2.4E+03	1.6E+03
		F	<b>2.2E+03</b>	3.5E+03	2.0E+04	6.2E+03	1.1E+04	3.6E+04	7.9E+04	9.9E+04	1.1E+05	7.0E+04
FF 311 Punch 2	B50	P	6.2E+01	8.8E+01	5.6E+02	1.6E+02	2.8E+02	1.0E+03	2.3E+03	2.9E+03	3.3E+03	2.2E+03
		F	2.7E+03	3.9E+03	2.4E+04	7.1E+03	1.2E+04	4.5E+04	1.0E+05	1.3E+05	1.4E+05	9.8E+04
FF 316	B50	P	6.3E+01	8.6E+01	3.0E+02	1.3E+02	1.3E+02	3.7E+02	1.1E+03	1.8E+03	2.7E+03	2.2E+03
		F	2.8E+03	3.8E+03	1.3E+04	5.6E+03	5.5E+03	1.6E+04	4.6E+04	7.7E+04	1.2E+05	9.6E+04
FF 331	B100	P	9.6E+01	2.2E+02	<b>1.6E+03</b>	<b>2.8E+02</b>	5.4E+01	5.4E+01	<b>6.1E+02</b>	9.2E+02	1.1E+03	8.0E+02
		F	4.2E+03	9.7E+03	<b>7.1E+04</b>	<b>1.2E+04</b>	2.4E+03	2.4E+03	<b>2.7E+04</b>	4.0E+04	5.0E+04	3.5E+04
FF 336 Punch 1	B100	P	<b>8.4E+01</b>	2.3E+02	<b>1.6E+03</b>	<b>2.3E+02</b>	<b>5.0E+01</b>	5.8E+01	5.7E+02	7.5E+02	1.0E+03	7.4E+02
		F	<b>3.7E+03</b>	9.9E+03	<b>7.0E+04</b>	<b>1.0E+04</b>	<b>2.2E+03</b>	2.5E+03	2.5E+04	3.3E+04	4.4E+04	3.2E+04
FF 336 Punch 2	B100	P	<b>8.4E+01</b>	2.3E+02	<b>1.6E+03</b>	2.0E+02	<b>4.6E+01</b>	<b>5.0E+01</b>	6.0E+02	7.7E+02	1.0E+03	7.5E+02
		F	<b>3.7E+03</b>	1.0E+04	<b>7.1E+04</b>	8.9E+03	<b>2.0E+03</b>	<b>2.2E+03</b>	2.6E+04	3.4E+04	4.5E+04	3.3E+04
FF 341	B100	P	<b>8.8E+01</b>	<b>2.5E+02</b>	<b>1.7E+03</b>	<b>2.1E+02</b>	<b>4.8E+01</b>	<b>5.8E+01</b>	4.9E+02	5.9E+02	7.4E+02	5.5E+02
		F	<b>3.9E+03</b>	<b>1.1E+04</b>	<b>7.3E+04</b>	<b>9.1E+03</b>	<b>2.1E+03</b>	<b>2.5E+03</b>	2.2E+04	2.6E+04	3.2E+04	2.4E+04



**Table B-3 Continued... This Table shows compounds docosane (DCSN) through hexatriacontane (HCTN).**

Filter #	BD Blend		DCSN	TRCS	TCSN	HCSN	OCSN	TCTN	DCTN	TECTN	HCTN
FF 256	B00	P	1.4E+03	5.7E+02	3.1E+02	4.6E+02	<b>8.1E+01</b>	1.2E+02	1.4E+02	<b>2.2E+02</b>	2.6E+02
		F	6.0E+04	2.5E+04	1.4E+04	2.0E+04	<b>3.5E+03</b>	5.2E+03	6.2E+03	<b>9.8E+03</b>	1.2E+04
FF 261 Punch 1	B00	P	1.1E+03	4.7E+02	3.1E+02	5.0E+02	<b>1.7E+02</b>	1.2E+02	1.4E+02	<b>2.2E+02</b>	<b>2.6E+02</b>
		F	4.9E+04	2.0E+04	1.4E+04	2.2E+04	<b>7.6E+03</b>	5.1E+03	6.1E+03	<b>9.5E+03</b>	<b>1.2E+04</b>
FF 261 Punch 2	B00	P	2.2E+03	8.0E+02	5.4E+02	4.3E+02	2.6E+02	1.5E+02	1.5E+02	<b>2.4E+02</b>	2.6E+02
		F	9.5E+04	3.5E+04	2.4E+04	1.9E+04	1.1E+04	6.5E+03	6.5E+03	<b>1.0E+04</b>	1.2E+04
FF 266	B00	P	1.8E+03	6.3E+02	4.5E+02	7.7E+02	1.1E+02	1.3E+02	<b>1.4E+02</b>	<b>2.3E+02</b>	2.6E+02
		F	8.1E+04	2.7E+04	1.9E+04	3.3E+04	4.6E+03	5.8E+03	<b>6.2E+03</b>	<b>1.0E+04</b>	1.2E+04
FF 276	B10	P	1.8E+03	5.9E+02	3.9E+02	6.0E+02	3.0E+02	9.3E+01	<b>1.4E+02</b>	<b>2.3E+02</b>	2.6E+02
		F	7.9E+04	2.6E+04	1.7E+04	2.6E+04	1.3E+04	4.0E+03	<b>6.0E+03</b>	<b>9.9E+03</b>	1.2E+04
FF 281 Punch 1	B10	P	1.3E+03	5.3E+02	3.3E+02	4.7E+02	7.9E+01	<b>1.1E+02</b>	1.4E+02	2.2E+02	<b>2.6E+02</b>
		F	5.8E+04	2.3E+04	1.4E+04	2.1E+04	3.5E+03	<b>4.7E+03</b>	6.1E+03	9.8E+03	<b>1.2E+04</b>
FF 281 Punch 2	B10	P	1.7E+03	7.2E+02	4.2E+02	6.1E+02	<b>3.6E+02</b>	1.2E+02	1.4E+02	2.5E+02	2.6E+02
		F	7.6E+04	3.2E+04	1.9E+04	2.7E+04	<b>1.6E+04</b>	5.3E+03	6.2E+03	1.1E+04	1.2E+04
FF 286	B10	P	1.5E+03	5.8E+02	3.8E+02	5.0E+02	1.1E+02	9.5E+01	1.4E+02	2.2E+02	2.6E+02
		F	6.6E+04	2.5E+04	1.6E+04	2.2E+04	5.0E+03	4.2E+03	6.1E+03	9.7E+03	1.2E+04
FF 291 Punch 1	B20	P	1.3E+03	5.4E+02	3.7E+02	4.6E+02	2.7E+02	1.7E+02	<b>1.4E+02</b>	<b>2.2E+02</b>	2.6E+02
		F	5.9E+04	2.3E+04	1.6E+04	2.0E+04	1.2E+04	7.3E+03	<b>6.2E+03</b>	<b>9.4E+03</b>	1.2E+04
FF 291 Punch 2	B20	P	1.2E+03	4.5E+02	2.9E+02	2.2E+02	9.9E+01	1.5E+02	1.4E+02	<b>1.9E+02</b>	<b>2.6E+02</b>
		F	5.4E+04	2.0E+04	1.3E+04	9.5E+03	4.3E+03	6.4E+03	6.1E+03	<b>8.3E+03</b>	<b>1.2E+04</b>
FF 296 Punch 1	B20	P	1.4E+03	5.6E+02	4.1E+02	4.9E+02	2.5E+02	<b>2.0E+02</b>	<b>1.5E+02</b>	<b>2.1E+02</b>	2.6E+02
		F	6.3E+04	2.4E+04	1.8E+04	2.1E+04	1.1E+04	<b>8.7E+03</b>	<b>6.3E+03</b>	<b>9.4E+03</b>	1.2E+04
FF 296 Punch 2	B20	P	1.4E+03	5.2E+02	3.7E+02	2.5E+02	3.2E+02	1.1E+02	1.4E+02	<b>1.9E+02</b>	<b>2.6E+02</b>
		F	6.0E+04	2.3E+04	1.6E+04	1.1E+04	1.4E+04	5.0E+03	6.1E+03	<b>8.3E+03</b>	<b>1.2E+04</b>
FF 301 Punch 1	B20	P	1.3E+03	4.9E+02	3.6E+02	4.7E+02	2.9E+02	1.4E+02	<b>1.5E+02</b>	<b>2.2E+02</b>	<b>2.6E+02</b>
		F	5.6E+04	2.1E+04	1.6E+04	2.1E+04	1.3E+04	6.2E+03	<b>6.6E+03</b>	<b>9.7E+03</b>	<b>1.2E+04</b>
FF 301 Punch 2	B20	P	1.2E+03	4.8E+02	3.5E+02	2.9E+02	2.3E+02	<b>2.1E+02</b>	<b>1.4E+02</b>	<b>1.9E+02</b>	<b>2.6E+02</b>
		F	5.1E+04	2.1E+04	1.5E+04	1.3E+04	1.0E+04	<b>9.1E+03</b>	<b>6.3E+03</b>	<b>8.3E+03</b>	<b>1.2E+04</b>
FF 306	B50	P	1.3E+03	5.9E+02	3.9E+02	4.1E+02	<b>4.9E+02</b>	<b>2.4E+02</b>	2.9E+02	<b>3.8E+02</b>	<b>5.3E+02</b>
		F	5.5E+04	2.6E+04	1.7E+04	1.8E+04	<b>2.1E+04</b>	<b>1.1E+04</b>	1.3E+04	<b>1.7E+04</b>	<b>2.3E+04</b>
FF 311 Punch 1	B50	P	1.0E+03	4.6E+02	2.9E+02	<b>1.9E+02</b>	3.3E+02	2.5E+02	2.8E+02	3.8E+02	<b>5.3E+02</b>
		F	4.5E+04	2.0E+04	1.3E+04	<b>8.2E+03</b>	1.4E+04	1.1E+04	1.2E+04	1.7E+04	<b>2.3E+04</b>
FF 311 Punch 2	B50	P	1.4E+03	5.5E+02	3.9E+02	3.7E+02	4.5E+02	<b>2.9E+02</b>	<b>2.8E+02</b>	<b>3.8E+02</b>	<b>5.3E+02</b>
		F	6.0E+04	2.4E+04	1.7E+04	1.6E+04	2.0E+04	<b>1.3E+04</b>	<b>1.2E+04</b>	<b>1.7E+04</b>	<b>2.3E+04</b>
FF 316	B50	P	1.5E+03	6.1E+02	3.9E+02	4.0E+02	<b>1.5E+02</b>	<b>2.2E+02</b>	<b>2.8E+02</b>	<b>3.8E+02</b>	<b>5.3E+02</b>
		F	6.6E+04	2.7E+04	1.7E+04	1.8E+04	<b>6.7E+03</b>	<b>9.6E+03</b>	<b>1.2E+04</b>	<b>1.7E+04</b>	<b>2.3E+04</b>
FF 331	B100	P	6.2E+02	<b>6.2E+02</b>	<b>3.7E+02</b>	<b>4.9E+02</b>	3.1E+02	3.6E+02	5.5E+02	7.9E+02	ND
		F	2.7E+04	<b>2.7E+04</b>	<b>1.6E+04</b>	<b>2.2E+04</b>	1.3E+04	1.6E+04	2.4E+04	3.4E+04	ND
FF 336 Punch 1	B100	P	6.9E+02	6.7E+02	4.4E+02	6.2E+02	3.0E+02	3.7E+02	5.6E+02	<b>7.8E+02</b>	<b>1.1E+03</b>
		F	3.0E+04	2.9E+04	1.9E+04	2.7E+04	1.3E+04	1.6E+04	2.4E+04	<b>3.4E+04</b>	<b>4.6E+04</b>
FF 336 Punch 2	B100	P	5.9E+02	7.1E+02	4.7E+02	5.9E+02	<b>2.8E+02</b>	<b>3.7E+02</b>	<b>5.6E+02</b>	<b>8.0E+02</b>	<b>1.1E+03</b>
		F	2.6E+04	3.1E+04	2.1E+04	2.6E+04	<b>1.2E+04</b>	<b>1.6E+04</b>	<b>2.4E+04</b>	<b>3.5E+04</b>	<b>4.6E+04</b>
FF 341	B100	P	5.0E+02	6.8E+02	<b>2.9E+02</b>	5.1E+02	3.2E+02	<b>3.6E+02</b>	5.5E+02	<b>7.9E+02</b>	<b>1.1E+03</b>
		F	2.2E+04	3.0E+04	<b>1.3E+04</b>	2.2E+04	1.4E+04	<b>1.6E+04</b>	2.4E+04	<b>3.5E+04</b>	<b>4.6E+04</b>

ND means the target analyte was "Not Detected" during GC/MS analysis. *Italicized* values mean that the mass spectrum of the target analyte did not match that of the routinely used authentic standards, but the Q-value of the target analyte was greater than 50%. **Bold Italicized** values mean that the Q-value for the target analyte was less than 50%.

**Table B-4 Mass (ng) of target n-alkanes in the soybean test engine sequence filters. P means mass detected in the ¼ inch punch extracted from each filter, while F means computed mass of analyte on entire filter calculated using Eq (2-2). This Table shows compounds dodecane (DDCN) through heneicosane (HNCN).**

Filter #	BD Blend		DDCN	TRDC	TDCN	PDCN	HDCN	HPCN	ODCN	NDCN	ECSN	HNCN
FF 386	B00	P	5.0E+01	5.3E+01	1.4E+02	2.9E+02	7.0E+02	2.6E+03	4.3E+03	3.9E+03	2.9E+03	1.6E+03
		F	2.2E+03	2.3E+03	6.0E+03	1.2E+04	3.1E+04	1.1E+05	1.9E+05	1.7E+05	1.3E+05	7.1E+04
FF 421 Punch 1	B00	P	2.0E+01	2.8E+01	5.1E+01	8.2E+01	1.0E+02	6.0E+02	1.6E+03	1.9E+03	1.9E+03	1.3E+03
		F	8.5E+02	1.2E+03	2.2E+03	3.6E+03	4.5E+03	2.6E+04	7.1E+04	8.4E+04	8.5E+04	5.9E+04
FF 421 Punch 2	B00	P	2.0E+01	2.9E+01	5.2E+01	7.8E+01	1.2E+02	7.1E+02	1.6E+03	2.1E+03	2.2E+03	1.5E+03
		F	8.8E+02	1.2E+03	2.3E+03	3.4E+03	5.1E+03	3.1E+04	7.0E+04	9.0E+04	9.4E+04	6.7E+04
FF 466 Punch 1	B20	P	2.0E+01	2.0E+01	1.2E+02	8.7E+01	1.4E+02	5.4E+02	1.3E+03	2.0E+03	2.5E+03	1.8E+03
		F	8.8E+02	8.8E+02	5.2E+03	3.8E+03	5.9E+03	2.4E+04	5.7E+04	8.8E+04	1.1E+05	7.9E+04
FF 466 Punch 2	B20	P	2.1E+01	2.4E+01	1.2E+02	6.9E+01	7.4E+01	3.0E+02	6.6E+02	1.0E+03	1.2E+03	9.0E+02
		F	9.2E+02	1.0E+03	5.3E+03	3.0E+03	3.2E+03	1.3E+04	2.9E+04	4.4E+04	5.3E+04	3.9E+04
FF 471 Punch 1	B20	P	2.3E+01	2.3E+01	9.4E+01	8.9E+01	1.5E+02	4.3E+02	9.3E+02	1.7E+03	2.5E+03	2.1E+03
		F	9.8E+02	9.8E+02	4.1E+03	3.9E+03	6.3E+03	1.9E+04	4.1E+04	7.3E+04	1.1E+05	9.4E+04
FF 471 Punch 2	B20	P	2.3E+01	2.3E+01	9.2E+01	8.9E+01	1.1E+02	4.0E+02	9.4E+02	1.7E+03	2.4E+03	2.1E+03
		F	1.0E+03	9.8E+02	4.0E+03	3.9E+03	4.9E+03	1.7E+04	4.1E+04	7.3E+04	1.1E+05	9.2E+04
FF 511	B100	P	8.2E+01	1.0E+02	2.5E+02	1.9E+02	6.2E+01	2.6E+02	9.2E+02	9.6E+02	9.8E+02	4.2E+02
		F	3.6E+03	4.6E+03	1.1E+04	8.4E+03	2.7E+03	1.1E+04	4.0E+04	4.2E+04	4.3E+04	1.8E+04
FF 516 Punch 1	B100	P	8.4E+01	9.6E+01	2.4E+02	1.9E+02	1.1E+02	1.5E+02	6.8E+02	8.7E+02	1.1E+03	5.9E+02
		F	3.7E+03	4.2E+03	1.0E+04	8.1E+03	4.9E+03	6.4E+03	3.0E+04	3.8E+04	4.8E+04	2.6E+04
FF 516 Punch 2	B100	P	8.0E+01	1.1E+02	2.7E+02	2.0E+02	1.1E+02	1.4E+02	6.3E+02	8.3E+02	1.0E+03	5.6E+02
		F	3.5E+03	4.8E+03	1.2E+04	8.7E+03	4.7E+03	6.0E+03	2.8E+04	3.7E+04	4.6E+04	2.5E+04

**Table B-4 Continued... Mass (ng) of target n-alkanes in the soybean test engine sequence filters. P means mass detected in the ¼ inch punch extracted from each filter, while F means computed mass of analyte on entire filter calculated using Eq (2-2). This Table shows compounds docosane (DCSN) through hexatriacontane (HCTN).**

Filter #	BD Blend		DCSN	TRCS	TCSN	HCSN	OCSN	TCTN	DCTN	TECTN	HCTN
FF 386	B00	P	8.5E+02	4.2E+02	2.8E+02	<i>3.5E+02</i>	<b>1.5E+02</b>	1.8E+02	<b>2.7E+02</b>	<b>3.8E+02</b>	<b>5.3E+02</b>
		F	3.7E+04	1.8E+04	1.2E+04	1.5E+04	<b>6.3E+03</b>	8.0E+03	<b>1.2E+04</b>	<b>1.7E+04</b>	<b>2.3E+04</b>
FF 421 Punch 1	B00	P	7.2E+02	3.0E+02	1.9E+02	<i>3.0E+02</i>	<i>8.0E+01</i>	<b>9.2E+01</b>	1.4E+02	<b>1.9E+02</b>	<b>2.6E+02</b>
		F	3.2E+04	1.3E+04	8.2E+03	1.3E+04	3.5E+03	<b>4.0E+03</b>	6.1E+03	<b>8.3E+03</b>	<b>1.2E+04</b>
P		8.3E+02	3.2E+02	2.0E+02	<i>3.7E+02</i>	<b>7.0E+01</b>	9.2E+01	1.4E+02	1.9E+02	<b>2.6E+02</b>	
F		3.6E+04	1.4E+04	8.6E+03	1.6E+04	<b>3.1E+03</b>	4.0E+03	6.0E+03	8.3E+03	<b>1.2E+04</b>	
FF 466 Punch 1	B20	P	9.1E+02	3.4E+02	2.4E+02	<i>3.4E+02</i>	<b>1.9E+02</b>	9.2E+01	<b>1.4E+02</b>	<b>1.9E+02</b>	<b>2.6E+02</b>
		F	4.0E+04	1.5E+04	1.1E+04	1.5E+04	<b>8.3E+03</b>	4.0E+03	<b>6.0E+03</b>	<b>8.3E+03</b>	<b>1.2E+04</b>
P		5.1E+02	2.1E+02	1.5E+02	<b>1.7E+02</b>	1.3E+02	9.1E+01	<b>1.4E+02</b>	1.9E+02	<b>2.6E+02</b>	
F		2.2E+04	9.3E+03	6.3E+03	<b>7.4E+03</b>	5.5E+03	4.0E+03	<b>6.1E+03</b>	8.3E+03	<b>1.2E+04</b>	
FF 471 Punch 1	B20	P	1.4E+03	5.2E+02	2.9E+02	<i>4.4E+02</i>	2.5E+02	<b>8.9E+01</b>	1.4E+02	1.9E+02	2.6E+02
		F	6.1E+04	2.3E+04	1.3E+04	1.9E+04	1.1E+04	<b>3.9E+03</b>	6.1E+03	8.3E+03	1.2E+04
FF 471 Punch 2		P	1.3E+03	5.1E+02	3.1E+02	<i>4.5E+02</i>	<b>1.4E+02</b>	9.4E+01	1.4E+02	<b>1.9E+02</b>	<b>2.6E+02</b>
		F	5.8E+04	2.2E+04	1.3E+04	2.0E+04	<b>6.3E+03</b>	4.1E+03	6.2E+03	<b>8.3E+03</b>	<b>1.2E+04</b>
FF 511	B100	P	5.3E+02	4.0E+02	4.3E+02	3.0E+02	<b>2.8E+02</b>	3.6E+02	<b>5.6E+02</b>	<b>7.5E+02</b>	<b>1.1E+03</b>
		F	2.3E+04	1.8E+04	1.9E+04	1.3E+04	<b>1.2E+04</b>	1.6E+04	<b>2.5E+04</b>	<b>3.3E+04</b>	<b>4.6E+04</b>
FF 516 Punch 1	B100	P	5.9E+02	4.2E+02	4.5E+02	<b>2.9E+02</b>	<b>2.8E+02</b>	3.6E+02	<b>5.5E+02</b>	7.6E+02	<b>1.1E+03</b>
		F	2.6E+04	1.8E+04	2.0E+04	<b>1.3E+04</b>	<b>1.2E+04</b>	1.6E+04	<b>2.4E+04</b>	3.3E+04	<b>4.6E+04</b>
P		6.0E+02	5.2E+02	4.5E+02	3.2E+02	2.8E+02	<b>3.6E+02</b>	<b>5.5E+02</b>	7.5E+02	<b>1.1E+03</b>	
F		2.6E+04	2.3E+04	2.0E+04	1.4E+04	1.2E+04	<b>1.6E+04</b>	<b>2.4E+04</b>	3.3E+04	<b>4.6E+04</b>	

ND means the target analyte was "Not Detected" during GC/MS analysis. *Italicized* values mean that the mass spectrum of the target analyte did not match that of the routinely used authentic standards, but the Q-value of the target analyte was greater than 50%. **Bold Italicized** values mean that the Q-value for the target analyte was less than 50%.

**Table B-5 Mass (ng) of target FAMES in the WVO test engine sequence filters. P means mass detected in the ¼ inch punch extracted from each filter, while F means computed mass of analyte on entire filter calculated using Eq (2-2).**

Filter #	BD Blend		C14:0	C16:0	C18:3n3	C18:2n6t	C18:2n6c	C18:1n9t	C18:1n9c	C18:0	C20:0	C22:0
FF 276	B10	P	2.0E+02	2.3E+03	9.0E+02	1.6E+03	5.7E+03	1.8E+03	4.8E+03	1.7E+03	4.5E+02	6.0E+02
		F	8.8E+03	9.8E+04	3.9E+04	7.0E+04	2.5E+05	7.9E+04	2.1E+05	7.2E+04	2.0E+04	2.6E+04
FF 281 Punch1	B10	P	1.5E+02	1.0E+03	7.0E+02	1.3E+03	3.6E+03	2.1E+03	3.3E+03	1.3E+03	3.0E+02	6.5E+02
		F	6.6E+03	4.4E+04	3.1E+04	5.5E+04	1.6E+05	9.0E+04	1.4E+05	5.5E+04	1.3E+04	2.8E+04
P		2.0E+02	3.5E+02	4.5E+02	2.2E+03	2.5E+03	1.7E+03	2.0E+03	1.1E+03	5.0E+02	7.0E+02	
F		8.8E+03	1.5E+04	2.0E+04	9.4E+04	1.1E+05	7.4E+04	8.8E+04	4.8E+04	2.2E+04	3.1E+04	
FF 286	B10	P	2.0E+02	1.8E+03	9.0E+02	1.5E+03	5.2E+03	2.5E+03	4.5E+03	1.7E+03	4.5E+02	6.0E+02
		F	8.8E+03	7.9E+04	3.9E+04	6.3E+04	2.3E+05	1.1E+05	2.0E+05	7.2E+04	2.0E+04	2.6E+04
FF 291 Punch1	B20	P	2.0E+02	6.1E+03	2.0E+03	2.0E+03	1.3E+04	5.0E+03	1.3E+04	4.2E+03	6.0E+02	8.0E+02
		F	8.8E+03	2.7E+05	8.5E+04	8.8E+04	5.9E+05	2.2E+05	5.7E+05	1.8E+05	2.6E+04	3.5E+04
P		2.0E+02	4.2E+03	1.6E+03	1.7E+03	9.7E+03	4.0E+03	9.0E+03	3.0E+03	4.5E+02	6.5E+02	
F		8.8E+03	1.8E+05	7.0E+04	7.2E+04	4.2E+05	1.8E+05	3.9E+05	1.3E+05	2.0E+04	2.8E+04	
FF 291 Punch2		P	2.0E+02	4.2E+03	1.6E+03	1.7E+03	9.7E+03	4.0E+03	9.0E+03	3.0E+03	4.5E+02	6.5E+02
		F	8.8E+03	1.8E+05	7.0E+04	7.2E+04	4.2E+05	1.8E+05	3.9E+05	1.3E+05	2.0E+04	2.8E+04
FF 296 Punch1	B20	P	2.0E+02	6.6E+03	1.9E+03	1.9E+03	1.6E+04	4.6E+03	1.2E+04	3.7E+03	6.5E+02	7.5E+02
		F	8.8E+03	2.9E+05	8.1E+04	8.3E+04	7.0E+05	2.0E+05	5.1E+05	1.6E+05	2.8E+04	3.3E+04
P		2.0E+02	6.1E+03	1.6E+03	1.9E+03	1.3E+04	4.8E+03	1.2E+04	3.7E+03	4.0E+02	8.0E+02	
F		8.8E+03	2.6E+05	6.8E+04	8.3E+04	5.5E+05	2.1E+05	5.2E+05	1.6E+05	1.8E+04	3.5E+04	
FF 296 Punch2		P	2.0E+02	6.1E+03	1.6E+03	1.9E+03	1.3E+04	4.8E+03	1.2E+04	3.7E+03	4.0E+02	8.0E+02
		F	8.8E+03	2.6E+05	6.8E+04	8.3E+04	5.5E+05	2.1E+05	5.2E+05	1.6E+05	1.8E+04	3.5E+04
FF 301 Punch1	B20	P	2.0E+02	4.8E+03	1.6E+03	1.9E+03	1.2E+04	4.0E+03	9.2E+03	3.4E+03	5.0E+02	7.5E+02
		F	8.8E+03	2.1E+05	7.0E+04	8.3E+04	5.4E+05	1.8E+05	4.0E+05	1.5E+05	2.2E+04	3.3E+04
P		2.0E+02	4.8E+03	1.7E+03	1.9E+03	9.7E+03	4.1E+03	8.9E+03	2.9E+03	4.0E+02	7.5E+02	
F		8.8E+03	2.1E+05	7.2E+04	8.3E+04	4.2E+05	1.8E+05	3.9E+05	1.3E+05	1.8E+04	3.3E+04	
FF 301 Punch2		P	2.0E+02	4.8E+03	1.7E+03	1.9E+03	9.7E+03	4.1E+03	8.9E+03	2.9E+03	4.0E+02	7.5E+02
		F	8.8E+03	2.1E+05	7.2E+04	8.3E+04	4.2E+05	1.8E+05	3.9E+05	1.3E+05	1.8E+04	3.3E+04
FF 306	B50	P	4.0E+02	2.2E+04	4.7E+03	6.3E+03	3.4E+04	1.4E+04	3.4E+04	1.0E+04	1.0E+03	1.6E+03
		F	1.8E+04	9.5E+05	2.1E+05	2.8E+05	1.5E+06	6.0E+05	1.5E+06	4.5E+05	4.4E+04	7.0E+04
FF 311 Punch1	B50	P	4.0E+02	1.7E+04	4.4E+03	4.1E+03	2.6E+04	1.0E+04	2.6E+04	8.1E+03	8.0E+02	1.5E+03
		F	1.8E+04	7.3E+05	1.9E+05	1.8E+05	1.1E+06	4.4E+05	1.1E+06	3.5E+05	3.5E+04	6.6E+04
P		5.0E+02	2.5E+04	4.5E+03	5.0E+03	3.7E+04	1.4E+04	3.9E+04	1.1E+04	5.0E+02	1.7E+03	
F		2.2E+04	1.1E+06	2.0E+05	2.2E+05	1.6E+06	6.2E+05	1.7E+06	4.9E+05	2.2E+04	7.4E+04	
FF311 Punch2		P	5.0E+02	2.5E+04	4.5E+03	5.0E+03	3.7E+04	1.4E+04	3.9E+04	1.1E+04	5.0E+02	1.7E+03
		F	2.2E+04	1.1E+06	2.0E+05	2.2E+05	1.6E+06	6.2E+05	1.7E+06	4.9E+05	2.2E+04	7.4E+04
FF 316	B50	P	4.0E+02	1.4E+04	5.0E+03	6.1E+03	2.8E+04	1.5E+04	2.9E+04	9.5E+03	1.0E+03	1.7E+03
		F	1.8E+04	5.9E+05	2.2E+05	2.7E+05	1.2E+06	6.7E+05	1.3E+06	4.2E+05	4.4E+04	7.4E+04
FF 331	B100	P	1.0E+03	9.6E+04	8.2E+03	1.4E+04	8.8E+04	4.7E+04	1.3E+05	3.7E+04	2.8E+03	4.4E+03
		F	4.4E+04	4.2E+06	3.6E+05	6.0E+05	3.8E+06	2.1E+06	5.7E+06	1.6E+06	1.2E+05	1.9E+05
FF 336 Punch1	B100	P	1.2E+03	9.2E+04	6.8E+03	1.3E+04	8.0E+04	4.5E+04	1.2E+05	3.4E+04	2.0E+03	4.4E+03
		F	5.3E+04	4.0E+06	3.0E+05	5.5E+05	3.5E+06	2.0E+06	5.2E+06	1.5E+06	8.8E+04	1.9E+05
P		8.0E+02	6.9E+04	3.2E+03	1.0E+04	6.1E+04	3.8E+04	9.3E+04	2.5E+04	2.0E+03	3.6E+03	
F		3.5E+04	3.0E+06	1.4E+05	4.6E+05	2.7E+06	1.6E+06	4.1E+06	1.1E+06	8.8E+04	1.6E+05	
FF 336 Punch2		P	8.0E+02	6.9E+04	3.2E+03	1.0E+04	6.1E+04	3.8E+04	9.3E+04	2.5E+04	2.0E+03	3.6E+03
		F	3.5E+04	3.0E+06	1.4E+05	4.6E+05	2.7E+06	1.6E+06	4.1E+06	1.1E+06	8.8E+04	1.6E+05
FF 341	B100	P	8.0E+02	5.9E+04	1.8E+03	1.0E+04	4.5E+04	3.2E+04	8.9E+04	2.5E+04	2.0E+03	4.2E+03
		F	3.5E+04	2.6E+06	7.9E+04	4.5E+05	2.0E+06	1.4E+06	3.9E+06	1.1E+06	8.8E+04	1.8E+05

**Table B-6 Mass (ng) of target FAMES in the soybean test engine sequence filters. P means mass detected in the ¼ inch punch extracted from each filter, while F means computed mass of analyte on entire filter calculated using Eq (2-2).**

Filter #	BD Blend		C14:0	C16:0	C18:3n3	C18:2n6t	C18:2n6c	C18:1n9t	C18:1n9c	C18:0	C20:0	C22:0
FF 466 Punch1	B20	P	2.0E+02	7.4E+03	2.5E+03	2.5E+03	1.9E+04	6.4E+03	1.4E+04	5.1E+03	6.0E+02	9.5E+02
		F	8.8E+03	3.2E+05	1.1E+05	1.1E+05	8.3E+05	2.8E+05	5.9E+05	2.2E+05	2.6E+04	4.2E+04
FF 466 Punch2		P	2.0E+02	8.9E+03	3.4E+03	3.9E+03	2.3E+04	8.1E+03	1.6E+04	6.0E+03	5.0E+02	9.5E+02
		F	8.8E+03	3.9E+05	1.5E+05	1.7E+05	1.0E+06	3.5E+05	7.1E+05	2.6E+05	2.2E+04	4.2E+04
FF 471 Punch1	B20	P	2.0E+02	6.4E+03	3.5E+03	3.2E+03	2.2E+04	7.1E+03	1.7E+04	6.2E+03	2.5E+02	9.0E+02
		F	8.8E+03	2.8E+05	1.5E+05	1.4E+05	9.6E+05	3.1E+05	7.3E+05	2.7E+05	1.1E+04	3.9E+04
FF 511	B100	P	1.0E+03	1.1E+05	2.2E+04	1.9E+04	1.9E+05	4.9E+04	1.4E+05	4.8E+04	4.0E+03	5.0E+03
		F	4.4E+04	4.9E+06	9.8E+05	8.1E+05	8.3E+06	2.1E+06	6.3E+06	2.1E+06	1.8E+05	2.2E+05
FF 516 Punch1	B100	P	1.0E+03	1.1E+05	2.2E+04	2.4E+04	1.7E+05	5.6E+04	1.4E+05	4.6E+04	3.4E+03	4.6E+03
		F	4.4E+04	4.7E+06	9.7E+05	1.1E+06	7.3E+06	2.4E+06	6.1E+06	2.0E+06	1.5E+05	2.0E+05
FF 516 Punch2		P	1.0E+03	7.2E+04	1.3E+04	1.6E+04	1.0E+05	3.8E+04	8.7E+04	3.0E+04	2.2E+03	4.0E+03
		F	4.4E+04	3.2E+06	5.6E+05	7.0E+05	4.4E+06	1.6E+06	3.8E+06	1.3E+06	9.6E+04	1.8E+05





**Table B-8 Mass (ng) of target POCs in the soybean test engine sequence filters. P means mass detected in the ¼ inch punch extracted from each filter, while F means computed mass of analyte on entire filter calculated using Eq (2-2). This Table shows compounds 2-pentanone (2PNN) through dodecanal (DDCL).**

Filter #	BD Blend		2PNN	3PNN	HXNL	HPTL	OCTL	2NNE	NNNL	DECL	UDCL	2HXN	2HPN	2-Oct	DDCL
FF 386 Punch 1	B00	P	2.7E+02	2.9E+02	1.0E+00	7.2E+01	6.2E+01	4.1E+01	7.0E+00	5.1E+01	4.0E+01	1.4E+02	1.3E+02	8.3E+01	3.9E+01
		F	1.2E+04	1.3E+04	4.4E+01	3.2E+03	2.7E+03	1.8E+03	3.1E+02	2.2E+03	1.8E+03	5.9E+03	5.8E+03	3.6E+03	1.7E+03
P		3.4E+02	3.7E+02	1.0E+01	8.1E+01	1.6E+02	4.1E+01	3.1E+01	3.6E+01	1.4E+02	1.6E+02	1.9E+02	1.7E+02	7.3E+01	
F		1.5E+04	1.6E+04	4.5E+02	3.5E+03	7.0E+03	1.8E+03	1.4E+03	1.6E+03	6.2E+03	6.8E+03	8.3E+03	7.3E+03	3.2E+03	
FF 386 Punch 2	B00	P	3.3E+01	1.6E+02	7.6E+00	3.8E+01	9.1E+01	2.1E+01	1.7E+01	3.2E+01	2.4E+01	8.3E+01	9.8E+01	4.7E+01	2.6E+01
F		1.5E+03	7.2E+03	3.3E+02	1.7E+03	4.0E+03	9.0E+02	7.4E+02	1.4E+03	1.0E+03	3.6E+03	4.3E+03	2.1E+03	1.1E+03	
FF 421 Punch 1	B00	P	1.6E+02	1.8E+02	3.7E+00	3.0E+01	8.0E+01	3.5E+01	6.5E+00	2.8E+01	2.4E+01	8.5E+01	9.1E+01	3.8E+01	2.2E+01
		F	7.1E+03	7.8E+03	1.6E+02	1.3E+03	3.5E+03	1.5E+03	2.8E+02	1.2E+03	1.0E+03	3.7E+03	4.0E+03	1.7E+03	9.4E+02
P		1.3E+02	1.4E+02	5.2E+00	2.9E+01	4.2E+01	2.1E+01	9.5E+00	1.1E+01	1.9E+01	9.5E+01	7.6E+01	5.1E+01	2.2E+01	
F		5.6E+03	6.1E+03	2.3E+02	1.3E+03	1.8E+03	9.0E+02	4.2E+02	4.6E+02	8.3E+02	4.1E+03	3.3E+03	2.2E+03	9.6E+02	
FF 421 Punch 3	B00	P	1.1E+02	1.3E+02	3.3E+00	2.8E+01	4.7E+01	2.1E+01	9.0E+00	1.1E+01	3.7E+01	6.7E+01	7.5E+01	4.4E+01	2.4E+01
		F	5.0E+03	5.8E+03	1.5E+02	1.2E+03	2.1E+03	9.0E+02	3.9E+02	4.6E+02	1.6E+03	2.9E+03	3.3E+03	1.9E+03	1.0E+03
P		7.3E+01	7.9E+01	3.4E+01	3.2E+01	2.9E+01	2.5E+01	1.7E+01	1.6E+01	1.5E+01	5.3E+01	5.7E+01	4.8E+01	9.0E+00	
F		3.2E+03	3.5E+03	1.5E+03	1.4E+03	1.3E+03	1.1E+03	7.2E+02	7.0E+02	6.3E+02	2.3E+03	2.5E+03	2.1E+03	3.9E+02	
FF 466 Punch 2	B20	P	2.8E+01	1.2E+02	7.5E+01	4.1E+01	4.1E+01	2.1E+01	3.1E+01	2.2E+01	2.1E+01	4.6E+01	5.7E+01	4.8E+01	1.9E+01
F		1.2E+03	5.4E+03	3.3E+03	1.8E+03	1.8E+03	9.0E+02	1.3E+03	9.6E+02	9.0E+02	2.0E+03	2.5E+03	2.1E+03	8.3E+02	
FF 471 Punch 1	B20	P	7.0E+01	7.6E+01	2.0E+01	3.1E+01	2.1E+01	2.5E+01	1.0E+01	6.5E+00	1.2E+01	4.8E+01	5.1E+01	4.1E+01	9.0E+00
		F	3.1E+03	3.3E+03	8.8E+02	1.3E+03	9.0E+02	1.1E+03	4.4E+02	2.8E+02	5.0E+02	2.1E+03	2.2E+03	1.8E+03	3.9E+02
P		6.1E+01	6.7E+01	1.4E+01	3.0E+01	2.9E+01	2.4E+01	1.5E+01	8.5E+00	1.7E+01	3.6E+01	4.5E+01	3.6E+01	9.0E+00	
F		2.7E+03	2.9E+03	6.3E+02	1.3E+03	1.2E+03	1.0E+03	6.6E+02	3.7E+02	7.2E+02	1.6E+03	1.9E+03	1.6E+03	3.9E+02	
FF 471 Punch 2	B20	P	7.3E+01	8.2E+01	3.6E+01	3.1E+01	3.4E+01	2.1E+01	2.3E+01	7.0E+00	1.6E+01	5.2E+01	3.3E+01	3.6E+01	1.6E+01
		F	3.2E+03	3.6E+03	1.6E+03	1.3E+03	1.5E+03	9.0E+02	1.0E+03	3.1E+02	6.8E+02	2.3E+03	1.4E+03	1.6E+03	6.8E+02
P		6.3E+01	7.1E+01	2.7E+01	2.9E+01	3.2E+01	2.1E+01	1.9E+01	1.5E+01	1.6E+01	3.8E+01	5.0E+01	3.4E+01	1.5E+01	
F		2.8E+03	3.1E+03	1.2E+03	1.3E+03	1.4E+03	9.0E+02	8.1E+02	6.6E+02	7.0E+02	1.7E+03	2.2E+03	1.5E+03	6.6E+02	
FF 471 Punch 3	B20	P	6.3E+01	7.1E+01	2.7E+01	2.9E+01	3.2E+01	2.1E+01	1.9E+01	1.5E+01	1.6E+01	3.8E+01	5.0E+01	3.4E+01	1.5E+01
		F	2.8E+03	3.1E+03	1.2E+03	1.3E+03	1.4E+03	9.0E+02	8.1E+02	6.6E+02	7.0E+02	1.7E+03	2.2E+03	1.5E+03	6.6E+02
P		1.6E+02	1.5E+02	7.2E+02	3.5E+02	1.7E+02	2.9E+02	2.3E+02	8.0E+01	6.2E+01	2.4E+02	1.6E+02	1.8E+02	5.0E+01	
F		6.8E+03	6.7E+03	3.2E+04	1.5E+04	7.3E+03	1.3E+04	1.0E+04	3.5E+03	2.7E+03	1.1E+04	7.1E+03	7.8E+03	2.2E+03	
FF 511	B100	P	2.2E+02	2.2E+02	9.0E+02	9.4E+01	2.0E+02	5.6E+02	2.9E+02	1.1E+02	7.0E+01	3.0E+02	2.0E+02	2.4E+02	3.6E+01
		F	9.6E+03	9.8E+03	3.9E+04	4.1E+03	8.7E+03	2.5E+04	1.3E+04	5.0E+03	3.1E+03	1.3E+04	8.8E+03	1.1E+04	1.6E+03
P		1.9E+02	1.9E+02	5.5E+02	4.1E+02	1.8E+02	2.6E+02	2.2E+02	1.0E+02	6.4E+01	2.6E+02	1.6E+02	2.1E+02	3.6E+01	
F		8.5E+03	8.5E+03	2.4E+04	1.8E+04	7.8E+03	1.1E+04	9.5E+03	4.4E+03	2.8E+03	1.1E+04	7.2E+03	9.2E+03	1.6E+03	
FF 516 Punch 1	B100	P	1.9E+02	1.9E+02	5.5E+02	4.1E+02	1.8E+02	2.6E+02	2.2E+02	1.0E+02	6.4E+01	2.6E+02	1.6E+02	2.1E+02	3.6E+01
F		8.5E+03	8.5E+03	2.4E+04	1.8E+04	7.8E+03	1.1E+04	9.5E+03	4.4E+03	2.8E+03	1.1E+04	7.2E+03	9.2E+03	1.6E+03	
FF 516 Punch 2	B100	P	1.9E+02	1.9E+02	5.5E+02	4.1E+02	1.8E+02	2.6E+02	2.2E+02	1.0E+02	6.4E+01	2.6E+02	1.6E+02	2.1E+02	3.6E+01
F		8.5E+03	8.5E+03	2.4E+04	1.8E+04	7.8E+03	1.1E+04	9.5E+03	4.4E+03	2.8E+03	1.1E+04	7.2E+03	9.2E+03	1.6E+03	



**Table B-8 Continued... This Table shows compounds benzaldehyde (BZDE) through anthraquinone (ATQ).**

Filter #	BD Blend		BZDE	mTOL	oTOL	pTOL	ACNE	1IND	9FLN	PNNN	BZP	BQN	NQN	ACNQ	ATQ
FF 386 Punch 1	B00	p	8.4E+01	5.4E+01	<b>3.6E+02</b>	6.9E+01	4.4E+01	<b>3.4E+01</b>	6.6E+01	2.0E+02	<b>4.8E-01</b>	2.3E+02	1.4E+02	<b>4.3E+03</b>	7.9E+01
		F	3.7E+03	2.4E+03	<b>1.6E+04</b>	3.0E+03	1.9E+03	<b>1.5E+03</b>	2.9E+03	8.8E+03	<b>2.1E+01</b>	1.0E+04	6.3E+03	<b>1.9E+05</b>	3.5E+03
FF 386 Punch 2		p	1.1E+02	6.6E+01	<b>4.9E+02</b>	8.7E+01	4.8E+01	<b>5.1E+01</b>	1.6E+02	3.0E+02	6.4E+01	2.5E+02	2.7E+02	<b>4.2E+03</b>	1.2E+02
		F	5.0E+03	2.9E+03	<b>2.1E+04</b>	3.8E+03	2.1E+03	<b>2.2E+03</b>	6.9E+03	1.3E+04	2.8E+03	1.1E+04	1.2E+04	<b>1.8E+05</b>	5.3E+03
FF 421 Punch 1	B00	p	4.6E+01	2.6E+01	<b>1.9E+02</b>	3.5E+01	2.7E+01	<b>1.8E+01</b>	5.7E+01	2.4E+02	2.0E+01	1.6E+02	1.1E+02	<b>2.3E+03</b>	8.5E+01
		F	2.0E+03	1.1E+03	<b>8.5E+03</b>	1.5E+03	1.2E+03	<b>7.7E+02</b>	2.5E+03	1.0E+04	8.7E+02	7.0E+03	4.6E+03	<b>1.0E+05</b>	3.7E+03
FF 421 Punch 2		p	3.4E+01	2.7E+01	<b>1.9E+02</b>	3.8E+01	3.0E+01	<b>2.7E+01</b>	4.6E+01	2.3E+02	1.0E+01	1.8E+02	1.0E+02	<b>2.0E+03</b>	8.3E+01
		F	1.5E+03	1.2E+03	<b>8.2E+03</b>	1.6E+03	1.3E+03	<b>1.2E+03</b>	2.0E+03	1.0E+04	4.5E+02	7.7E+03	4.5E+03	<b>8.6E+04</b>	3.6E+03
FF 421 Punch 3		p	3.8E+01	2.5E+01	<b>9.9E+01</b>	3.3E+01	2.2E+01	<b>2.0E+01</b>	4.5E+01	1.8E+02	2.2E+01	1.4E+02	9.5E+01	<b>2.2E+03</b>	5.9E+01
		F	1.7E+03	1.1E+03	<b>4.3E+03</b>	1.4E+03	9.6E+02	<b>8.9E+02</b>	2.0E+03	7.8E+03	9.5E+02	6.2E+03	4.1E+03	<b>9.8E+04</b>	2.6E+03
FF 421 Punch 4		p	3.7E+01	2.7E+01	<b>1.5E+02</b>	3.2E+01	2.3E+01	<b>1.5E+01</b>	4.5E+01	2.1E+02	2.4E+01	1.3E+02	9.4E+01	<b>1.7E+03</b>	7.9E+01
		F	1.6E+03	1.2E+03	<b>6.4E+03</b>	1.4E+03	1.0E+03	<b>6.7E+02</b>	2.0E+03	9.3E+03	1.0E+03	5.7E+03	4.1E+03	<b>7.3E+04</b>	3.4E+03
FF 466 Punch 1	B20	p	2.7E+01	2.2E+01	<b>9.4E+01</b>	2.3E+01	2.0E+01	<b>1.3E+01</b>	1.9E+01	8.5E+01	1.1E+00	5.7E+01	3.3E+01	<b>2.0E+03</b>	4.3E+01
		F	1.2E+03	9.4E+02	<b>4.1E+03</b>	9.8E+02	8.5E+02	<b>5.5E+02</b>	8.3E+02	3.7E+03	4.7E+01	2.5E+03	1.4E+03	<b>8.6E+04</b>	1.9E+03
FF 466 Punch 2		p	3.4E+01	2.2E+01	<b>3.8E+01</b>	2.1E+01	2.1E+01	<b>1.2E+01</b>	3.6E+01	9.9E+01	2.0E+01	5.4E+01	5.6E+01	<b>3.9E+02</b>	4.9E+01
		F	1.5E+03	9.6E+02	<b>1.7E+03</b>	9.0E+02	9.0E+02	<b>5.1E+02</b>	1.6E+03	4.3E+03	8.9E+02	2.3E+03	2.4E+03	<b>1.7E+04</b>	2.1E+03
FF 471 Punch 1	B20	p	2.6E+01	2.4E+01	<b>9.0E+01</b>	2.3E+01	1.9E+01	<b>1.1E+01</b>	3.5E+01	1.0E+02	<b>2.2E-01</b>	5.3E+01	4.6E+01	<b>7.6E+02</b>	4.9E+01
		F	1.1E+03	1.0E+03	<b>3.9E+03</b>	9.8E+02	8.1E+02	<b>4.7E+02</b>	1.5E+03	4.5E+03	<b>9.8E+00</b>	2.3E+03	2.0E+03	<b>3.3E+04</b>	2.1E+03
FF 471 Punch 2		p	2.7E+01	2.1E+01	<b>8.2E+01</b>	2.3E+01	1.9E+01	<b>1.1E+01</b>	2.7E+01	9.7E+01	<b>5.8E-01</b>	5.2E+01	4.6E+01	<b>5.6E+02</b>	3.4E+01
		F	1.2E+03	9.2E+02	<b>3.6E+03</b>	1.0E+03	8.1E+02	<b>4.9E+02</b>	1.2E+03	4.2E+03	<b>2.5E+01</b>	2.3E+03	2.0E+03	<b>2.4E+04</b>	1.5E+03
FF 471 Punch 3		p	2.8E+01	2.1E+01	<b>5.1E+01</b>	2.2E+01	2.0E+01	<b>1.1E+01</b>	2.9E+01	8.5E+01	7.3E-01	4.5E+01	4.1E+01	<b>3.3E+02</b>	4.2E+01
		F	1.2E+03	9.2E+02	<b>2.2E+03</b>	9.4E+02	8.5E+02	<b>5.0E+02</b>	1.3E+03	3.7E+03	3.2E+01	1.9E+03	1.8E+03	<b>1.4E+04</b>	1.8E+03
FF 471 Punch 4		p	2.7E+01	2.1E+01	<b>5.8E+01</b>	2.2E+01	1.9E+01	<b>1.1E+01</b>	2.3E+01	8.8E+01	2.0E+00	4.2E+01	3.7E+01	<b>4.1E+02</b>	3.9E+01
		F	1.2E+03	9.2E+02	<b>2.5E+03</b>	9.4E+02	8.3E+02	<b>5.0E+02</b>	1.0E+03	3.8E+03	8.7E+01	1.8E+03	1.6E+03	<b>1.8E+04</b>	1.7E+03
FF 511	B100	p	<b>9.8E+01</b>	<b>8.4E+01</b>	<b>1.8E+02</b>	<b>1.1E+02</b>	7.2E+01	<b>4.0E+01</b>	<b>7.8E+01</b>	<b>7.2E+01</b>	<b>1.4E+01</b>	<b>1.0E+02</b>	<b>8.1E+01</b>	<b>3.4E+03</b>	<b>5.2E+01</b>
		F	<b>4.3E+03</b>	<b>3.7E+03</b>	<b>7.8E+03</b>	<b>4.7E+03</b>	3.2E+03	<b>1.8E+03</b>	<b>3.4E+03</b>	<b>3.2E+03</b>	<b>6.3E+02</b>	<b>4.5E+03</b>	<b>3.6E+03</b>	<b>1.5E+05</b>	<b>2.3E+03</b>
FF 516 Punch 1	B100	p	<b>1.1E+02</b>	<b>9.4E+01</b>	<b>2.6E+02</b>	<b>1.1E+02</b>	7.4E+01	<b>4.4E+01</b>	<b>1.6E+02</b>	<b>1.1E+02</b>	<b>9.8E+01</b>	<b>1.1E+02</b>	<b>9.6E+01</b>	<b>5.8E+03</b>	<b>7.2E+01</b>
		F	<b>5.0E+03</b>	<b>4.1E+03</b>	<b>1.1E+04</b>	<b>4.8E+03</b>	3.2E+03	<b>1.9E+03</b>	<b>6.9E+03</b>	<b>4.8E+03</b>	<b>4.3E+03</b>	<b>4.8E+03</b>	<b>4.2E+03</b>	<b>2.6E+05</b>	<b>3.2E+03</b>
FF 516 Punch 2		p	<b>1.0E+02</b>	<b>9.0E+01</b>	<b>2.8E+02</b>	<b>1.1E+02</b>	7.4E+01	<b>4.5E+01</b>	<b>1.4E+02</b>	<b>1.1E+02</b>	<b>6.0E+01</b>	<b>1.2E+02</b>	<b>1.1E+02</b>	<b>7.8E+02</b>	<b>7.2E+01</b>
		F	<b>4.5E+03</b>	<b>3.9E+03</b>	<b>1.2E+04</b>	<b>4.7E+03</b>	3.2E+03	<b>2.0E+03</b>	<b>6.1E+03</b>	<b>4.7E+03</b>	<b>2.6E+03</b>	<b>5.3E+03</b>	<b>4.8E+03</b>	<b>3.4E+04</b>	<b>3.2E+03</b>

*Italicized* values mean that the mass spectrum of the target analyte did not match that of the routinely used authentic standards, but the Q-value of the target analyte was greater than 50%. **Bold Italicized** values mean that the Q-value for the target analyte was less than 50%. **Bold** values mean that the mass of the target analyte was less than the Engine Blank concentration.

## APPENDIX C

### Determination of number of ozone molecules in the system

Concentration of ozone used in the system = 0.4 ppm

$$0.4 \text{ ppm of ozone} = \frac{0.4 \text{ cm}^3 \text{ ozone}}{10^6 \text{ cm}^3 \text{ air}}$$

1 mole of gas contains approx.  $24.5 \times 10^3 \text{ cm}^3$  at room temperature,  $T=25 \text{ }^\circ\text{C}$

$$\text{Therefore, the concentration of ozone in air} = \frac{0.4 \text{ moles ozone}}{24.5 \times 10^3 \times 10^6 \text{ cm}^3 \text{ air}} = 1.63 \times 10^{-11} \frac{\text{moles ozone}}{\text{cm}^3 \text{ air}}$$

1 mole of a substance contains  $6.022 \times 10^{23}$  molecules

$$\begin{aligned} \text{Therefore, the \# of molecules of ozone in 0.4 ppm} &= 1.63 \times 10^{-11} \times 6.022 \times 10^{23} \text{ molecules/cm}^3 \\ &= \mathbf{1 \times 10^{13} \text{ molecules/cm}^3} \end{aligned}$$

# of molecules of ozone in each reaction chamber at any time = # of ozone molecules in 0.4 ppm  $\times$  volume of reaction chamber

Volume of reaction chamber = 164 mL

$$\begin{aligned} \text{\# of molecules of ozone in each reaction chamber at any given time} &= 1 \times 10^{13} \text{ molecules/cm}^3 \times 164 \text{ cm}^3 \\ &= \mathbf{1.64 \times 10^{15} \text{ molecules of ozone}} \end{aligned}$$

Table C1 shows the number of molecules of PAHs and FAMES spiked on the ¼-inch filter punches. At  $t=0$ , each ¼-inch punch spiked with only the 16 PAH mix had  $1.44 \times 10^{15}$  molecules, while each ¼-inch punch spiked with the 16 PAH mix and the 10 FAME mix had  $2.48 \times 10^{16}$  molecules. If we assume that each molecule of PAH or FAME consumed one molecule of ozone, and that the reactions between ozone and the FAME or PAH molecules were instantaneous, it therefore implies that the  $1.64 \times 10^{15}$  molecules of ozone in each reaction chamber at  $t=0$  were not in excess of the PAH and FAME total molecules. Further, given that each reaction chamber was loaded with 3 to 6 punches, it suggests that at  $t=0$ , there was not an excess of ozone in the system. However, at time points greater than  $t=0$  (i.e. at  $t=1, 2, 4, 8,$  and 24 hours), there was always excess ozone in the system.

**Table C-1 Molecules of PAHs and FAMES per punch in the reaction chambers**

Compounds	Mass at t=0 (ng)	MW (g/mol)	Moles at t=0	Molecules at t=0
Naphthalene	30	128	2.34E-10	1.41E+14
Acenaphthylene	30	152	1.97E-10	1.19E+14
Acenaphthene	30	154	1.95E-10	1.17E+14
Fluorene	30	166	1.81E-10	1.09E+14
Phenanthrene	30	178	1.69E-10	1.02E+14
Anthracene	30	178	1.69E-10	1.02E+14
Fluoranthene	30	202	1.49E-10	8.95E+13
Pyrene	30	202	1.49E-10	8.95E+13
Benzo[a]anthracene	30	228	1.32E-10	7.93E+13
Chrysene	30	228	1.32E-10	7.93E+13
Benzo[b]fluoranthene	30	252	1.19E-10	7.17E+13
Benzo[k]fluoranthene	30	252	1.19E-10	7.17E+13
Benzo[a]pyrene	30	252	1.19E-10	7.17E+13
Indeno[1,2,3-cd]pyrene	30	276	1.09E-10	6.55E+13
Benzo[ghi]perylene	30	276	1.09E-10	6.55E+13
Dibenz[a,h]anthracene	30	278	1.08E-10	6.50E+13
<b>Total Moles of PAHs</b>				<b>1.44E+15</b>
Methyl myristate (C14:0)	535.0	242	2.21E-09	1.33E+15
Methyl palmitate (C16:0)	1315.0	270	4.87E-09	2.93E+15
Methyl linolenate (C18:3n3)	460.0	292	1.58E-09	9.49E+14
Methyl linolelaidate (C18:2n6t)	270.0	294	9.18E-10	5.53E+14
Methyl linoleate (C18:2n6c)	2905.0	294	9.88E-09	5.95E+15
Methyl elaidate (C18:1n9t)	1490.0	296	5.03E-09	3.03E+15
Methyl oleate (C18:1n9c)	3100.0	296	1.05E-08	6.31E+15
Methyl stearate (C18:0)	710.0	298	2.38E-09	1.44E+15
Methyl arachidate (C20:0)	220.0	326	6.75E-10	4.06E+14
Methyl behenate (C22:0)	255.0	354	7.20E-10	4.34E+14
<b>Total Moles of FAMES</b>				<b>2.33E+16</b>
<b>Total Moles of PAHs+FAMES</b>				<b>2.48E+16</b>

**Table C-2 Descriptive statistics of ozone concentrations (ppm) measured during the ozone exposure experiments.**

Date	Experiment Type	Avg* (ppm)	Std Dev* (ppm)	%RSD
4/24/2014	PAHs Only O <sub>3</sub> Exposure	0.444	0.037	8.3
4/28/2014	PAHs and FAMES O <sub>3</sub> Exposure	0.407	0.023	5.8
5/7/2014	B20 Filter O <sub>3</sub> Exposure	0.407	0.026	6.4

\*values are based on 30 sec data over 24 hours of each experiment.

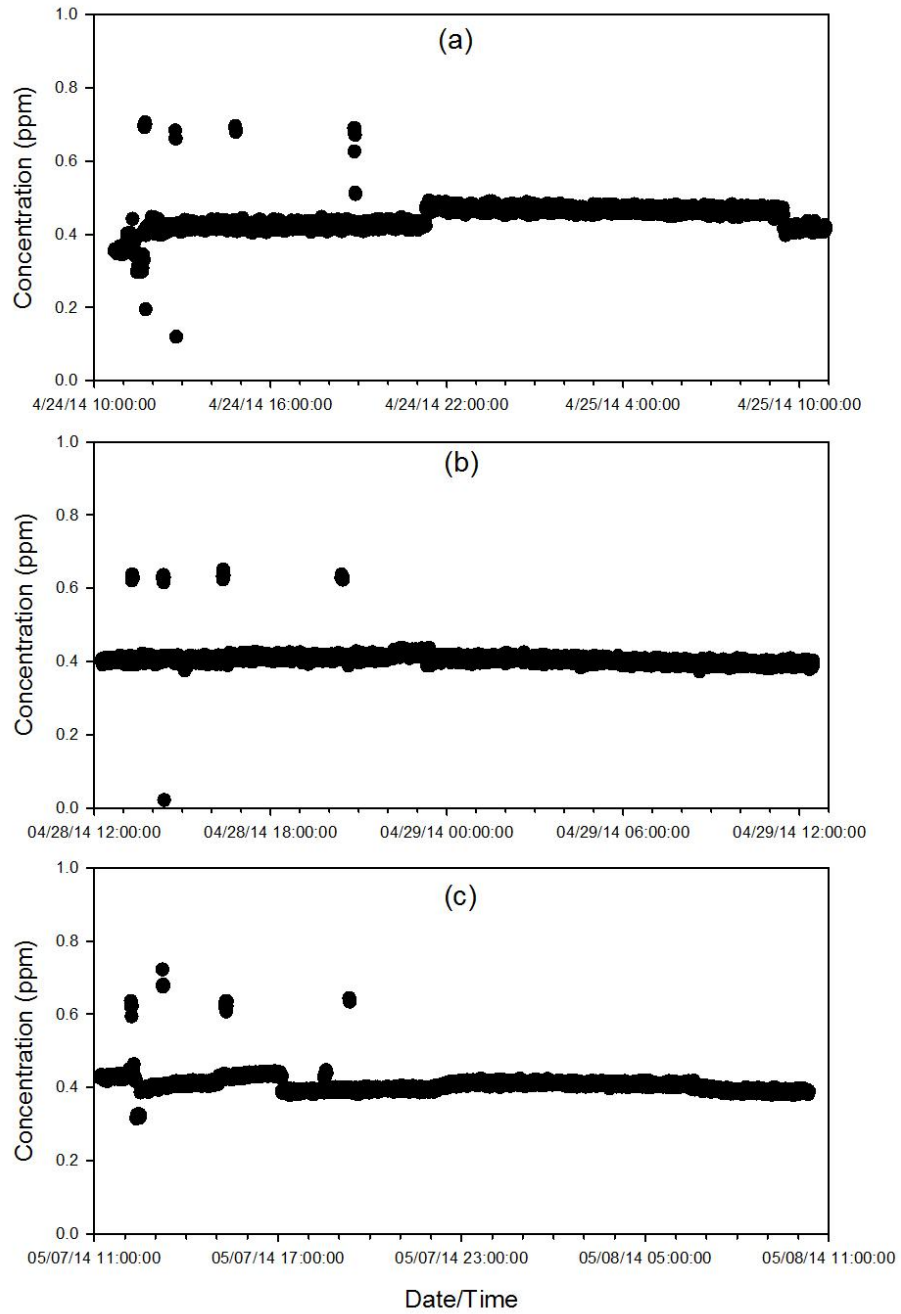


**Figure C-1 Ozone concentrations (ppm) measured during the ozone exposure experiments conducted for 24 hours on (a) 04/24/14, (b) 04/28/14, and (c) 05/07/14.**

**Table C-3 Descriptive statistics of total exit flow (SLPM) measured during the control and ozone exposure experiments.**

Date	Experiment Type	Average Total Exit Flow (SLPM)	Total Exit Flow STD Dev (SLPM)	Total Exit Flow %RSD
4/8/2014	PAHs Only (Control)	1.197	0.015	1.3
4/9/2014	PAHs and FAMES (Control)	1.215	0.015	1.3
4/24/2014	PAHs Only O <sub>3</sub> Exposure	1.162	0.014	1.2
4/28/2014	PAHs and FAMES O <sub>3</sub> Exposure	1.168	0.020	1.7
5/5/2014	B20 Filter (Control)	1.196	0.023	1.9
5/7/2014	B20 Filter O <sub>3</sub> Exposure	1.218	0.017	1.4

**Table C-4 Descriptive statistics of temperature (°C) and RH (%) measured during the control and ozone exposure experiments.**

Date	Experiment Type	Average Temp (°C)	Temp STD Dev (°C)	Temp %RSD	Average RH (%)	RH STD Dev (%)	RH %RSD
4/8/2014	PAHs Only (Control)	21.3	0.6	2.9	49.5	1.9	3.9
4/9/2014	PAHs and FAMES (Control)	21.0	0.3	1.7	49.8	1.2	2.4
4/24/2014	PAHs Only O <sub>3</sub> Exposure	22.6	0.6	2.7	49.2	2.4	4.8
4/28/2014	PAHs and FAMES O <sub>3</sub> Exposure	23.8	0.2	0.7	46.9	1.4	2.9
5/5/2014	B20 Filter (Control)	22.5	0.3	1.1	50.4	1.0	2.0
5/7/2014	B20 Filter O <sub>3</sub> Exposure	21.7	1.0	4.4	50.3	3.5	7.0

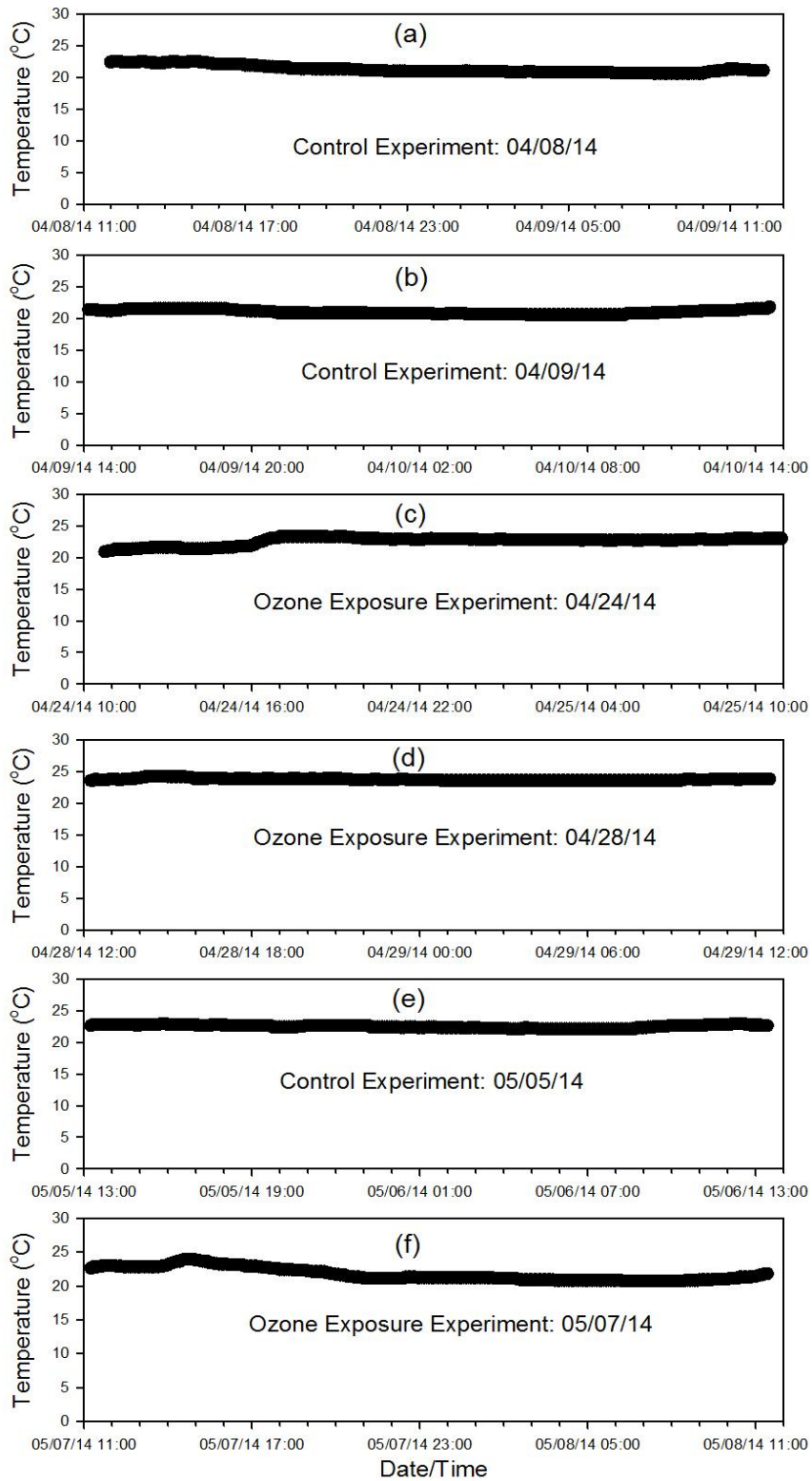


**Figure C-2** Temperatures ( $^{\circ}\text{C}$ ) measured in the ozone exposure chamber during the ozone exposure experiments and control conducted for 24 hours on (a) 04/08/14, (b) 04/09/14, (c) 04/24/14, (d) 04/28/14, (e) 05/05/14, and (f) 05/07/14.

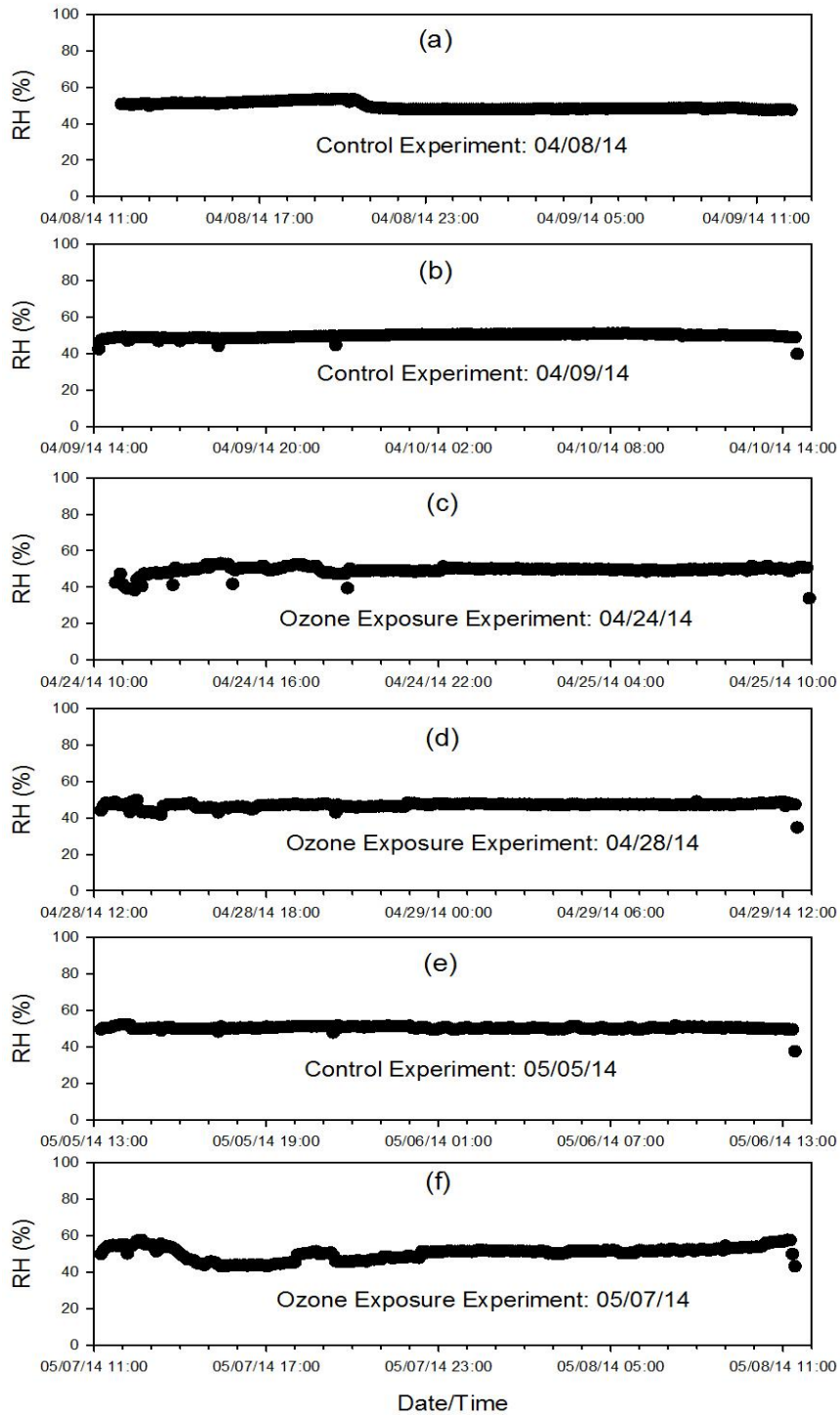


**Figure C-3 RH (%) measured in the ozone exposure chamber during the ozone exposure experiments and control conducted for 24 hours on (a) 04/08/14, (b) 04/09/14, (c) 04/24/14, (d) 04/28/14, (e) 05/05/14, and (f) 05/07/14.**

**Figures for the kinetics experiments of (PAHs), (PAHs and FAMES), and (FF291 biodiesel exhaust PM) exposed to 0.4 ppm ozone.**

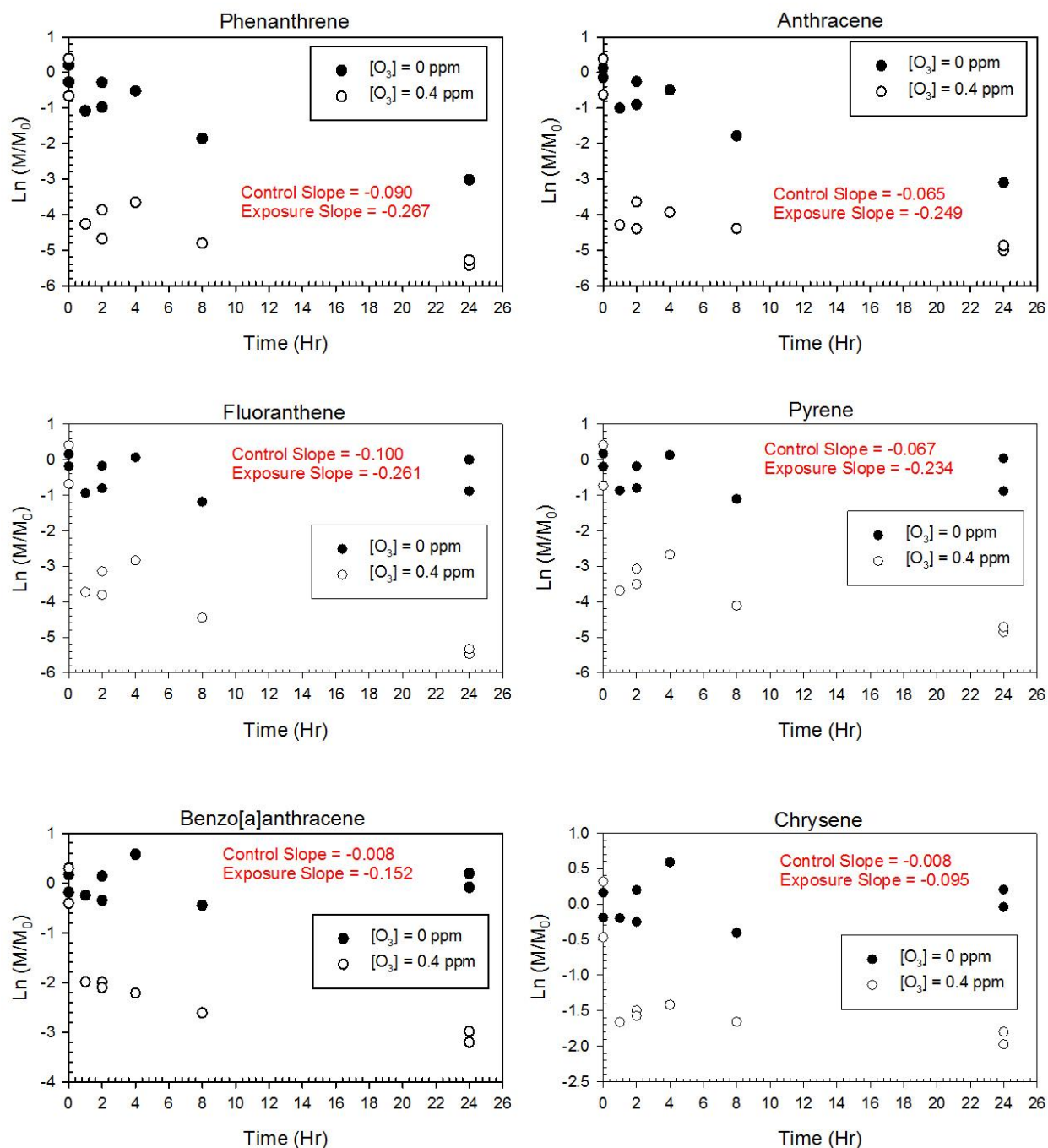


**Figure C-4(a). PAHs Only exposed to ozone. (Phenanthrene to Chrysene).**



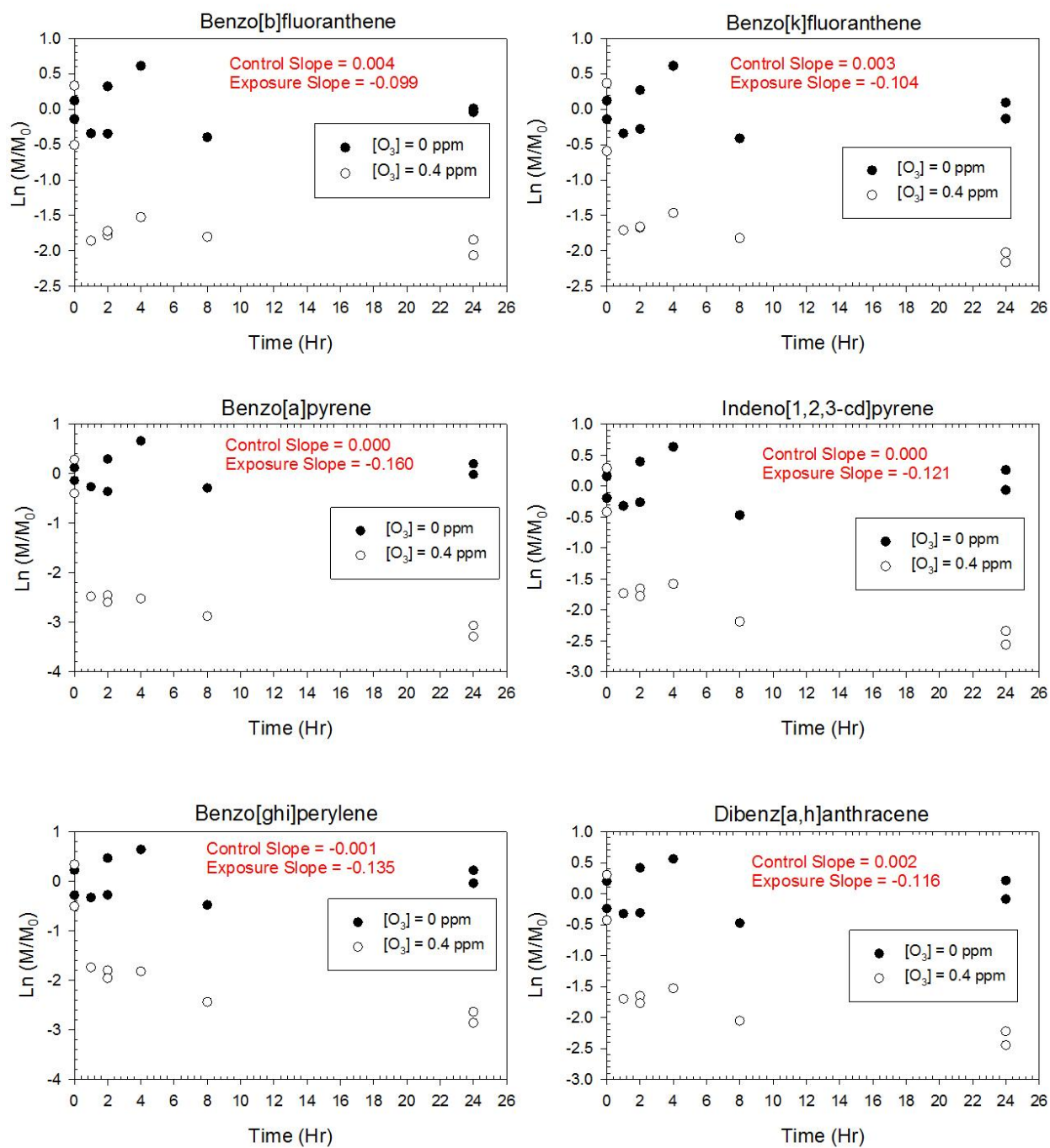


**Figure C-4(b). PAHs Only exposed to ozone. (Benzo[b]fluoranthene to Dibenz[a,h]anthracene).**

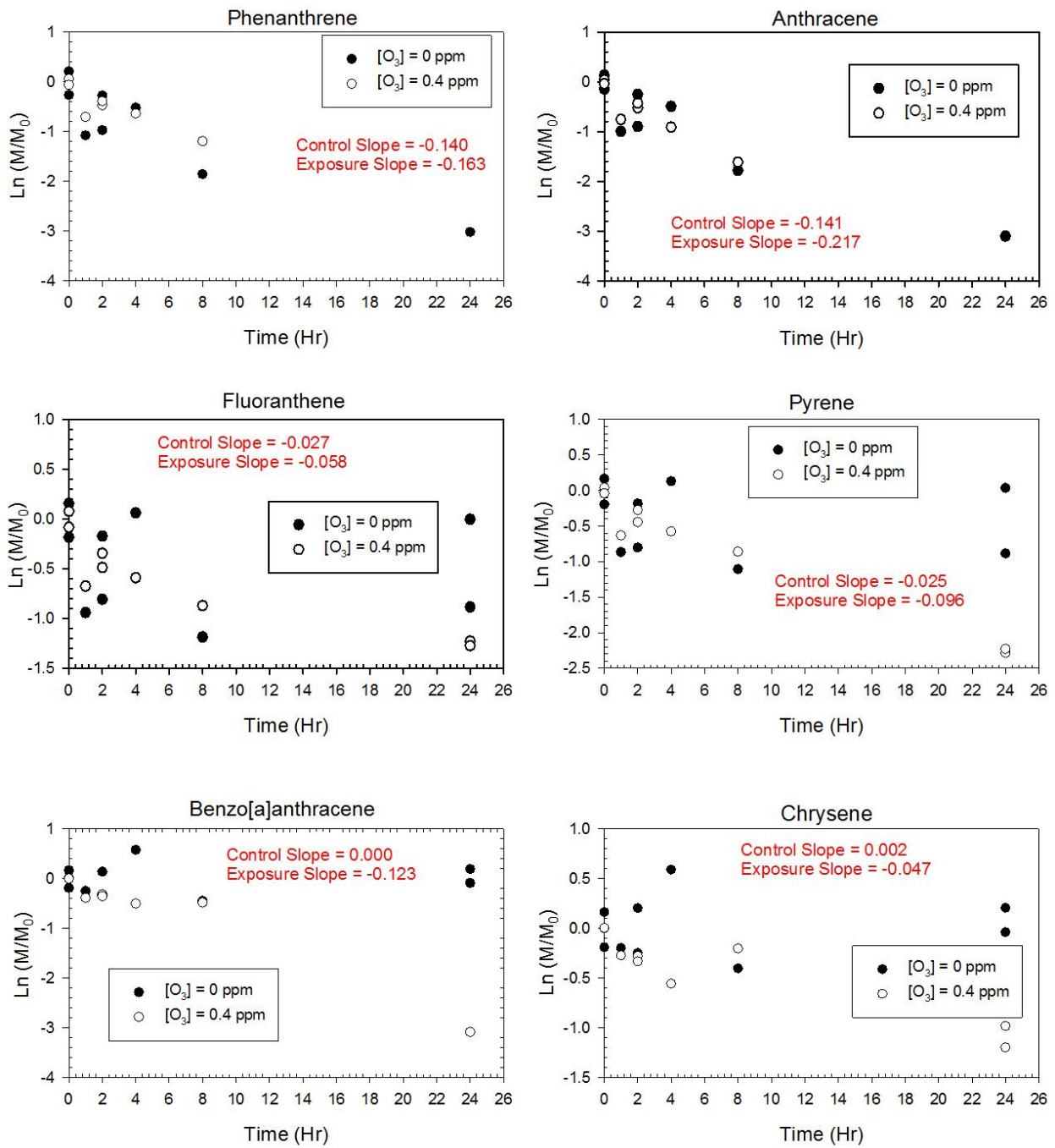


**Figure C-5(a). PAHs and FAMES exposed to ozone. (Phenanthrene to Chrysene).**

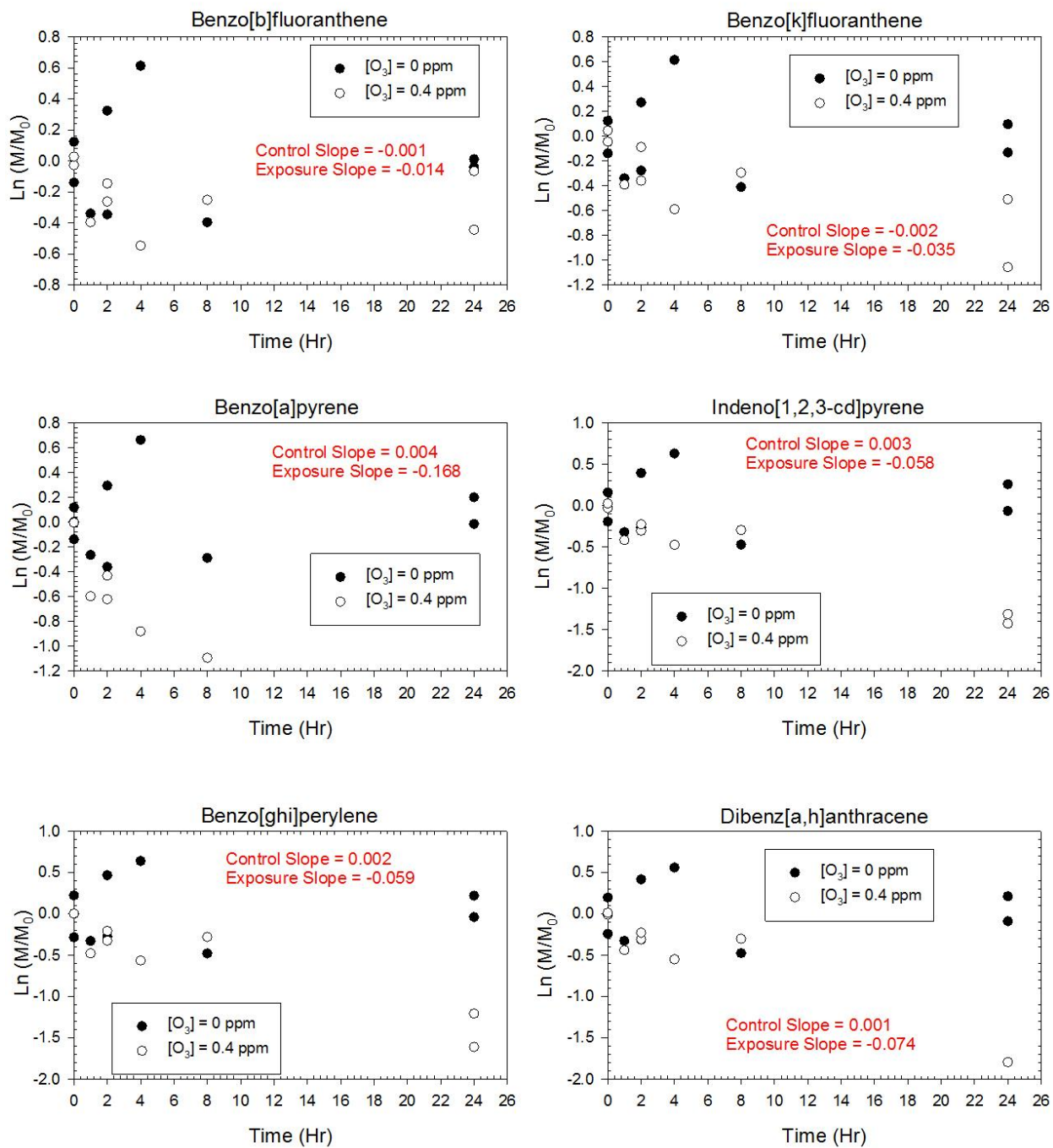


**Figure C-5(b). PAHs and FAMEs exposed to ozone. (Benzo[b]fluoranthene to Dibenz[a,h]anthracene).**

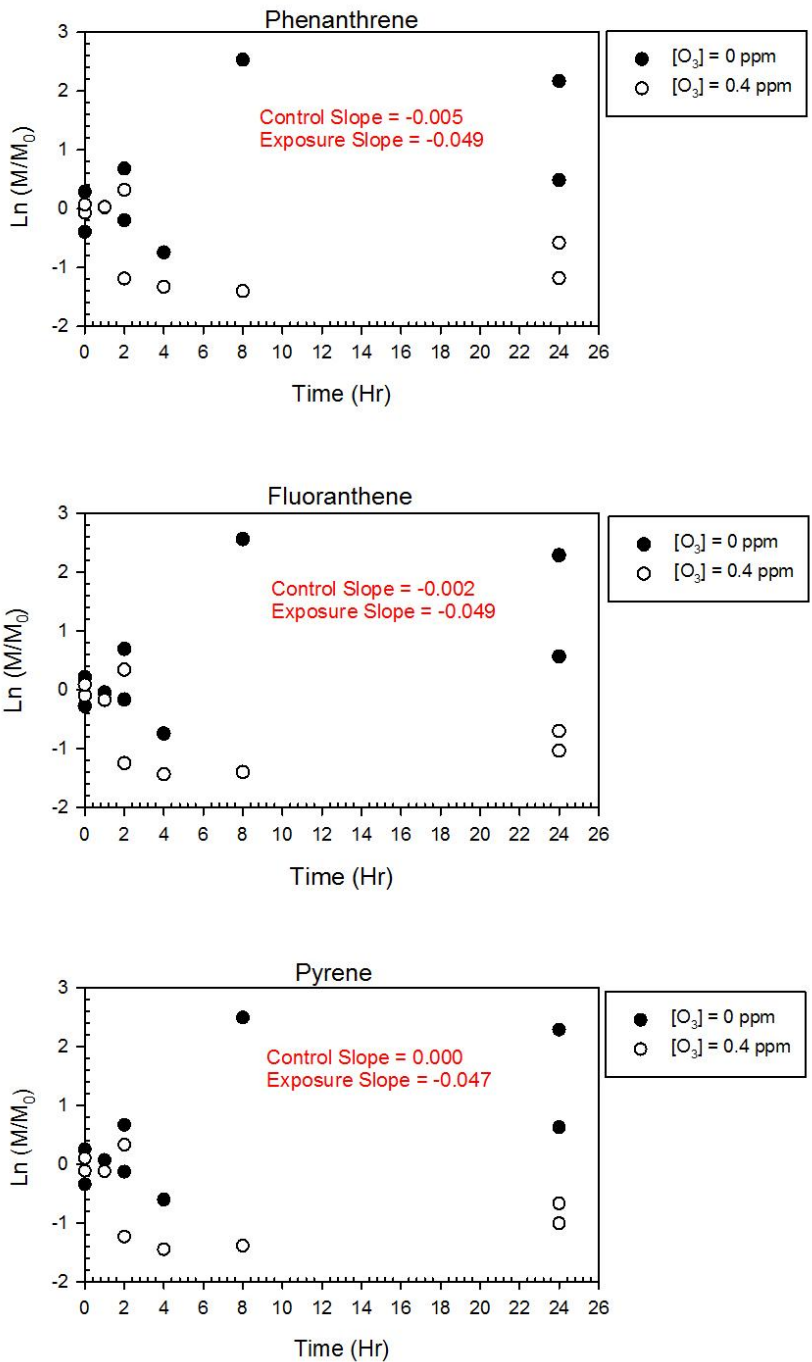


**Figure C-6. PAHs in biodiesel exhaust PM (FF 291) exposed to ozone.**

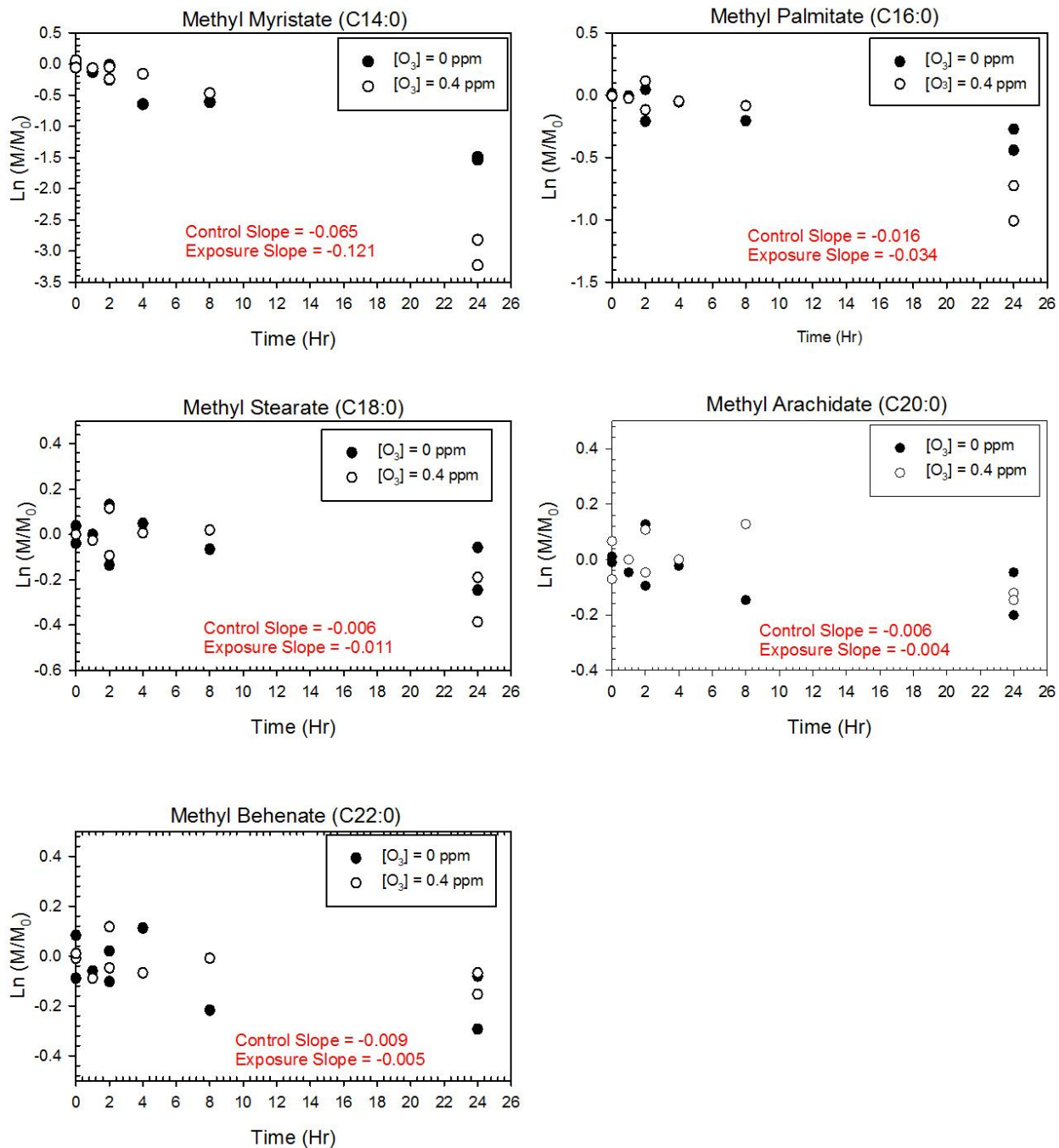


**Figure C-7(a). Saturated FAMES for the exposure of PAHs and FAMES to ozone.**

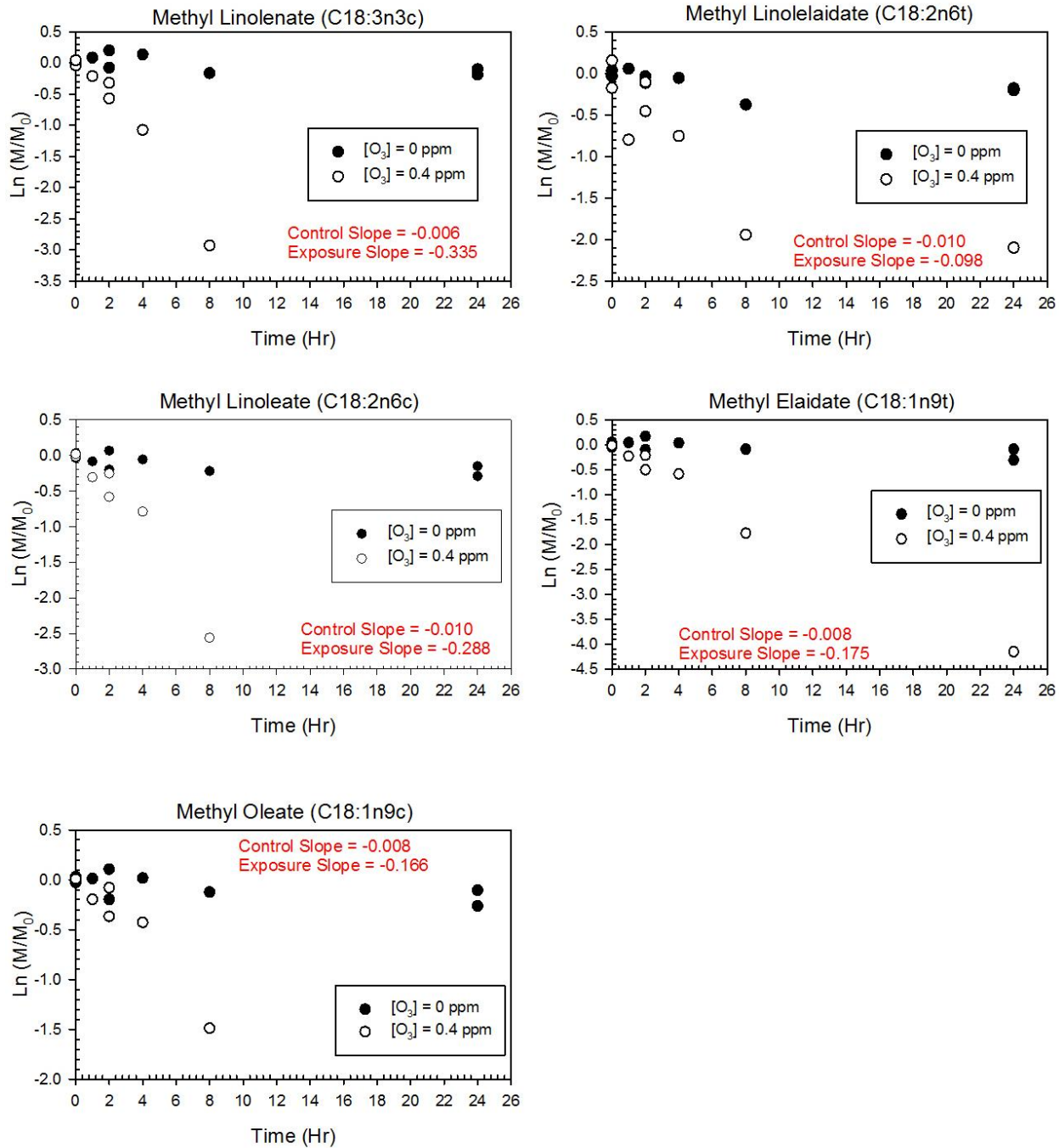


**Figure C-7(b). Unsaturated FAMES for the exposure of PAHs and FAMES to ozone.**



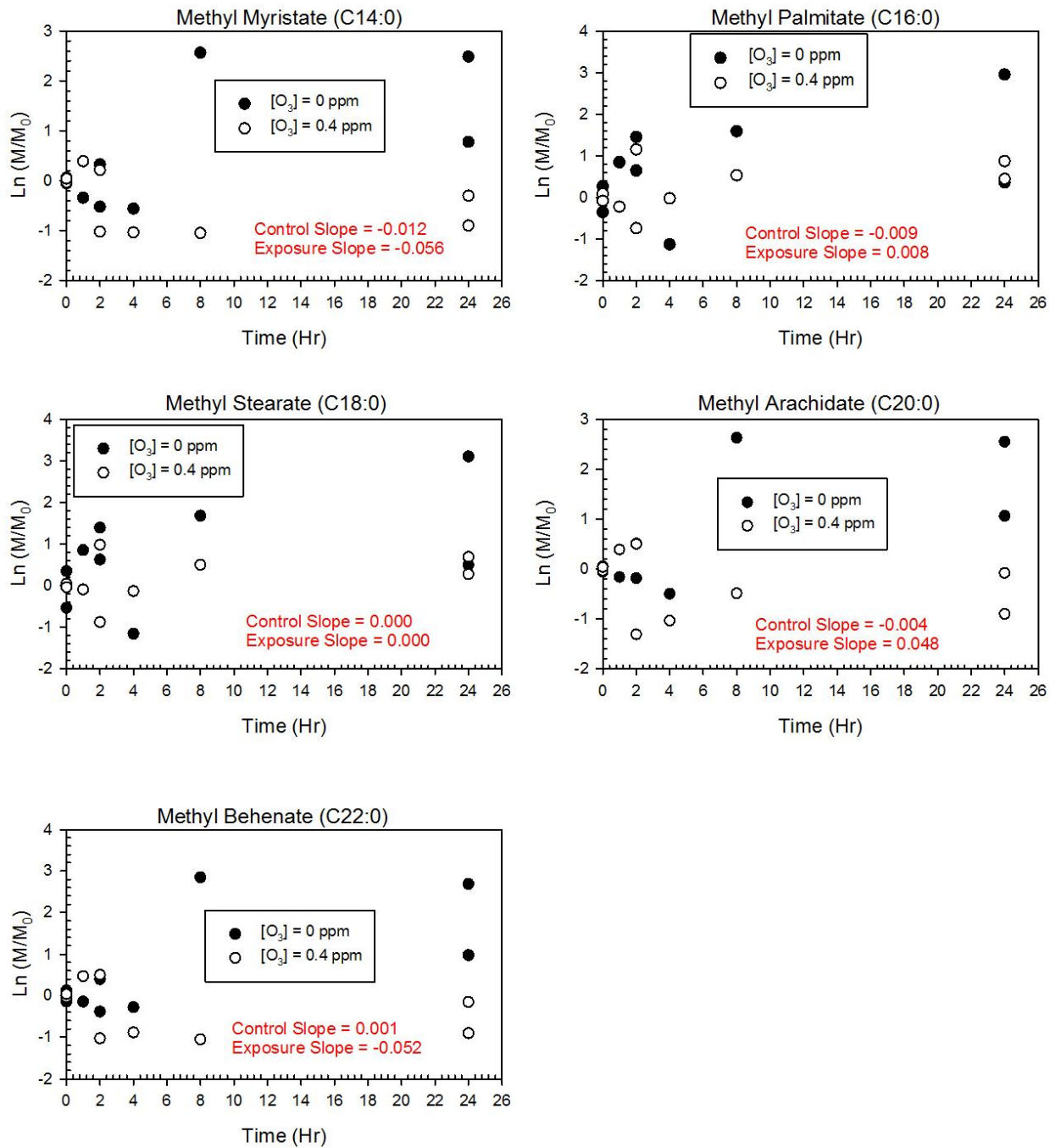


**Figure C-8(a). Saturated FAMES for the exposure of FF 291 to ozone. FAMES were corrected for %recovery based on tetracosane-d50.**

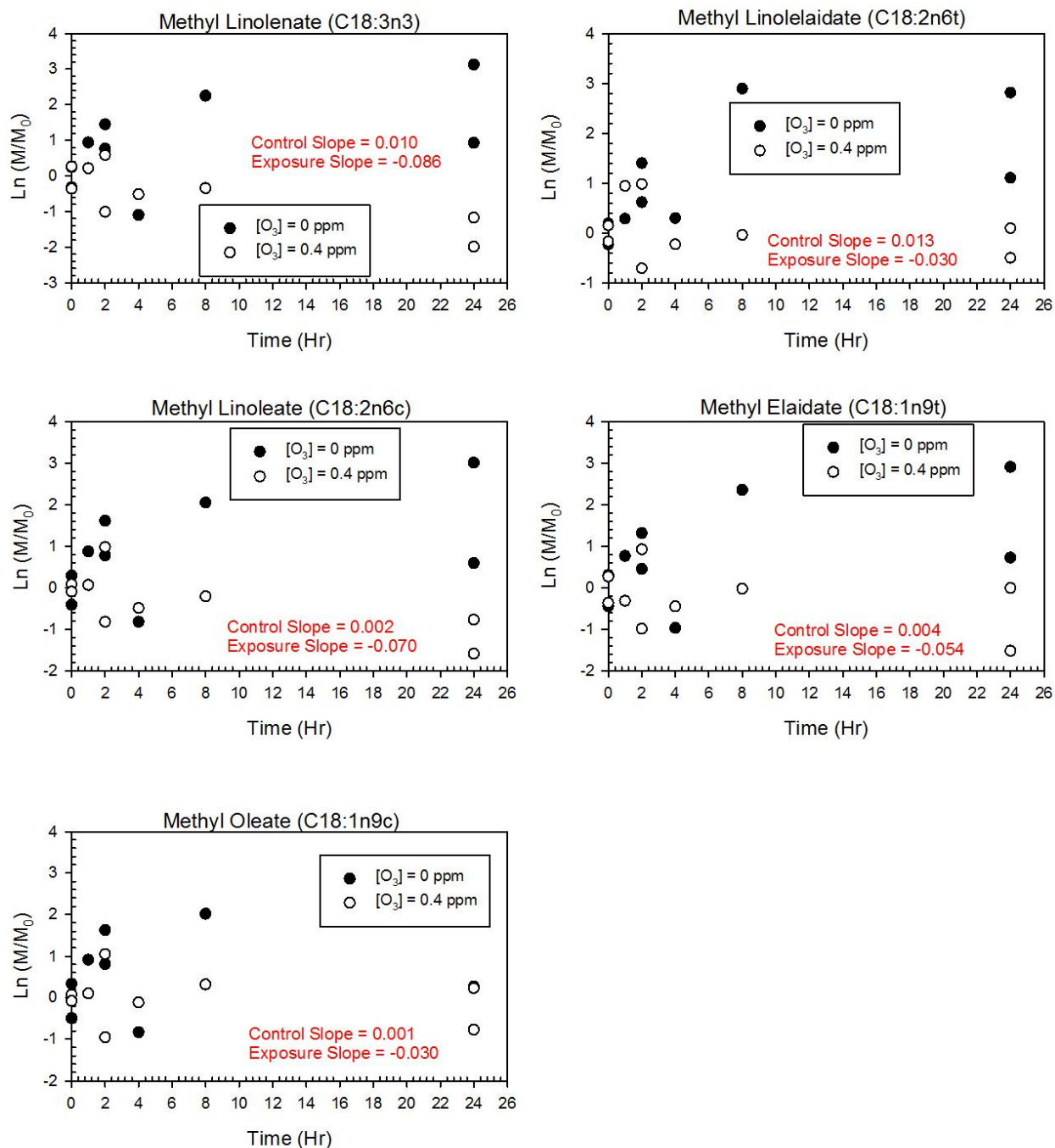


**Figure C-8(b). Unsaturated FAMES for the exposure of FF 291 to ozone. FAMES were corrected for %recovery based on tetracosane-d50.**



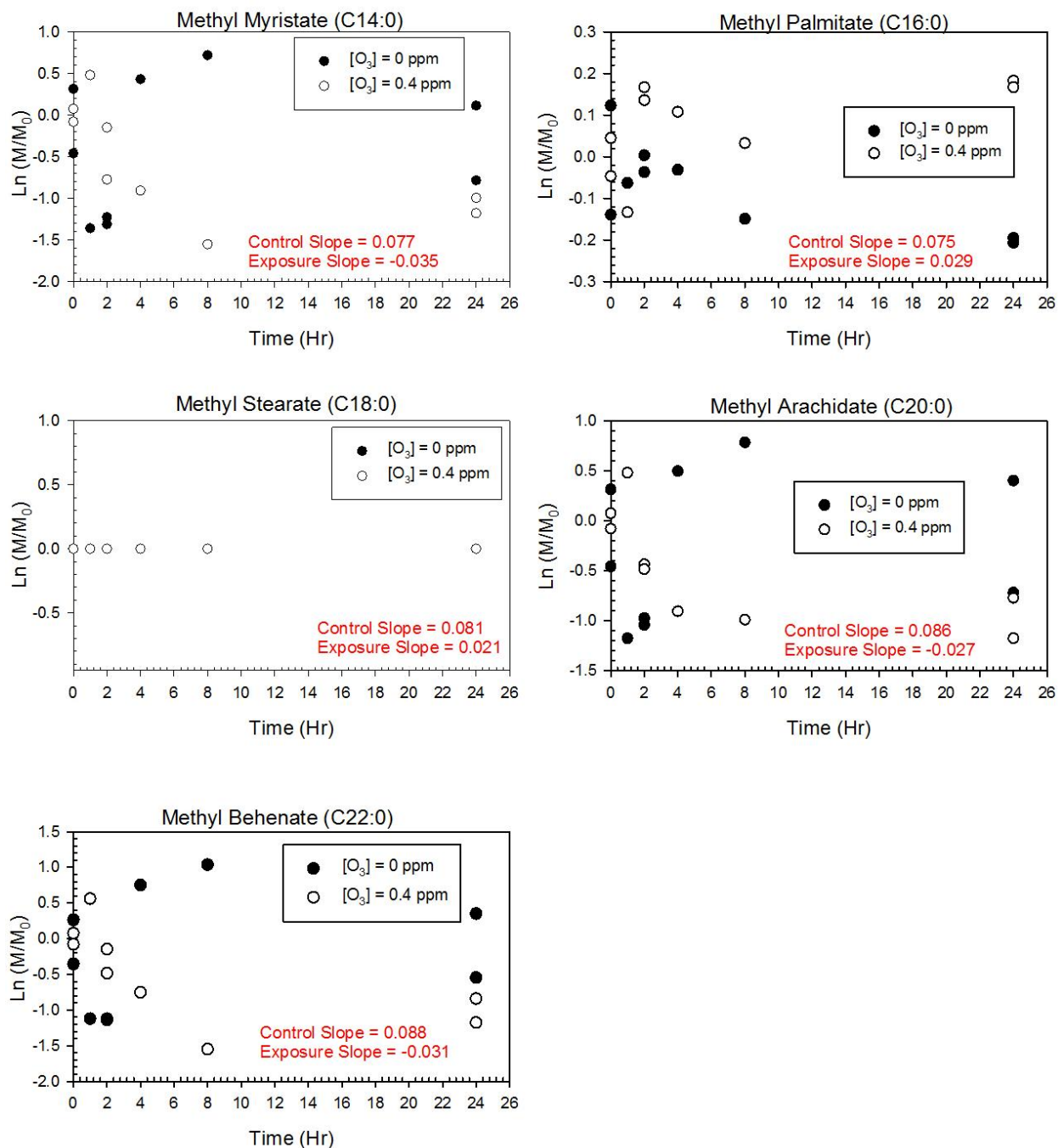


**Figure C-9(a). Saturated FAMES for the exposure of FF 291 to ozone. Mass of each FAMES was normalized to the mass of Methyl Stearate at  $t=t$ .**

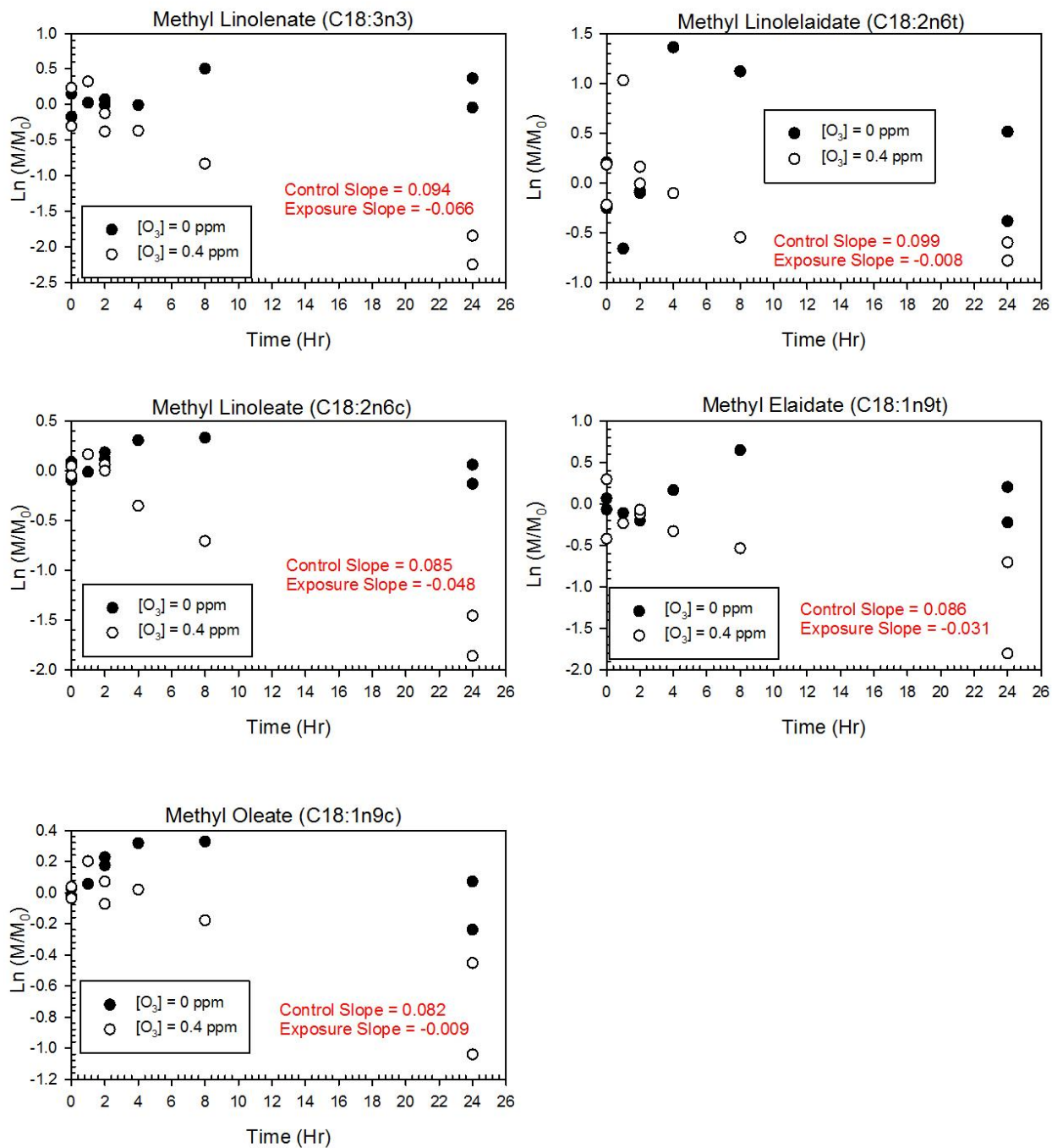


**Figure C-9(b). Unsaturated FAMES for the exposure of FF 291 to ozone. Mass of each FAMES was normalized to the mass of Methyl Stearate at t=t.**

## APPENDIX D

### **Agricultural PM<sub>10</sub> Emissions from Cotton Field Disking in Las Cruces, NM**

John Kasumba<sup>1</sup>, Britt Holmén<sup>1</sup>, April Hiscox<sup>2</sup>, Junming Wang<sup>3</sup>, David Miller<sup>4</sup>

1. School of Engineering, University of Vermont, Burlington, VT 05401
2. School of Coast and Environment, Louisiana State University, Baton Rouge, LA 7083
3. Department of Plant and Environmental Sciences, New Mexico State University, Las Cruces, NM 88003
4. Department of Natural Resources Management and Engineering, University of Connecticut, Storrs, CT 06269

#### **Abstract**

Various studies have shown a relationship between elevated levels of inhalable particulate matter (PM) and agricultural practices, especially in the vicinity of agricultural fields. Airborne particle concentrations and meteorological variables were measured during nine agricultural field events on a cotton field in Las Cruces, NM in March 2008. A variety of real-time and integrated PM<sub>10</sub> and total suspended particles (TSP) samplers were used during sampling. The field events were designed to measure particle concentrations at different heights, near (4 meter) and far (20 – 150 meters) from a disking tractor. Particle concentrations decreased with increasing distance from the ground for near-source disking events, whereas particle concentrations were almost independent of height for far-source disking and background events. Near-source disking event particle concentrations were 4 to 7 times higher than those for far-source disking and background events. Near-source disking events had emission factors ranging from 71 – 237 mg m<sup>-2</sup>, while those for far-source disking events ranged from 10 – 162 mg m<sup>-2</sup>. Plume heights for near-source disking events were between 3 – 5 m, whereas those for far-source disking events were between 6 and 8 m. Meteorological variables were found to influence emission factors, with wind speed showing a strong nonlinear relationship with emission factors. No clear relationship was found between soil moisture content and emission factors.

Key words: Air quality, Agricultural fields, Disking, PM<sub>10</sub>, Emission factors

## 1. Introduction

Agriculture has been linked to increases in particulate matter (PM) concentrations during periods of high wind speed or during agricultural land preparation activities such as disking, harvesting and tillage operations in the vicinity of agricultural fields (Clausnitzer and Singer, 1997; Kjelgaard et al. 2004; Qiu and Pattey, 2008). Most of the atmospheric dust  $>2 \mu\text{m}$  is thought to arise from agricultural activities and livestock operations and other mechanical operations (Pye, 1987). Elevated concentrations of agricultural dust are associated with a number of health and environmental problems. Inhalable particles (particles less than  $10 \mu\text{m}$  in aerodynamic diameter) are of most interest to public health because they penetrate deep into the respiratory system and cause adverse health effects. Elevated levels of  $\text{PM}_{10}$  and  $\text{PM}_{2.5}$  have previously been linked to cardiovascular and respiratory illness, hospitalization and increased mortality (Pope et al., 2002; Schwartz et al., 2003; von Klot et al., 2005).

A number of studies measuring agricultural PM emissions have reported considerable concentrations of PM due to agricultural operations. Erisman et al., 2008 reported that PM is responsible for about 20% of the agricultural field emissions in Europe. In the United States, industrialized agriculture in the Central Valley of California has been reported to contribute to the seasonal variability of the region's air quality (California Air Resources Board, 1986-1994). Some studies have quantified PM agricultural field emissions in terms of crop-specific emission factors, where PM emissions have been found to be a function of the type of crop grown e.g. (Cassel et al., 2003; Gaffney and Yu, 2003). Other studies have investigated the vertical profiles of PM ( $\text{PM}_{2.5}$ ,  $\text{PM}_{10}$  and TSP) on agricultural fields during land preparation activities, e.g. (Flocchini et al., 1994; Holmén et al., 2001(a and b)). Generally, all previous studies demonstrated the significant influence that agricultural practices have on air quality on and around agricultural fields. Thus, it is important to measure the concentrations of PM emitted from agricultural practices to better understand their effects on air quality and human health. Control techniques can then be devised in order to protect the people highly exposed to such emissions, especially personnel operating agricultural machinery and those living near the fields.

In this study, agricultural field PM emissions were measured during six disking events on a cotton field in New Mexico. Estimation of  $\text{PM}_{10}$  plume heights, fluxes, and emission factors was done for different disking events where PM sampling arrays of different designs were deployed during sampling periods ranging from 2 hours to overnight (8 hours). Particle size distributions and total particle mass concentrations emitted during near and far-source disking operations were determined. Sampling involved measurement of particle concentrations at different horizontal and vertical distances (height above ground) using a variety of instruments. The data indicate that agricultural disking operations increase  $\text{PM}_{10}$  concentrations, and that near-source disking

operations had the greatest effect on particle concentrations. Furthermore, meteorological variables were found to influence PM<sub>10</sub> emission factors.

## **2. Methods**

### *2.1 Sampling site and Samplers*

A cotton field in the New Mexico State University Leyendecker Plant Science Research Farm in Rio Grande valley south of Las Cruces (Lat. 32° 11' 50.46" N Long. 106° 44' 20.46" W Elevation 1176 m), NM was used for the disking experiments in March 2008. The cotton field, 246 m long and 100 m wide, oriented with its long axis about 135 degrees clockwise from true N. The soil type is an Armijo clay loam, and Harkey loam (USDA, 2005). Concentrations of particles and meteorological parameters were measured using a variety of sampling instruments during nine sampling events (Table 1) located at heights above ground from 0.5 – 9 meters. Two sonic anemometers, (MOI model 50.5) were used for measuring meteorological variables such as temperature, wind speed and wind direction. The sonic anemometers were located at the southern edge of the field, one at 1.34 m and the other at 8 m from the ground.

The micro-orifice uniform deposit impactor (MOUDI) had cut diameters at 0.056, 0.1, 0.18, 0.32, 0.56, 1, 1.8, 3.2, 5.6, 10, and 18µm (inlet). Some of the samplers were positioned on a tractor-mounted platform that maintained a constant position, about three rows (4 meters) downwind from each operational pass across the field during near-source sampling events. At the same time, the MetOne samplers were positioned on vertical arrays on portable towers above the field at the upwind and downwind edges of the field. The distance between the disking tractor and the tractor-mounted platform with samplers varied between 20 meters and 150 meters for the far-source disking events. During the far-source disking events, the disking tractor started disking far from the tractor-mounted platform with samplers, and got closer to it with the subsequent passes. Plume heights were estimated using PM<sub>10</sub> data measured by the DustTrak samplers (as outlined below).

**Table 1. Field particle instruments deployed during sampling events 1 to 9.**

<b>Instrument</b>	<b>Methodology</b>	<b>Sampling Resolution</b>	<b>Units</b>	<b>Type of PM</b>	<b>Events Instrument Sampled</b>
MOUDI, (MSP model 100)	Cascade impactor	Event integrated duration	$\mu\text{g}/\text{m}^3$	Size-resolved (0.056-18) $\mu\text{m}$	1, 2, 4, 5, 6
MetOne, (MOI model ES-640)	Light Scattering	1 Minute	$\text{mg}/\text{m}^3$	2 measured $\text{PM}_{10}$ while 1 measured TSP	1, 2, 3, 4, 5, 6, 7
DustTrak, (TSI model 8520)	Light Scattering	1 Second	$\text{mg}/\text{m}^3$	All 4 instruments measured $\text{PM}_{10}$	1, 2, 3, 4, 5, 6, 7

## 2.2 Sampling events

PM sampling events were classified into 3 types: Background, near-source, and far-source disking. A total of 4 background events (Events 1, 7, 8, and 9) occurred where the disking tractor was not operating, and PM samples were collected on vertical arrays located on the south edge of the field. Event 1 was prior to application of pre-emergence herbicides, prometryn and trifluralin. The rest of the events occurred after herbicide application. Events 7 and 9 were nighttime sampling events, and were 8 and 40 days after herbicide application, respectively. Event 8 was a daytime sampling event and it occurred 38 days after herbicide application. Furthermore, Events 8 and 9 were sampled with Filter/PUF samplers only. Events 2, 3, and 4 were near-source disking events, while Events 5 and 6 were far-source disking events. Disking events lasted about 2-3 hours, while background events lasted about 8-10 hours. It is important to note that samplers were positioned at different heights during the various sampling events as shown in Table 2. The reason for positioning the DustTrak and the filter/PUF samplers at different heights during each event was to characterize the plumes as best as possible.

In order to determine soil moisture, surface soil samples (upper 10 cm) were collected from at least four locations on the field during each sampling event. Soil moisture was then determined by the gravimetric method after Gardner (1986).

**Table 2. Summary of the sampler heights (meters) from the ground during sampling.**

Event	Date and Time of Event	DustTrak	MetOne
<b>Event 1:</b> Daytime Background/ pre-herbicide	03/08/08	0(Ground) 0(Ground)	1.5(NE)
	10:30-18:30	4.8(NE), 8.8(SW)	1(SE)
			1(SW)
<b>Event 2:</b> Pre-herbicide/ near-source disking	03/11/08	0(Ground), 1.5(PT)	1.5(NE), 1(PT)
	11:50-13:42	2.15(PT), 4.15(PT)	1(SW)
<b>Event 3:</b> Post-herbicide/ near-source disking	03/12/08	0.5(PT), 1.66(PT)	1.5(NE), 1(PT)
	13:47-15:19	2.15(PT), 4.15(PT)	1(SW)
<b>Event 4:</b> Post-herbicide/ near-source disking	03/13/08	0.5(PT), 1.66(PT)	1.5(NE), 1(PT)
	13:09-14:31	2.15(PT), 4.15(PT)	1(SW)
<b>Event 5:</b> Post-herbicide/ far-source disking	03/17/08	0.43(PT), 1.33(PT)	1.5(NE), 1(PT)
	13:01-14:31	4.61(PT), 6.5(PT)	1(SW)
<b>Event 6:</b> Post-herbicide/ far-source disking	03/19/08	0.62(PT), 2.2(PT)	1.5(NE), 1(PT)
	11:42-12:12	4.16(PT), 9(PT)	1(SW)
<b>Event 7:</b> Nighttime Background Post-herbicide	19:00 (03/19/08)	0.62(PT), 2.2(PT)	1.5(NE), 1(PT)
	07:00 (03/20/08)	4.16(PT), 9(PT)	1(SW)
<b>Event 8:</b> Daytime Background Post-herbicide	04/18/08	DustTraks	MetOnes
	08:33-20:30	Not Used	Not Used
<b>Event 9:</b> Nighttime Background Post-herbicide	20:10 (04/20/08)	DustTraks	MetOnes
	08:20 (04/21/08)	Not Used	Not Used

The relative locations of the samplers on the field are shown in parentheses; NE, SE, and SW mean northeast, southeast, and southwest corners of field. PT means tractor-mounted platform with array of samplers. The MOUDI and PQ200 were always positioned on the tractor-mounted platform, 1.5 m from the ground.

### 2.3 Emission factor calculations

Agricultural PM emission factors for operations like disking, tilling and harvesting are usually calculated on the basis of land worked because the source being quantified is the field where the operation takes place, not the moving tractor/implement (Holmén et al., 2001b). In this study, vertical profiles of wind speed and DustTrak PM<sub>10</sub> concentrations were used to calculate PM<sub>10</sub> fluxes and emission factors for the disking operations. Plume heights were estimated by the polynomial extrapolation of height-concentration plots to define plume height H, as the height above the ground surface where PM<sub>10</sub> concentration, C, was not distinguished from background (or C → 0). A polynomial particle concentration profile model was then used to fit the measured vertical PM<sub>10</sub> concentration profiles, C(h), and the log wind law (Equation 1) was used for wind speed profiles, U(h):

$$u_h = \frac{u^*}{K_1} \ln\left(\frac{h}{z_o}\right) \quad \text{Eq (1)}$$

where  $u^*$  is the friction velocity,  $u_h$  is the wind speed at height  $h$ ,  $K_1$  is the von Karman constant (0.4),  $h$  is the distance from the ground, and  $z_o$  is the roughness length.

$$\text{Emission Factor (mg m}^{-2}\text{)} = \int_{z_o}^H \frac{C(h)U(h)t}{w} dh \quad \text{Eq (2)}$$

Emission factors were calculated as the integrated particle flux,  $C(h) \times U(h)$  normalized to the field width worked, and the duration of the event (Equation 2).

where  $C(h)$  is the PM<sub>10</sub> concentration at height  $h$ ,  $U(h)$  is the component of wind speed perpendicular to the long axis of the field,  $t$  is the time of the test,  $w$  is the average fractional width of soil worked during the test period.  $w$  was computed from the field width (W), total number of tractor passes, and DustTrak peak widths and observed tractor start-stop times per tractor pass.

The uncertainties in the calculated emission factors, plume heights and particle fluxes were estimated using propagation of error techniques (Coleman and Steele, 1989).



Emission factors and plume heights were estimated for disking events only. Particle and meteorological data were screened and only those data that were realistic were used for the analyses. Wind direction changed during Event 6, and therefore, samplers were moved to opposite end of field. Therefore, this event was subdivided into two sub-events, i.e., Event 6A - measurements made before the change in wind direction, while Event 6B represents measurements made after the change in wind direction.

### 3. Results and Discussion

#### 3.1 Event particle size distributions

Figure 1 shows the MOUDI particle size distributions measured during sampling events 1, 2, 4, 5, and 6. It can be observed in Figure 1 that most of the particle mass was contributed by particles with diameters greater than 1  $\mu\text{m}$ . Particles less than 1  $\mu\text{m}$  generally contributed between 10 and 40% to the total particle mass concentrations for all the events in which the MOUDI was used. This is consistent with previous studies; for example Tuch et al., 1997 observed that the contribution of small particles to the total mass was almost negligible for ambient air sampled in an urban area. Because the MOUDI did not have a stage at 2.5  $\mu\text{m}$  cut-point diameter, it was not possible to quantify the contribution of  $\text{PM}_{2.5}$  particles to the  $\text{PM}_{18}$  measured by the MOUDI. The contribution of  $\text{PM}_{10}$  particles to the  $\text{PM}_{18}$  ranged between 76 and 90%.

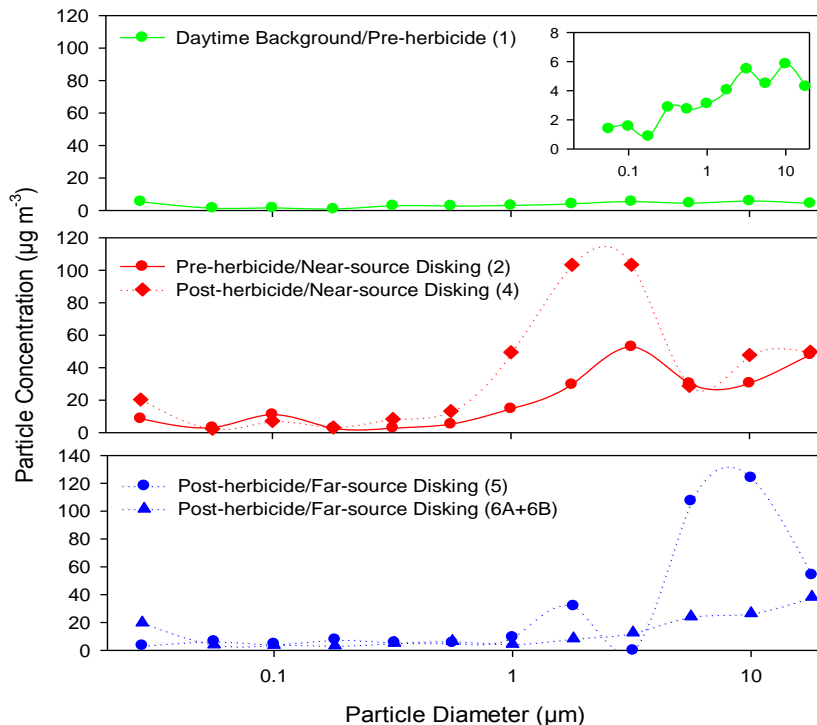


**Figure 1. Particle size distributions measured by the MOUDI (at 1.5 m from the ground) during five sampling events (indicated by number in parenthesis).**

*3.2 Particle concentration variations with height*

The DustTrak data were used to study the variations in particle concentration with respect to height above the ground. Particle concentrations did not vary significantly with height for background and far-source disking events except for Event 5 (Figure 2). This observation suggests that the concentration of particles is independent of height in the absence of a particle source, or when a receptor is far from the source. The exceptional behavior of Event 5 could be linked to an unstable atmosphere or variations in wind speed during that event, but this explanation has not been confirmed. Conversely, the high particle concentrations observed for event number 5 could be due to interference from emissions on the neighboring fields. It is noteworthy that this anomaly was also observed in the MOUDI size distribution data for event number 5 (Figure 1) where particle concentrations for particles larger than 1  $\mu\text{m}$  were about 3 times greater than those for event number 6. It is also important to note that for Event 5, data for three DustTrak samplers were used to obtain the vertical profile for this event (Figure 2). The reason was because the DustTrak at 4 m height was not functioning during the period of the event.

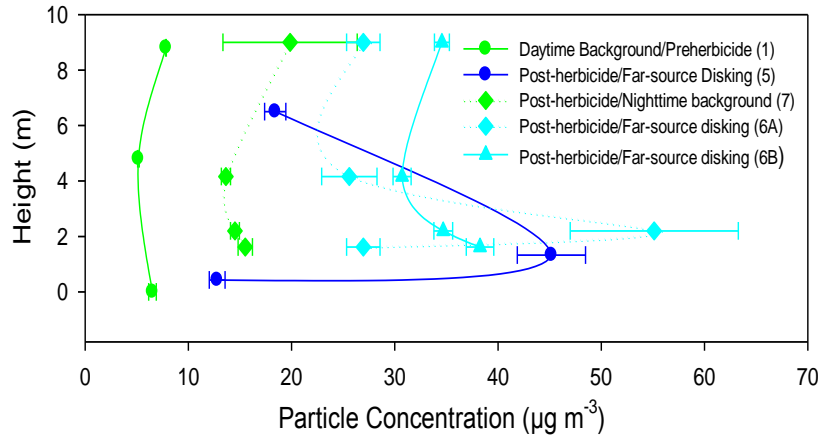


**Figure 2. Height vs average particle mass concentration for the DustTraks for the background and far-source disking events. Error bars represent standard error. Note that the mass concentrations (x-axis) were very low for these events.**

Particle mass concentrations decreased with increasing sampler height for near-source disking events (Figure 3). This is expected for a ground level source (disking

tractor). This observation could also be due to wind speed changes with height. Because wind speed and turbulence increase with height from the ground, particles far from the ground are expected to be dispersed more than those near the ground. Near-source disking event particle concentrations (Figure 3) were 4 to 7 times higher than those for far-source disking and background events (Figure 2).

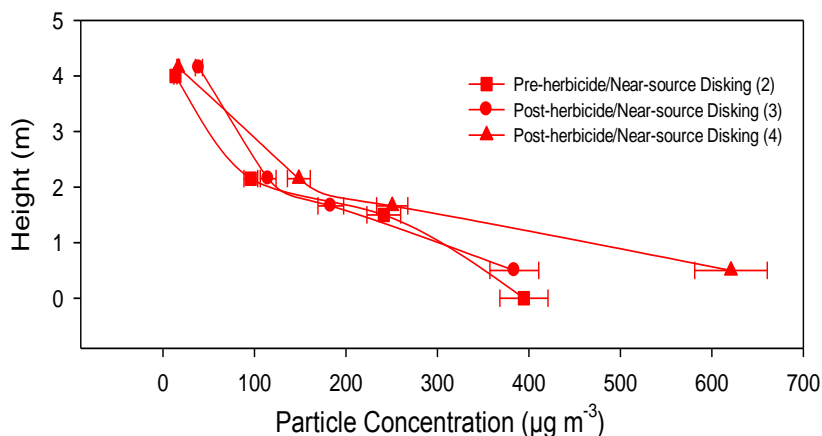


**Figure 3. Height vs average particle mass concentration for the DustTraks during near-source disking events. Error bars represent standard error.**

### 3.3 Particle concentration variations with horizontal distance

Particle concentrations decreased with increasing horizontal distance from the disking tractor (Figure 4) as expected. The MetOne sampler mounted on a trailer located near the disking tractor measured higher particle concentrations during the disking events (especially near-source disking events) than the MetOne samplers positioned upwind and downwind of the disking tractor. For background events (Events 1 and 7), the effect of uniform particle dispersion in the absence of a source was observed in Figure 4 as all three MetOne samplers measured similar concentrations. Ideally, we would expect the downwind sampler to measure higher particle concentrations than the upwind sampler during the far-source and near-source disking events, but this was not observed as can be seen in Figure 4. However, Wang et al., 2007 observed that wind speed and downwind distance of the samplers from the source affect the collection efficiency of agricultural PM<sub>10</sub> by EPA-approved PM<sub>10</sub> samplers. This is mainly due to the gravitational settling of larger particles before they are sampled. The same reasoning could explain the observation made in this study, where the downwind concentrations of TSP were almost similar to the upwind PM<sub>10</sub> concentrations for the far-source disking events as observed in Figure 4.

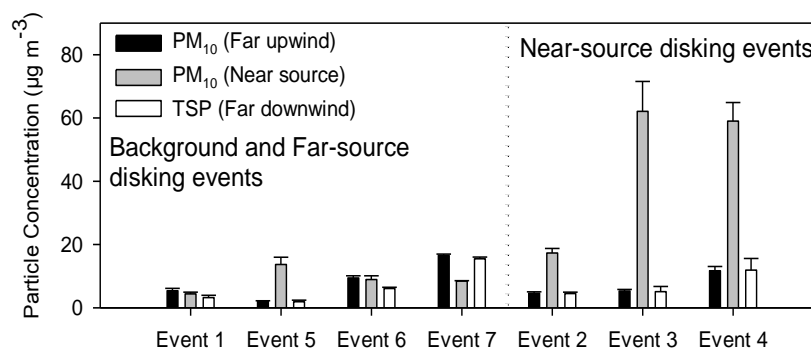


**Figure 4. Average particle mass concentrations measured by the MetOne samplers during all events. Error bars represent standard error.**

### 3.4 Plume Heights

Plume heights appeared to be greater for the far-source disking events than for the near-source disking events (Table 3). This observation is expected for a plume dispersing from a ground source. Essentially, samplers near the source are not able to fully characterize the plume as effectively as samplers farther from the plume. Height-particle flux plots showed that there was no direct relationship observed between plume height and temperature. We would expect plume height to increase with increasing temperature because as temperature increases, particle resuspension increases and this leads to an increase in plume heights. No obvious relationship was found between wind speed and plume heights. Plume heights would be expected to decrease with increasing wind speed because the wind blows away the particles horizontally as soon as they are emitted. This hinders the particles from rising far up into the atmosphere.

### 3.5 Emission Factors

Unlike plume heights, the PM<sub>10</sub> emission factors were observed to be greater for near-source disking events than for far-source disking events (Table 3) with the exception of Event 5. This was expected because samplers near the particle source should capture more particles than samplers farther away from the source. Because of dispersion, samplers far from the source are exposed to fewer particles than samplers near the source. The exceptional behavior of event five was observed in other measurements such as the MOUDI and MetOne measurements (see Figures 1 and 4). The PM<sub>10</sub> emission factors obtained in this study are in agreement with those reported in previous studies: Holmén et al. (2001a) reported emission factors ranging from zero to 800 mg m<sup>-2</sup> for different operations including disking; Qiu and Pattey (2008) estimated an average PM<sub>10</sub> emission factor of 74 mg m<sup>-2</sup> for a harvesting operation on a wheat field in Canada; Bogman et al. (2005) predicted PM<sub>10</sub> emission factors ranging from 150 to 230 mg m<sup>-2</sup> for agricultural tillage and harvesting operations in Flanders, Belgium.

**Table 3. Estimated plume heights, emission factors, and meteorological variables for the different events. Values in parentheses represent uncertainties.**

Event	Plume Height (m)	Emission Factor (mg/m <sup>2</sup> )	Mean Wind Speed (m/s)	Mean Wind Direction (deg)	Wind Direction Standard Dev (deg)	Mean Temp (°C)	Average Soil Moisture (%)
Event # 2, Near-source disking (Pre-herbicide)	3.1 (2.2)	163.5 (116.0)	3.71	78.2	22.5	19.0	1.49
Event # 3, Near-source disking (Post-herbicide)	4.5 (5.0)	71.1 (78.8)	2.04	113.2	151.3	18.9	1.16
Event # 4, Near-source disking (Post-herbicide)	4.0 (5.5)	237.1 (326.2)	5.48	2.0	14.7	23.0	2.47
Event # 5, Far-source disking (Post-herbicide)	7.6 (6.3)	162.3 (133.9)	4.53	31.4	73.7	11.5	1.76
Event # 6A, Far-source disking (Post-herbicide)	5.9 (6.2)	9.9 (10.5)	2.10	204.4	46.5	15.2	2.34
Event # 6B, Far-source disking (Post-herbicide)	5.9 (3.6)	17.4 (10.7)	1.81	168.5	78.9	17.1	2.34

No obvious relationship was observed between emission factors and plume heights, while it appears that emission factors increased with ambient air temperature. For example, Event 4 had the highest temperature (23 °C), and at the same time the highest emission factor (237 mg m<sup>-2</sup>); Events 2 and 3, also near-source disking events like Event 4, had lower temperatures (~ 19 °C) than event four, and therefore their corresponding emission factors were lower than that for event 4. The effect of temperature on emission factors is not well-manifested for the far-source disking events because of the behavior of Event 5. It is, however, observed that the average temperature for event 6B was greater than that for 6A, and as expected, the emission factor for event

6B was greater than that for event 6A. Clausnitzer and Singer (2000) observed that the measured respirable dust (or PM<sub>4</sub>, particles with aerodynamic diameter less than 4 μm) concentrations for cultivation operations increased with increasing ambient temperature. The increase in respirable dust as air temperature increased was attributed to the increasingly unstable atmospheric conditions near the ground that helped to loft detached soil particles into the atmosphere.

Wind direction also influenced the PM<sub>10</sub> measurements, and hence the emission factors. During Event 3, high variability in wind direction (wind frequently changed directions as indicated by high standard deviation, SD = 151 degrees, Table 3) is believed to have affected the PM<sub>10</sub> emission factors. The emission factor for Event 3 was lower than those for the other two near-source disking events where little variability in wind direction occurred (Events 2 and 4, see Table 3).

It was generally observed that emission factors increased with wind speed (Figure 5). Although near-source disking events were different from far-source disking events, it can be clearly observed in Figure 5 that the emission factor increased with wind speed irrespective of the type of event. A logarithmic fit was found to best describe the relationship between emission factors and wind speed, with an  $r^2$  value of 0.922. This kind of relationship between emission factors and wind speed is expected because more particles are expected to be resuspended from the ground as wind speed increases for a dry type of soil. Kjelgaard et al (2004) observed that particle concentrations from the Columbia Plateau region increased during periods of high wind speeds. The predominant type of soil in the Columbia Plateau was Ritzville silt loam, a mixture of loess, volcanic ash particles, and very low (<1%) organic matter.

There was no obvious relationship observed between soil moisture and emission factors. Under normal circumstances, emission factors are expected to decrease with increasing soil moisture. In this study, there were no significant variations in soil moisture during the different sampling events. Soil moisture values ranged between 1.49 and 2.47%, mainly because the disking events number 2 to 6 were conducted the same season of the year, just a few days apart. The very narrow range of soil moisture does not allow the observation of any significant effects of soil moisture on emission factors in this study. The dependence of emission factors on soil moisture could also be due to the soil type, whereby certain soil types will most likely exhibit relationships between soil moisture and emission factors, while others will not. Clausnitzer and Singer (2000) observed that for tillage operations, the concentrations of PM<sub>4</sub> decreased as a power function as soil water content increased between 2 and 14%. They attributed this relationship to the increased cohesion between the adsorbed water films surrounding the soil particles, the increased adhesion between water molecules and soil surfaces, and the added weight of the soil particles as soil water content increased.

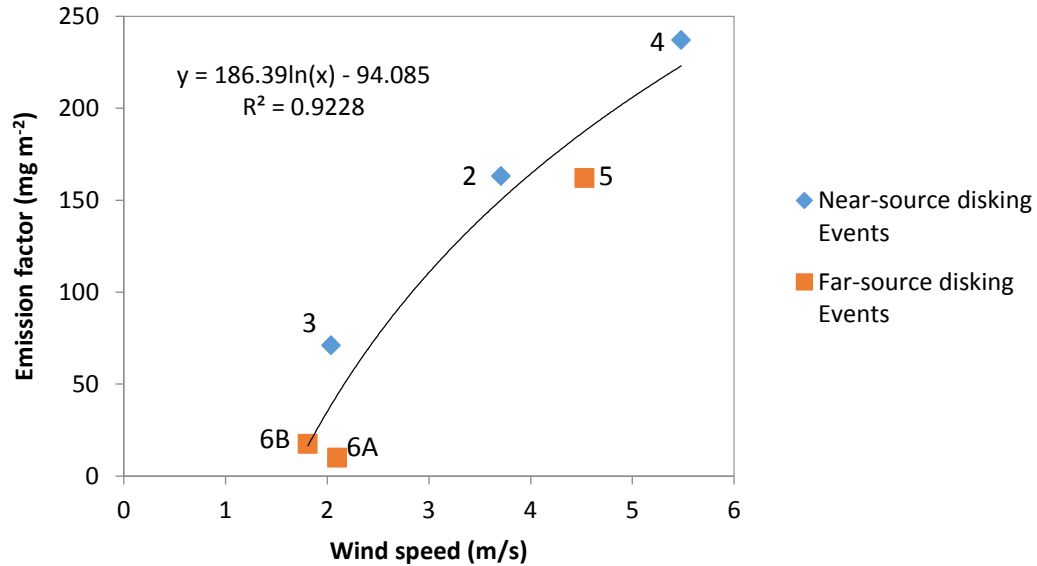


**Figure 5. Emission factor variations with changes in wind speed for six events. Symbol shows type of event, Numbers indicate Event number. Line is best fit.**

#### 4 Conclusions

This study has demonstrated the influence of agricultural disking operations on the PM<sub>10</sub> concentrations and emission factors on an agricultural field. As expected, near-source disking events had higher emission factors than far-source disking events. Emission factors for near-source disking events ranged from 71 – 237 mg m<sup>-2</sup>, while those for far-source disking events ranged from 10 – 162 mg m<sup>-2</sup>. Although event number five was a far-source disking event, it had an unexpectedly high emission factor. This abnormal behavior of event number five was partly attributed to particle sources outside the boundaries of the sampling field. Near-source disking events were responsible for the observed high particle concentrations because the particle concentrations for such events were about 4 – 7 times higher than those for the background and far-source disking events. Vertical particle concentration profiles showed that the concentrations of PM<sub>10</sub> decreased with increasing height for near-source disking events, whereas particle concentrations did not significantly change with height for background and far-source disking events.

Meteorological variables were found to influence emission factors during the disking events. A strong nonlinear relationship was found between emission factors and wind speed. Wind direction was also found to affect the emission factors. For example, Event 3 was a near-source disking event but because of the multiple changes in wind direction during this event, its emission factor was relatively lower than the other near-source disking events that had stable wind directions. Ambient temperature was also

found to affect emission factors because emission factors increased with increasing ambient air temperature.

Although previous studies have shown a relationship between emission factors and soil moisture content, no significant relationship was observed between soil moisture and emission factors in this study because only narrow soil moisture range was sampled.

Far-source disking events had higher plume heights than near-source disking events. No clear relationship was observed between plume height and meteorological variables.

According to the results of this study, more research needs to be done in order to better understand the effects of agricultural operations on air quality and human health. The emissions from agricultural fields can directly affect the people operating agricultural machinery and people living near agricultural fields. Therefore, exposure studies on agricultural fields need to be performed in order to quantify the exact effects of agricultural PM emissions on human health. Understanding the exposure effects of agricultural emissions can lead to development of better agricultural operations. Furthermore, the duration of elevated concentrations of PM can be may as well be studied. The duration of exposure can be correlated with the duration of elevated peak concentrations. All this can lead to regulation of agricultural field emissions, and hence reduced exposure.

It is also important to note that the equation used to estimate emission factors in this study does not incorporate some of the factors believed to influence emission factors on agricultural fields. An equation including meteorological variables like temperature and probably relative humidity may possibly give a better estimate of emission factors over a wider range of field conditions than studied here. Soil variables such as soil moisture content and silt content would also need to be incorporated into the emission factor equation for better estimates. The agricultural implement characteristics would as well be important in the emission factor determination.

### **Acknowledgements**

This work was supported by the United States Department of Agriculture (USDA) under contract 023199. The authors also wish to express their gratitude to Anna Conterato and Nick Meltzer for their assistance during field sampling.



## References

- Bogman, P., Cornelis, W., Rolle H., Gabriels D., (2005). Prediction of TSP and PM<sub>10</sub> emissions from agricultural operations in Flanders, Belgium. 14th International Conference "Transport and Air Pollution". Graz, Austria, June 1-3, 2005.
- California Air Resources Board, 1986-1994. California air quality data. Quarterly summaries. Technical Support Division, California Air Resources Board, Sacramento, CA.
- Cassel, T., Trzepla-Nabaglo, K., Flocchini, R., (2003). PM<sub>10</sub> Emission Factors for Harvest and Tillage of Row Crops. 12th International Emission Inventory Conference - "Emission Inventories - Applying New Technologies". San Diego, April 29 - May 1, 2003.
- Clausnitzer, H., Singer, M.J., 1997. Intensive land preparation emits respirable dust. *California Agriculture* 51, 27-30.
- Clausnitzer, H., Singer, M.J., 2000. Environmental influences on respirable dust production from agricultural operations in California. *Atmospheric Environment* 34, 1739-1745.
- Coleman, H.W., Steele, W.G., 1989. Experimentation and uncertainty analysis of engineers. Wiley, New York, pp. 205.
- Erisman, J.W., Bleeker, A., Hensen, A., Vermeulen, A., 2008. Agricultural air quality in Europe and the future perspectives. *Atmospheric Environment* 42, 3209-3217.
- Flocchini, R.G., Cahill, T.A., Matsumura, R.T., Carvacho, O., Lu, Z., 1994. Study of fugitive PM<sub>10</sub> emissions for selected agricultural practices on selected agricultural soils. SJV Grant File # 20960. University of California, Davis, CA.
- Gaffney, P., Yu, H., (2003). Computing agricultural PM<sub>10</sub> fugitive dust emissions using process specific emission rates and GIS. 12th International Emission Inventory Conference - "Emission Inventories - Applying New Technologies". San Diego, April 29 - May 1, 2003.
- Holmén, B.A., James, T.A., Ashbaugh, L.L., Flocchini, R.G., 2001. Lidar-assisted measurement of PM<sub>10</sub> emissions from agricultural tilling in California's San Joaquin Valley – Part I: lidar. *Atmospheric Environment* 35, 3251-3264.
- Holmén, B.A., James, T.A., Ashbaugh, L.L., Flocchini, R.G., 2001. Lidar-assisted measurement of PM<sub>10</sub> emissions from agricultural tilling in California's San

- Joaquin Valley – Part II: emission factors. *Atmospheric Environment* 35, 3265-3277.
- Kjelgaard, J., Sharratt, B., Sundram, I., Lamb, B., Claiborn, C., Saxton, K., Chandler, D., 2004. PM<sub>10</sub> emission from agricultural soils on the Columbia Plateau: comparison of dynamic and time-integrated field-scale measurements and entrainment mechanisms. *Agricultural and Forestry Meteorology* 125, 259-277.
- Pope, C. A. III., Burnett, R. T., Thurston, G. D., Thun, M. T., Calle, E. E., Ito, K., Krewski, D., 2002. Lung cancer, cardiovascular mortality and long-term exposure to fine particulate air pollution. *Journal of American Medical Association*, 287:1132-1141.
- Pye, K., 1987. *Aeolian Dust and Dust Deposits*. Academic Press, New York, pp. 334
- Qiu, G., Pattey, E., 2008. Estimating PM<sub>10</sub> emissions from spring wheat harvest using an atmospheric tracer technique. *Atmospheric Environment* 42, 8315-8321.
- Schwartz, J., Zanobetti, A., Bateson, T. F., 2003. Mortality and morbidity among elderly residents of cities with daily PM measurements. Revised analyses of time-series studies of air pollution and health Boston: Health Effects Institute, 2003, 25-58.
- Tuch, T., Brand, P., Wichmann, H.E., Heyder, J., 1997. Variation of particle number and mass concentration in various size ranges of ambient aerosols in Eastern Germany. *Atmospheric Environment* 31, 4193-4197.
- USDA NRCS., 2005. Soil Survey Geographics (SSURGO) database for Dona Ana County area, New Mexico. Fort Worth, Texas: USDA NRCS.
- von Klot, S., Peters, A., Aalto, P., Bellander, T., Berglind, N., and D'Ippoliti, D., Elosua, R., Hormann, A., Kulmala, M., Lanki, T., Lowel, H., Pekkanen, J., Picciotto, S., Sunyer, J., Forastiere, F., 2005. Ambient air pollution is associated with increased risk of hospital cardiac readmissions of myocardial infarction survivors in five European cities. *Circulation* 112, 3073-3079.
- Wang, L., Parnell, Jr. C.B., Buser, M.D., 2007. Theoretical study of the impact of particulate matter gravitational settling on ambient coarse particulate matter monitoring for agricultural emissions. *Air & Waste Manage. Assoc.* 57, 111-115.

## APPENDIX E

### **Mechanized and Natural Soil-to-Air Transfer of Trifluralin and Prometryn from a Cotton Field in Las Cruces, New Mexico**

Britt A. Holmén<sup>1,\*</sup>, John Kasumba<sup>1</sup>, April Hiscox<sup>2</sup>, Junming Wang<sup>3</sup>, David Miller<sup>4</sup>

<sup>1</sup>School of Engineering, University of Vermont, Burlington, VT 05405

<sup>2</sup>Department of Geography, University of South Carolina, Columbia, SC 29208

<sup>3</sup>School of Agriculture and Consumer Sciences, Tennessee State University, Nashville, TN  
37209

<sup>4</sup>Department of Natural Resources Management and Engineering, University of Connecticut,  
Storrs, CT 06269

KEYWORDS Herbicide; Disk harrow; Prometryn; Trifluralin; Gas/particle partitioning; Agricultural emissions; Air-soil distribution; Soil preparation

\*Author to whom correspondence should be directed. e-mail: [bholmen@uvm.edu](mailto:bholmen@uvm.edu)

## ABSTRACT

Two pre-emergence herbicides (trifluralin and prometryn) were applied on a cotton field in Las Cruces, NM and their atmospheric particle and gas-phase concentrations measured during mechanized soil preparation and natural wind erosion sampling events before and after herbicide application. Air sampling was conducted using samplers mounted at various heights from the ground and at various locations on the field. During mechanized soil management with a disk harrow, sampling occurred at two distances from the tractor (“near-source”, 4 meters downwind and “far-source”, 20 – 100 meters from the disking tractor). Natural background (no disking) sampling events occurred during daytime and at night. Both herbicides were quantifiable for all post-application sampling events, including background sampling that occurred 8, 38, and 40 days after herbicide application. Average concentrations in both the gas and particle phases ranged from about 10 to 350 ng/m<sup>3</sup>. Averaging by event type, mean total prometryn concentrations were 2 (night background) to 8 (near-source) times higher than the corresponding trifluralin concentrations. Prometryn/trifluralin ratios were higher in airborne samples than in soil, indicative of trifluralin losses during daytime sampling, possibly via atmospheric reactions. Prometryn particle phase mass fractions were generally higher than those for trifluralin for all sampling events, consistent with  $K_{\text{air/soil-oc}}$  partition coefficients, and particle-phase mass fractions were higher for near-source disking and daytime background sampling compared to far-source and nighttime. Daytime natural background prometryn concentrations could be as high as those measured during disking and background samples showed significant relationships to meteorological parameters (air temperature, relative humidity and dewpoint). Mechanical disturbance by tilling operations reduced the ability to predict airborne herbicide concentrations on the basis of meteorological conditions. Prometryn concentrations were higher for larger

particle sizes ( $D_p > 1.8 \mu\text{m}$ ), while no clear patterns with particle size were observed for trifluralin. Trifluralin concentrations in the smallest size bin ( $\text{PM}_{0.18}$ ) were 2 to 50 times higher than prometryn for the three disking events where an impactor was used, indicating the importance of measuring size-resolved herbicide distributions in future studies.

## **Introduction**

Trifluralin and prometryn are widely used pre-emergence herbicides, applied to agricultural fields prior to field planting and cultivation. The transport of these herbicides to the atmosphere via gas-phase volatilization and resuspension of particles by wind erosion (“natural” or background events), or by mechanized operations such as disking, tillage, and other agricultural operations is of concern for downwind environmental and human health. Prometryn is moderately toxic<sup>1</sup> and the EPA has classified trifluralin as a Group C possible human carcinogen<sup>2</sup>. When in the atmosphere, herbicides distribute between the gas and particle phases depending on their concentrations, their physical and chemical properties, and atmospheric conditions such as temperature and relative humidity<sup>3</sup>. Knowledge of the gas/particle partitioning of herbicides is important because this process affects long-range transport of herbicides from their application sites, the potential removal of herbicides by wet and dry deposition, and the rate of atmospheric reactions such as oxidation and photodegradation<sup>4</sup>. Consideration of these herbicide transport processes is often overlooked due to the lack of field measurements on atmospheric gas and particle herbicide concentrations, especially during soil management practices.

Partitioning of semi-volatile organic compounds (SVOCs) to aerosol particles and removal of aerosol particles through dry deposition or rainfall have been identified as key factors determining long-range transport potential and overall SVOC persistence<sup>5</sup>. Herbicides and

pesticides present in the particle phase typically have higher atmospheric lifetimes because gas-phase compounds are more susceptible to oxidation by hydroxyl radicals<sup>6</sup>. Understanding the gas/particle partitioning behavior of herbicides can thus help us understand or predict the long-range transport of herbicides to non-target sites. Recent studies have quantified the ambient gas/particle partitioning of herbicides and pesticides<sup>4a, 6c, 7</sup>, but few studies have measured the herbicide content of airborne particulate matter (PM) from agricultural fields during mechanized agricultural operation events such as disking and tillage<sup>8</sup>. In addition, very few studies have measured the vertical profiles of herbicides on agricultural fields, while no studies have reported the distribution of herbicides in different airborne particle size fractions. In our previous study, pendimethalin and metolachlor concentrations were measured during disking events in California; pendimethalin but not metolachlor was found in airborne PM released during disking and there was a measurable increase in pendimethalin's particle/gas partition coefficient with distance from the tractor<sup>8b</sup>.

The objectives of this study were to: (1) quantify the total airborne herbicide load and gas/particle distribution of two herbicides under field conditions; (2) determine the distribution of the particle-phase herbicides as a function of airborne particle size; and (3) compare the herbicide concentrations with respect to event type (disking vs. background) in order to determine the relative importance of human-induced versus natural-process herbicide emissions from agricultural fields. Airborne gaseous and particulate herbicide (trifluralin and prometryn) concentrations were measured during nine sampling events (one pre-herbicide daytime background, one pre-herbicide disking, four post-herbicide disking, one post-herbicide daytime background, and two post-herbicide nighttime background) on a cotton field in Las Cruces, New Mexico in March and April 2008.

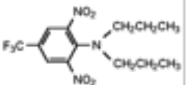
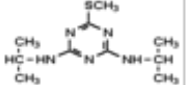
## Experimental Methods

### Herbicide Application and Sampling Events

Two pre-emergence herbicides, prometryn and trifluralin (Table 1), were applied to bare soil in a cotton field in Las Cruces, NM in March 2008 as the trade herbicides Caparol (Syngenta, Greensboro, NC) and Trust (Dow AgroSciences, Indianapolis, IN), respectively. The active ingredient for Caparol is prometryn (2,4-bis(isopropylamino)-6-(methylthio)-1,3,5-triazine [44.4%]) while that for Trust is trifluralin ( $\alpha,\alpha,\alpha$ -trifluoro-2,6-dinitro-*N,N*-dipropyl-*p*-toluidine [46%]). The applied formulation contained 0.05% Placement<sup>®</sup> (AgriSolutions) a drift control and deposition agent. Prometryn and trifluralin target application rates were 0.850 lb/acre (0.095 g/m<sup>2</sup>) and 0.518 lb/acre (0.058 g/m<sup>2</sup>), respectively, based on the formulation mixture. The structures and physical-chemical properties of both herbicides are shown in Table 1<sup>9</sup>. The theoretical air-soil partition coefficients ( $K_{air/soil}$ ) for both herbicides were calculated using Table 1 values and Equation (1):

$$K_{air/soil} = \frac{K_H}{K_{oc}} \quad [1]$$

where  $K_H$  is the dimensionless 25 °C Henry's law constant, and  $K_{OC}$  is the organic carbon sorption partition coefficient. Equation (1) assumes the majority of soil sorption is due to organic matter and ignores mineral sorption that has been shown to be important for dry field conditions<sup>10</sup>. The air/soil partition coefficient ( $K_{air/soil}$ ) for trifluralin is three orders of magnitude greater than the value for prometryn due to its much higher vapor pressure. Trifluralin's reported short half-life in air (25 - 193 minutes) as compared to prometryn (~10 hours) is likely due to a higher photodegradation or oxidation rate<sup>4b</sup>.

Herbicide	Chemical Structure	Molecular Weight (g/mol)	Vapor Pressure (Pa) at 25° C	H (Pa.m <sup>3</sup> /mol) at 25° C	Log K <sub>oc</sub>	Melting Point (° C)	Half-life in soil (days)	Half-life in air (min)	K <sup>[b]</sup> <sub>air/soil</sub>
Trifluralin C <sub>13</sub> H <sub>16</sub> F <sub>3</sub> N <sub>3</sub> O <sub>4</sub>		335	1.47 × 10 <sup>-2</sup>	16.61	4.14	49	~93	25-193	4.87 × 10 <sup>-7</sup>
Prometryn C <sub>10</sub> H <sub>19</sub> N <sub>5</sub> S		241	1.33 × 10 <sup>-4</sup>	1.39E-03	2.91	119	~60	~600 <sup>[a]</sup>	6.90 × 10 <sup>-10</sup>
<sup>[a]</sup> <a href="http://www.nlm.nih.gov/pubs/factsheets/toxnetfs.html">http://www.nlm.nih.gov/pubs/factsheets/toxnetfs.html</a>									
<sup>[b]</sup> computed from H and K <sub>oc</sub>									

The field site, sampling events and samplers were described previously<sup>11</sup>. Table 2 briefly summarizes the nine sampling events with more detailed description in the Supporting Information. Light-weight Filter-PUF samplers comprised of an Apex personal air sampling pump (Casella, Amherst, NH) that had both a Teflon filter (47 mm, Pall Gelman) and a polyurethane foam (PUF) cartridge at its inlet sampled particle-phase and gas-phase herbicides, respectively, at a flow rate of 4 liters per minute. During all the sampling events, three Filter-PUF samplers were mounted at different heights on a portable platform vertical array located either in the middle, corner or edge of the field to capture herbicide vertical profiles, while two other Filter-PUF samplers were always placed at the downwind and upwind corners of the field at ~1m height. A Micro-Orifice Uniform Deposition Impactor (MOUDI, Model 110-R, MSP Corp.) operating at 30 Lpm was located on the platform to measure herbicide distributions in 10 particle size fractions (<0.18 to 18 μm diameter) using aluminum foil substrates. During the disking events, the disking tractor was always moving while the samplers were stationary only for the far-source disking events. During near-source disking, the sampler platform was moved after each tractor pass to maintain a 4-meter downwind distance from the disking tractor. No disking took place during “natural” background events, and the samplers were stationary. Two sonic anemometers (CSAT3, Campbell Scientific) located at the southern edge of the field at



1.34 m and 8 m from the ground measured air temperature, wind speed, and wind direction at 20 Hz resolution. Because the meteorological data for Events 7, 8, and 9 were incomplete, the nearby Las Cruces international airport meteorological data<sup>12</sup> summarize conditions for all nine sampling events (Table 2). Surface soil samples collected from random locations on the field during Events 4, 6, and 9 were used to determine the herbicide concentrations at various times (1, 7 and 40 days, respectively) after herbicide application (duplicate 1 gram subsamples were extracted and analyzed). Samples collected by the MOUDI stages, filters, and PUFs, together with soil samples were all stored in a -80 °C freezer after shipment to the University of Vermont until they were extracted and analyzed.

**Table 2. Meteorological parameters during sampling events.**

Event#	Event Type	Days After Applied	Mean Temp (°C)	Mean WS (m/s)	Mean WD (Deg)	Mean RH (%)	Stability Parameter	Mean T <sub>dew</sub> (°C)	Mean Soil Moisture (%)
1	Pre-herbicide Background	-4	NA	NA	NA	NA	NA	NA	NA
2	Pre-herbicide Near-Source Disking	-1	19	3.71	134.1	NA	0.1	NA	1.45
3	Near-Source Disking	0	23.7	9.6	264.3	8.4	1.8	-11.91	1.35
4	Near-Source Disking	1	24.2	18.8	258	10.4	0.3	-8.85	2.47
5	Far-Source Disking	5	13.2	12.4	258	13	-0.2	-14.62	1.76
6	Far-Source Disking	7	18.3	2.6	93.3	9.1	0.7 to 0.4	-14.99	3.06
7	Nighttime Background	8	8.9	4.2	125.8	18.9	NA	-13.53	2.29
8	Daytime Background	38	20.6	3.5	139.7	5.6	NA	-19.05	NA
9	Nighttime Background	40	13.7	6.5	258.4	11.9	NA	-15.29	NA

WS = wind speed, WD = wind direction, RH = relative humidity, NA = Not Available

Stability from Kasumba et al. (2011) based on sonic anemometers used during "active" events; Soil moisture measured by TDR probe and moisture cans.

## Laboratory analysis of the real-world samples for the field-applied herbicides

The Filter-PUF, soil and MOUDI field samples were extracted by supercritical fluid extraction (SFE) and analyzed by gas chromatography-mass spectrometry (GC/MS) for the two field-applied herbicides, prometryn and trifluralin. During extraction, the MOUDI aluminum foils were combined into four composite size fractions to obtain sufficient herbicide mass for GC/MS analysis; particles with aerodynamic diameter between 10 and 18 µm (PM<sub>10-18</sub>) were

extracted together, as were particles between 1.8 and 10  $\mu\text{m}$  ( $\text{PM}_{1.8-10}$ ), 0.18 and 1.8  $\mu\text{m}$  ( $\text{PM}_{0.18-1.8}$ ), and less than or equal to 0.18  $\mu\text{m}$  ( $\text{PM}_{0.18}$ ).

Using a Spe-ed 2 Supercritical Fluid Extractor (Applied Separations, Allentown, PA), supercritical fluid carbon dioxide was used as the herbicide extraction solvent with a 10% v/v acetone modifier at 200 bar, 86°C (MOUDI foil, 75 min, 100mL vessel; Teflon filters, 45 min, 25 mL vessel) or 98°C (PUFs, 120 min, 1L vessel), and a flow rate of 2 mL/min. Reproducibility of the extraction methods was ensured by extracting replicate samples of laboratory herbicide standards for each method and surrogate (terbutryn) addition prior to extraction of all samples. Herbicide standard percent recoveries ranged from 77 to 106% with relative standard deviations from 4 to 12%.

All sample extracts were analyzed by GC/MS (Agilent 6890GC/5973MSD) using methane positive chemical ionization (PCI) as the ionization mode. Exactly 2.25  $\mu\text{g}$  of each of two herbicide internal standards (benfluralin, 98.7% and propazine, 99.5% (ChemService Inc., West Chester, PA) were added to each sample just before GC/MS analysis for quantification. The GC conditions were: Restek (Rxi-XLB) capillary GC column (30 m, 0.25 mm i.d, and 0.25  $\mu\text{m}$  film thickness), 99.999% helium carrier gas at 1 mL/min, 290 °C injector operated in splitless mode, and 290 °C detector. Particle-phase concentrations for the filters were expressed in terms of herbicide mass collected per volume of air sampled, rather than herbicide mass sampled per gravimetric mass of PM collected because some filters had pre-weights greater than their respective post-weights, thus leading to negative PM concentrations for samples with little particle mass collected. The detailed SFE extraction procedures and GC/MS analysis conditions, including laboratory quality control and detection limits can be found in the Supporting Information.

Measured concentrations of trifluralin and prometryn in blanks for the different sampling media were used to define minimum mass detection limits for the field samples (see Supporting Information). For each sampling medium, the herbicide concentration was considered to be “*certain*” if the sample herbicide mass was greater than the average blank mass ( $M_b$ ) plus one standard deviation of the field blank mass ( $s_b$ ) for the same sampling medium; “*uncertain*” if the measured herbicide mass was less than  $(M_b + 1s_b)$ , but greater than  $M_b$ ; and “*below blank detection*” (*BBD*) if the measured herbicide mass was less than  $M_b$ . The number of samples that had detectable concentrations for prometryn (30 PUF and 33 Filter) was greater than the number of samples that had detectable trifluralin concentrations (14 PUF and 34 Filter), likely due to the higher prometryn application rate, but these data may also reflect sampling or analytical losses of trifluralin from the PUF samples. One Event 5 sample that had extremely low total volume sampled but detectable herbicide mass was omitted from statistical analysis.

### **Statistical Analysis**

JMP software (version 9.0.0, SAS Institute Inc., 2010) was used for statistical analysis (Student’s t-tests (assuming unequal variances) and Analysis Of Variance (ANOVA); defining “statistical significance” at the 5% level ( $\alpha = 0.05$ )). To compare the herbicide concentrations based on the type of sampling event, the events were classified into four types: near-source disking (Events 3 and 4), far-source disking (Events 5 and 6), daytime background (Event 8), and nighttime background (Events 7 and 9). Herbicides were not detected in the two pre-application events (Events 1 and 2), so they are not discussed further.

## Results and Discussion

### Soil Sample Herbicide Concentrations.

Measured trifluralin concentrations in soil samples were higher than prometryn concentrations, with the ratio of prometryn to trifluralin concentrations ranging from 0.08 to 0.21 (Table 3) showing no discernable trend over time (Event 9 was 40 days after herbicide application), possibly due to sample heterogeneity across the field. The 30-40% difference in herbicide concentrations of the two different soil samples collected during Event 4 indicates the field sample heterogeneity by sampling location. The low measured prometryn/trifluralin ratios in soil samples were surprising because ratio of prometryn to trifluralin in the applied herbicide formulation was 1.6. It is unknown to what extent the Placement<sup>®</sup> deposition additive may have differentially affected the sorption and volatilization behavior of the two herbicides. This product is intended to generate positively charged micelles that encase the herbicide and reduce evaporation. It is likely that the effect of Placement<sup>®</sup> would be enhanced for the lower solubility herbicide in our study, trifluralin. Trifluralin has a much higher computed  $K_{air/soil_{oc}}$  even given its 10 times higher organic carbon sorption coefficient compared to prometryn (see Table 1), but this computed equilibrium value assumes wet conditions and previous studies have shown, sorption and volatilization processes depend on the soil moisture conditions<sup>3, 10, 13</sup>. The longer half-life of trifluralin in soil (93 days) compared to prometryn (60 days) is, however, consistent with the higher measured trifluralin soil concentrations. It is also important to note that there were detectable concentrations of both herbicides in the surface soil collected 40 days after herbicide application (Event 9). These data agree with previous measurements of trifluralin in soil samples over 100 days after application even in higher moisture environments<sup>14</sup>.

**Table 3. Average herbicide concentrations in soil samples (ng/g soil).**

Herbicide	Event 1	Event 2	Event 3	Event 4	Mean Concn Soil ng/g
	Sample 1 n=2	Sample 2 n=2	Sample 3 n=2	Sample 4 n=2	
Days Since Application	1	1	7	40	
Trifluralin (ng/g soil)	661 (754)	468 (116)	141 (154)	528 (385)	449
Prometryn (ng/g soil)	127 (137)	71.5 (8.4)	13.7 (16.7)	89.5 (85.4)	75.5
Prometryn/trifluralin concentration ratio	0.21 (0.04)	0.16 (0.02)	0.08 (0.03)	0.15 (0.05)	0.15

n represents number of subsamples extracted

Values in parentheses represent one standard deviation.

Considering the variability among samples, no decreasing trend in soil herbicide concentrations was observed, therefore the mean soil concentrations reported in Table 3 are considered representative over all events after soil incorporation of herbicides. There was no rain during the study so conditions were dry: soil moisture ranged from 1.3 to 3%, somewhat lower than observed in our California study<sup>8b</sup> (2.3 – 3.5%). Atmospheric conditions were also drier and colder than Clymo et al.<sup>8b</sup>: daytime relative humidity was 5-13%, nighttime 12-20% and air temperature was 10-20°C (see Table 2) vs. 40-60% and 20-30 °C in our previous daytime study.

### Airborne Herbicide Load.

No herbicides were detected in pre-application events (Events 1 and 2), as expected. Thus, there was no carryover of herbicides from previous applications on the field, and there was no contamination from neighboring fields.

Generally, when both herbicides were detected in a given PUF or filter sample, prometryn concentrations were higher than trifluralin concentrations in both the gas and particle phases for all sampling locations and sampling events (Table S3). Mean prometryn total (particle + gas phases) concentrations were statistically ( $\alpha = 0.05$ ) higher for near-source disking

events (Events 3 and 4; mean = 351.5 ng/m<sup>3</sup>) than far-source disking (Events 5 and 6; mean = 123.0 ng/m<sup>3</sup>), daytime background (Event 8; mean = 116.8 ng/m<sup>3</sup>) and nighttime background events (Events 7 and 9; mean = 60.5 ng/m<sup>3</sup>) as shown in Figure 1. For trifluralin, near-source disking total concentrations were statistically 1.5 – 2 times higher than the far-source and daytime background samples, but not statistically different from nighttime background (Events 7 and 9) due to higher variability in nighttime samples. For both herbicides, the event type pattern observed for total herbicide concentration was also observed for the gas-phase samples collected on PUFs, but particle-phase concentrations were not statistically different between event types for either herbicide. This latter result may be related to computing herbicide concentrations on an air-volume sampled, not PM mass, basis due to missing PM mass data for some samples.

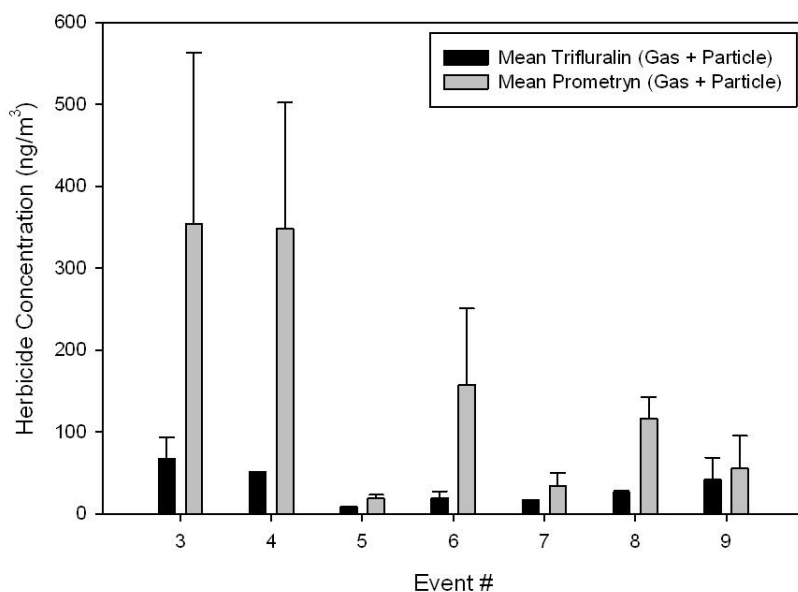


**Figure 1. Mean total (gas + particle phases combined) herbicide concentrations measured in Apex Filter-PUF samplers by sampling event. Error bars represent one standard deviation.**

Similar relationships were found previously for PM<sub>10</sub>: near-source disking events had about 4 to 10 times higher PM<sub>10</sub> concentrations than far-source disking and background events<sup>11</sup>. Thus, soil management practices taking place on the agricultural field during sampling increase both PM<sub>10</sub> and herbicide airborne concentrations approximately 1-10 times above background levels, depending on the sampler distance from the tractor. No direct relationship was found as a function of tractor distance, however, suggesting airborne herbicide concentrations also depend on field meteorological conditions (temperature, wind speed, humidity) which control herbicide volatilization and soil resuspension rates.

Averaging over all the Filter-PUF samplers by event type, the *total* (gas + particle) prometryn concentrations were 2 to 8 times higher than the corresponding trifluralin total concentrations, the gas-phase prometryn concentrations were 2 to 4 times higher than the gas-phase trifluralin concentrations, and the particle-phase prometryn concentrations were 2 to 14 times higher than the particle-phase trifluralin concentrations. These differences in herbicide concentrations in airborne samples likely result from a combination of: (1) different herbicide application rates; (2) the shorter half-life of trifluralin in the air, which means that more trifluralin than prometryn would decompose after entering the atmosphere; (3) differences in prometryn/trifluralin ratio by particle size (MOUDI, see below); and (4) higher loss of gas-phase trifluralin than prometryn during storage or breakthrough during sampling due to its higher vapor pressure. The higher number of PUF sample non-detects for trifluralin compared to prometryn suggests losses during air sampling for some samples, but samples with uncertain PUF concentrations did not always have low filter concentrations and no data are available to assess PUF breakthrough during sampling. Trifluralin loss during laboratory handling is unlikely because very good recoveries were obtained for spiked PUFs and filters.

The higher prometryn/trifluralin concentration ratios measured in the gas and particle phases cannot be fully accounted for by the herbicide target application rates determined from the spray formulation. Prometryn was applied at a rate of 0.85 lb/acre while trifluralin was applied at a rate of 0.52 lb/acre, a ratio of 1.6. Compared to the application rate, the higher ratio in air samples and lower ratio measured in surface soil samples (see Table 3) suggest processes occurred to modify the prometryn/trifluralin ratio either prior to or during air sampling, assuming laboratory losses can be ruled out. Loss of trifluralin during air sampling would explain the higher prometryn/trifluralin ratios measured in the airborne samples. We do not have field data to further quantify the possible herbicide loss mechanisms, but the herbicides' physical-chemical properties (Table 2) imply that trifluralin might degrade more quickly than prometryn when both herbicides were either resuspended (as dust-bound herbicide) or volatilized into air from the soil surface particles, thus trifluralin measured air concentrations would always be lower than those for prometryn. For example, trifluralin photolysis is known to be fast and it also reacts with atmospheric hydroxyl radical with lifetimes of 15 min to 8.5 hours, respectively<sup>4b, 15</sup>. For the soil samples, either prometryn was preferentially lost from the soil samples prior to sample collection (Event 4) or trifluralin was more easily extracted from the soil, the latter is unlikely based on the relative properties in Table 2. More data, such as the relative rates of soil biodegradation of the two herbicides during soil sample storage, would be needed to evaluate these possible explanations of why the herbicide mass concentration ratio varied with sample type.

Given that prometryn/trifluralin ratios in Filter/PUF samples were generally greater than 1, prometryn should have a longer atmospheric residence time and therefore longer transport distance probability than trifluralin after being released to the atmosphere via agricultural disking or natural daytime resuspension. The total airborne concentrations of trifluralin and prometryn



were not statistically different for Events 7 and 9, the two nighttime passive sampling events ( $p = 0.1487$ ). Nighttime concentrations were also typically lower than daytime for both herbicides. The observed similar concentrations of the two herbicides for nighttime sampling could be explained by higher in-soil prometryn degradation/loss given that these nighttime events occurred days after herbicide application (8 days for Event 7, and 40 days for Event 9). Appreciable soil degradation did not occur, however, evidenced by the high airborne prometryn concentrations measured during the daytime background event (Event 8), 38 days after herbicide application. It is more likely that time-of-day affected the resuspension, volatilization, and degradation of the two herbicides differently in the absence of soil management. Either more prometryn than trifluralin volatilized or was resuspended from the soil during daytime Event 8 than for nighttime Events 7 and 9, or photodegradation of trifluralin preferentially removed trifluralin from the atmosphere during daytime Event 8, but not at night. Meteorological parameters such as temperature, wind speed, and relative humidity could also have played a role in affecting the relative concentrations of both herbicides during day and night background sampling events. The mean temperature during Event 8 (20.6 °C) was higher than the temperatures for Events 7 (8.9 °C) and 9 (13.7 °C) (Table 2) and could have resulted in higher volatilization and dust resuspension during Event 8. Trifluralin's higher air/soil partition coefficient is consistent with greater gas-phase trifluralin loss in air relative to prometryn only during the day due to higher photodegradation and/or gas-phase oxidation *after* release from the soil. Further examination of the gas and particle phase behavior of these herbicides may shed light on these competing processes.

### **Gas- and Particle-Phase Herbicide Concentrations by Event Type**

Figure 2 shows the average particle-phase and gas-phase concentrations of both herbicides in each sampling event for the three Filter-PUF samplers located on the tower/platform. Prometryn mean concentrations were typically higher than trifluralin mean concentrations for all filter and PUF samples in each event (Figure 2, note y-axis scales), and airborne herbicide concentrations appreciably decreased with time after herbicide application. Events 7, 8 and 9 occurred 8, 38 and 40 days after herbicide application, respectively, and the concentrations of both herbicides during Event 9 were lower than those for the earlier nighttime background event (Event 7). The 2-4 times higher prometryn particle-to-gas concentration ratio for daytime Event 8 compared to Events 7 and 9 supports the hypothesis that daytime conditions released more surface soil particles and particle-bound herbicides from the soil compared to nighttime conditions. Such natural erosion conditions are not uncommon in dry climates where solar insolation heats the ground and leads to development of vertical convection currents that incorporate fine soil particles into the atmosphere (“dust devils”).

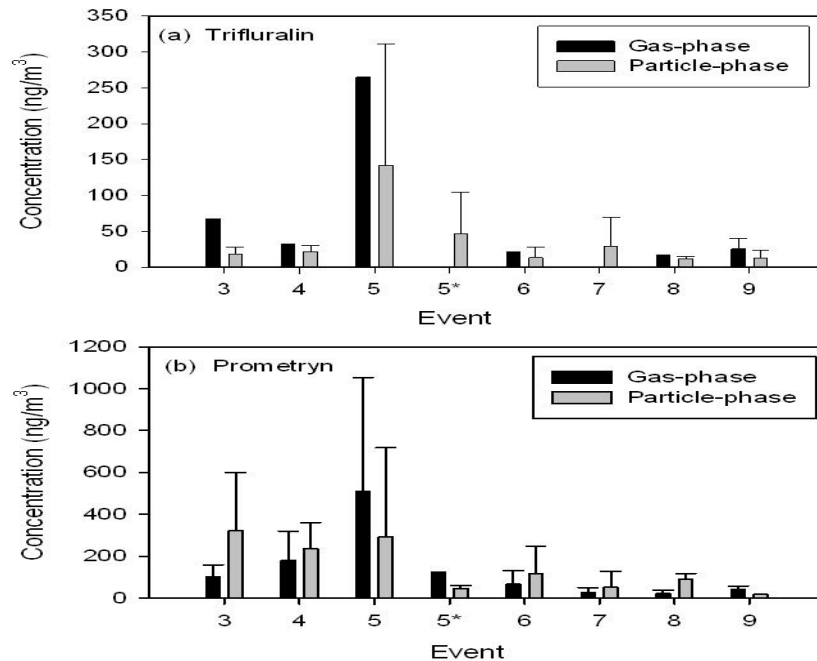


**Figure 2. Average gas and particle-phase concentrations of (a) trifluralin and (b) prometryn (for the three filter/PUF samplers on the tower). \* indicates Event 5 data plotted without the outlier concentration.**

During Event 5 disking, the DustTrak sampler located at 5.5m height measured unusually high  $PM_{10}$  concentrations compared to the other DustTraks<sup>11</sup>. Samplers located at this spot on the platform were apparently exposed to more herbicide and particles than other samplers for an unknown reason, possibly due to a localized dust devil soil disturbance event during this relatively windy far-source disking event (see Table 2). Because the Filter-PUF sampling unit located at the 5.5 m height of the platform during Event 5 clogged, these data were not included in statistical analyses.

### Herbicide Concentrations and Sampler Height

Based on our  $PM_{10}$  study<sup>11</sup>, vertical profile patterns of decreasing herbicide concentrations with sampling height were expected, especially for the near-source disking

events. For PM<sub>10</sub>, concentrations decreased with height from the ground for near-source disking events, while there were no consistent vertical profile shapes for far-source disking events and background events<sup>11</sup>. The vertical profiles observed for both herbicides differed from event to event for both gas and particle-phase herbicides (Supporting Information, Figures S1 and S2). Even replicate types of sampling events (Near-source disking Events 3 and 4; Far-source disking Events 5 and 6), however, did not have similar vertical herbicide profiles. Thus, no distinct vertical profile patterns existed for the herbicides trifluralin and prometryn despite being found for PM<sub>10</sub>.

### Herbicide Gas/Particle Fractionation

The mass fraction of herbicide measured in the particle phase ( $\Phi_p$ ) was determined (Eq. 2) to evaluate the gas-particle behavior of the two herbicides by event type:

$$\Phi_p = \frac{M_p}{M_p + M_g} \quad [2]$$

where  $M_p$  is the herbicide mass in the particle phase (filter sample) and  $M_g$  is the herbicide mass in the gas phase (PUF sample). The measured  $\Phi_p$  for prometryn was generally higher than  $\Phi_p$  for trifluralin in individual samples, in agreement with the herbicides' relative air/soil partition coefficients. Over all sampling events,  $\Phi_p$  ranged from 0.08 to 0.90 (mean =  $0.44 \pm 0.21$ ) for trifluralin and from 0.13 to 0.99 for prometryn (mean =  $0.55 \pm 0.26$ ). For prometryn, there was a significant difference in the particle mass fraction by event type, with  $\Phi_p$  greater than 0.5 for the daytime background and near-source disking events and less than 0.5 for far-source and nighttime events (Figure S3). High  $\Phi_p$  during disking events was expected because herbicide-bound particles were mechanically resuspended from the ground. There apparently was not sufficient time for prometryn to desorb from the dust during near-source disking,

resulting in increased mass fractions in the particle phase. During background sampling, in contrast, no particles were mechanically disturbed from the ground, thus the concentration of herbicide-bound particles in the atmosphere was determined by natural wind erosion and compound volatilization from the soil. The significantly (at 95% probability level) lower  $\Phi_p$  ratios for nighttime background and far-source disking compared to near-source and daytime background sampling suggest volatilization processes were greater than wind erosion of particle-bound herbicides under nighttime background sampling. In contrast, for the single daytime background sampling (Event 8), wind erosion of herbicide-bound dust dominated over volatilization of prometryn to generate the observed high particle mass fractions.

Event 8 was the only event with a distinct pattern of increasing  $\Phi_p$  with increasing sampling height (Figure S3), suggesting that high near-ground gas-phase volatilization from soil at low ambient air relative humidity and high temperature (Event 8, See Table 2) combined with intermittent events of soil particle erosion under these daytime background conditions. The increase in particle mass fraction with height indicates prometryn was preferentially sorbed to particles as they were transported away from the ground-level source. The highest sampling height (9 m) had the highest  $\Phi_p$  measured in the study and the lowest PUF concentrations of all passive events. Thus, prometryn was either lost from the gas-phase, relative to particle phase, as soil particles were vertically transported from the ground or gas-to-particle re-adsorption of (near-ground) volatilized prometryn may have occurred under conditions of daytime soil heating and dust resuspension. Natural wind erosion may resuspend different particle sizes compared to active mechanical disking and the tendency of prometryn to desorb from airborne particles may be a function of particle size and organic matter content. With increasing height, the volume fraction of smaller particles with higher  $f_{oc}$  typically increases; both these factors would explain

the higher  $\Phi_p$  with sampler height. As discussed below, however, prometryn concentrations were not higher in the smaller size fractions during the disking events where particle size distribution was measured. Future studies should examine the distribution of herbicides as a function of particle size and sampling height concurrently to better quantify these background herbicide transport processes.

The background events (7, 8 and 9) showed statistically significant relationships between airborne prometryn total concentrations and  $\Phi_p$  with mean event meteorological parameters, but disking event relationships to meteorological conditions were not as strong. For example, total airborne prometryn increased with (i) increased ambient air temperature ( $R^2 = 0.61$ ,  $p = 0.0048$ ), (ii) decreased relative humidity ( $R^2 = 0.51$ ,  $p = 0.0127$ ), and (iii) decreased dewpoint ( $R^2 = 0.61$ ,  $p = 0.0048$ ) for *background* events whereas mean temperature explained 50% of the variability ( $R^2 = 0.50$ ,  $p = 0.0015$ ), humidity had no significant relationship to total prometryn concentration and dewpoint ( $R^2 = 0.33$ ,  $p = 0.0165$ ) explained only 33% of the variability for *disking* events. These data indicate that mechanical disturbance by tilling operations reduces the ability to predict airborne herbicide concentrations on the basis of meteorological conditions alone.

The measured gas/particle relative herbicide concentrations were consistent with the calculated air/soil partition coefficients. Prometryn particle phase mass fractions were generally higher than those for trifluralin during all events (see Figure S3). More research on a wide range of herbicides is needed to achieve better quantitative understanding of the factors that influence gas/particle partitioning of herbicides under field conditions. The findings of the gas/particle partitioning of trifluralin in the present study are consistent with previous studies. For instance, in a Strasbourg, France gas/particle partitioning study of 71 pesticides, trifluralin was one of the

pesticides found to mostly partition to the gas phase with an average mass fraction in the gas phase of 66.5%<sup>7a</sup>.

The range of herbicide particle-phase mass fractions measured in this study were similar to those measured by Clymo et al. (2005)<sup>8b</sup> for pendimethalin, but not metolachlor, during near-source disking in California. Relationships between herbicide properties and  $\Phi_p$  were examined, but not found to be significant except for a distinct increase in the range of measured  $\Phi_p$  for herbicides with Log  $K_{oc}$  greater than 2.5 (See Figure S4). Other properties, including vapor pressure,  $K_{air/soil}$ , Henry's constant, Abraham's H acceptor/donor parameters showed no relationship. Compound polarizability, as quantified by ACD Labs iLab2 software (<http://ilab/acdlabs.com/iLab2/index.php>), and which may be indicative of compound sorption to both organic matter and mineral surfaces in soil particles, showed a non-linear relationship to  $\Phi_p$ , with a distinct increase in  $\Phi_p$  for polarizability less than  $31 \times 10^{-24} \text{ cm}^3$ . Data from more herbicides are needed to better predict  $\Phi_p$  as a function of chemical properties.

### **Particle Size and Herbicide Concentration**

The sorption capacity of particulate organic matter has been previously found to be controlled by the size of PM because of a greater number of sorptive sites associated with a greater surface-to-volume ratio with decreasing particle size<sup>16</sup>. Size-resolved airborne particles were collected here for disking Events 4, 5 and 6 only. For the combined MOUDI-binned particle size fractions, prometryn concentrations increased with increasing particle size fraction for most of the sampling events while no clear pattern was observed for trifluralin (Figure 3). Prometryn concentrations were usually higher than trifluralin concentrations in all size fractions except in the smallest fraction,  $PM_{0.18}$ . Because trifluralin is more hydrophobic than prometryn, it

was expected that trifluralin concentrations in the smallest size fraction,  $PM_{0.18}$  (expected to have the highest organic matter content) would be higher than prometryn concentrations, and this was observed (Figure 3). The trifluralin concentration in  $PM_{0.18}$  was 50 times higher than that for prometryn during Event 4, about 2 times higher during Event 5, and about 5 times higher during Event 6. Given the observed relationship for prometryn with particle size, it is unlikely that the increase in Event 8 particle mass fraction was due to size-fractionation of particles during resuspension events, unless convection due to daytime soil heating under low humidity, high temperature atmospheric conditions preferentially suspends larger diameter particles than are suspended during mechanical tilling. Data are needed to compare the particle size distributions of herbicides during *natural background erosion* events to those associated with managed soil activities (disking, cultivation, etc.).

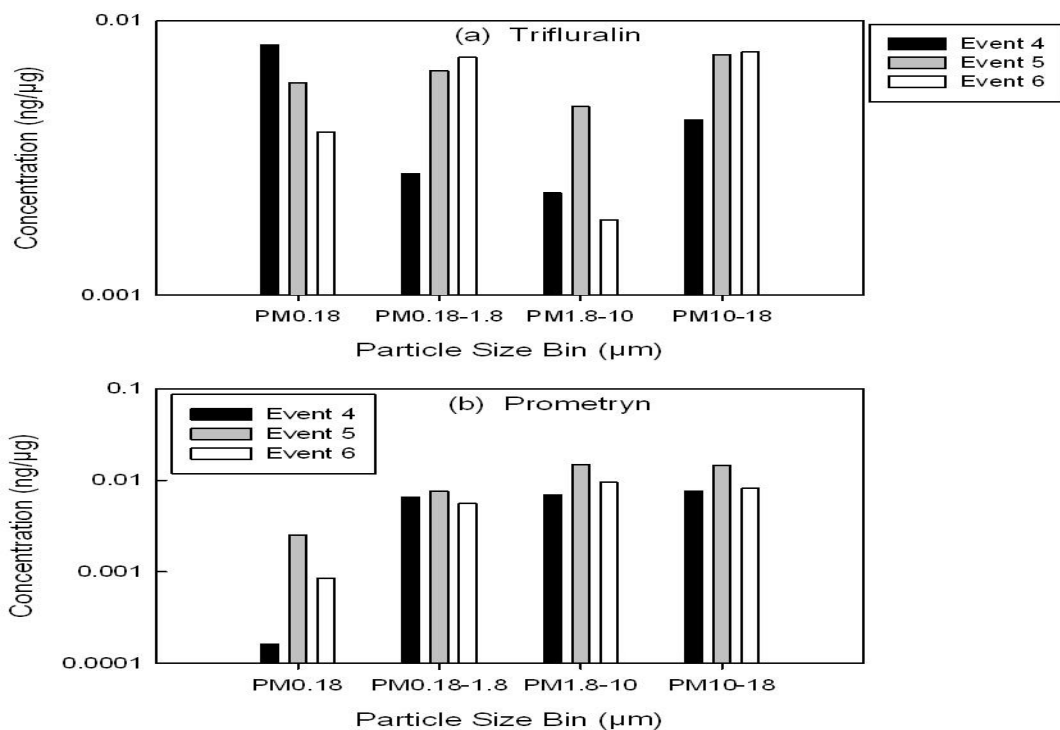


**Figure 3. (a) Trifluralin and (b) Prometryn concentrations measured on the particles sampled by the MOUDI (ng/μg of total MOUDI mass sampled). Note that the y-axis is on a log scale.**



Previous field studies have used high volume samplers in order to sample considerable mass of herbicides and pesticides during sampling. For example, flow rates ranging from 31 to 38 m<sup>3</sup>/h sampled gaseous and particle-bound PAHs in air at a deciduous forest in Borden, Ontario <sup>17</sup>; 15 m<sup>3</sup>/h sampled gaseous and particulate phase pesticides (83 pesticides) at two sites in Quebec, Canada <sup>7b</sup>; and 10 to 15 m<sup>3</sup>/h flows were used to sample gas and particle-phase herbicides at three sites in France <sup>4a</sup>. Here, the 0.24 m<sup>3</sup>/h flow rate for the light-weight Filter-PUF samplers enabled sampling gas- and particle-phase herbicides at different heights from the ground (0-9 meters), but also resulted in low measured mass of herbicides, especially trifluralin, during some events despite sampling very close to the source compared to other studies. It is not known to what extent the number of trifluralin PUF samples below detection were the result of the low sample flow rates employed vs. atmospheric oxidation/photolysis. It should be noted that an intermittent source was sampled in this study: except during the short periods of time when the disking tractor passed immediately upwind of the tower, background ambient air was being sampled, even during the disking events (Events 3-6). This may explain why background event herbicide concentrations could be of similar magnitude to those measured during both near- and far-source mechanized events that greatly disturbed the dry soil.

This work suggests two important avenues for future real-world measurement of airborne herbicides downwind of agricultural operations: extensive background gas/particle sampling as a function of height and as a function of particle size should be conducted for a wider range of herbicide compounds. These studies should also examine the effects of herbicide formulation on volatilization and particle resuspension processes. Higher sampler flow rates and methods to quantify filter “blow-off” artifacts should be employed in future field campaigns. Collection of

this data will enable calculation of pre-emergent herbicide fluxes downwind after soil application.

### **Acknowledgments**

This work was supported by the United States Department of Agriculture (USDA) under contract CSREES #2006-04701. The authors express their gratitude to Anna Conterato and Nick Meltzer for their assistance during field sampling and Timothy Kelly for his assistance during the laboratory analysis of the field samples.

### **Supporting Information**

Field sampling details, laboratory QA/QC procedures, filter and PUF herbicide concentrations by event and mass fractions for individual samples are documented separately. This material is available free of charge via the Internet at <http://pubs.acs.org>.

### **References Cited**

1. Gosselin, R. E.; Smith, R. P.; Hodge, H. C.; Braddock, J. E., *Clinical Toxicology of Commercial Products*. Williams and Wilkins: Baltimore, MD, 1984.
2. Agency, U. S. E. P. Integrated Risk Information System: Trifluralin. <http://www.epa.gov/iris/subst/0268.htm>.
3. Yang, W.; Holmén, B. A., Effects of relative humidity on chloroacetanilide and dinirtoaniline herbicide desorption from agricultural PM<sub>2.5</sub> and quartz fiber filters. *Environ. Sci. Technol.* **2007**, *41*, 3843-3849.
4. (a) Scheyer, A.; Morville, S.; Mirabel, P.; Millet, M., Gas/Particle Partitioning of Lindane and Current-used Pesticides and their Relationship with Temperature in Urban and Rural

- Air in Alsace Region (East of France). *Atmos Environ* **2008**, *42*, 7695–7705; (b) Le Person, A.; Mellouki, A.; Muñoz, A.; Borrás, E.; Martín-Reviejo, M.; Wirtz, K., Trifluralin: Photolysis under sunlight conditions and reaction with OH radicals. *Chemosphere* **2007**, *67*, 376-383.
5. (a) Götz, C. W. S., M.; MacLeod, M.; Wegmann, F.; Schenker, U.; Hungerbühler, K. , Dependence of Persistence and Long-Range Transport Potential on Gas-Particle Partitioning in Multimedia Models. *Environmental Science & Technology* **2008**, *42*, 3690–3696; (b) Scheringer, M., Characterization of the Environmental Distribution Behavior of Organic Chemicals by Means of Persistence and Spatial Range. *Environmental Science & Technology* **1997**, *31*, 2891–2897; (c) Scheringer, M., Long-range Transport and Global Fractionation of POPs: Insights from Multimedia Modeling Studies. *Environmental Pollution* **2004**, *128*, 177–188; (d) Lohmann, R. L., G. , Adsorptive and Absorptive Contributions to the Gas-Particle Partitioning of Polycyclic Aromatic Hydrocarbons: State of Knowledge and Recommended Parametrization for Modeling *Environmental Science & Technology* **2004**, *38*, 3793–3803.
6. (a) Atkinson, R., Estimation of OH Radical Reaction Rate Constants and Atmospheric Lifetimes for Polychlorobiphenyls, Dibenzo-p-dioxins, and Dibenzofurans. *Environmental Science & Technology* **1987**, *21*, 305–307; (b) Atkinson, R.; Guicherit, R.; Hites, R. A.; Palm, W.-U.; Seiber, J. N.; de Voogts, P., Transformations of Pesticides in the Atmosphere: A State of the Art. *Water, Air, & Soil Pollution* **1999**, *115*, 219–243; (c) Schummer, C.; Mothiron, E.; Appenzeller, B. M. R.; Rizet, A.-L.; Wennig, R.; Millet, M., Temporal Variations of Concentrations of Currently used Pesticides in the Atmosphere of Strasbourg, France *Environmental Pollution* **2010**, *158*, 576–584.

7. (a) Schummer, C.; Mothiron, E.; Appenzeller, B. M. R.; Wennig, R.; Millet, M., Gas/Particle Partitioning of Currently used Pesticides in the Atmosphere of Strasbourg (France) *Air Quality, Atmosphere & Health* **2010**, *3*, 171–181; (b) Sadiki, M.; Poissant, L., Atmospheric Concentrations and Gas-Particle Partitions of Pesticides: Comparisons between Measured and Gas-Particle Partitioning Models from Source and Receptor Sites. *Atmos Environ* **2008**, *42*, 8288–8299; (c) Sauret, N.; Wortham, H.; Streckowski, R.; Herckès, P.; Nieto, L. I., Comparison of Annual Dry and Wet Deposition Fluxes of Selected Pesticides in Strasbourg, France. *Environmental Pollution* **2009**, *157*, 303–312.
8. (a) Clymo, A. Downwind Concentrations of Metolachlor and Pendimethalin Sorbed to Airborne Particulate Matter Suspended During Soil Incorporation. M.S., University of California, Davis, 2002; (b) Clymo, A. S.; Shin, J. Y.; Holmén, B. A., Herbicide Sorption to Fine Particulate Matter Suspended Downwind of Agricultural Operations: Field and Laboratory Investigations. *Environ. Sci. & Technol.* **2005**, *39* (2), 421 - 430.
9. Mackay, D.; Shiu, W.-Y.; Ma, K.-C., *Handbook of physical-chemical properties and environmental fate for organic chemicals*. CRC Press: Boca Raton, FL, 2006.
10. Goss, K.-U.; Buschmann, J.; Schwarzenbach, R. P., Adsorption of Organic Vapors to Air-Dry Soils: Model Predictions and Experimental Validation. *Environ. Sci. Technol.* **2004**, *38* (13), 3667 -3673.
11. Kasumba, J.; Holmén, B. A.; Hiscox, A.; Wang, J.; Miller, D., Agricultural PM10 Emissions from Cotton Field Disking in Las Cruces, NM. . *Atmos Environ* **2011**, *45*, 1668–1674.
12. National Climatic Data Center <http://cdo.ncdc.noaa.gov/qclcd/QCLCD?prior=N>.

13. Schneider, M.; Goss, K.-U., Volatilization Modeling of Two Herbicides from Soil in a Wind Tunnel Experiment under Varying Humidity Conditions. *Environ. Sci. Technol.* **2012**, *46*, 12527-12533.
14. Bedos, C.; Rousseau-Djabri, M. F.; Gabrielle, B.; Flura, D.; Durand, B.; Barriuso, E.; Cellier, P., Measurement of trifluralin volatilization in the field: Relation to soil residue and effect of soil incorporation. *Environmental Pollution* **2006**, *144* 958-966.
15. Burrows, H. D.; Canle L., M.; Santaballa, J. A.; Steenken, S., Reaction pathways and mechanisms of photodegradation of pesticides. *Journal of Photochemistry and Photobiology B: Biology* **2002**, *67* 71–108.
16. (a) Benoit, P.; Madrigal, I.; Preston, C. M.; Chenu, C.; Barriuso, E., Sorption and Desorption of non-ionic Herbicides onto Particulate Organic Matter from Surface Soils under Different Land Uses. *European Journal of Soil Science* **2008**, *59*, 178–189; (b) Bidleman, T. F.; Christensen, E. J., Atmospheric Removal Processes for High Molecular Weight Organochlorines. *Journal of Geophysical Research* **1979**, *84*, 7857-7862.
17. Su, Y.; Lei, Y. D.; Wania, F.; Shoeib, M.; Harner, T., Regressing gas/particle partitioning data for polycyclic aromatic hydrocarbons. *Environ. Sci. Technol.* **2006**, *40*, 3558-3564.